ISSN 1881-7815 Online ISSN 1881-7823

BST BioScience Trends

Volume 18, Number 4
August, 2024

IRCA BSSA

IACMHR

www.biosciencetrends.com

BST
BioScience Trends

ISSN: 1881-7815
Online ISSN: 1881-7823
CODEN: BTIRCZ
Issues/Year: 6
Language: English
Publisher: IACMHR Co., Ltd.

BioScience Trends is one of a series of peer-reviewed journals of the International Research and Cooperation Association for Bio & Socio-Sciences Advancement (IRCA-BSSA) Group. It is published bimonthly by the International Advancement Center for Medicine & Health Research Co., Ltd. (IACMHR Co., Ltd.) and supported by the IRCA-BSSA.

BioScience Trends devotes to publishing the latest and most exciting advances in scientific research. Articles cover fields of life science such as biochemistry, molecular biology, clinical research, public health, medical care system, and social science in order to encourage cooperation and exchange among scientists and clinical researchers.

BioScience Trends publishes Original Articles, Brief Reports, Reviews, Policy Forum articles, Communications, Editorials, News, and Letters on all aspects of the field of life science. All contributions should seek to promote international collaboration.

Editorial Board

Editorial and Head Office

Pearl City Koishikawa 603,
2-4-5 Kasuga, Bunkyo-ku, Tokyo 112-0003, Japan
E-mail: office@biosciencetrends.com

BioScience Trends

Editorial and Head Office

Pearl City Koishikawa 603, 2-4-5 Kasuga, Bunkyo-ku,
Tokyo 112-0003, Japan

E-mail: office@biosciencetrends.com
URL: www.biosciencetrends.com

Editorial Board Members

Original Article

Correspondence

Original Article

DOI: 10.5582/bst.2024.01178

Genetic screening of newborns for deafness over 11 years in Beijing, China: More infants could benefit from an expanded program

Yu Ruan[1,2,3], Cheng Wen[1,2,3], Xiaohua Cheng[1,2,3], Wei Zhang[1,2,3], Liping Zhao[1,2,3], Jinge Xie[1,2,3], Hongli Lu[4], Yonghong Ren[4], Fanlin Meng[4], Yue Li[1,2,3], Lin Deng[1,2,3], Lihui Huang[1,2,3,*], Demin Han[1,2,3,*]

[1] Otolaryngology-Head and Neck Surgery, Beijing Tongren Hospital, Capital Medical University, Beijing, China;
[2] Beijing Institute of Otolaryngology, Beijing, China;
[3] Key Laboratory of Otolaryngology Head and Neck Surgery (Capital Medical University), Ministry of Education, Beijing, China;
[4] CapitalBio Corporation & National Engineering Research Center for Beijing Biochip Technology, Beijing, China.

SUMMARY Genetic screening of newborns for deafness plays an important role in elucidating the etiology of deafness, diagnosing it early, and intervening in it. Genetic screening of newborns has been conducted for 11 years in Beijing. It started with a chip to screen for 9 variants of 4 genes in 2012; the chip screened for 15 variants of those genes in 2018, and it now screens for 23 variants of those genes. In the current study, a comparative analysis of three screening protocols and follow-up for infants with pathogenic variants was performed. The rates of detection and hearing test results of infants with pathogenic variants were analyzed. Subjects were 493,821 infants born at 122 maternal and child care centers in Beijing from April 2012 to August 2023. Positivity increased from 4.599% for the chip to screen for 9 variants to 4.971% for the chip to screen for 15 variants, and further to 11.489% for the chip to screen for 23 variants. The carrier frequency of the *GJB2* gene increased from 2.489% for the chip to screen for 9 variants and 2.422% for the chip to screen for 15 variants to 9.055% for the chip to screen for 23 variants. The carrier frequency of the *SLC26A4* gene increased from 1.621% for the chip to screen for 9 variants to 2.015% for the chip to screen for 15 variants and then to 2.151% for the chip to screen for 23 variants. According to the chip to screen for 9 variants and the chip to screen for 15 variants, the most frequent mutant allele was c.235delC. According to the chip to screen for 23 variants, the most frequent mutant allele was c.109G>A. The chip to screen for 15 variants was used to screen 66.67% (14/21) of newborns with biallelic variants in the *SLC26A4* gene for newly added mutations. The chip to screen for 23 variants was used to screen 92.98% (53/57) of newborns with biallelic variants in the *GJB2* gene (52 cases were biallelic c.109G>A) and 25% (1/4) of newborns with biallelic variants in the *SLC26A4* gene for newly added mutations. Among the infants with pathogenic variants (biallelic variants in *GJB2* or *SLC26A4*), 20.66% (25/121) currently have normal hearing. In addition, 34.62% (9/26) of newborns who passed the hearing screening were diagnosed with hearing loss. Findings indicate that a growing number of newborns have benefited, and especially in the early identification of potential late-onset hearing loss, as the number of screening sites has increased. Conducting long-term audiological monitoring for biallelic variants in individuals with normal hearing is of paramount significance.

Keywords deafness genes, genetic screening of newborns, hearing screening for newborns, hearing loss, follow-up

1. Introduction

Hearing loss (HL) is the most common human neurosensory disorder, with a lifelong impact that may be ameliorated by early detection and intervention (*1*). The reported incidence of HL ranges from 1.33 to 1.86 per 1,000 newborns; more than half of these newborns have a genetic etiology (*2,3*).

In 2012, the Beijing Municipal Government launched a large-scale project for the genetic screening of

newborns, which included 9 variants of 4 genes associated with deafness, including c.235delC (p.Leu79Cysfs*3), c.299_300delAT (p.His100Argfs*14), c.176_191del16 (p.Gly59Alafs*18), and c.35delG (p.Gly12Valfs*2) of *GJB2* (MIM: 121011); c.919-2A>G and c.2168A>G (p.His723Arg) of *SLC26A4* (MIM: 605646); m.1555A>G and m.1494C>T of mtDNA *12SrRNA* (MIM: 561000); c.538C>T (p.Arg180*) of *GJB3* (MIM: 603324). Genetic screening of newborns can effectively increase the early rate of detection of hereditary HL, ototoxicity-related deafness, and delayed-onset HL, providing an early warning and diagnosis of HL and facilitating early intervention. Dai *et al.* conducted a study on 180,469 newborns born between 2013 and 2014 who underwent concurrent hearing and deafness genetic screening using the chip to screen for 9 variants (*4*). Results revealed that 25% of infants with pathogenic combinations of *GJB2* or *SLC26A4* variants and 99% of infants with an m.1555A>G or m.1494C>T variant passed the routine hearing screening for newborns. This highlights the importance of genetic screening in identifying infants at risk for HL, even when they may initially pass conventional hearing screening.

In 2018, to further enhance the early detection of large vestibular aqueduct syndrome (LVAS), the Beijing Municipal Government used an enhanced genetic screening chip. Based on the chip to screen for 9 variants, 6 additional variants of the *SLC26A4* gene were added to provide a chip to screen for 15 variants of the 4 genes, including c.1975G>C (p.Val659Leu), c.1707+5G>A, c.1229C>T (p.Thr410Met), c.1226G>A (p.Arg409His), c.2027T>A (p.Leu676Gln), and c.1174A>T (p.Asn392Tyr). Wen *et al.* analyzed 76,460 newborns who underwent concurrent hearing and deafness genetic screening using the chip to screen for 15 variants in 2019 and 2020 and found that 28.57% (2/7) of the newborns with the *SLC26A4* mutation causing deafness passed hearing screening (*5*).

In December 2022, the Beijing Municipal Government began using a chip to screen for 23 variants of the 4 genes. Based on the chip to screen for 15 variants, 5 additional variants of the *GJB2* gene and 3 variants of the *SLC26A4* gene were included: c.109G>A (p.Val37Ile), c.257C>G (p.Thr86Arg), c.512insAACG, c.427C>T (p.Arg143Trp) and c.35insG of *GJB2*; c.589G>A (p.Gly197Arg), c.917insG and c.281C>T (p.Thr94Ile) of *SLC26A4*. This upgrade has significantly broadened the scope of the screening, allowing for the identification of a greater variety of deafness-causing mutations and contributing to more comprehensive and accurate diagnoses of hereditary HL in newborns. Few studies have evaluated the performance of the chip to screen for 23 variants and few have compared the rate of detection with other protocols within the same category.

Since April 2012, the genetic screening of newborns in Beijing has been in clinical practice for more than a decade, with the screening protocols being continually updated. It started with a chip to screen for 9 variants of 4 genes in 2012; the chip screened for 15 variants of those genes in 2018, and the current chip now screens for 23 variants of those genes. This study involved an analysis of 493,821 newborns from Beijing born from April 2012 to August 2023. This study compared positivity, rates of detection of various genotypes, carrier frequencies, allele frequencies, and pathogenic genotypes according to three distinct screening protocols. In addition, the hearing phenotypes of individuals with pathogenic variants were analyzed. The aim of this study was to analyze the results of three screening protocols and hearing testing of infants with pathogenic variants in order to optimize protocols for current genetic screening and to improve interventions and management strategies for HL.

2. Materials and Methods

2.1. Clinical data

Subjects were 493,821 infants born at 122 maternal and child care centers in Beijing who underwent concurrent hearing and genetic screening from April 2012 to August 2023. Both hearing screening and genetic screening for newborns were conducted within 72 h after birth for all neonates at no charge.

A chip was used to screen 273,647 of those newborns born from April 2012 to December 2017 for 9 variants of 4 genes, which is referred to here as the chip to screen for 9 variants. A chip was used to screen 195,767 newborns born from January 2018 to November 2022 for 15 variants of those genes, which is referred to here as the chip to screen for 15 variants. A chip was used to screen 24,407 newborns born from December 2022 to August 2023 for 23 variants of those genes, which is referred to here as the chip to screen for 23 variants. The newborns who were screened for pathogenic variants were followed up systematically to obtain hearing screening and hearing test results. Figure 1 shows the study flow. Hearing screening was conducted using the otoacoustic emissions (OAEs) or automated auditory brainstem response (AABR) test.

2.2. Genetic screening

Dried blood spots were collected for genetic testing of genes associated with deafness: *GJB2*, *SLC26A4*, mtDNA *12SrRNA*, and *GJB3*. The Deafness Gene Variant Detection Array Kit (CapitalBio) was used to identify 9 variants of 4 genes in newborns born from April 2012 to December 2017, including c.235delC (p.Leu79Cysfs*3), c.299_300delAT (p.His100Argfs*14), c.176_191del16 (p.Gly59Alafs*18), and c.35delG (p.Gly12Valfs*2) of *GJB2* (MIM: 121011); c.919-2A>G and c.2168A>G (p.His723Arg) of *SLC26A4* (MIM: 605646); c.538C>T

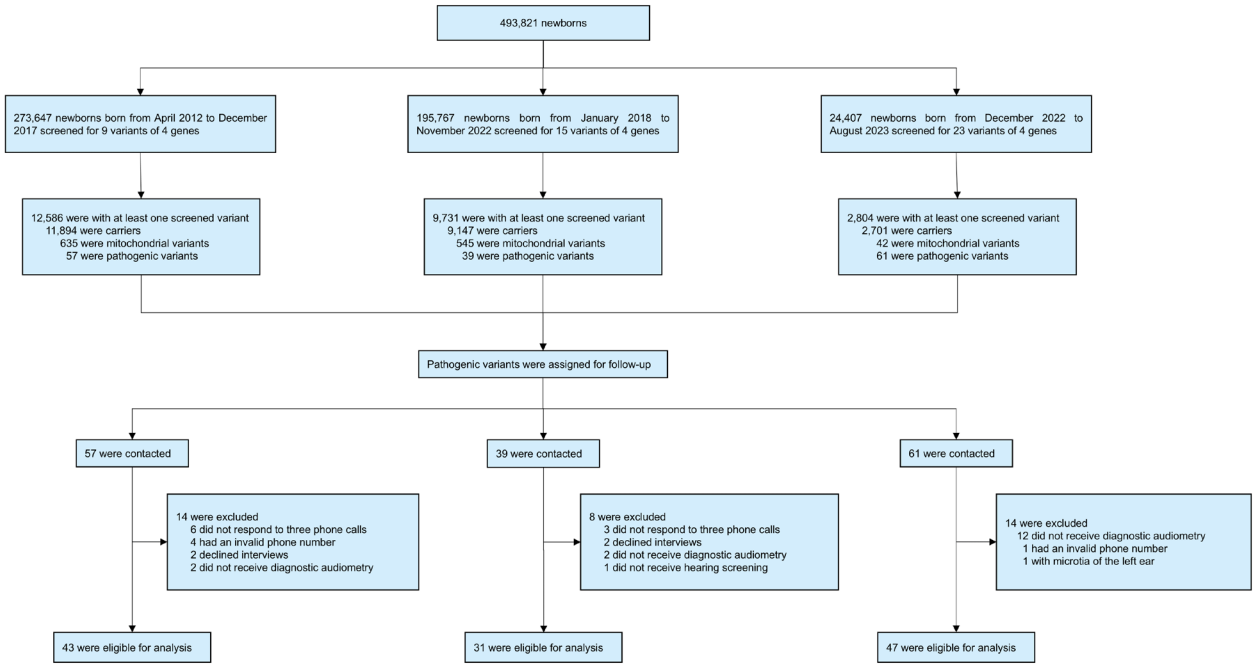

Figure 1. Participation in genetic screening and outcomes for 493,821 newborns. Genetic screening results were classified as follows: pathogenic variants (homozygote or compound heterozygote for *GJB2* or *SLC26A4*), carriers (heterozygote for *GJB2* or *SLC26A4* and heterozygote or homozygote for *GJB3*), mitochondrial variants (any mtDNA*12SrRNA* variant), and wild (no variant). Newborns with pathogenic variants were followed up.

(p.Arg180*) of *GJB3* (MIM: 603324); and m.1555A>G and m.1494C>T of mtDNA *12SrRNA* (MIM: 561000). The Deafness Gene Variant Detection Array Kit (CapitalBio) was used to identify 15 variants of 4 genes in newborns born from January 2018 to November 2022. Based on the chip to screen for 9 variants, 6 variants of the *SLC26A4* gene have been added: c.1975G>C (p.Val659Leu), c.1707+5G>A, c.1229C>T (p.Thr410Met), c.1226G>A (p.Arg409His), c.2027T>A (p.Leu676Gln), and c.1174A>T (p.Asn392Tyr). The Deafness Gene Variant Detection Array Kit (CapitalBio) was used to identify 23 variants of 4 genes in newborns born from December 2022 to August 2023. Based on the chip to screen for 15 variants, 5 variants of the *GJB2* gene and 3 variants of the *SLC26A4* gene have been added: c.109G>A(p.Val37Ile), c.257C>G(p.Thr86Arg), c.512insAACG, c.427C>T(p.Arg143Trp), c.35insG of *GJB2*; c.589G>A (p.Gly197Arg), c.917insG, c.281C>T (p.Thr94Ile) of *SLC26A4*. Genetic screening was conducted at Beijing Tongren Hospital, where genetic screening laboratories were authorized by the Beijing Municipal Health Commission (*4*). Results were recorded on a report card as wild or positive. Positive included carriers (heterozygous for *GJB2* or *SLC26A4* and heterozygous or homozygous for *GJB3*), pathogenic variants (homozygous or compound heterozygous for *GJB2* or *SLC26A4*) and mitochondrial variants (any mtDNA *12SrRNA* variant). Positive infants in genetic screening were referred to Beijing TongRen Hospital for diagnostic audiological testing, genetic counseling, and genetic diagnosis.

Genotypes with homozygous and compound heterozygous variants in *GJB2* or *SLC26A4* were diagnosed as deafness-causing genotypes, and those with mtDNA *12SrRNA* variants were diagnosed as drug-susceptible. Each subject was categorized into only one group based on genetic results. When a subject's results fell into more than one category, the subject was assigned to a group in the following order of priority: pathogenic variants, mitochondrial variants, carriers, and wild.

2.3. Hearing testing

Audiological evaluations of infants with pathogenic variants were performed at the Pediatric Hearing Diagnostic Center at Beijing Tongren Hospital. These assessments included objective and subjective hearing tests to ensure a thorough analysis of auditory function. Objective audiological tests consisted of the auditory brainstem response (ABR), distortion product otoacoustic emissions (DPOAEs), auditory steady state response (ASSR), and acoustic immittance. Subjective audiological tests included pediatric behavioral audiometry and pure tone audiometry.

According to the WHO 1997 criteria, the degree of HL was classified based on the average hearing thresholds of pediatric behavioral audiometry at 500 Hz, 1,000 Hz, 2,000 Hz, and 4,000 Hz for the better ear: normal (≤ 25 dB HL), mild (26-40 dB HL), moderate (41-60 dB HL), severe (61-80 dB HL), and profound (>80dB HL).

2.4. Statistical analysis

The software SPSS 27.0 was used to perform chi-square tests to compare positivity, rates of detection of various genotypes, carrier frequencies, and allele frequencies among the three screening protocols.

2.5. Ethics statement

This study was approved by the Ethics Committee of the Beijing Institute of Otolaryngology. Fully informed written consent was obtained from parents before screening.

3. Results

3.1. Comparison of positivity according to three genetic screening protocols

As shown in Table 1, total positivity was 5.087% (25,121/493,821). Positivity with the protocol for the chip to screen for 9 variants was 4.599% (12,586/273,647), and positivity with the protocol for the chip to screen for 15 variants was 4.971% (9,731/195,767), and positivity with the protocol for the chip to screen for 23 variants was 11.489% (2,804/24,407). Positivity according to the three screening protocols increased significantly ($P < 0.001$).

3.2. Comparison of the rates of detection of various genotypes according to three genetic screening protocols

As shown in Table 2, the rates of detection of pathogenic variants among three screening protocols, from highest to lowest, were as follows: the chip to screen for 23 variants (0.250%, 61/24,407), the chip to screen for 9 variants (0.021%, 57/273,647), and the chip to screen for 15 variants (0.020%, 39/195,767). The rates differed significantly ($P < 0.001$).

The rates of detection of mitochondrial variants, from highest to lowest, were as follows: the chip to screen for 15 variants (0.279%, 545/195,767), the chip to screen for 9 variants (0.232%, 635/273,647), and the chip to screen for 23 variants (0.176%, 42/24,407). The rates differed significantly ($P < 0.001$).

The rates of detection of carriers, from highest to lowest, were as follows: the chip to screen for 23 variants (11.066%, 2,701/24,407), the chip to screen for 15 variants (4.672%, 9,147/195,767), and the chip to screen for 9 variants (4.346%, 11,894/273,647). The rates

Table 1. Positivity according to three genetic screening protocols

Genotypes	Chip to screen for 9 variants *n* (%)	Chip to screen for 15 variants *n* (%)	Chip to screen for 23 variants *n* (%)	Total number (%)	*P* value
Positive	12,586 (4.599)	9,731 (4.971)	2,804 (11.489)	25,121 (5.087)	< 0.001
Wild type	261,061 (95.401)	186,036 (95.029)	21,603 (88.511)	468,700 (94.913)	
Total	273,647 (100.000)	195,767 (100.000)	24,407 (100.000)	493,821 (100.000)	

n: number of newborns.

Table 2. Rates of detection of various genotypes according to three genetic screening protocols

Genotypes	Chip to screen for 9 variants *n* (%)	Chip to screen for 15 variants *n* (%)	Chip to screen for 23 variants *n* (%)	*P* value
Pathogenic variants				
GJB2 homozygote/compound heterozygote	48 (0.018)	18 (0.009)	57 (0.234)	
SLC26A4 homozygote/compound heterozygote	9 (0.003)	21 (0.011)	4 (0.016)	
total	57 (0.021)	39 (0.020)	61 (0.250)	< 0.001
Mitochondrial variants	635 (0.232)	545 (0.279)	42 (0.176)	< 0.001
Carrier				
GJB2 heterozygote	6,615 (2.417)	4,597 (2.348)	2,096 (8.588)	
SLC26A4 heterozygote	4,287 (1.567)	3,783 (1.932)	471 (1.930)	
GJB3 heterozygote/homozygote	846 (0.309)	632 (0.323)	80 (0.328)	
Multiple gene heterozygote	146 (0.053)	135 (0.069)	54 (0.221)	
total	11,894 (4.346)	9,147 (4.672)	2,701 (11.066)	< 0.001
Total for all screened	12,586 (4.599)	9,731 (4.971)	2,804 (11.489)	

n: number of newborns. According to the protocol for the chip to screen for 9 variants, there were 25 cases of mitochondrial variants heterozygous for *GJB2* or *SLC26A4* or *GJB3*, and 146 cases of multiple gene heterozygotes who were heterozygous for *GJB2* and *SLC26A4* or heterozygous for *GJB2* and *GJB3* or heterozygous for *SLC26A4* and *GJB3*. According to the protocol for the chip to screen for 15 variants, there was 1 case of a *GJB2* homozygote with mitochondrial variants, 1 case of an *SLC26A4* homozygote heterozygous for *GJB2*, 29 cases of mitochondrial variants heterozygous for *GJB2* or *SLC26A4* or *GJB3*, and 1 case of a multiple gene heterozygote who was heterozygous for *GJB2* and *SLC26A4* and *GJB3*. According to the protocol for the chip to screen for 23 variants, there was 1 case of a *GJB2* homozygote with mitochondrial variants, 1 case of a *GJB2* compound heterozygote heterozygous for *GJB3*, 1 case of a *GJB2* compound heterozygote heterozygous for *SLC26A4*, and 5 cases of mitochondrial variants who were heterozygous for *GJB2* or *SLC26A4*.

differed significantly ($P < 0.001$).

3.3. Comparison of carrier frequency according to three genetic screening protocols

As shown in Table 3, the carrier frequency for the 4 screened genes, from highest to lowest, was the *GJB2* gene, *SLC26A4* gene, *GJB3* gene, and mtDNA *12SrRNA* gene. The carrier frequency for the *GJB2* gene was highest according to the chip to screen for 23 variants (9.055%, 2,210/24,407), followed by the chip to screen for 9 variants (2.489%, 6,811/273,647), and then the chip to screen for 15 variants (2.422%, 4,742/195,767). The differences were significant ($P < 0.001$).

The carrier frequency for the *SLC26A4* gene was highest according to the chip to screen for 23 variants (2.151%, 525/24,407), followed by the chip to screen for 15 variants (2.015%, 3,944/195,767), and then the chip to screen for 9 variants (1.621%, 4,435/273,647). The differences were significant ($P < 0.001$).

The carrier frequency of the *GJB3* gene was 0.320% (876/273,647) according to the chip to screen for 9 variants, 0.340% (666/195,767) according to the chip to screen for 15 variants, and 0.361% (88/24,407) according to the chip to screen for 23 variants. The differences were not significant ($P = 0.346$).

The carrier frequency of the mtDNA *12SrRNA* gene was highest according to the chip to screen for 15 variants (0.279%, 546/195,767), followed by the chip to screen for 9 variants (0.232%, 635/273,647), and then the chip to screen for 23 variants (0.176%, 43/24,407). The differences were significant ($P < 0.001$).

3.4. Comparison of allele frequency according to three genetic screening protocols

The allele frequencies according to three screening protocols are shown in Table 4. According to the

Table 3. Carrier frequencies according to three genetic screening protocols

Gene	Chip to screen for 9 variants *n* (%)	Chip to screen for 15 variants *n* (%)	Chip to screen for 23 variants *n* (%)	*P* value
GJB2	6,811 (2.489)	4,742 (2.422)	2,210 (9.055)	< 0.001
SLC26A4	4,435 (1.621)	3,944 (2.015)	525 (2.151)	< 0.001
GJB3	876 (0.320)	666 (0.340)	88 (0.361)	0.346
mtDNA *12S rRNA*	635 (0.232)	546 (0.279)	43 (0.176)	< 0.001
Total	12,586 (4.599)	9,731 (4.971)	2,804 (11.489)	

n: number of newborns. According to the protocol for the chip to screen for 9 variants, there were 171 cases of digenic gene variants. According to the protocol for the chip to screen for 15 variants, there were 165 cases of digenic gene variants and 1 case of trigenic gene variants. According to the protocol for the chip to screen for 23 variants, there were 62 cases of digenic gene variants. Therefore, the sum of the carrier frequencies for each gene is greater than the overall positivity according to genetic screening.

Table 4. Allele frequencies according to three genetic screening protocols

Variants	Chip to screen for 9 variants			Chip to screen for 15 variants			Chip to screen for 23 variants			*P* value
	Het (*n*)	Hom (*n*)	AF (%)	Het (*n*)	Hom (*n*)	AF (%)	Het (*n*)	Hom (*n*)	AF (%)	
GJB2 c.235delC	4,998	27	0.923	3,537	11	0.909	424	0	0.869	0.425
GJB2 c.299_300delAT	1,378	2	0.253	945	1	0.242	120	1	0.250	0.591
GJB2 c.176_191del16	381	1	0.070	217	0	0.055	37	0	0.076	0.014
GJB2 c.35delG	42	0	0.008	37	0	0.009	5	0	0.010	0.519
GJB2 c.109G>A	/	/	/	/	/	/	1,579	30	3.358	
GJB2 c.257C>G	/	/	/	/	/	/	6	0	0.012	
GJB2 c.512insAACG	/	/	/	/	/	/	15	0	0.031	
GJB2 c.427C>T	/	/	/	/	/	/	8	0	0.016	
GJB2 c.35insG	/	/	/	/	/	/	11	0	0.023	
SLC26A4 c.919-2A>G	3,719	7	0.682	2,597	6	0.666	350	3	0.729	0.243
SLC26A4 c.2168A>G	709	1	0.130	513	0	0.131	57	0	0.117	0.710
SLC26A4 c.1174A>T	/	/	/	165	0	0.042	24	0	0.049	0.480
SLC26A4 c.1226G>A	/	/	/	133	0	0.034	12	0	0.025	0.281
SLC26A4 c.1229C>T	/	/	/	125	0	0.032	24	0	0.049	0.061
SLC26A4 c.1975G>C	/	/	/	244	0	0.062	20	0	0.041	0.069
SLC26A4 c.2027T>A	/	/	/	110	1	0.029	14	0	0.029	0.993
SLC26A4 c.1707+5G>A	/	/	/	64	0	0.016	8	0	0.016	0.994
SLC26A4 c.589G>A	/	/	/	/	/	/	7	0	0.014	
SLC26A4 c.917insG	/	/	/	/	/	/	1	0	0.002	
SLC26A4 c.281C>T	/	/	/	/	/	/	6	0	0.012	
GJB3 c.538C>T	875	1	0.160	666	0	0.170	88	0	0.180	0.357

n: number of newborns, Het: heterozygote, Hom: homozygote, AF: allele frequency.

protocol for the chip to screen for 9 variants, the most frequent mutant alleles were c.235delC (0.923%, 5,052/547,294), c.919-2A>G (0.682%, 3,733/547,294), and c.299_300delAT (0.253%, 1,382/547,294), in descending order. According to the protocol for the chip to screen for 15 variants, the most frequent mutant alleles were c.235delC (0.909%, 3,559/391,534), c.919-2A>G (0.666%, 2,609/391,534), and c.299_300delAT (0.242%, 947/391,534). According to the protocol for the chip to screen for 23 variants, the most frequent mutant alleles were c.109G>A (3.358%, 1,639/48,814), c.235delC (0.869%, 424/48,814), and c.919-2A>G (0.729%, 356/48,814).

The allele frequencies of 7 sites (No.1-4, 10-11 and 21 in Table 4) according to three screening protocols were compared. The allele frequency of c.176_191del16 according to the chip to screen for 23 variants (0.076%, 37/48,814) was higher than that according to the chip to screen for 9 variants (0.070%, 383/547,294) and that according to the chip to screen for 15 variants (0.055%, 217/391,534); the difference was significant ($P = 0.014$). There were no differences in the other 6 sites among the three genetic screening protocols.

The allele frequencies for the 6 sites (No.12-17 in Table 3) according to the chip to screen for 15 variants and the chip to screen for 23 variants were compared, and no significant differences were found.

3.5. Comparison of pathogenic genotype according to three genetic screening protocols

The comparison of pathogenic genotypes according to three genetic screening protocols is shown in Table 5. According to the protocol for the chip to screen for 9 variants, the rate of detection of the c.235delC/c.235delC genotype was the highest (47.37%, 27/57), followed by c.235delC/c.299_300delAT (17.54%, 10/57). According to the protocol for the chip to screen for 15 variants, the rate of detection of the c.235delC/c.235delC genotype was the highest (28.21%, 11/39), followed by c.919-2A>G/c.919-2A>G (15.38%, 6/39). According to the protocol for the chip to screen for 23 variants, the rate of detection of the c.109G>A/c.109G>A genotype was the highest (49.18%, 30/61), followed by c.235delC/c.109G>A (24.59%, 15/61).

A point worth noting is that according to the protocol for the chip to screen for 15 variants, 66.67% (14/21) of newborns with biallelic variants in the *SLC26A4* gene were detected with newly added mutations based on the chip to screen for 9 variants. According to the protocol for the chip to screen for 23 variants, 92.98% (53/57) of newborns with biallelic variants in the *GJB2* gene were detected with the newly added mutations based on the protocol for the chip to screen for 15 variants, 52 of whom were biallelic c.109G>A variant. In addition, 25%

Table 5. Pathogenic genotypes according to three genetic screening protocols

Genotypes	Chip to screen for 9 variants *n* (%)	Chip to screen for 15 variants *n* (%)	Chip to screen for 23 variants *n* (%)
c.235delC/c.235delC	27	11	0
c.235delC/c.299_300delAT	10	5	0
c.235delC/c.176_191del16	5	1	2
c.299_300delAT/c.176_191del16	2	0	0
c.299_300delAT/c.35delG	1	0	0
c.299_300delAT/c.299_300delAT	2	1	1
c.176_191del16/c.176_191del16	1	0	0
c.235delC/c.35delG	0	0	1
c.919-2A>G/c.919-2A>G	7	6	3
c.2168A>G/c.2168A>G	1	0	0
c.919-2A>G/c.2168A>G	1	1	0
c.2027T>A/c.2027T>A	/	1	0
c.919-2A>G/c.1229C>T	/	5	0
c.1229C>T/c.1975G>C	/	3	0
c.2168A>G/c.2027T>A	/	2	0
c.2168A>G/c.1975G>C	/	1	0
c.919-2A>G/c.1226G>A	/	1	0
c.919-2A>G/c.1975G>C	/	1	0
c.109G>A/c.109G>A	/	/	30
c.235delC/c.109G>A	/	/	15
c.299_300delAT/c.109G>A	/	/	6
c.109G>A/c.35insG	/	/	1
c.235delC/c.35insG	/	/	1
c.919-2A>G/c.281C>T	/	/	1
Total	57	39	61

n: number of newborns. According to the protocol for the chip to screen for 15 variants, there was 1 case of a c.299_300delAT homozygote with m.1555A>G homoplasmy and 1 case of a c.2027T>A homozygote with a c.235delC heterozygote. According to the protocol for the chip to screen for 23 variants, there was 1 case of a c.109G>A homozygote with m.1555A>G homoplasmy, 1 case of c.235delC/c.109G>A with a c.538C>T heterozygote, and 1 case of c.235delC/c.109G>A with a c.919-2A>G heterozygote.

(1/4) of newborns with biallelic variants in the *SLC26A4* gene were detected with newly added mutations based on the protocol for the chip to screen for 15 variants.

3.6. Hearing testing of individuals with pathogenic variants

Among 121 newborns with pathogenic variants, 43 were identified by the protocol for the chip to screen for 9 variants, 31 were identified by the protocol for the chip to screen for 15 variants, and 47 were identified by the protocol for the chip to screen for 23 variants (Figure 2). Of the 121 newborns, 95 (78.51%, 95/121) failed the hearing screening, while 26 (21.49%, 26/121) passed.

All 95 newborns who failed the hearing screening underwent hearing testing, and the age at hearing testing ranged from 2 to 8 months. Results revealed that 87 newborns (91.58%, 87/95) were diagnosed with HL and 8 (8.42%, 8/95) were diagnosed with normal hearing. Among those with HL, 77 (88.51%, 77/87) had bilateral HL and 10 (11.49%, 10/87) had unilateral HL. All 8 newborns with normal hearing were detected by the protocol for the chip to screen for 23 variants, with the following genotypes: c.109G>A/c.109G>A in 4 newborns, c.235delC/c.109G>A in 1, c.235delC/c.109G>A/c.919-2A>G in 1, c.299_300delAT/c.109G>A in 1, and c.109G>A/c.35insG in 1.

As shown in Table 6, all 26 newborns who passed the hearing screening underwent hearing testing, and the age at hearing testing ranged from 2 to 12 months. Results revealed that 9 newborns (34.62%, 9/26) were diagnosed with HL and 17 (65.38%, 17/26) were diagnosed with normal hearing. Among those with HL, 8 (88.89%, 8/9) had bilateral HL and 1 (11.11%, 1/9) had unilateral HL. Among the 17 newborns with normal hearing, 3 were detected by the protocol for the chip to screen for 15 variants and 14 were detected by the protocol for the chip to screen for 23 variants, with the following genotypes: c.2027T>A/c.2027T>A/c.235delC in 1 newborn, c.1229C>T/c.1975G>C in 1, c.919-2A>G/c.1229C>T in 1, c.919-2A>G/c.919-2A>G in 1, c.109G>A/c.109G>A in 4, c.235delC/c.109G>A in 6, c.235delC/c.109G>A/c.538C>T in 1, c.299_300delAT/c.109G>A in 2.

4. Discussion

This study analyzed the genetic screening of 493,821 newborns for deafness in Beijing according to three different screening protocols over 11 years since the initiation of a project for the genetic screening of newborns in 2012. Here, positivity, rates of detection of various genotypes, carrier frequencies and allele frequencies, pathogenic genotypes of genetic screening, and hearing testing of infants with pathogenic variants

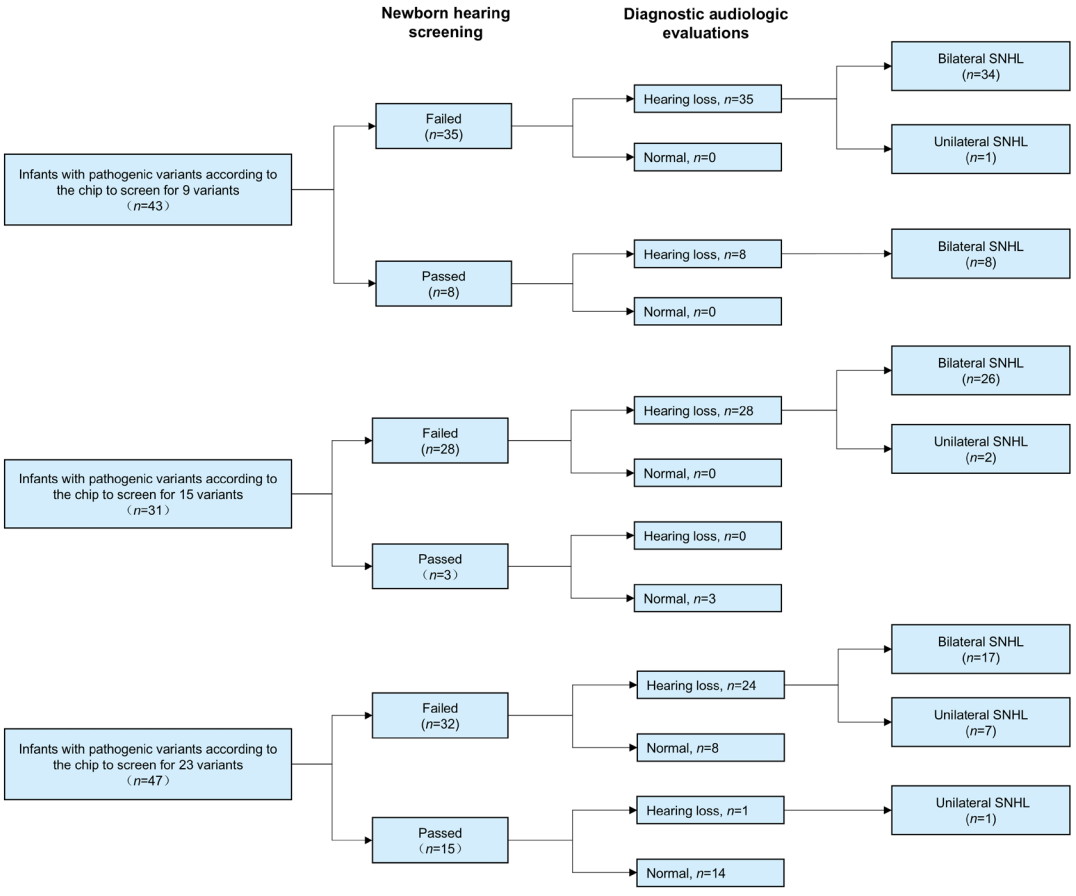

Figure 2. Auditory performance of infants with pathogenic variants.

Table 6. Hearing test results for 26 infants with pathogenic variants who passed hearing screening

No.	Sex	Year	Genetic screening protocol	Genotypes	Age at diagnosis (months)	Hearing test results	
						R	L
1	F	2013	Chip to screen for 9 variants	c.235delC/c.176_191del16	unavailable	Severe	Severe
2	F	2013	Chip to screen for 9 variants	c.235delC/c.176_191del16	unavailable	Severe	Moderate
3	F	2014	Chip to screen for 9 variants	c.235delC/c.235delC	2	Moderate	Moderate
4	M	2015	Chip to screen for 9 variants	c.919-2A>G/c.919-2A>G	3	Normal	Moderate
5	F	2016	Chip to screen for 9 variants	c.299_300delAT/c.299_300delAT	3	Severe	Profound
6	F	2016	Chip to screen for 9 variants	c.919-2A>G/c.2168A>G	22	Profound	Severe
7	M	2016	Chip to screen for 9 variants	c.176_191del16/c.176_191del16	3	Profound	Profound
8	M	2017	Chip to screen for 9 variants	c.235delC/c.235delC	3	Severe	Mild
9	M	2020	Chip to screen for 15 variants	c.2027T>A/c.2027T>A/c.235delC	12	Normal	Normal
10	F	2020	Chip to screen for 15 variants	c.1229C>T/c.1975G>C	10	Normal	Normal
11	F	2022	Chip to screen for 15 variants	c.919-2A>G/c.1229C>T	3	Normal	Normal
12	F	2022	Chip to screen for 23 variants	c.919-2A>G/c.919-2A>G	2	Normal	Normal
13	M	2022	Chip to screen for 23 variants	c.109G>A/c.109G>A	4	Normal	Normal
14	F	2022	Chip to screen for 23 variants	c.235delC/c.109G>A	6	Normal	Normal
15	F	2023	Chip to screen for 23 variants	c.299_300delAT/c.109G>A	2	Mild	Normal
16	F	2023	Chip to screen for 23 variants	c.299_300delAT/c.109G>A	4	Normal	Normal
17	F	2023	Chip to screen for 23 variants	c.109G>A/c.109G>A	3	Normal	Normal
18	M	2023	Chip to screen for 23 variants	c.235delC/c.109G>A/ c.538C>T	4	Normal	Normal
19	F	2023	Chip to screen for 23 variants	c.109G>A/c.109G>A	6	Normal	Normal
20	M	2023	Chip to screen for 23 variants	c.299_300delAT/c.109G>A	6	Normal	Normal
21	M	2023	Chip to screen for 23 variants	c.235delC/c.109G>A	3	Normal	Normal
22	F	2023	Chip to screen for 23 variants	c.235delC/c.109G>A	3	Normal	Normal
23	M	2023	Chip to screen for 23 variants	c.235delC/c.109G>A	3	Normal	Normal
24	M	2023	Chip to screen for 23 variants	c.235delC/c.109G>A	4	Normal	Normal
25	F	2023	Chip to screen for 23 variants	c.109G>A/c.109G>A	3	Normal	Normal
26	F	2023	Chip to screen for 23 variants	c.235delC/c.109G>A	4	Normal	Normal

are discussed.

4.1. Positivity according to genetic screening

Positivity with the protocol for the chip to screen for 9 variants was reported to be 4.508% (8,136/180,469) according to Dai *et al.* (*4*). The current authors' research team reported that 4.510% (3,412/75,649) of infants carried at least one mutant allele according to genetic screening with the chip to screen for 9 variants (*6*). Gao *et al.* (*7)* analyzed 10 years of data from genetic screening of newborns at Peking Union Medical College Hospital and found that positivity with the protocol for the chip to screen for 9 variants was 4.629% (4,262/92,080). The results of the current study indicated that positivity with the protocol for the chip to screen for 9 variants was 4.599%, which was consistent with the findings of the aforementioned studies.

Positivity with the screening protocol for the chip to screen for 15 variants was reported to be 4.922% (3,763/76,460) from 2019 to 2020 according to Wen *et al*. (*5*). Gao *et al*. (*7*) reported on the genetic screening of 73,733 newborns at Peking Union Medical College Hospital using the chip to screen for 15 variants, and positivity was 5.095%. The current study noted that the positivity with the screening protocol for the chip to screen for 15 variants was 4.971%, which was consistent with the findings of the aforementioned studies.

There are only few studies on positivity with the screening protocol for the chip to screen for 23 variants. The current study found that positivity with the screening protocol for the chip to screen for 23 variants was 11.489%, which was higher than that with the chip to screen for 9 variants (4.599%) and that with the chip to screen for 15 variants (4.971%). The increase could be attributed to the addition of c.109G>A in the *GJB2* gene, which had a higher carrier frequency in the Chinese population, ranging from 6.930% to 12.500% (*8*).

In summary, the current study reported increasing positivity in genetic screening for deafness using a more powerful microfluidic chip to screen for 23 variants than the chip to screen for 15 variants and the chip to screen for 9 variants. These findings may provide a reference for the development of genetic screening for deafness in the Chinese population in other regions.

4.2. Rate of detection of various genotypes of genetic screening

The results of the current study indicated that screening protocol for the chip to screen for 23 variants had a higher rate of detection of carriers (11.066%) compared to that with the chip to screen for 15 variants (4.672%) and the chip to screen for 9 variants (4.346%). Therefore, an increasing number of individuals with deafness-associated variants were identified by

microfluidics technology. These individuals are at risk for HL. Through reproductive counseling and avoidance of potential triggers (*e.g.*, noise exposure, slapping, and head injury) in individuals with such variants, the incidence of HL could be significantly reduced.

According to the three screening protocols, the rates of detection of *GJB2* heterozygotes were 2.417%, 2.348%, and 8.588%, respectively, in the current study. Recent research on hereditary deafness has indicated that *GJB2* hetero-mutation carriers exhibit heightened auditory sensitivity, potentially attributable to enhanced cochlear amplification (*9*). The increase in cochlear amplification heightens sensitivity to noise. Exposure to daily-level noise can cause permanent hearing threshold shifts in $Cx26^{+/-}$ mice, leading to HL. *GJB2* hetero-mutation carriers are vulnerable to noise and should avoid exposure to noise in daily life. Consequently, offering targeted guidance on strategies to avoid daily exposure to noise to *GJB2* heterozygous carriers could be instrumental in preserving their hearing health.

According to the three screening protocols, the rates of detection of *SLC26A4* heterozygotes were 1.567%, 1.932%, and 1.930%, respectively, in the current study. *SLC26A4* gene mutations are closely related to LVAS (*10*), with 67-90% of patients with enlarged vestibular aqueduct (EVA) having biallelic *SLC26A4* mutations (*11-16*). According to previous studies, however, 7.4-36% of patients with EVA had a monoallelic *SLC26A4* mutation (*17-23*). Proactive counseling needs to be provided to *SLC26A4* hetero-mutation carriers, who are predisposed to EVA. This guidance should address the potential hazards associated with external stimuli, notably strenuous physical activities, to ensure their auditory well-being. Hence, implementing genetic screening can facilitate the early identification of at-risk individuals. This allows for the provision of timely and proactive guidance to mitigate potential hearing impairments.

In addition, all three screening protocols in the current study included the most common mtDNA *12SrRNA* variants in the Chinese population (m.1555A>G and m.1494C>T). Individuals with mtDNA *12SrRNA* variants were susceptible to drug-induced HL. By extending pharmacological counseling to individuals and their maternal lineage, coupled with vigilant avoidance of aminoglycoside antibiotics, the risk of HL could be significantly mitigated.

4.3. Carrier frequency and allele frequency according to genetic screening

According to the three screening protocols, the carrier frequency of the *GJB2* gene was the highest. Specifically, the carrier frequency of the *GJB2* gene according to the screening protocol for the chip to screen for 23 variants (9.055%) was significantly higher than that with the protocols for the chip to screen for 15 variants (2.422%) and that with the chip to screen for 9 variants (2.489%). The *GJB2* gene was reported to be the most common gene associated with over 50% of non-syndromic HL cases (*24*). The current research indicated that the screening protocol for the chip to screen for 23 variants significantly enhances the detection of *GJB2* gene mutations and has an advantage in early identification of newborns with mutations in the *GJB2* gene.

The *SLC26A4* gene was found to be the second most common gene in the screened population. The carrier frequency of the *SLC26A4* gene in the current study was highest according to the chip to screen for 23 variants (2.151%), followed by the chip to screen for 15 variants (2.015%), and then the chip to screen for 9 variants (1.621%). This suggested that the screening protocol for the chip to screen for 23 variants could identify more newborns at risk for EVA.

In the current study, the most frequent variant was *GJB2* c.109G>A, with an allele frequency of 3.358%. Another prevalent variant, c.235delC, was the second most common variant in *GJB2*, with an allele frequency of 0.869%-0.923%. The c.919-2A>G variant was the most prevalent in *SLC26A4*, with an allele frequency of 0.666%-0.729%. Wu *et al*. (*25*) conducted a longitudinal study on genetic screening in 5,173 newborns in Taiwan and found that the allele frequencies, from highest to lowest, were c.109G>A (8.535%), c.235delC (0.638%), and c.919-2A>G (0.580%). Li *et al*. (*26*) reported allele frequencies of c.109G>A and c.235delC in newborns in Shanghai, with 6.168% (187/3,032) and 0.759% (23/3,032), respectively. Zhang *et al*. (*27*) investigated the spectrum of deafness-associated variants in 3,555,336 newborns across 32 provinces nationwide and found that c.235delC and c.919-2A>G were the most common variants in the Chinese population, with allele frequencies of 0.990% and 0.667%, respectively. Our previous study (*5*) on concurrent hearing and genetic screening of newborns in Beijing found that the most frequent mutations were c.235delC and c.919-2A>G, with allele frequencies of 0.920% (767/83,380) and 0.680% (567/83,380), respectively. The allele frequencies of c.235delC and c.919-2A>G in the current study were close to those of the aforementioned studies. The allele frequency of c.109G>A in the current study was lower than those reported by Wu *et al.* and Li *et al*., possibly due to regional differences between Taiwan, Shanghai, and the Beijing area.

4.4. Pathogenic genotypes according to genetic screening

The current study found that screening protocol for the chip to screen for 15 variants detected 66.67% (14/21) more newborns with *SLC26A4* deafness-causing mutations than the protocol with the chip to screen for 9 variants, which was close to the 71.43% (5/7) reported

by Wen *et al.* (*5*).

The screening protocol for the chip to screen for 23 variants detected 92.98% (53/57) more newborns with *GJB2* deafness-causing mutations than the protocol for the chip to screen for 15 variants, 52 of whom had the biallelic c.109G>A variant. A study has reported that the biallelic c.109G>A variant was associated with an increasing incidence of HL with age (*28*). Therefore, more biallelic c.109G>A individuals could benefit from early diagnosis and intervention through the screening protocol for the chip to screen for 23 variants. In addition, the screening protocol for the chip to screen for 23 variants detected 25% (1/4) more newborns with *SLC26A4* deafness-causing mutations than the protocol for the chip to screen for 15 variants, suggesting that the protocol for the chip to screen for 23 variants also had advantages in screening newborns with EVA.

These findings highlighted the significant advantage of utilizing enhanced genetic screening chips, which are crucial to the identification of a broader spectrum of individuals with mutations associated with deafness.

4.5. Hearing testing of children with pathogenic variants

Of the 121 individuals with pathogenic variants in the current study, 21.49% (26/121) of newborns passed hearing screening, 34.62% (9/26) of whom were diagnosed with HL. Dai *et al*. (*4*) reported that 25% (10/40) of newborns with pathogenic variants passed hearing screening. The current results are consistent with the findings reported by Dai *et al*. The data underscores the pivotal role of genetic screening in the early identification of individuals with potential HL, including those who may be missed by conventional hearing screening for newborns. By preemptively identifying such individuals, genetic screening enables timely intervention and management strategies to be implemented.

Among the 121 individuals with pathogenic variants, 96 (79.34%) were diagnosed with HL. Zhu *et al*. (*29*) conducted a concurrent hearing and genetic screening of 32,512 individuals in Nantong and found that 86.36% (19/22) of individuals with biallelic variants in the *GJB2* or *SLC26A4* gene had HL. The results of the current study are similar to those reported by Zhu *et al*. Among the 121 individuals with pathogenic variants, 25 were diagnosed with normal hearing, with the age at diagnosis ranging from 2 to 12 months. Four of the individuals had biallelic variants in the *SLC26A4* gene and 21 had a biallelic c.109G>A variant in the *GJB2* gene. The occurrence of delayed HL in these 25 children remains a significant concern. Fang *et al*. emphasized the importance of incorporating long-term follow-up in the detection of and interventions for children with delayed HL (*30*).

Among the 4 infants with confirmed normal hearing and biallelic variants in the *SLC26A4* gene listed in Table 6 (No. 9-12), 3 underwent computed tomography of the temporal bone. In one, there was no enlargement of the vestibular aqueduct bilaterally and poor medial parietal morphology of the cochlea bilaterally. In another, there was no enlargement of the vestibular aqueduct bilaterally and no obvious abnormalities in the bilateral inner, middle, or outer ear. A subsequent MRI scan of the inner ear was recommended for these two infants. In the third infant, prominent enlargement of the vestibular aqueduct was noted bilaterally. Moreover, continuous and close clinical follow-up is required for all 4 of these infants.

Chai *et al*. (*31*) reported that among hearing impaired subjects with homozygous c.109G>A, the onset of hearing impairment was congenital in 65% (11/17) and delayed in 35% (6/17). Chen *et al*. (*28*) found that among biallelic c.109G>A newborns, 43.91% (18/41) passed hearing screening for newborns or had normal hearing. The incidence of moderate or higher grades of HL in individuals with biallelic c.109G>A increases with age, with 9.52% at ages of 7 to 15, 23.08% at ages of 20 to 40, 59.38% at ages of 40 to 60, and 80.00% at ages of 60 to 85. Therefore, conducting long-term audiological monitoring and regular follow-up for newborns who are homozygous or compound heterozygous for c.109G>A in the *GJB2* gene is imperative.

In conclusion, the key points and highlights of the current study lie in its comparative analysis of three protocols for genetic screening of newborns and follow-up for infants with pathogenic variants. This study first analyzed the advantages of the chip to screen for 23 variants compared to the chip to screen for 15 variants and the chip to screen for 9 variants. Findings suggest that a growing number of newborns have benefited, and especially in the early identification of potential late-onset HL, as the number of screening sites has increased. Individuals with biallelic variants could have normal hearing, indicating that long-term audiological monitoring is imperative. This is of significant clinical importance to improve interventions and management strategies for HL.

Acknowledgements

The authors wish to thank all of the subjects and family members for their participation in this study.

Funding: This work was supported by a grant from the Capital's Funds for Health Improvement and Research (grant no. CFH 2022-2-1092) and from the National Natural Science Foundation of China General Program (grant nos. 82071064 and 81870730).

Conflict of Interest: The authors have no conflicts of interest to disclose.

References

1. Kennedy CR, McCann DC, Campbell MJ, Law CM, Mullee M, Petrou S, Watkin P, Worsfold S, Yuen HM, Stevenson J. Language ability after early detection of permanent childhood hearing impairment. N Engl J Med. 2006; 354:2131-2141.
2. Kennedy C, McCann D. Universal neonatal hearing screening moving from evidence to practice. Arch Dis Child Fetal Neonatal Ed. 2004; 89:F378-383.
3. Fortnum HM, Summerfield AQ, Marshall DH, Davis AC, Bamford JM. Prevalence of permanent childhood hearing impairment in the United Kingdom and implications for universal neonatal hearing screening: questionnaire based ascertainment study. BMJ. 2001; 323:536-540.
4. Dai P, Huang LH, Wang GJ, *et al.* Concurrent hearing and genetic screening of 180,469 neonates with follow-up in Beijing, China. Am J Hum Genet. 2019; 105:803-812.
5. Wen C, Yang X, Cheng X, *et al.* Optimized concurrent hearing and genetic screening in Beijing, China: A cross-sectional study. Biosci Trends. 2023; 17:148-159.
6. Ruan Y, Wen C, Zhao XL, Wang XL, Cheng XH, Zhao LP, Zhang W, Huang LH. A follow-up study of 75,649 newborn genetically screened for deafness and patients with confirmed deafness. Chin J Otology. 2019; 17:661-669.
7. Gao RZ, Fan Y, Yang TY, Li DD, Guo Y, Jiang H, Xu YC, Chen XW. Results of neonatal genetic screening for hearing loss in peking union medical college hospital in the past 10 years. Med J Peking Union Med Coll Hospital. 2022; 13:1020-1027.
8. Chinese clinical multicenter research collaborative group for deafness gene screening and diagnosis. A guidelines for genetic screening of hereditary deafness genes. Natl Med J China. 2021; 101:97-102.
9. Liu LM, Liang C, Chen J, Fang S, Zhao HB. Cx26 heterozygous mutations cause hyperacusis-like hearing oversensitivity and increase susceptibility to noise. Sci Adv. 2023; 9:eadf4144.
10. Du Y, Huang L, Wang X, Cui Q, Cheng X, Zhao L, Ni T. Clinical data analysis of genotypes and phenotypes of deafness gene mutations in newborns: A retrospective study. Biosci Trends. 2017; 11:460-468.
11. Mey K, Muhamad AA, Tranebjaerg L, Rendtorff ND, Rasmussen SH, Bille M, Caye-Thomasen P. Association of SLC26A4 mutations, morphology, and hearing in pendred syndrome and NSEVA. Laryngoscope. 2019; 129:2574-2579.
12. Choi BY, Stewart AK, Nishimura KK, *et al.* Efficient molecular genetic diagnosis of enlarged vestibular aqueducts in East Asians. Genet Test Mol Biomarkers. 2009; 13:679-687.
13. Miyagawa M, Nishio SY, Usami S, Deafness Gene Study Consortium. Mutation spectrum and genotype-phenotype correlation of hearing loss patients caused by SLC26A4 mutations in the Japanese: A large cohort study. J Hum Genet. 2014; 59:262-268.
14. Reyes S, Wang G, Ouyang X, Han B, Du LL, Yuan HJ, Yan D, Dai P, Liu XZ. Mutation analysis of SLC26A4 in mainland Chinese patients with enlarged vestibular aqueduct. Otolaryngol Head Neck Surg. 2009; 141:502-508.
15. Wang QJ, Zhao YL, Rao SQ, Guo YF, Yuan H, Zong L, Guan J, Xu BC, Wang DY, Han MK, Lan L, Zhai SQ, Shen Y. A distinct spectrum of SLC26A4 mutations in patients with enlarged vestibular aqueduct in China. Clin Genet. 2007; 72:245-254.
16. Zhao FF, Lan L, Wang DY, Han B, Qi Y, Zhao Y, Zong L, Li Q, Wang QJ. Correlation analysis of genotypes, auditory function, and vestibular size in Chinese children with enlarged vestibular aqueduct syndrome. Acta Otolaryngol. 2013; 133:1242-1249.
17. Wu CC, Lu YC, Chen PJ, Yeh PL, Su YN, Hwu WL, Hsu CJ. Phenotypic analyses and mutation screening of the SLC26A4 and FOXI1 genes in 101 Taiwanese families with bilateral nonsyndromic enlarged vestibular aqueduct (DFNB4) or Pendred syndrome. Audiol Neurootol. 2010; 15:57-66.
18. Zhao J, Yuan Y, Chen J, Huang S, Wang G, Han D, Dai P. SLC26A4 gene copy number variations in Chinese patients with non-syndromic enlarged vestibular aqueduct. J Transl Med. 2012; 10:82.
19. Pang XH, Chai YC, Chen P. The incidence and pathogenic correlation of SLC26A4 mono-allelic mutations in deaf patients with enlarged vestibular aqueduct. Chin Sci J Hearing Speech Rehab. 2015; 3:190-194.
20. Rah YC, Kim AR, Koo JW, Lee JH, Oh SH, Choi BY. Audiologic presentation of enlargement of the vestibular aqueduct according to the SLC26A4 genotypes. Laryngoscope. 2015; 125:E216-222.
21. Tsukamoto K, Suzuki H, Harada D, Namba A, Abe S, Usami S. Distribution and frequencies of PDS (SLC26A4) mutations in Pendred syndrome and nonsyndromic hearing loss associated with enlarged vestibular aqueduct: A unique spectrum of mutations in Japanese. Eur J Hum Genet. 2003; 11:916-922.
22. Pryor SP, Madeo AC, Reynolds JC, Sarlis NJ, Arnos KS, Nance WE, Yang Y, Zalewski CK, Brewer CC, Butman JA, Griffith AJ. SLC26A4/PDS genotype-phenotype correlation in hearing loss with enlargement of the vestibular aqueduct (EVA): Evidence that Pendred syndrome and non-syndromic EVA are distinct clinical and genetic entities. J Med Genet. 2005; 42:159-165.
23. Albert S, Blons H, Jonard L*, et al.* SLC26A4 gene is frequently involved in nonsyndromic hearing impairment with enlarged vestibular aqueduct in Caucasian populations. Eur J Hum Genet. 2006; 14:773-779.
24. Kenneson A, Van Naarden Braun K, Boyle C. GJB2 (connexin 26) variants and nonsyndromic sensorineural hearing loss: A HuGE review. Genet Med. 2002; 4:258-274.
25. Wu CC, Tsai CH, Hung CC, Lin YH, Lin YH, Huang FL, Tsao PN, Su YN, Lee YL, Hsieh WS, Hsu CJ. Newborn genetic screening for hearing impairment: A population-based longitudinal study. Genet Med. 2017; 19:6-12.
26. Li L, Lu J, Tao Z, Huang Q, Chai Y, Li X, Huang Z, Li Y, Xiang M, Yang J, Yao G, Wang Y, Yang T, Wu H. The p.V37I exclusive genotype of GJB2: A genetic risk-indicator of postnatal permanent childhood hearing impairment. PLoS One. 2012; 7:e36621.
27. Zhang J, Wang H, Yan C, Guan J, Yin L, Lan L, Li J, Zhao L, Wang Q. The frequency of common deafness-associated variants among 3,555,336 newborns in China and 141,456 individuals across seven populations worldwide. Ear Hear. 2023; 44:232-241.
28. Chen Y, Wang Z, Jiang Y, *et al.* Biallelic p.V37I variant in GJB2 is associated with increasing incidence of hearing loss with age. Genet Med. 2022; 24:915-923.
29. Zhu QW, Li MT, Zhuang X, Chen K, Xu WQ, Jiang YH, Qin G. Assessment of hearing screening combined with

limited and expanded genetic screening for newborns in Nantong, China. JAMA Netw Open. 2021; 4:e2125544.
30. Fang BX, Cen JT, Yuan T, Yin GD, Gu J, Zhang SQ, Li ZC, Liang YF, Zeng XL. Etiology of newborn hearing impairment in Guangdong Province: 10-year experience with screening, diagnosis, and follow-up. World J Pediatr. 2020; 16:305-313.
31. Chai Y, Chen D, Sun L, Li L, Chen Y, Pang X, Zhang L, Wu H, Yang T. The homozygous p.V37I variant of GJB2 is associated with diverse hearing phenotypes. Clin Genet. 2015; 87:350-355.

Received June 28, 2024; Revised August 14, 2024; Accepted August 20, 2024.

*Address correspondence to:
Lihui Huang and Demin Han, Otolaryngology-Head and Neck Surgery, Beijing Tongren Hospital, Capital Medical University, Beijing, P.R. China 100730; Beijing Institute of Otolaryngology, Beijing, P. R. China 100005; Key Laboratory of Otolaryngology Head and Neck Surgery (Capital Medical University), Ministry of Education, Beijing, China 100005.
E-mail: huangpub@126.com (LH); enthandm@126.com (DH)

Released online in J-STAGE as advance publication August 25, 2024.

Original Article

DOI: 10.5582/bst.2024.01168

High social capital facilitates the alleviation of psychological distress in breast cancer patients: Insights from a cross-sectional study in Anhui Province, China

Wen Zhu[1,§], Zhongliang Bai[3,§], Xiangyang Liao[3], Xiaoyue Xie[3], Yue Fang[2,4,*], Ren Chen[3,5,*]

[1] Graduate Student Affairs Office, the First Affiliated Hospital of Anhui Medical University, Hefei , Anhui, China;
[2] Galactophore Oncology Center, Hefei Cancer Hospital, Chinese Academy of Sciences, Hefei, Anhui, China;
[3] Department of Health Services Management, School of Health Services Management, Anhui Medical University, Hefei, Anhui, China;
[4] Science Island Branch, Graduate School of University of Science and Technology of China, Hefei, Anhui, China;
[5] School of Public Health, Anhui Medical University, Hefei, Anhui, China.

SUMMARY Differences in social capital have been shown to impact psychological distress in cancer patients, but few studies have examined the relationship between social capital and the distress thermometer (DT) in breast cancer patients who have undergone modified radical surgery. To fill this research gap, our study aimed to investigate the association between social capital and the DT among breast cancer patients who underwent modified radical surgery in Anhui Province, China. This cross-sectional study used multi-stage stratified random sampling. Data on demographic characteristics, eight dimensions of social capital, and the DT were collected using a questionnaire. Logistic regression models were subsequently utilized to assess the relationship between social capital and DT, adjusting for confounding factors. A total of 253 participants were included in the final analysis. Results indicated that individuals with higher levels of social capital, including participation in the local community (OR = 3.437; 95% CI: 1.734-6.814), social agency or proactivity in a social context (OR = 69.700; 95% CI: 20.142-241.195), feelings of trust and safety (OR = 26.287; 95% CI: 7.646-90.374), neighborhood connections (OR = 7.022; 95% CI: 3.020-16.236), family and friend connections (OR = 59.315; 95% CI: 17.182-204.760), tolerance of diversity (OR = 9.785; 95% CI: 4.736-20.216), value of life (OR = 65.142; 95% CI: 19.994-212.242), and work connections (OR = 31.842; 95% CI: 12.612-80.397), had higher odds of reporting poor DT scores compared to those with lower levels of social capital. These findings indicate an association between social capital and DT scores in breast cancer patients who have undergone modified radical surgery, suggesting that social capital may play a crucial role in alleviating psychological distress within this community.

Keywords social capital, psychological distress, modified radical surgery for breast cancer, cross-sectional study, China

1. Introduction

Breast cancer is a significant public health concern worldwide. Nowadays, breast cancer is the most common cancer among women around the world and ranks first in the incidence of female malignant tumors in most countries or regions, including China (*1*). According to recent studies, breast cancer accounts for approximately 25% of all cancer cases and 15% of cancer-related deaths in women globally (*2*). The incidence of breast cancer varies in different countries or regions, and especially in developing countries or regions where the mortality rate for women with breast cancer is significantly higher than in developed countries (*3*).

Breast cancer is associated with many factors, including family history and reproductive risk factors, early age of menarche, late age of menopause, older age of first birth, hormone replacement therapy after menopause, alcohol intake, and obesity (*4*). The age at which women are at risk of developing breast cancer also varies, but the majority of cases occur in women age 40 and older (*5-7*). Surgery is a preferred treatment option for most patients with early to mid-stage breast cancer. Modified radical surgery has emerged as a preferred procedure due to its less invasive nature compared to traditional radical surgery and its ability to partially

remove cancer lesions. However, modified radical surgery involves removing part or all of the patient's breast, which disrupts the local lymphatic and vascular circulation, leading to changes in appearance. Common adverse reactions such as lymphedema and local numbness can cause significant distress and pain. During the lengthy treatment process, breast cancer patients who undergo modified radical surgery often experience various forms of psychological distress, including depression, anxiety, pain, and social isolation. This psychological distress is a standard and adaptive reaction to unpleasant stimuli or threats (*8*), which seriously affect patients' quality of life and prognosis (*9,10*). Therefore, the psychological suffering of breast cancer patients who undergo modified radical surgery has gradually garnered the attention of many researchers (*11-14*).

Currently, the Social Capital Scale has good structural validity, internal consistency, reliability, and good external validity (*15-17*). The growing recognition of the social determinants of health has highlighted the importance of social capital in health research. Social capital consists of resources within a social structure that are utilized or activated for specific purposes. Moreover, one distinction that has gained currency dichotomizes social capital into "bonding" and "bridging" varieties. Specifically, bonding social capital refers to trusting and cooperative relations within homogeneous groups, while bridging social capital describes relationships between individuals who are dissimilar with respect to social identity and power (*18*). And social capital is further separated into individual and collective social capital. Individual social capital has been broadly defined as the ability of actors to secure benefits through membership in social networks and other social structures. In contrast, collective social capital is viewed as a collective feature and refers to the rules that promote collective action, and the former is reported to protect health more than the latter (*17*). Sufficient social capital promotes enhanced self-efficacy, which, in turn, assists patients in forming accurate cognitive assessments and improving their life satisfaction.

Psychological distress has been associated with reduced health-related quality of life (*19,20*), low satisfaction with medical care, and decreased treatment adherence (*21,22*). The US National Comprehensive Cancer Network (NCCN) guideline for distress management was the first to recommend screening all cancer patients with the Distress Thermometer (DT), a questionnaire specifically developed for cancer patients (*23*). Cancer patients could benefit from social support, which is useful in reducing anxiety, depression, and distress (*24*). A cross-sectional study in China noted both a higher rate and greater degree of psychological distress in patients with cancer (*25*). Strong social cohesion had a protective effect on the inverse association between social support and psychological distress, which, in turn, had a protective effect on the indirect effect of social support on pain through psychological distress (*26*). Some researchers are reevaluating breast cancer treatment, placing greater emphasis on the influence of social contextual factors on the psychological well-being of patients who have undergone modified radical surgery. Studies of breast cancer patients have found that improving individual social capital can enhance cancer treatment compliance, help reduce cancer-related pain, and increase resilience to cancer side effects (*27,28*).

In addition, higher levels of social capital have been associated with better body image and overall life satisfaction among breast cancer patients (*29*). Social capital can help identify the unique needs and preferences of breast cancer patients, facilitating the creation of customized interventions to address the specific challenges that individuals or communities encounter. However, most previous studies examining the relationship between social capital and the distress levels of breast cancer patients have been conducted in developed or Eastern countries. There are few such studies in China, the largest developing country (*30*). For example, Kim *et al.* conducted a randomized controlled trial to explore the impact of an exercise adherence intervention with social capital on breast cancer survivors with moderate fatigue (*31*). A study in the US has discussed how social support can provide hope to cancer patients, concluding that family support, community support, and the support of health care providers is most effective in helping cancer patients integrate social capital (*32*). To fill this research gap and contribute to existing knowledge, the aim of the current study was to investigate the relationship between social capital and psychological distress among breast cancer patients who have undergone modified radical surgery in Anhui Province, China.

2. Materials and Methods

2.1. Study design and data collection

A cross-sectional survey was conducted in Anhui Province, eastern China, between August and December 2023. Ethical approval for this study was obtained from the Ethics Committee of Hefei Cancer Hospital, Chinese Academy of Sciences (No.YXLL-2024-35).

Three representative hospitals from Anhui Province, China, each with 100 patients, were randomly selected to represent the overall level of breast cancer patients who underwent surgery in Anhui Province: the First Affiliated Hospital of Anhui Medical University, the Second Hospital of Anhui Medical University, and the Chinese Academy of Sciences, Hefei Cancer hospital. Inclusion criteria were: 1) age 18 and older, 2) participants were not deaf or mute, did not have dementia or cognitive impairment, and were willing to participate in the survey, and 3) individuals who underwent modified radical

mastectomy for a pathologically confirmed diagnosis of breast cancer. Exclusion criteria were: 1) individuals with other primary tumors, 2) individuals with severe systemic infections or autoimmune diseases, and 3) individuals with an expected survival time of ≥ 6 months or a Karnofsky Performance Status (KPS) of ≥ 80.

A total of 273 breast cancer patients who underwent modified radical mastectomy were included in the study. Structured face-to-face interviews were conducted by skilled or trained graduate students, with assistance from hospital staff. Of the 273 survivors who agreed to participate, 253 completed the entire survey and were eligible for analysis. Thus, the response rate was 92.67% (253 out of 273). The sampling process is outlined in Figure 1 below. Before beginning the investigation, the study's objectives and procedures were verbally communicated to each participant, ensuring that informed consent was obtained from all individuals.

2.2. Measures

2.2.1. Measurement of psychological distress

The DT, a brief 0–10 visual analogue scale, was developed to routinely assess psychological distress in cancer patients (*33-35*). The scale is a single-item visual analog scale, where patients rate their pain level from 0 (no pain) to 10 (extreme pain), reflecting their pain experience over the past week. A score on the DT below either four or five, depending on the country and setting, has been propagated as an optimal cut-off to rule out significant distress in patients with cancer (*34,36*). Some studies have shown that the cut-off for intracranial tumors is six or higher, five for breast cancer patients who underwent modified radical surgery, and four for brain cancer patients. Given this, the cut-off for this study was chosen as five (*37,38*). Specifically, this study divided the participants into two groups based on their DT score, a low group (score of 0-4) and a high group (score greater than 4).

2.2.2. Measurement of social capital

Based on the World Bank's Social Capital Assessment Tool and previous works, a tool consisting of 36 items was used to assess social capital, the main independent variable (*39*). Responses were assessed using a 4-point Likert-type scale ranging from 1 (no, not at all) to 4 (yes, frequently), with higher scores representing higher levels of social capital. The scale consisted of 8 dimensions. Each dimension was calculated as the sum of its associated items, namely participation in the local

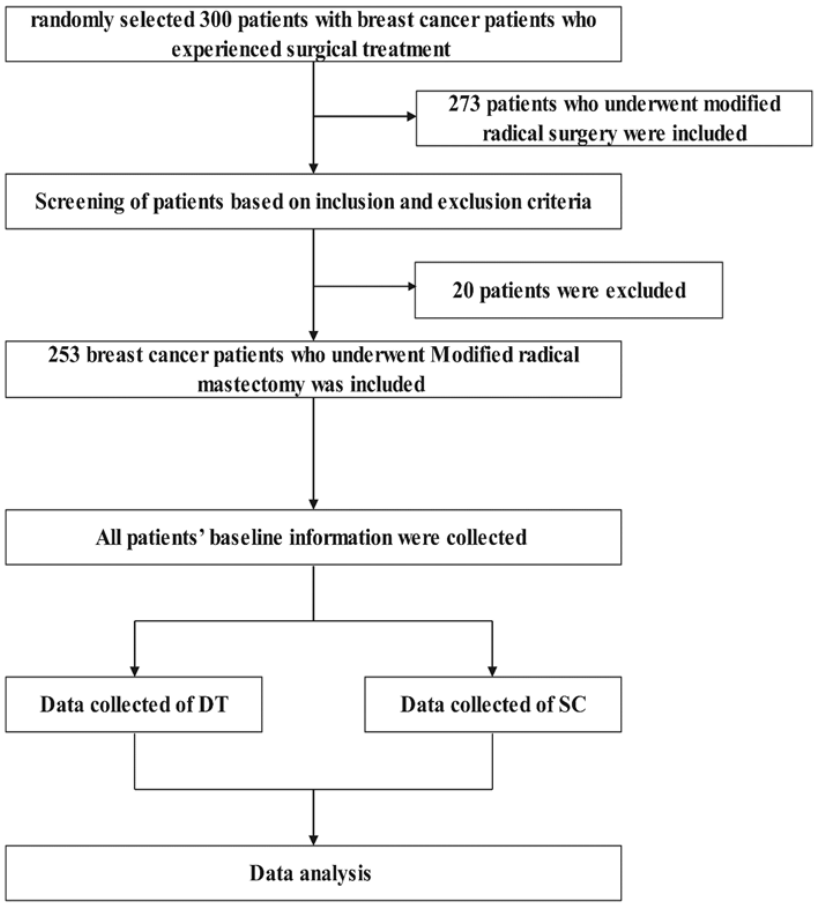

Figure 1. Flow chart for record selection.

community (range: 7-28), social agency or proactivity in a social context (range: 7-28), feelings of trust and safety (range: 5-20), neighborhood connections (range: 5-20), family and friend connections (range: 3-12), tolerance of diversity (range: 2-8), value of life (range: 2-8) and work connections (range: 3-12) (*40*). A point worth noting is that entries 35 and 36 do not count toward the scale total. In data analysis, the scores of each dimension of social capital were dichotomized into two categories by taking the median value as the cut-off (*41,42*). The Cronbach's α of the questionnaire was 0.964.

2.2.3. Measurement of other variables

Information on demographic and health-related variables was also collected. Essential demographic variables included name, age, marital status, level of education, breast cancer stage (based on the American Joint Committee on Cancer (AJCC) staging manual, 8th edition) (*43*), and treatment modality.

2.3. Statistical analysis

First, continuous and categorical variables were expressed as numbers and percentages, and then the difference between different DT groups (high DT versus low DT) and social capital (high SC versus low SC) was examined using a Chi-squared test. Second, a one-way ANOVA and Kendall correlation analysis were performed to assess the correlation between the DT and social capital. Third, a binary logistic regression model was used to further explore the interactive relationship between the DT and social capital. Social capital variables were coded with subjects having a lower level as the reference group in all models. The results of the binary logistic regression analyses are reported as odds ratios (OR) and adjusted odds ratios (AOR), along with their respective 95% confidence intervals (95% CI).

All statistical analyses were performed using the statistical software SPSS 23.0 (SPSS Inc., Chicago, IL, USA). P value < 0.05 was considered to represent statistical significance in this study.

3. Results

3.1. Results of descriptive analysis

The characteristics of the participants are summarized in Table 1. In total, 253 breast cancer patients who underwent modified radical surgery were included in the data analysis. Participant characteristics included: age < 40 (17%), 40-49 (23.72%), 50-59(28.06%), 60-69 (22.13%), ≥ 70 (9.09%), unmarried (5.93%), married (69.57%), widowed or divorced (24.50%), with most having an education level of illiteracy. Approximately three-quarters (73.91%) of participants were classified as AJCC Stage 2. Statistical differences in age, education, and marital status were noted ($P < 0.01$).

Table 2 shows significant differences in DT scores among breast cancer patients who underwent modified radical surgery across all eight dimensions of social capital.

The Kendall's r correlation results are shown in Table 3, revealing significant negative correlations ($P < 0.01$). The correlation coefficients for each dimension were as follows: participation in the local community (r = -0.279), social agency or proactivity in a social context (r = -0.675), feelings of trust and safety (r = -0.384),

Table 1. Descriptive results for participant characteristics (N = 253)

Variables	N	Frequency (%)	DT		P-value*
			Low (≤ 4)	High (> 4)	
Age					< 0.01
<40	43	17.00%	22	21	
40-49	60	23.72%	45	15	
50-59	71	28.06%	44	27	
60-69	56	22.13%	17	39	
≥70	23	9.09%	9	14	
Level of education					< 0.01
Illiterate	102	40.32%	32	70	
Primary school	70	27.67%	39	31	
Junior school (High school)	58	22.92%	47	11	
Junior college and higher	23	9.09%	19	4	
Marital status					0.007
Unmarried	15	5.93%	10	5	
Married	176	69.57%	104	72	
Widowed or divorced	62	24.50%	23	39	
AJCC Stage					0.709
1	23	9.09%	12	11	
2	187	73.91%	104	83	
3	43	17.00%	21	22	

*Chi-squared test.

Table 2. Descriptive results for social capital and the distress thermometer (N = 253)

Variables	Total (N = 253)	DT		P-value*
		Low (≤ 4)	High (> 4)	
Participation in the local community				< 0.01
low	134	55	79	
high	119	82	37	
Social agency or proactivity in a social context				< 0.01
low	83	5	78	
high	170	132	38	
Feelings of trust and safety				< 0.01
low	53	9	44	
high	200	128	72	
Neighborhood connections				< 0.01
low	58	16	42	
high	195	121	74	
Family and friend connections				< 0.01
low	80	10	70	
high	173	127	46	
Tolerance of diversity				< 0.01
low	124	38	86	
high	129	99	30	
Value of life				< 0.01
low	141	34	107	
high	112	103	9	
Work connections				< 0.01
low	126	26	100	
high	127	111	16	

*Chi-squared test.

Table 3. Correlation between the distress thermometer and social capital

Factors[a]	1	2	3	4	5	6	7	8	9
1	1	0.321**	0.407**	0.363**	0.266**	0.29**	0.196**	0.258**	-0.279**
2	0.321**	1	0.426**	0.4**	0.738**	0.578**	0.606**	0.634**	-0.675**
3	0.407**	0.426**	1	0.505**	0.548**	0.408**	0.439**	0.361**	-0.384**
4	0.363**	0.4**	0.505**	1	0.58**	0.443**	0.278**	0.209**	-0.291**
5	0.266**	0.738**	0.548**	0.58**	1	0.643**	0.589**	0.564**	-0.568**
6	0.29**	0.578**	0.408**	0.443**	0.643**	1	0.524**	0.478**	-0.462**
7	0.196**	0.606**	0.439**	0.278**	0.589**	0.524**	1	0.744**	-0.676**
8	0.258**	0.634**	0.361**	0.209**	0.564**	0.478**	0.744**	1	-0.67**
9	-0.279**	-0.675**	-0.384**	-0.291**	-0.568**	-0.462**	-0.676**	-0.67**	1

[a]Factor1 = Participation in the local community; Factor 2= Social agency or proactivity in a social context; Factor 3 = Feelings of trust and safety; Factor 4 = Neighborhood connections; Factor 5 = Family and friend connections; Factor 6= Tolerance of diversity; Factor 7 = Value of life; Factor 8 = Work connections; Factor 9 = Distress thermometer. *P<0.05, **P<0.01.

neighborhood connections (r = -0.291), family and friend connections (r = -0.568), tolerance of diversity (r = -0.462), value of life (r = -0.676), and work connections (r = -0.67).

The results of the binary regression logistic analysis of the relationships between social capital and the DT are shown in Table 4. Among eight social capital dimensions, compared to reference groups, a higher level of social capital was linked to the DT. After adjusting for all covariate variables, in comparison to reference groups, higher levels of participation in the local community (OR = 3.437; 95% CI: 1.734 - 6.814), social agency or proactivity in a social context (OR = 69.700; 95% CI: 20.142 - 241.195), feelings of trust and safety (OR = 26.287; 95% CI: 7.646 - 90.374), neighborhood connections (OR = 7.022; 95% CI: 3.020 - 16.236), family and friend connections (OR = 59.315; 95% CI: 17.182 - 204.760), tolerance of diversity (OR = 9.785; 95% CI: 4.736 - 20.216), value of life (OR = 65.142; 95% CI: 19.994 - 212.242), and work connections (OR = 31.842; 95% CI: 12.612 - 80.397) were associated with the DT, which indicated that a lower level of social capital was a risk factor for a higher DT score among breast cancer patients who underwent modified radical surgery.

4. Discussion

This study investigated the relationship between social capital and psychological distress among breast cancer

Table 4. Logistic analysis examining associations between the distress thermometer and social capital ($N = 253$)

Social capital dimensions	Unadjusted OR (95% CI)	Adjusted AOR (95% CI)
Participation in the local community		
low	Ref.	Ref.
high	3.183 (1.895-5.348)**	3.437 (1.734-6.814)**
Social agency or proactivity in a social context		
low	Ref.	Ref.
high	54.189 (20.470-143.452)**	69.700 (20.142-241.195)**
Feelings of trust and safety		
low	Ref.	Ref.
high	8.691 (4.012-18.827)**	26.287 (7.646-90.374)**
Neighborhood connections		
low	Ref.	Ref.
high	4.292 (2.253-8.176)**	7.022 (3.020-16.236)**
Family and friend connections		
low	Ref.	Ref.
high	19.326 (9.189-40.648)**	59.315 (17.182-204.760)**
Tolerance of diversity		
low	Ref.	Ref.
high	7.468 (4.270-13.063)**	9.785 (4.736-20.216)**
Value of life		
low	Ref.	Ref.
high	30.016 (16.461-78.801)**	65.142 (19.994-212.242)**
Work connections		
low	Ref.	Ref.
high	26.683 (13.533-52.609)**	31.842 (12.612-80.397)**

Adjusted Participation in the local community, Social agency or proactivity in a social context, Feelings of trust and Safety, Neighborhood connections, Family and friend connections, Tolerance of diversity, Value of life, Work connections. *$p < 0.05$. **$p < 0.01$.

patients who underwent modified radical surgery in Anhui, China. Results revealed a negative association between social capital dimensions and DT scores. Specifically, individuals with higher levels of social capital exhibited less psychological distress. In addition, the interactive relationship between social capital and various variables related to psychological distress was identified in breast cancer patients who underwent modified radical surgery.

Breast cancer is one of the most common malignant tumors seriously affecting women's physical and mental health. It not only causes physiological pain but also often imposes great psychological pressure on patients because of the disfigurement it causes. Psychological distress can lead to the weakening of patients' cellular immune function, and the weakening of cellular immune function can lead to the emergence of more clinical discomfort in the patients, which affects their quality of life and the effectiveness of treatment, and it even has direct adverse effects on prognosis. Previous studies have shown that intervention in social factors can improve patients' quality of life and alleviate psychological distress (*44-46*). A cohort study in Sweden found that individuals living in neighborhoods with highly connected social capital may receive adequate health promotion information and adopt healthy behaviors due to trusting relationships between neighbors (*47*). In line with the current findings, prior studies have also found that improving individual social capital can enhance cancer treatment compliance, help reduce cancer-related pain, and increase resilience to cancer side effects (*27,28*). The current study showed that a higher level of social capital was associated with less psychological distress, as corroborated by previous studies reporting that more social capital is linked to less likelihood of having psychological distress (*16*).

The current results indicated that psychological distress is correlated with age, level of education, and marital status in breast cancer patients who underwent modified radical surgery. However, there is a minimal association between psychological distress and the AJCC stage. One possible explanation is that female patients often exhibit a heightened concern for the implications of breast cancer itself, rather than the treatment process, due to their cognitively emotional reasoning. The relationship between social capital and psychological distress was investigated in breast cancer patients who underwent modified radical surgery. Findings revealed that various dimensions of social capital were associated with psychological distress in this patient population. For example, in this study, social support was defined as resources that are available to breast cancer patients who undergo modified radical surgery when they are in pain (*42*). Eight dimensions were utilized to evaluate social capital. This variation further highlighted the necessity to determine a universal and consent definition and measurement of social capital (*48*).

Moreover, all dimensions of social capital exhibit a significant negative correlation with psychological distress. One potential explanation is that advances in medical technology and improved care may provide

more significant social capital to support breast cancer patients who have undergone modified radical surgery, consequently reducing the risk of psychological distress. Conversely, patients with higher levels of social capital are more likely to receive support through engagement in formal or informal groups, voluntary activities, and community services, thereby alleviating psychological distress. Building upon the current findings, breast cancer patients who have undergone modified radical surgery should be encouraged to more actively engage in society to establish and maintain their social capital, enabling them to access increased social support and mitigate psychological distress.

Results of a logistic regression model indicated that participation in the local community, social agency or proactivity in a social context, feelings of trust and safety, neighborhood connections, family and friend connections, tolerance of diversity, value of life, and work connections were statistically associated with the psychological distress of breast cancer patients who underwent modified radical surgery, which also agrees with previous studies (*49,50*). Results from China demonstrated that social roles and functions of women are often limited by family, politics, and traditional cultural factors (*16*). For women with breast cancer, the scope of social capital and the level of social participation are more likely to be limited than those of healthy women and men (*51*). On one hand, the pain associated with breast cancer treatment significantly restricts the range of activities available to female patients and diminishes their social participation. On the other hand, post-surgical alterations to the body frequently lead to decreased self-esteem and heightened anxiety among female patients, further diminishing their social capital. In addition, a clinical trial involving patients with breast cancer in Iran found that after receiving social capital interventions, the occurrence of social capital in breast cancer patients had a positive impact on patients' psychology (*27*). In order to enhance the quality of life and alleviate psychological distress among breast cancer patients who have undergone modified radical surgery, programs or initiatives aimed at building and reinforcing social capital should be implemented. These efforts should focus on fostering participation in the local community, promoting social agency or proactivity, nurturing feelings of trust and safety, strengthening neighborhood connections, enhancing family and friend connections, fostering tolerance of diversity, promoting the value of life, and facilitating work connections. Such programs should involve support from family members, relatives, neighbors, and friends.

Our study has several notable strengths. First, prior research has established that, akin to other forms of cancer, breast cancer's high morbidity and mortality rates have significant psychological impacts, resulting in severe psychological reactions such as psychological distress in the majority of patients (*9,10*). To the extent known, the current study is the first to present empirical evidence from a Chinese context regarding the influence of social capital factors on psychological distress among breast cancer patients. This study specifically proposes the establishment of a social support system encompassing community and familial support in order to foster increased communication between patients and their relatives, friends, and neighbors. This initiative seeks to cultivate a supportive community that is conducive to alleviating the adverse emotional experiences of patients. On the one hand, the findings of this study offer valuable insights into the role of social capital in the mental health of cancer patients. On the other hand, the findings of this study have the potential to enhance clinicians' comprehension of the psychological distress experienced by patients undergoing breast cancer treatment. In addition, future investigations could draw on these insights to improve the quality of life for breast cancer patients undergoing modified radical surgery by emphasizing the role of social capital in mitigating psychological distress. Second, a highly reliable and valid social capital scale was utilized. This scale encompasses eight dimensions that more accurately capture the characteristics of social capital, including trust, reciprocity, and social networks. Third, the representativeness of the sample was ensured through the implementation of a multistage sampling strategy and the inclusion of an appropriate sample size. The sampling process took into account the representation and influence of hospitals. This greatly contributed to the successful attainment of the study's objectives.

However, there are a few limitations that should be acknowledged. First, this was a cross-sectional study, which precluded determining the causality of social capital and the psychological distress of breast cancer patients who underwent modified radical surgery. A longitudinal study design is warranted for the future. Second, the generalization of these findings is limited since the study only involved breast cancer patients who underwent modified radical surgery in Anhui Province. Future studies that include larger areas and samples need to be conducted. Third, data in this study were based on self-reports and might be subject to a recall or reporting bias.

Finally, this study only analyzed the relationship between social capital and psychological distress in breast cancer patients who underwent modified radical surgery and did not include psychological distress and social capital in other cancer patients. Future research considering social capital in cancer patients may help to understand the role of social capital better and thus improve the quality of life of cancer patients.

5. Conclusion

In summary, the current study revealed an association between social capital and psychological distress among

breast cancer patients who underwent modified radical surgery. Specifically, higher levels of participation in the local community, social agency or proactivity in a social context, feelings of trust and safety, neighborhood connections, family and friend connections, tolerance of diversity, value of life, and work connections were associated with less psychological distress among breast cancer patients. Therefore, tailored attention should be given to breast cancer patients who have undergone modified radical surgery, and especially those from regions with varying levels of social capital. These findings should inform the formulation of strategies to enhance treatment, nursing, and rehabilitation services to mitigate damaging physical and psychological impacts, thus improving the quality of life of breast cancer patients who have undergone modified radical surgery.

Acknowledgements

The authors wish to thank the breast cancer patients who participated in this study.

Funding: This work was supported by grants from the Outstanding Research and Innovation Team Program of the Education Department of Anhui Province (no. 2023AH010036), the Outstanding Young Medical Talent Program, Hefei Cancer Hospital, Chinese Academy of Sciences, China (no. 2000000005), and the First Hospital Affiliated with Anhui Medical University's Foundation to Nurture Youth (2020kj21).

Conflict of Interest: The authors have no conflicts of interest to disclose.

Ethics approval and consent to participate: Ethical approval for this study was obtained from the Ethics Committee of Hefei Cancer Hospital, Chinese Academy of Sciences (No.YXLL-2024-35). All participants provided written informed consent before participating in the study. Participants were informed of the study's purpose, procedures, potential risks, benefits, and their right to withdraw at any time without penalty. Confidentiality and anonymity were maintained throughout the study, and all data collected were stored securely to protect participants' privacy. In addition, all methods used in this study are in accordance with the Declaration of Helsinki.

References

1. Youlden DR, Cramb SM, Yip CH, Baade PD. Incidence and mortality of female breast cancer in the Asia-Pacific region. Cancer Biol Med. 2014; 11:101-115.
2. Bray F, Ferlay J, Soerjomataram I, Siegel RL, Torre LA, Jemal A. Global cancer statistics 2018: GLOBOCAN estimates of incidence and mortality worldwide for 36 cancers in 185 countries. CA Cancer J Clin. 2018; 68:394-424.
3. Sung H, Ferlay J, Siegel RL, Laversanne M, Soerjomataram I, Jemal A, Bray F. Global cancer statistics 2020: GLOBOCAN estimates of incidence and mortality worldwide for 36 cancers in 185 countries. CA Cancer J Clin. 2021; 71:209-249.
4. Hua T, Fan R, Fan Y, Chen F. Immune response of COVID-19 vaccines in solid cancer patients: A meta-analysis. Hum Vaccin Immunother. 2024; 20:2357424.
5. Baron RC, Rimer BK, Breslow RA, Coates RJ, Kerner J, Melillo S, Habarta N, Kalra GP, Chattopadhyay S, Wilson KM, Lee NC, Mullen PD, Coughlin SS, Briss PA. Client-directed interventions to increase community demand for breast, cervical, and colorectal cancer screening a systematic review. Am J Prev Med. 2008; 35:S34-55.
6. Jylhä M. What is self-rated health and why does it predict mortality? Towards a unified conceptual model. Soc Sci Med. 2009; 69:307-316.
7. Winters S, Martin C, Murphy D, Shokar NK. Breast cancer epidemiology, prevention, and screening. Prog Mol Biol Transl Sci. 2017; 151:1-32.
8. Kim J, Cho J, Lee SK, Choi EK, Kim IR, Lee JE, Kim SW, Nam SJ. Surgical impact on anxiety of patients with breast cancer: 12-month follow-up prospective longitudinal study. Ann Surg Treat Res. 2020; 98:215-223.
9. Dinapoli L, Colloca G, Di Capua B, Valentini V. Psychological aspects to consider in breast cancer diagnosis and treatment. Curr Oncol Rep. 2021; 23:38.
10. Lovelace DL, McDaniel LR, Golden D. Long-term effects of breast cancer surgery, treatment, and survivor care. J Midwifery Womens Health. 2019; 64:713-724.
11. Mokhtari-Hessari P, Montazeri A. Health-related quality of life in breast cancer patients: Review of reviews from 2008 to 2018. Health Qual Life Outcomes. 2020; 18:338.
12. Phoosuwan N, Lundberg PC. Psychological distress and health-related quality of life among women with breast cancer: A descriptive cross-sectional study. Support Care Cancer. 2022; 30:3177-3186.
13. Segrin C, Badger T, Sikorskii A. Psychological distress and social support availability in different family caregivers of Latinas with breast cancer. J Transcult Nurs. 2021; 32:103-110.
14. Verri V, Pepe I, Abbatantuono C, Bottalico M, Semeraro C, Moschetta M, De Caro MF, Taurisano P, Antonucci LA, Taurino A. The influence of body image on psychological symptomatology in breast cancer women undergoing intervention: A pre-post study. Front Psychol. 2024; 15:1409538.
15. Wan C, Fang J, Jiang R, Shen J, Jiang D, Tu X, Messing S, Tang W. Development and validation of a quality of life instrument for patients with drug dependence: Comparisons with SF-36 and WHOQOL-100. Int J Nurs Stud. 2011; 48:1080-1095.
16. Zhao J, Ma Y, Tanimoto T, Ozaki A, Chen WL, Wang JY, Zhang YX, Chen LL, Wang JW, Yu JM. Effects of physical activity and stress on the relationship between social capital and quality of life among breast cancer survivors. Sci Rep. 2020; 10:17746.
17. Zhu M, Zhang Y, He H, Chen L, Chen J, Zhang M. Social participation and acceptance of disability in young and middle-aged breast cancer patients after surgery: A 6-month follow-up study. Asia Pac J Oncol Nurs. 2023; 10:100266.
18. Kim S, Ko YH, Song Y, Kang MJ, Lee H, Kim SH, Jeon JY, Cho YU, Yi G, Han J. Pre-post analysis of a social capital-based exercise adherence intervention for breast cancer survivors with moderate fatigue: A randomized

controlled trial. Support Care Cancer. 2020; 28:5281-5289.
19. Pelletier G, Verhoef MJ, Khatri N, Hagen N. Quality of life in brain tumor patients: The relative contributions of depression, fatigue, emotional distress, and existential issues. J Neurooncol. 2002; 57:41-49.
20. Von Essen L, Larsson G, Oberg K, Sjödén PO. 'Satisfaction with care': Associations with health-related quality of life and psychosocial function among Swedish patients with endocrine gastrointestinal tumours. Eur J Cancer Care (Engl). 2002; 11:91-99.
21. Admiraal JM, Hoekstra-Weebers J, Schröder CP, Tuinier W, Hospers GAP, Reyners AKL. Distress, problems, referral wish, and supportive health care use in breast cancer survivors beyond the first year after chemotherapy completion. Support Care Cancer. 2020; 28:3023-3032.
22. Henselmans I, Helgeson VS, Seltman H, de Vries J, Sanderman R, Ranchor AV. Identification and prediction of distress trajectories in the first year after a breast cancer diagnosis. Health Psychol. 2010; 29:160-168.
23. Gradishar WJ, Moran MS, Abraham J, *et al*. Breast Cancer, Version 3.2022, NCCN Clinical Practice Guidelines in Oncology. J Natl Compr Canc Netw. 2022; 20:691-722.
24. Blasco T, Jovell E, Mirapeix R, Leon C. Patients' desire for psychological support when receiving a cancer diagnostic. Int J Environ Res Public Health. 2022; 19.
25. Rao WW, Yang MJ, Cao BN, You YY, Zhang YY, Liu YY, Kou C, Yu Y, Cassidy RM, Yu Q, Zhang XY. Psychological distress in cancer patients in a large Chinese cross-sectional study. J Affect Disord. 2019; 245:950-956.
26. Yamada K, Kimura T, Cui M, Kubota Y, Ikehara S, Iso H. Social support, social cohesion and pain during pregnancy: The Japan Environment and Children's Study. Eur J Pain. 2021; 25:872-885.
27. Aflakseir A, Nowroozi S, Mollazadeh J, Goodarzi MA. The role of psychological hardiness and marital satisfaction in predicting posttraumatic growth in a sample of women with breast cancer in Isfahan. Iran J Cancer Prev. 2016; 9:e4080.
28. Alizadeh S, Khanahmadi S, Vedadhir A, Barjasteh S. The relationship between resilience with self- compassion, social support and sense of belonging in women with breast cancer. Asian Pac J Cancer Prev. 2018; 19:2469-2474.
29. Keyvanara M, Afshari M, Dezfoulian E. The relationship between social capital and quality of life among patients referring to diabetes centers in Isfahan, Iran. J Diabetes Res. 2018; 2018:9353858.
30. Ji K, Bai Z, Zhao Y, Sang L, Wang D, Chen R. Relationship between social capital and quality of life among adult stroke patients: a cross-sectional study in Anhui Province, China. Health Qual Life Outcomes. 2022; 20:19.
31. Kim S, Ko YH, Song Y, Kang MJ, Lee H, Kim SH, Jeon JY, Cho YU, Yi G, Han J. Correction to: Pre-post analysis of a social capital-based exercise adherence intervention for breast cancer survivors with moderate fatigue: A randomized controlled trial. Support Care Cancer. 2021; 29:1141-1144.
32. Banas JR, Victorson D, Gutierrez S, Cordero E, Guitleman J, Haas N. Developing a peer-to-peer mHealth application to connect Hispanic cancer patients. J Cancer Educ. 2017; 32:158-165.
33. Donovan KA, Grassi L, McGinty HL, Jacobsen PB. Validation of the distress thermometer worldwide: state of the science. Psychooncology. 2014; 23:241-250.
34. Ma X, Zhang J, Zhong W, Shu C, Wang F, Wen J, Zhou M, Sang Y, Jiang Y, Liu L. The diagnostic role of a short screening tool--the distress thermometer: A meta-analysis. Support Care Cancer. 2014; 22:1741-1755.
35. Mitchell AJ. Pooled results from 38 analyses of the accuracy of distress thermometer and other ultra-short methods of detecting cancer-related mood disorders. J Clin Oncol. 2007; 25:4670-4681.
36. Tuinman MA, Gazendam-Donofrio SM, Hoekstra-Weebers JE. Screening and referral for psychosocial distress in oncologic practice: Use of the Distress Thermometer. Cancer. 2008; 113:870-878.
37. Iskandarsyah A, de Klerk C, Suardi DR, Soemitro MP, Sadarjoen SS, Passchier J. The Distress Thermometer and its validity: A first psychometric study in Indonesian women with breast cancer. PLoS One. 2013; 8:e56353.
38. Keir ST, Calhoun-Eagan RD, Swartz JJ, Saleh OA, Friedman HS. Screening for distress in patients with brain cancer using the NCCN's rapid screening measure. Psychooncology. 2008; 17:621-625.
39. Xu L, Guo M, Nicholas S, Sun L, Yang F, Wang J. Disease causing poverty: Adapting the Onyx and Bullen social capital measurement tool for China. BMC Public Health. 2020; 20:63.
40. Lachance L, Coombe CM, Brush BL, Lee SD, Jensen M, Taffe B, Bhardwaj P, Muhammad M, Wilson-Powers E, Rowe Z, Caldwell CH, Israel BA. Understanding the benefit-cost relationship in Long-standing community-based participatory research (CBPR) partnerships: Findings from the Measurement Approaches to Partnership Success (MAPS) study. J Appl Behav Sci. 2022; 58:513-536.
41. Calkins E. OARS methodology and the "medical model". J Am Geriatr Soc. 1985; 33:648-649.
42. Ito T, Okuyama K, Abe T, Takeda M, Hamano T, Nakano K, Nabika T. Relationship between individual social capital and cognitive function among older adults by gender: A cross-sectional study. Int J Environ Res Public Health. 2019; 16.
43. Teichgraeber DC, Guirguis MS, Whitman GJ. Breast Cancer Staging: Updates in the AJCC Cancer Staging Manual, 8th Edition, and Current Challenges for Radiologists, From the AJR Special Series on Cancer Staging. AJR Am J Roentgenol. 2021; 217:278-290.
44. Luebbert K, Dahme B, Hasenbring M. The effectiveness of relaxation training in reducing treatment-related symptoms and improving emotional adjustment in acute non-surgical cancer treatment: A meta-analytical review. Psychooncology. 2001; 10:490-502.
45. Meyer TJ, Mark MM. Effects of psychosocial interventions with adult cancer patients: A meta-analysis of randomized experiments. Health Psychol. 1995; 14:101-108.
46. van't Spijker A, Trijsburg RW, Duivenvoorden HJ. Psychological sequelae of cancer diagnosis: A meta-analytical review of 58 studies after 1980. Psychosom Med. 1997; 59:280-293.
47. Hamano T, Li X, Sundquist J, Sundquist K. Is neighbourhood linking social capital associated with colorectal cancer incidence and mortality? A national cohort study from Sweden. J Prim Prev. 2021; 42:493-510.
48. FarrHenderson M, Di Marco MH, Evans DP. Perceptions

of social capital before and after the perpetration of femicide, homicide, and other serious crimes: Evidence from Argentina. J Interpers Violence. 2024; 8862605241265918.
49. Snyder CF, Wu AW, Miller RS, Jensen RE, Bantug ET, Wolff AC. The role of informatics in promoting patient-centered care. Cancer J. 2011; 17:211-218.
50. Zhang S, Bantum EO, Owen J, Bakken S, Elhadad N. Online cancer communities as informatics intervention for social support: Conceptualization, characterization, and impact. J Am Med Inform Assoc. 2017; 24:451-459.
51. David-Barrett T, Rotkirch A, Carney J, Behncke Izquierdo I, Krems JA, Townley D, McDaniell E, Byrne-Smith A, Dunbar RI. Women favour dyadic relationships, but men prefer clubs: Cross-cultural evidence from social networking. PLoS One. 2015; 10:e0118329.

Received June 22, 2024; Revised August 16, 2024; Accepted August 22, 2024.

[§]These authors contributed equally to this work.

*Address correspondence to:
Yue Fang, Galactophore Oncology Center, Hefei Cancer Hospital, Chinese Academy of Sciences, Hefei, Anhui, China.
E-mail: fangle@cmpt.ac.cn

Ren Chen, Department of Health Services Management, School of Health Services Management, Anhui Medical University, Hefei, Anhui, China.
E-mail: chenren2006@hotmail.com

Released online in J-STAGE as advance publication August 25, 2024.

Original Article

DOI: 10.5582/bst.2024.01199

Association of the national level of human development with the incidence and mortality of congenital birth defects in 2019: A cross-sectional study from 189 countries

Chen Du[1,§], Ziquan Zhang[2,§], Shuzhe Xiao[1,§], Yanwen Li[1], Ruiwen Jiang[1], Weihua Jian[3], Zhuxiao Ren[4], Yiting Lv[1], Zhizhang Pan[1], Jie Yang[1,*]

[1] Department of Neonatology, Nanfang Hospital, Southern Medical University, Guangzhou, Guangdong, China;
[2] School of Artificial Intelligence, Sun Yat-sen University, Zhuhai, Guangdong, China.
[3] Department of Neonatology, Zhongshan City People's Hospital, Zhongshan, Guangdong, China;
[4] Department of Neonatology, Guangdong Women and Children Hospital, Guangzhou, Guangdong, China.

SUMMARY Congenital birth defects (CBD) play a significant role in causing child mortality globally. The incidence and mortality of CBD vary widely across countries, and the underlying causes for this divergence remain incompletely comprehended. We conducted an analysis to investigate the relationship between the incidence and mortality of CBD in 189 countries and their Human Development Index (HDI). In this study, CBD data from 189 countries was used from the Global Burden of Diseases Study (GBD) 2019, and HDI data was collected for the same countries. Later, the relationship between CBD and HDI was analyzed, and the impact of gross national income (GNI) per capita, expected years of schooling, mean years of schooling and life expectancy at birth was quantified using principal component regression. The age-standardized incidence rate (ASIR) varied between 66.57 to 202.24 per 100,000, with a 95% uncertainty interval (UI) of 57.20-77.51 and 165.87-241.48 respectively. The age-standardized mortality rate (ASMR) also showed a rang from 1.38 to 26.53 (14.03-39.90) per 100,000, with the 95%UI of 0.91-2.09 and 14.03-39.90 respectively. Both the incidence and mortality rates of CBD decreased with the increased HDI (incidence: r = -0.38, $p < 0.001$, mortality: r = -0.77, $p < 0.001$). Our investigation revealed significant variations in the incidence and mortality of CBD among countries with different development levels. In conclusion, the global incidence and mortality of CBD vary significantly among countries, possibly due to differences in the accessibility of health services.

Keywords congenital abnormalities, human development index, child death.

1. Introduction

Congenital birth defects (CBD) is one of the leading causes of death among children worldwide (*1*). As embryonic development progresses, CBD appears to be a spectrum of structural, functional, or metabolic abnormalities (*2*). Concurrence of CBD correlates with multi-factors such as genes, environment, economics, education, literacy, and so on (*3,4*). As morality in children below five years is an index of country development, rising incidence of CBD and related mortality have been an issue in developing countries for years. The age-standardized incidence rate (ASIR) and age-standardized mortality rate (ASMR) are statistical measures used for evaluating the different populations' incidence and mortality rates so that the effect of differing age distributions can be eliminated.

The United Nations Development Program (UNDP) established the Human Development Index (HDI) to assess a country's degree of development. The HDI takes into account factors such as education, literacy, gross national income (GNI) per capita, and life expectancy. From 0 to 1, higher values of the index indicate higher levels of development. Gross national income (GNI) measures the total income earned by residents of a country (*5*). Previous studies have shown that socioeconomic, human race, environmental pollution, and hereditary genes affected the incidence of CBD and related mortality, respectively (*6,7*). However, the correlation between HDI and CBD has never been reported.

In this study, we gained ASIR and ASMR of 2019

from the Global Burden of Diseases, Injuries, and Risk Factors Study (GBD), which divided the world into 21 regions, GBD, based on the geographic locations of countries around the world. We devided HDI into very high, high, middle, low levels, and investigated the associations of HDI and the incidence of CBD and related mortality.

2. Materials and Methods

2.1. Data sources

ASIR and ASMR of CBD in 2019 are available on the GBD dataset on the website: *https://ghdx.healthdata.org/gbd-results-tool* (accessed 25 Sep 2023) . HDI data were available on the website: *https:// hdr.undp.org/data-center/ human-development-index#/ indicies/HDI* (accessed 20 Oct 2023).

2.2. Case definition

CBD included eleven congenital malformations, deformations, and chromosomal abnormalities (*8*), including congenital heart diseases, congenital musculoskeletal anomalies, gastrointestinal congenital anomalies, neural tube defects, orofacial clefts, Down syndrome, Klinefelter syndrome, Turner syndrome, other chromosomal abnormalities, urogenital congenital anomalies. CBD Case was defined in accordance with the 10th version of the International Classification of Diseases (ICD-10).

The HDI is a comprehensive measure of a country's development level compiled by the UNDP. The UNDP classifies countries into four categories based on their HDI: Very High (0·80 ≤ HDI ≤1), High (0·70 ≤ HDI < 0·80), Medium (0.55 ≤ HDI < 0·70), and Low (0 ≤ HDI < 0·55) (*9*).

2.3. Statistical analysis

The ASIR and ASMR were calculated by the GBD global population (*8*). The districts that need higher priority for incidence and mortality reduction were identified based on the 3×4 grouping of districts in tertiles of ASIR and ASMR in 2019 and the four categories of countries classified with HDI (*9*). The Spearman correlation coefficient was assessed between ASR of incidence and mortality with the HDI of the countries in 2019. There is an uncertainty interval (UI) of 95% for the incidence number, deaths, ASIR, and ASMR, which were calculated by using the 25th and 975th sorted values among 1000 draws. ASIR and ASMR were reported per 100,000 populations and later normalized (such that the total rate of each CBD equals 1) and mean-centered before Principal Component Analysis (PCA). The principal component regression was employed to quantify the relative contributions of the four indicators constituting HDI to the ASIR and ASMR of CBD. GraphPad Prism 10 and R version 4.3.1 were used for the statistical analyses. In order to be considered statistically significant, a significance level of $P < 0·05$ was required.

3. Results

3.1. Total CBD

In 2019, data from 189 countries showed variations in the incidence and mortality of CBD at the national level. At the national level, ASIR varied 3.04 times among the 189 countries of the world, ranging from 66.57 (95% UI 57·20-77·51) to 202·24 (165·87-241·48) per 100,000 livebirths (Figure 1A and Supplemental Table S1, *http://www.biosciencetrends.com/action/getSupplementalData.php?ID=208*). ASIR was 130 or more per 100,000 livebirths in 25 (75.76%) of the 33 low HDI countries, in 12 (31.58%) of the 38 medium HDI countries, in 11 (21.57%) of the 51 high HDI countries, and in 15 (22.39%) of the 67 very high HDI countries (Figure 1B and Supplemental Table S1, *http://www.biosciencetrends.com/action/getSupplementalData.php?ID=208*).

At the national level, ASMR varied 19.22 times among the 189 countries of the world, ranging from 1.38 (0.91-2.09) to 26.52 (14.03-39.90) per 100,000 livebirths (Figure 2A and Supplemental Table S2, *http://www.biosciencetrends.com/action/getSupplementalData.php?ID=208*). ASIR was 8 or more per 100,000 livebirths in 31 (93.94%) of the 33 low HDI countries, in 15 (39.47%) of the 38 medium HDI countries, in 13 (25.49%) of the 51 high HDI countries, and in 4 (5.97%) of the 67 very high HDI countries (Figure 2B and Supplemental Table S2, *http://www.biosciencetrends.com/action/getSupplementalData.php?ID=208*).

The total incidence and mortality of CBD decreased with increasing HDI (incidence $r = -0.38$, $p < 0.001$ and mortality $r = -0.77$, $p < 0.001$) (Figure 3). Additionally, we discovered that the proportional impact of the four elements comprising HDI on the incidence and mortality of CBD is comparable (Figure 4). Not only should we pay attention to socioeconomic inequalities, but we should also address the disparities prevailing in the education and healthcare systems of different countries.

3.2. Levels and trends of CBD in 21 regions

The incidence and deaths varied significantly among different national levels of human development and regions (Figure 1C-D and Figure 2C-D). While variations in the incidence of CBD were observed across 21 regions, congenital heart diseases ranked highest in affected individuals in nine regions, and

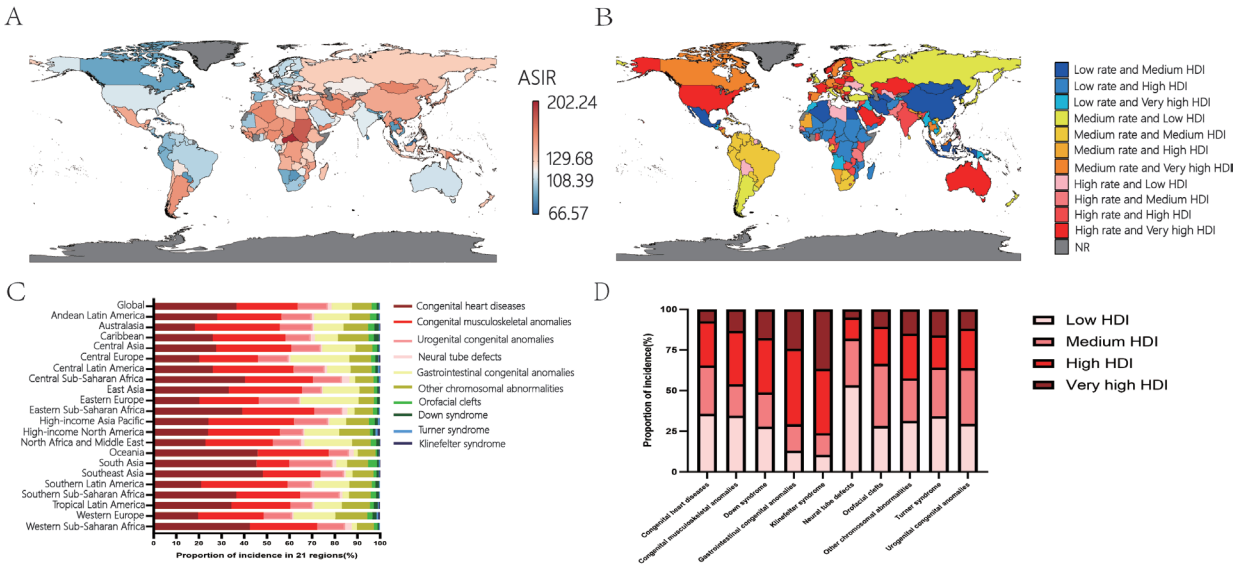

Figure 1. (A) Global distribution map of the total ASIR of CBD in 2019; **(B)** District groupings of the total ASIR of CBD in 2019: High, medium, and low groupings are based on the tertile of the ASIR. The tertile cutoffs for ASIR were 108.39 and 129.68. The HDI was divided into four levels: Very High (HDI ≥ 0.8), High (0.7 ≤ HDI < 0.8), Medium (0.55 ≤ HDI < 0.7), and Low (HDI < 0.55). **(C)** The proportional incidence of various CBD in 21 regions in 2019. **(D)** The proportional incidence of various CBD in 2019 was classified by low, medium, high, and very high HDI globally. ASIR = age-standardized incidence rate, HDI = Human development index.

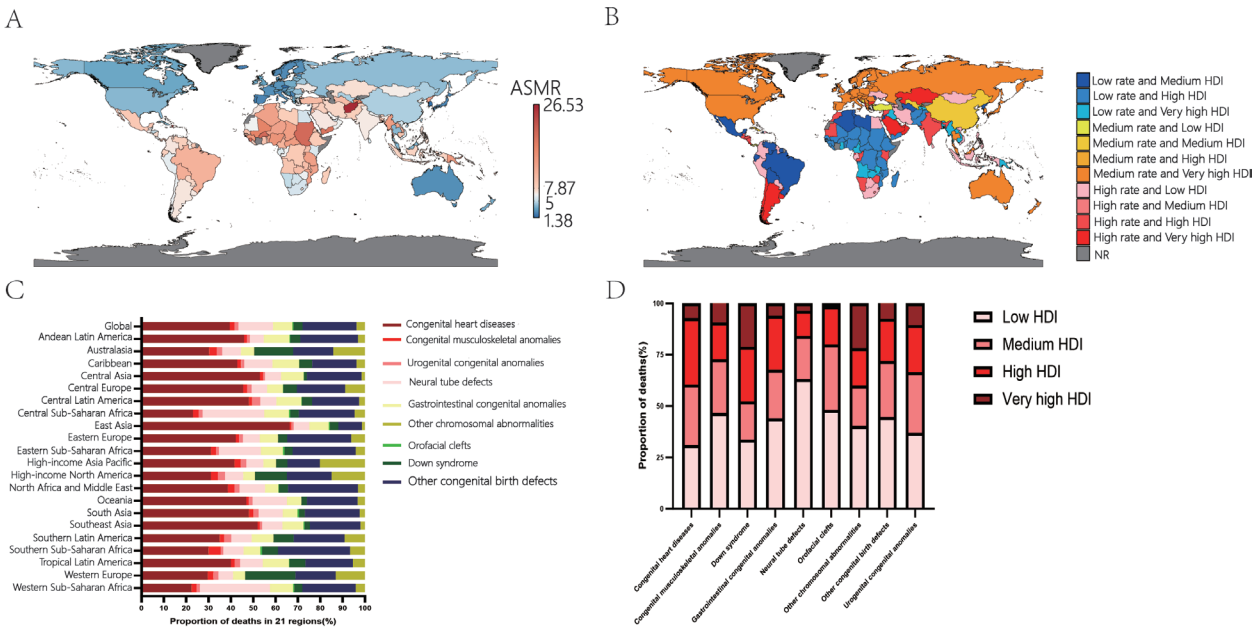

Figure 2. (A) Global distribution map of the total ASMR of CBD in 2019; **(B)** District groupings of the total ASMR of CBD in 2019: High, medium, and low groupings are based on the tertile of ASMR. The tertile cutoffs for age-standardized mortality rate were 5.00 and 7.87. The HDI was divided into four levels: Very High (HDI ≥ 0.8), High (0.7 ≤ HDI < 0.8), Medium (0.55 ≤ HDI < 0.7), and Low (HDI < 0.55). **(C)** The proportional death of various CBD in 21 regions in 2019. **(D)** The proportional death of various CBD in 2019 was classified by low, medium, high, and very high HDI globally. ASMR = age-standardized mortality rate, HDI = Human development index, NR = not report.

congenital musculoskeletal anomalies in twelve regions. Additionally, gastrointestinal congenital anomalies ranked second in ASIR in the Central Europe and Eastern Europe regions (Figure 1C).

Across 21 regions, congenital heart diseases stood out as the primary cause of death in 18 regions. Neural tube defects were a notable cause of death in Central Sub-Saharan Africa and Western Sub-Saharan Africa, while Other CBD played a significant role in Southern Sub-Saharan Africa (Figure 2C). These three regions all belong to Sub-Saharan Africa, which has lots of low HDI countries.

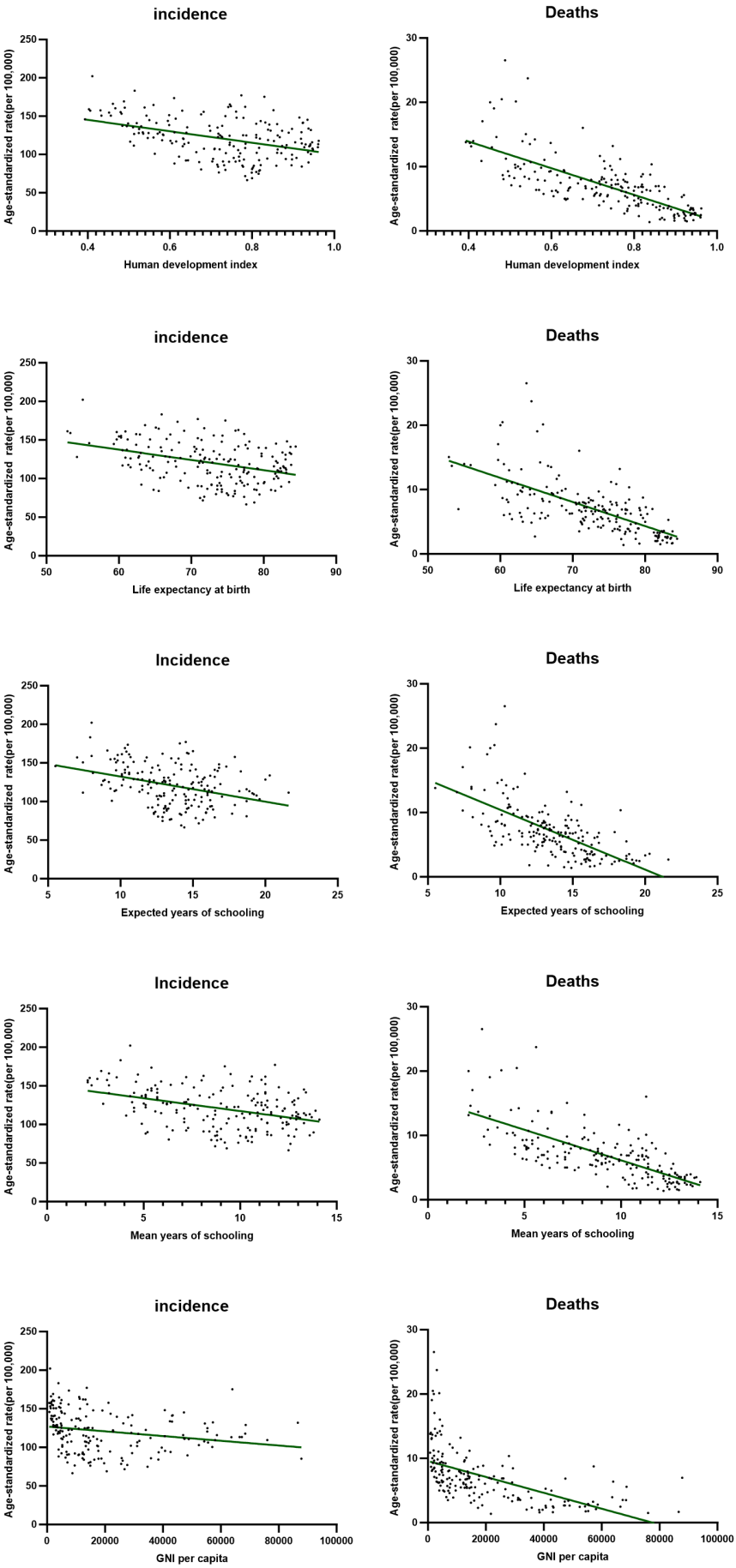

Figure 3. Correlation between the ASIR and ASMR of CBD and HDI, expected years of schooling, mean years of schooling, GNI per capita, and life expectancy at birth.

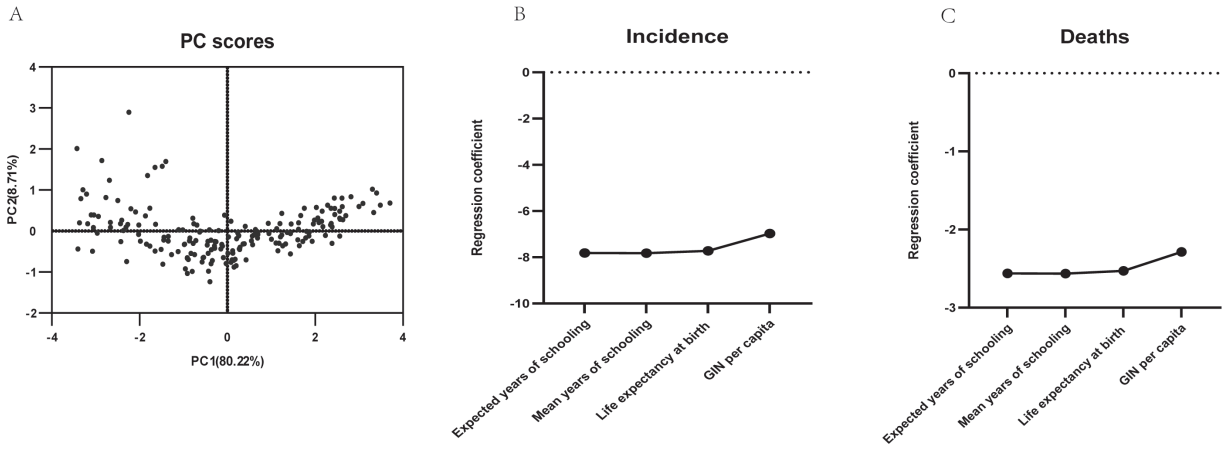

Figure 4. Principal component analysis of the incidence and mortality of CBD. (A) Principal component (PC) score. The first and second principal components are plotted. **(B)** Regression coefficients of ASIR, calculated as a weighted sum, demonstrate the relative contribution to the model of each of the four indicators constituting HDI that were used to generate the model. **(C)** Regression coefficients of ASMR, calculated as a weighted sum, demonstrate the relative contribution to the model of each of the four indicators constituting HDI that were used to generate the model. The four indicators included expected years of schooling, mean years of schooling, GNI per capita, and life expectancy at birth. ASIR = age-standardized incidence rate. HDI = Human Development Index.

Based on the analysis of the incidence and mortality of various CBD in 21 global regions, five specific defects with higher incidence and mortality rates may exert a more significant impact on human development. Consequently, another purpose of our study was to find the correlation between the ASIR and ASMR of five specific birth defects (Figure 5).

3.3. Congenital heart diseases

At the national level, ASIR of congenital heart diseases varied 6.26 times among the 189 countries of the world, ranging from 14.02 (10.13-20.58) to 87.71 (66.73-116.83) per 100,000 livebirths in 189 countries (Supplemental Table S3, *http://www.biosciencetrends.com/action/getSupplementalData.php?ID=208*). The ASMR varied 25.92 times among the 189 countries of the world, ranging from 0.38 (10.13-20.58) to 9.85 (4.27-16.17) per 100,000 livebirths in 189 countries (Supplemental Table S3, *http://www.biosciencetrends.com/action/getSupplementalData.php?ID=208*). The ASIR of congenital heart diseases decreases with increased HDI (r = -0·77, $p < 0.001$). Similarly, the ASMR exhibits a reduction with the rise in HDI (r = -0·61, $p < 0.001$) (Figure 5).

3.4. Congenital musculoskeletal diseases

ASIR of congenital musculoskeletal diseases varied 5.39 times among the 189 countries of the world, ranging from 13.31 (8.08-19.55) to 71.70 (44.44-102.87) per 100,000 livebirths in 189 countries (Supplemental Table S4, *http://www.biosciencetrends.com/action/getSupplementalData.php?ID=208*). The ASMR varied 27.33 times among the 189 countries of the world, ranging from 0.03 (0.01-0.05) to 0.82 (0.40-1.31) per 100,000 livebirths in 189 countries (Supplemental Table S4, *http://www.biosciencetrends.com/action/getSupplementalData.php?ID=208*). The ASIR of congenital musculoskeletal diseases decreases with increased HDI (r = -0·38, $p < 0.001$). Similarly, the ASMR exhibits a reduction with the rise in HDI (r = -0·57, $p < 0.001$) (Figure 5)

3.5. Urogenital congenital anomalies

ASIR of urogenital congenital anomalies varied 4.20 times among the 189 countries of the world, ranging from 6.29 (4.41-8.68) to 26.43 (18.54-37.82) per 100,000 livebirths in 189 countries (Supplemental Table S5, *http://www.biosciencetrends.com/action/getSupplementalData.php?ID=208*). The ASMR varied 25.50 times among the 189 countries of the world, ranging from 0.02 (0.01-0.04) to 0.51 (0.25-0.99) per 100,000 livebirths in 189 countries (Supplemental Table S5, *http://www.biosciencetrends.com/action/getSupplementalData.php?ID=208*). The ASIR of urogenital congenital anomalies decreases with increased HDI (r = -0·20, $p < 0.001$). Similarly, the ASMR exhibits a reduction with the rise in HDI (r = -0·49, $p < 0.001$) (Figure 5).

3.6. Neural tube defects

ASIR of neural tube defects varied 17.56 times among the 189 countries of the world, ranging from 0.43 (0.35-0.53) to 7.55 (5.75-9.62) per 100,000 livebirths in 189 countries (Supplemental Table S6, *http://www.biosciencetrends.com/action/getSupplementalData.php?ID=208*). The ASMR varied 292 times among the 189 countries of the world, ranging from 0.02 (0.01-0.03) to 5.84 (2.20-12.40) per 100,000 livebirths in

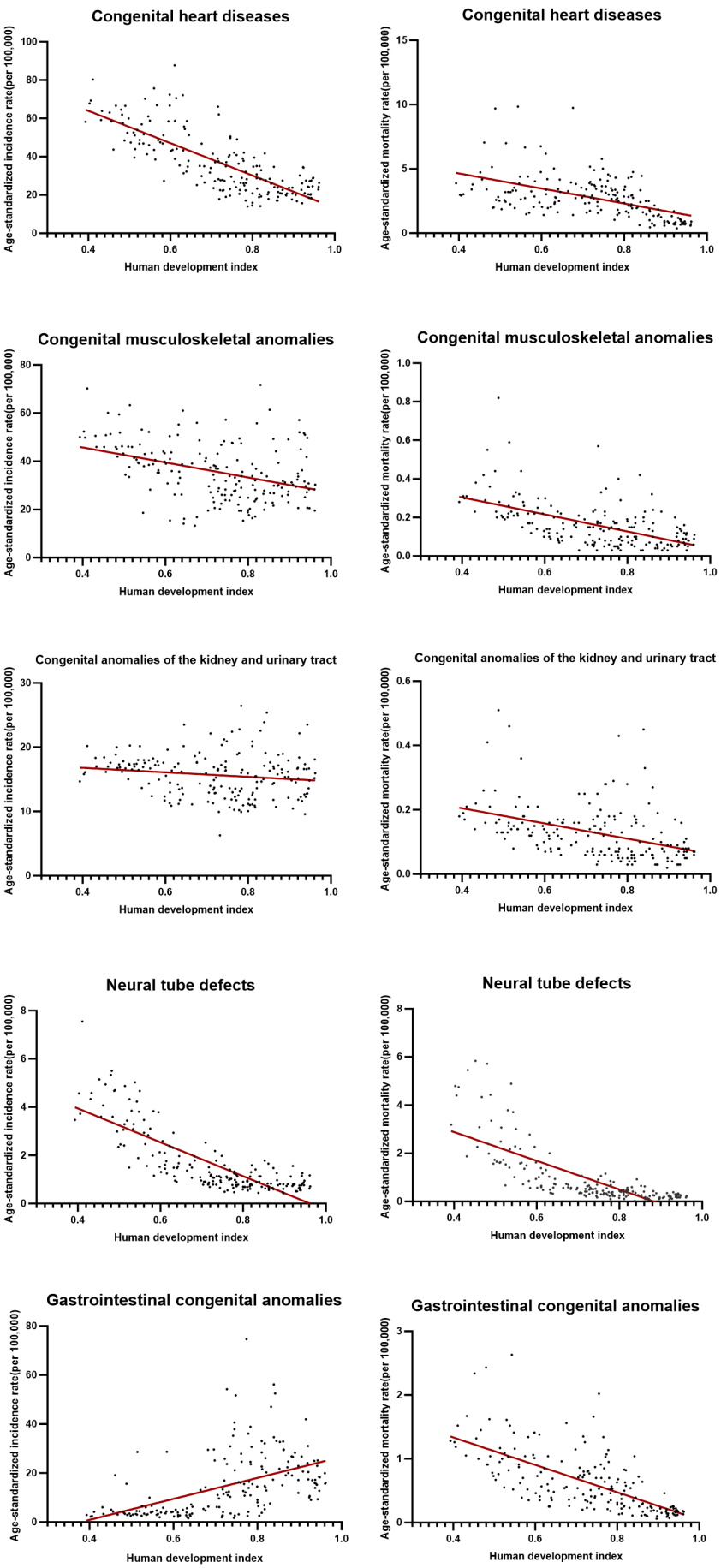

Figure 5. Correlation between the ASIR and ASMR of five types of CBD and HDI.

189 countries (Supplemental Table S6, *http://www.biosciencetrends.com/action/getSupplementalData.php?ID=208*). The ASIR of neural tube defects decreases with increased HDI (r = -0·78, $p < 0.001$). Similarly, the ASMR exhibits a reduction with the rise in HDI (r = -0·84, $p < 0.001$) (Figure 5).

3.7. Gastrointestinal congenital anomalies

ASIR of gastrointestinal congenital anomalies varied 47.52 times among the 189 countries of the world, ranging from 1.57 (1.21-2.00) to 74.60 (49.75-103.10) per 100,000 livebirths in 189 countries (Supplemental Table S7, *http://www.biosciencetrends.com/action/getSupplementalData.php?ID=208*). The ASMR varied 43.83 times among the 189 countries of the world, ranging from 0.06 (0.04-0.12) to 2.63 (0.72-5.13) per 100,000 livebirths in 189 countries (Supplemental Table S7, *http://www.biosciencetrends.com/action/getSupplementalData.php?ID=208*). The ASIR of gastrointestinal congenital anomalies decreases with an increased in HDI (r = 0.61, $p < 0.001$). Similarly, the ASMR exhibits a reduction with the rise in HDI (r = -0·74, $p < 0.001$) (Figure 5).

4. Discussion

In this study, we revealed a negative correlation of the national levels of human development with the incidence and mortality of CBD. We also quantified the similar contributions of education, life expectancy, and socioeconomic to the incidence and mortality of CBD. Previous studies illustrated the national disparities remained, and there were negative correlations between the annual changes from 1990 to 2019 in ASIR and ASMR with socio-demographic index (SDI) (*4,10*). SDI was based on the assessment of incomes per capita, education level, and fertility rates (*4*). HDI is of greater importance to people's health problems than SDI, as it represents medical accessibility in each country. The difference was that our findings further explain the relationship between national differences in CBD and access to health services by applying the HDI. Our findings suggested the potential targeted countries to decrease the incidence and mortality of CBD.

The similarity in the variability of CBD rates for conditions like congenital heart diseases, congenital musculoskeletal diseases, and urogenital anomalies across 189 countries suggests global consistency in diagnostic standards and genetic prevalence. These conditions are generally recognizable at birth or early infancy, aiding in consistent identification across diverse healthcare systems worldwide (*11-13*), enabling consistent recognition and early treatment worldwide.

Finally, we found that CBD mortality in Haiti and Afghanistan deviates from overall trends. Afghanistan's long-term armed conflict and Haiti's Zika virus outbreak likely contributed to this divergence (*14,15*). Future research should focus on the impact of these factors on CBD in these countries.

On the one hand, the low and medium HDI countries can be the targeted areas to improve their accessibility to health services or their national policy to CBD. In low and medium HDI countries, conflict and social unrest often lead to data based on unverified estimates. Limited diagnostic capabilities, resources, and infrastructure hinder comprehensive CBD surveillance. Severe CBD cases are usually identified, but milder conditions often go undiagnosed and untreated. Enhancing healthcare resources in these nations is a crucial public health priority (*10*). On the other hand, in very high HDI countries, 15 (22.39%) of 67 have high incidence, and 4 (5.97%) have high mortality. Improving management in those with high mortality could enhance outcomes. These countries can learn from better-performing peers, and the data in this article may aid in developing targeted CBD prevention and control policies.

This study also revealed a negative correlation of HDI with the incidence and mortality of congenital heart diseases. Previous research has demonstrated that heterogeneity among geographical regions existed, and the mortality rate declined with increasing SDI (*9,16,17*). They commonly illustrated the importance of access to health care in reducing congenital heart diseases. Prior research has shown that routine ultrasound scans conducted around the 11th to 13th weeks of pregnancy can identify over 50% of congenital heart defects (*18*). There has been a rise in the use of prenatal ultrasound in nations with low and medium HDI (*19*). However, physicians may lack sufficient training in these countries (*20*). Limited access to early pregnancy ultrasounds and underdeveloped healthcare systems may contribute to the higher incidence of congenital heart diseases in these countries. Previous studies have shown that lower income countries face a shortage of cardiac surgeons, with national socioeconomic status positively correlating with access to cardiac surgery (*21*). Therefore, the high mortality from congenital heart diseases in low HDI countries is likely due to limited access to healthcare. Improving healthcare accessibility and quality in these regions is crucial.

Our study revealed a negative correlation of HDI with the incidence and mortality of congenital musculoskeletal diseases. In previous studies, it was demonstrated that the distribution inequity of congenital musculoskeletal diseases was associated with national income, which was consistent with our findings (*22*). Therefore, in low and medium HDI countries, the abilities of these countries' healthcare systems are enhanced, and the experience of the countries that perform better with the same HDI level is learned.

It was illustrated in a past study that the annual change from 1990 to 2019 in the incidence and

mortality of urogenital congenital anomalies were negatively associated with HDI (*23*). Our research revealed a negative correlation between the HDI and the mortality rate of urogenital congenital abnormalities across various countries worldwide. Patients with urogenital congenital anomalies, regardless of whether they have abnormal kidney function at birth, require long-term and continuous monitoring of renal function (*24*). Close follow-up by renal specialists and protective measures for renal function, such as avoiding certain antibiotics and optimal timing for surgery, was crucial for the long-term survival of these patients (*24,25*). However, there is still a shortage of renal specialists in low HDI countries (*13,26,27*). To reduce the mortality rate of urogenital congenital anomalies in countries with low HDI, it is crucial to increase the number of renal specialists and improving the accessibility of healthcare services. The relationship between the incidence of urogenital congenital anomalies and HDI was not significant, possibly due to its development being impacted by both hereditary and environmental variables (*13,26,27*).

However, our study focused on the national disparities of ASIR and ASMR of neural tube defects, and we found a negative correlation of HDI with the incidence and mortality of neural tube defects. The leading cause of neural tube defects is pregnant women early in pregnancy if the lack of folic acid (*28,29*). The higher variability in the ASIR of neural tube defects across different countries underscores disparities in folic acid supplementation policies. Low HDI countries often face challenges in awareness and implementation of folic acid programs, leading to higher incidence rates. Nutritional deficiencies in these countries further exacerbate the risk of such birth defects, coupled with a lack of medical resources for early screening and diagnosis. Previous research has indicated that in developing countries, the coverage of folic acid supplementation is low (*28-31*). In contrast, in developed countries, the incidence of neural tube defects has decreased through public initiatives encouraging folic acid supplementation, even implementing fortified foods (*30,32,33*). Therefore, the initial step in low HDI countries is to enhance the crises of nutritional shortages and the healthcare systems. However, in the medium and high HDI countries, policies such as mandatory folic acid consumption and folic acid-enriched food supplements are important.

Our study found a positive correlation between ASIR of gastrointestinal congenital anomalies and HDI. In very high HDI countries, the advanced medical equipment and greater professional training of medical staff likely lead to more diagnosed cases of gastrointestinal anomalies, thus increasing the reported incidence rates. Residents in very high HDI countries may have more frequent exposure to certain environmental factors, such as the use of specific drugs and chemicals, that are linked to gastrointestinal anomalies (*34*). Additionally, the dietary habits inherent in modern lifestyles might also influence fetal development (*35*). We found a negative correlation between ASMR and HDI. Previous studies, consistent with our findings, showed that mortality for gastrointestinal congenital anomalies differs between developing and developed countries (*7*), highlighting the critical role of healthcare accessibility in reducing incidence and mortality.

5. Limitations

Firstly, the study relies on secondary data, which might be subject to reporting biases and inaccuracies, particularly in low and medium HDI countries. In future research, we would testify it in birth cohort so as to mitigate these biases. Secondly, the study identifies significant correlations, it does not establish causation. In our future research, causal relationships should be more explored. The HDI used in our study is highly sensitive to extreme values and cannot comprehensively reflect a national level of human development. Human Development Composite Indices could complement HDI to provide a more comprehensive evaluation of human development in future research (*9*). Thirdly, the estimation data utilized in this study may be subject to the influence of the restricted quality and scope of worldwide GBD data collection, particularly in low and medium HDI countries. Given these limitations, our analysis only demonstrates broad associations rather than causal relationships.

6. Conclusion

In conclusion, this study investigated the latest epidemiologic patterns of and risk factors for CBD at the global, regional, and national levels by HDI (such as education, literacy, GNI per capita, and life expectancy). Compared with other research, our research mainly provided the leading risk factors for the CBD disease burden in different HDI regions, which have important public health significance for the prevention of CBD all over the world.

Funding: This work was supported by the National Key R&D Program of China(2021YFC2701701).

Conflict of Interest: The authors have no conflicts of interest to disclose. The study's sponsors had no involvement in the research design, data collecting, data analysis, data interpretation, or report writing. The corresponding author was granted full access to the data in the study and took on the ultimate responsibility for deciding to submit it for publication.

References

1. Organizaton WH. Congenital disorders. *https://www.*

who.int/news-room/fact-sheets/detail/birth-defects (accessd January 8, 2024).
2. Zhou Y, Mao X, Zhou H, Wang L, Qin Z, Cai Z, Yu B. Birth Defects Data From Population-Based Birth Defects Surveillance System in a District of Southern Jiangsu, China, 2014-2018. Front Public Health. 2020; 8:378.
3. Lipinski RJ, Krauss RS. Gene-environment interactions in birth defect etiology: Challenges and opportunities. Curr Top Dev Biol. 2023; 152:1-30.
4. Kang L, Cao G, Jing W, Liu J, Liu M. Global, regional, and national incidence and mortality of congenital birth defects from 1990 to 2019. Eur J Pediatr. 2023; 182:1781-1792.
5. Data OWi. Gross national income (GNI) per capita, 2022. *https://ourworldindata.org/grapher/gross-national-income-per-capita* (accessd August 08, 2024).
6. Lee KS, Choi YJ, Cho J, Lee H, Lee H, Park SJ, Park JS, Hong YC. Environmental and Genetic Risk Factors of Congenital Anomalies: an Umbrella Review of Systematic Reviews and Meta-Analyses. J Korean Med Sci. 2021; 36:e183.
7. Mortality from gastrointestinal congenital anomalies at 264 hospitals in 74 low-income, middle-income, and high-income countries: a multicentre, international, prospective cohort study. Lancet. 2021; 398:325-339.
8. Wang H, Abbas KM, Abbasifard M, *et al*. Global age-sex-specific fertility, mortality, healthy life expectancy (HALE), and population estimates in 204 countries and territories, 1950–2019: a comprehensive demographic analysis for the Global Burden of Disease Study 2019. Lancet. 2020; 396:1160-1203.
9. Programme UND. Human Development Index | Human Development Reports. *https://hdr.undp.org/data-center/human-development-index#/indicies/HDI* (accessd January 08, 2024).
10. Li XY, Hou MJ, Kong XM, Lv JJ, Yang CH, Li DT, Zhang RH. The congenital birth defects burden in children younger than 14 years of age, 1990 - 2019: An age-period-cohort analysis of the global burden of disease study. J Glob Health. 2024; 14:04012.
11. Kuitunen I, Uimonen MM, Haapanen M, Sund R, Helenius I, Ponkilainen VT. Incidence of Neonatal Developmental Dysplasia of the Hip and Late Detection Rates Based on Screening Strategy: A Systematic Review and Meta-analysis. JAMA Netw Open. 2022; 5:e2227638.
12. Plana MN, Zamora J, Suresh G, Fernandez-Pineda L, Thangaratinam S, Ewer AK. Pulse oximetry screening for critical congenital heart defects. Cochrane Database Syst Rev. 2018; 3:Cd011912.
13. Murugapoopathy V, Gupta IR. A Primer on Congenital Anomalies of the Kidneys and Urinary Tracts (CAKUT). Clin J Am Soc Nephrol. 2020; 15:723-731.
14. Journel I, Andrécy LL, Metellus D, *et al*. Transmission of Zika Virus - Haiti, October 12, 2015-September 10, 2016. MMWR Morb Mortal Wkly Rep. 2017; 66:172-176.
15. Keasley J, Blickwedel J, Quenby S. Adverse effects of exposure to armed conflict on pregnancy: a systematic review. BMJ Glob Health. 2017; 2:e000377.
16. Higashi H, Barendregt JJ, Kassebaum NJ, Weiser TG, Bickler SW, Vos T. The burden of selected congenital anomalies amenable to surgery in low and middle-income regions: Cleft lip and palate, congenital heart anomalies and neural tube defects. Archives of Disease in Childhood. 2015; 100:233-238.
17. Liu Y, Chen S, Zühlke L, Black GC, Choy M-k, Li N, Keavney BD. Global birth prevalence of congenital heart defects 1970–2017: updated systematic review and meta-analysis of 260 studies. Int J Epidemiol. 2019; 48:455-463.
18. Minnella GP, Crupano FM, Syngelaki A, Zidere V, Akolekar R, Nicolaides KH. Diagnosis of major heart defects by routine first-trimester ultrasound examination: association with increased nuchal translucency, tricuspid regurgitation and abnormal flow in ductus venosus. Ultrasound Obstet Gynecol. 2020; 55:637-644.
19. Horn D, Edwards E, Ssembatya R, DeStigter K, Dougherty A, Ehret D. Association between antenatal ultrasound findings and neonatal outcomes in rural Uganda: a secondary analysis. BMC Pregnancy Childbirth. 2021; 21:756.
20. Becker DM, Tafoya CA, Becker SL, Kruger GH, Tafoya MJ, Becker TK. The use of portable ultrasound devices in low- and middle-income countries: a systematic review of the literature. Trop Med Int Health. 2016; 21:294-311.
21. Vervoort D, Meuris B, Meyns B, Verbrugghe P. Global cardiac surgery: Access to cardiac surgical care around the world. J Thorac Cardiovasc Surg. 2020; 159:987-996.e986.
22. Mody KS, Henstenburg J, Herman MJ. The Health & Economic Disparities of Congenital Musculoskeletal Disease Worldwide: An Analysis of 25 Years (1992-2017). Glob Pediatr Health. 2021; 8:2333794x21994998.
23. Huang X, Tang J, Chen M, Xiao Y, Zhu F, Chen L, Tian X, Hong L. Sex difference and risk factors in burden of urogenital congenital anomalies from 1990 to 2019. Sci Rep. 2023; 13:13656.
24. Nef S, Neuhaus TJ, Spartà G, Weitz M, Buder K, Wisser J, Gobet R, Willi U, Laube GF. Outcome after prenatal diagnosis of congenital anomalies of the kidney and urinary tract. Eur J Pediatr. 2016; 175:667-676.
25. Wühl E, van Stralen KJ, Verrina E, Bjerre A, Wanner C, Heaf JG, Zurriaga O, Hoitsma A, Niaudet P, Palsson R, Ravani P, Jager KJ, Schaefer F. Timing and Outcome of Renal Replacement Therapy in Patients with Congenital Malformations of the Kidney and Urinary Tract. Clin J Am Soc Nephrol. 2013; 8:67-74.
26. Nicolaou N, Renkema KY, Bongers EMHF, Giles RH, Knoers NVAM. Genetic, environmental, and epigenetic factors involved in CAKUT. Nature Reviews Nephrology. 2015; 11:720-731.
27. Kolvenbach CM, Shril S, Hildebrandt F. The genetics and pathogenesis of CAKUT. Nature Reviews Nephrology. 2023; 19:709-720.
28. Lu VM. Global, regional, and national epidemiological trends in neural tube defects between 1990 and 2019: a summary. Child's Nervous System. 2023; 39:3103-3109.
29. Viswanathan M, Urrutia RP, Hudson KN, Middleton JC, Kahwati LC. Folic Acid Supplementation to Prevent Neural Tube Defects: Updated Evidence Report and Systematic Review for the US Preventive Services Task Force. JAMA. 2023; 330:460-466.
30. Kancherla V, Botto LD, Rowe LA, *et al*. Preventing birth defects, saving lives, and promoting health equity: an urgent call to action for universal mandatory food fortification with folic acid. Lancet Glob Health. 2022; 10:e1053-e1057.
31. Gernand AD, Schulze KJ, Stewart CP, West KP,

Christian P. Micronutrient deficiencies in pregnancy worldwide: health effects and prevention. Nature Reviews Endocrinology. 2016; 12:274-289.
32. Toivonen KI, Lacroix E, Flynn M, Ronksley PE, Oinonen KA, Metcalfe A, Campbell TS. Folic acid supplementation during the preconception period: A systematic review and meta-analysis. Prev Med. 2018; 114:1-17.
33. Tong H, Walker N. Current levels of coverage of iron and folic acid fortification are insufficient to meet the recommended intake for women of reproductive age in low- and middle-income countries. J Glob Health. 2021; 11:18002.
34. Murase JE, Heller MM, Butler DC. Safety of dermatologic medications in pregnancy and lactation: Part I. Pregnancy. J Am Acad Dermatol. 2014; 70:401.e401-414; quiz 415.
35. Persson M, Cnattingius S, Villamor E, Söderling J, Pasternak B, Stephansson O, Neovius M. Risk of major congenital malformations in relation to maternal overweight and obesity severity: cohort study of 1.2 million singletons. BMJ. 2017; 357:j2563.

Received July 17, 2024; Revised August 22, 2024; Accepted August 24, 2024.

[§]These authors contributed equally to this work.
**Address correspondence to:*
Jie Yang, Department of Neonatology, Nanfang Hospital, Southern Medical University, Guangzhou, China
E-mail: jieyang0830@126.com

Released online in J-STAGE as advance publication August 27, 2024.

Original Article

DOI: 10.5582/bst.2024.01211

Evaluation of the value of *Synechococcus* 7942 as a sensitizer for photo-sonodynamic therapy against breast cancer

Ruimei Zhao[1,2,§], Pengfei Zhao[3,§,*], Ziyuan Zhou[4,§], Deliang Liu[3,§], Yang Zhou[3], Mingbin Zheng[3,5,*], Tetsuya Asakawa[3,*], Xin Kuang[1,*]

[1] Department of Anesthesiology, People's Hospital of Longhua, Shenzhen, Guangdong Province, China;
[2] Department of Anesthesiology, Hunan Aerospace Hospital, Changsha, Hunan Provence, China;
[3] Institute of Neurology, National Clinical Research Center for Infectious Diseases, Shenzhen Third People's Hospital, Shenzhen, Guangdong Province, China;
[4] National Cancer Center, National Clinical Research Center for Cancer, Cancer Hospital & Shenzhen Hospital, Chinese Academy of Medical Sciences and Peking Union Medical College, Shenzhen, Guangdong Province, China;
[5] Key Laboratory for Nanomedicine, Guangdong Medical University, Dongguan, Guangdong, Guangdong Province, China.

SUMMARY This study was conducted to investigate the value of *Synechococcus* 7942 (Syne) as a sensitizer for photo-sonodynamic therapy (PSDT). Syne was characterized. The efficacy of Syne-mediated PSDT were verified *in vitro* (in 4T1 breast cancer cells) and *in vivo* (in a breast tumor-bearing mouse model). The safety of Syne-mediated PSDT was verified *in vivo.* Results indicated that Syne triggered the generation of oxygen and ROS during PSDT, thereby inducing cell death in 4T1 cells. Syne-mediated PSDT induced the death of tumor cells both *in vitro* and *in vivo.* The speed of tumor growth was delayed in animals receiving PSDT. Syne-mediated PSDT was more effective than photodynamic therapy or sonodynamic therapy alone. In addition, administration of a Syne monomer resulted in satisfactory tumor targeting. Syne-mediated PSDT affected neither the animal body weight nor the major organs, indicating satisfactory safety. Accordingly, Syne is an efficient, safe, and readily available sensitizer that is ideal for potential clinical use of PSDT to treat breast cancer. The findings of this study are useful for exploration of a novel sensitizer for PSDT, which might be a promising alternative therapy against breast cancer.

Keywords sensitizer, *Synechococcus* 7942 (Syne), photo-sonodynamic therapy (PSDT), breast cancer

1. Introduction

Breast cancer is the most common malignancy among women and stands as the second leading cause of tumor-related death in women. Nevertheless, conventional strategies thus far, such as surgery, radiotherapy, and chemotherapy, have not achieved satisfactory efficacy, particularly in patients with cancer at an advanced stage. Due to the knotty nature of treatments against breast cancer, many alternative treatments were considered, and photodynamic therapy (PDT), sonodynamic therapy (SDT), and photo-sonodynamic therapy (PSDT, a combination of PDT and SDT) have garnered considerable attention (*1*).

PDT is a non-invasive cancer therapy based on generation of reactive oxygen species (ROS) triggered by activation of photosensitized agents with specific wavelengths of light. Use of PDT alone has many limitations, such as limited penetration (often less than 1 cm), uncertain efficacy, potential damage to normal cells, and the generation of tolerance in targeted cells (*1*), which have further limited the use of PDT. SDT is another therapy that is also based on the generation of ROS. It has satisfactory penetration (often more than 8 cm) and less damage to normal cells/tissues (*1*). Due to the deep penetration and greater focusing of ultrasound, SDT is often combined with PDT to provide a more practical PSDT for use in cancer treatment. Early in 2000, Zhao *et al*. reported that combined use of PDT and SDT resulted in tumor necrosis approximately 2-3 times deeper than use of either therapy alone in mice with squamous cell carcinoma of the skin (*2*). PSDT has been used to treat breast cancer. Liu *et al*. used composite peptide amphiphile-indocyanine green (ICG) nanomicelles in conjunction with a sono-/photosensitizer of ICG encapsulation for combined SDT, PDT, and photothermal therapy (PTT). They found that this treatment had ideal efficacy in both *in vivo* and *in vitro*

breast cancer models (*3*). Zheng *et al*. used a carrier-free nanosensitizer, oleanolic acid (OC), consisting of an anti-cancer drug, oleanolic acid, and a photosensitizer, chlorin e6 (Ce6), to treat orthotopic 4T1 breast tumor-bearing mice. They found that self-assembled carrier-free nanosensitizer OC satisfactorily mediated the efficacy of PSDT to treat breast cancer-bearing mice (*4*). Moshfegh *et al*. used hematoporphyrin as a sensitizer for PSDT, and they found that hematoporphyrin-mediated PSDT delayed tumor growth (*5*). Learning from these previous studies, we understand that selection of an ideal sensitizer might play a vital role in achieving efficacious PDT, SDT, and PSDT.

An ideal sensitizer for PDT, SDT, and particularly for PSDT should have several characteristics: *i*) It should have satisfactory biocompatibility so it can thus be used in both PDT and SDT (good as both a photosensitizer and sonosensitizer). Importantly, it should enhance the synergistic effects of PDT and SDT. *ii*) It should have the ability to trigger the generation of ROS. *iii*) It has good solubility and aggregation to avoid ROS quenching (*6*). *iv*) Its safety and efficacy can be verified. *v*) It should be easily synthesized or produced (ready availability). To have these characteristics, sensitizers were often modified using nanotechnology-based technologies in particular. So far, several modified sensitizers for PSDT to treat breast cancer have been reported, such as OC (*4*), Ce6 (*4,7*), hematoporphyrin (*5*), cationic morpholino-phthalocyanines conjugated to nitrogen and nitrogen-sulfur doped graphene quantum dots (*8*), and sinoporphyrin sodium (DBDMS) (*9*). However, all of these sensitizers have their special advantages and weaknesses. Accordingly, exploration of a novel sensitizer for PSDT to treat breast cancer is an indispensable task for researchers. Cyanobacteria, a group of non-pathogenic bacteria, are coming into the picture due to their capacity to produce large volumes of oxygen (*10*). A previous study by our laboratory found that *Synechococcus* 7942 (Syne), a cyanobacterium, mediated the efficacy of PDT to treat breast cancer by relieving tumor hypoxia and enhancing the generation of ROS (*11*). Moreover, Syne is moderately effective at immune stimulation. Hence, Syne has been identified as a good photosensitizer for PDT (*11*). Based on the findings of the previous study, we hypothesized that Syne is also a good sonosensitizer that could display anti-tumor action in PSDT as well. We therefore conducted the current study to verify whether Syne can exhibit its efficacy as a sensitizer for PSDT in breast cancer models. We believe the findings of the current study will facilitate for exploration of novel sensitizers for PSDT, which is an important promising alternative therapy against breast cancer.

2. Materials and Methods

2.1. Materials and animals

Syne was purchased from the freshwater algae seed bank of the Institute of Aquatic Biology (FACHB, Wuhan, China). 4T1 breast cancer cells were obtained from the cell culture bank of the Chinese Academy of Sciences (CAS, Shanghai, China).

A total of 42 BALB/c mice (female, 6 weeks old, weighing 15–18 g, Beijing Charles River Laboratory Animal Technology, Ltd, Beijing, China) were used in this study. Mice were raised under conditions of 60% humidity, room temperature of 23°C, and a 12-h light-dark rhythm (7:00 AM–7:00 PM) with food and water freely available.

They were treated in strict compliance with the National Institutes of Health Guidelines for the Care and Use of Laboratory Animals. All experiments were approved of and supervised by the Animal Ethics Committee of the Shenzhen Third People's Hospital (approval number 2022-018)

2.2. Experimental design

Experiments included the confirmation of the characterization of Syne, evaluation of Syne-related photosynthetic oxygen production and photo-sonodynamic effects, and verification of the efficacy of Syne in photo-sonodynamic treatments *in vitro* and *in vivo*. The protocol for this study is shown in Figure 1.

2.3. Conformation of the characterization of Syne

Syne solution samples were subjected to UV-visible spectrophotometry (B-600 Ultra-micro–UV Spectrophotometer, METASH, China). Absorbance was configured to confirm the absorption peaks of Syne solutions.

2.4. Evaluation of Syne-related photosynthetic oxygen production and photo-sonodynamic effects

Oxygen production by Syne solutions at concentrations of 1, 2.5, 5, and 10 $\times 10^7$ CFU/mL in 30 min, as well as at times of 0, 10, 20, 30, 40, 50, 60 min at 1×10^8 CFU/mL was detected using a dissolved oxygen meter (S4 -Standard Kit, METTLER TOLEDO, Shanghai, China). The probe of the oxygen-dissolving instrument was inserted into the Syne solutions, and the dissolved oxygen levels were measured in real time. Wavelength was selected as λ = 660 nm in light of a previous study (*11*). ROS production was detected with a 2′,7′-dichlorofluorescence diacetate (DCFH-DA) probe (Sigma, St. Louis, USA) ex/em: λ = 485/525 nm.

Then, 2 mL of each Syne solution (10 $\times 10^7$ CFU/mL) was placed into five dishes, mixed with 10 μL of DCFH-DA, and treated user the following conditions. The Syne group was the control without any treatment. The Syne + US group was treated with an ultrasound probe (1.0 W/cm2, 50% duty cycle, XK-2011R, Xingkang Ltd,

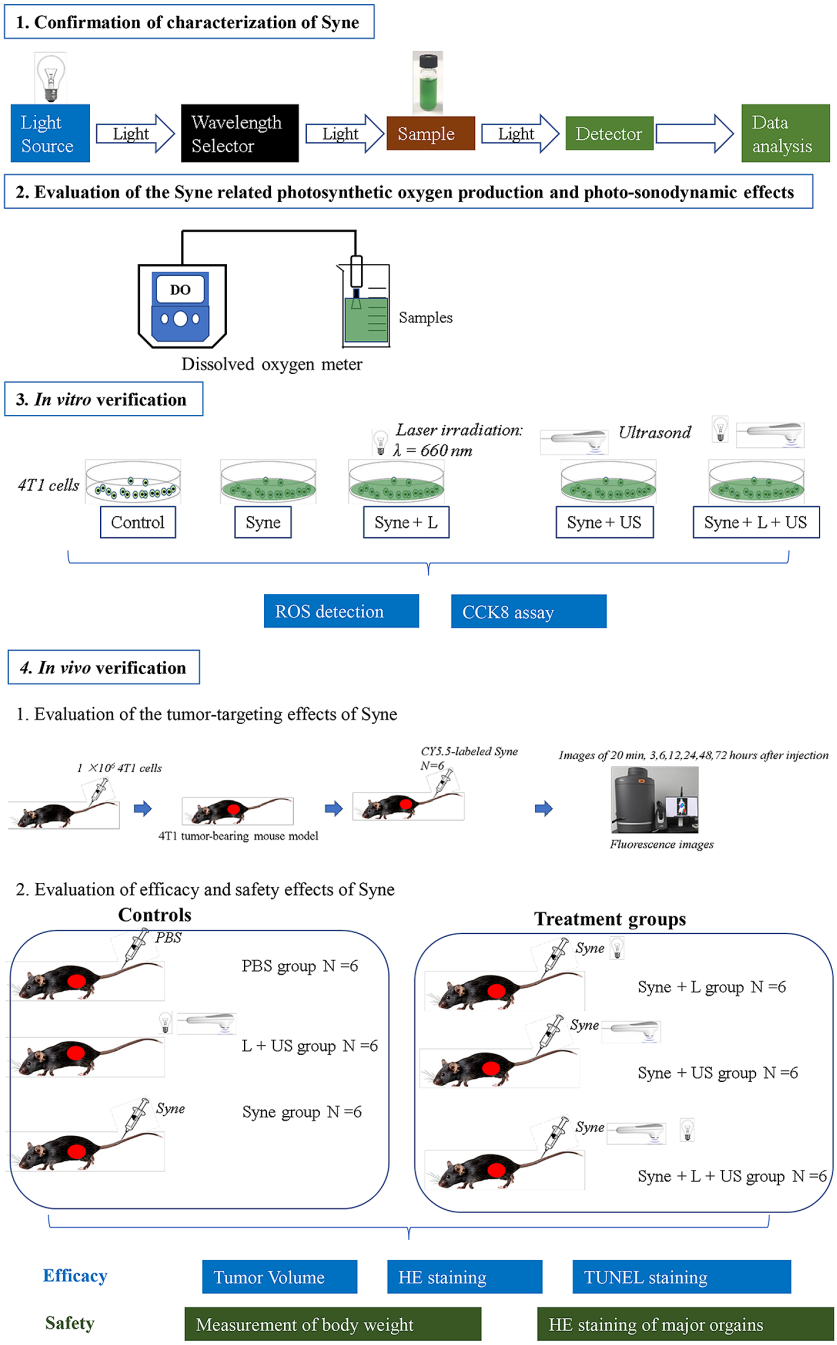

Figure 1. Protocol of the current study.

Wuhan, China) for 8 min. The Syne + L + US group was treated with laser irradiation (λ = 660 nm, LWRL, Laserwave, Beijing, China) for 1 min followed by the aforementioned ultrasound treatment. After the initiation of the treatments, a 100-μL sample of the Syne solution was extracted every minute from each group and placed into a 96-well plate. The fluorescence intensity of each well was observed and measured using a microplate reader (Model, Biotek Instruments, Vermont, USA)

2.5. *In vitro* verification of the efficacy of Syne in photo-sonodynamic treatments

4T1 breast cancer cells were seeded in 96-well plates and incubated in 37°C, 5% CO_2 for 24 h. When the cells covered approximately 80% of the plate bottom, they could be used for subsequent experiments. Then, cells were divided into 5 groups. The Control group was the intact 4T1 cells (1×10^4 cells/well) with distilled water and incubated at 37°C in 5% CO_2 for 3 h. Syne-related groups were prepared by incubating Syne (1×10^7 CFU/mL) with 4T1 cells (1×10^4 cells/well) at 37°C in 5% CO_2 for 3 h for subsequent experiments. The Syne group was only the Syne solution without any treatments. The Syne + L group was treated with laser irradiation (λ = 660 nm) for 1 min. The Syne + US group was treated with an ultrasound probe (1.0 W/cm^2, 50% duty cycle, XK-2011R, Xingkang Ltd, Chengdu, China) for 3

min. The Syne + L + US group was treated with laser irradiation followed by ultrasound treatment with the aforementioned parameters. After the treatments, all samples were incubated at 37℃ in 5% CO_2 for 24 h for subsequent CCK8 assays. Each group included at least 5 wells for repetition of the experiments.

A conventional CCK8 assay was used to assess cellular viability. For preparation of the CCK8 reagent, 10 μL of the original CCK8 solution (Beyotime, Shanghai, China) was mixed with 90 μL of 1640 medium. This mixture was added to a well, and cells in each group (1×10^4 cells/well) were incubated at 37℃ in 5% CO_2 for 10 min. Fluorescence images of ROS generation were obtained by confocal microscopy (SpinSR, Olympus, Tokyo, Japan). Absorbance was measured at a wavelength of 450 nm using an enzyme meter. The optical density (OD) values of each well were recorded, and the cell viability in each group was calculated using the formula: Cell viability (%) = (OD treatment group - OD blank group) / (OD control group - OD blank group) × 100%.

DCFH-DA and Hoechst staining were also performed to check the generation of ROS and the nucleus of 4T1 cells. Analogous with the aforementioned experiments measuring ROS generation, 4T1 cells (2×10^4 cells per well) were cultured in an 8-well culture chamber. When the cells covered 80% of the chamber, they were used for subsequent experiments. For the Syne-related groups, Syne (1×10^7 cells/mL) was added to the cells, and the mixture was incubated for 3 h. Then, the supernatant was discarded and 200 μL of fresh culture medium containing 10 μL DCFH-DA (1 mg/mL) was added, and the mixture was incubated for 30 min. Then, cells were grouped and treated as described earlier. After the treatments, cells were incubated for 2 h and washed with PBS twice. Then, fresh medium containing Hoechst 33258 was added, and cells were stained for 30 min. Fluorescence images of ROS generation were obtained by confocal microscopy (CLSM) to determine the amount of ROS. The average fluorescence intensity of the fluorescence images was semi-quantitatively analyzed using the software ImageJ (ImageJ1.51K, NIH, USA).

For viability/cytotoxicity assay, all groups of cells after treatments were returned to the incubator and incubated at 37°C in 5% CO_2 for 21 h. Then, the cells were incubated with prepared Calcein and propidium iodide (PI) in the dark for 1 hour. Cell staining was examined using a fluorescence microscope (BZ-X800E, Keyence, Tokyo, Japan, ex/em: λ = 545/605 nm).
Semi-quantitative analyses were also performed to calculate the ROS intensity, cell viability, and PI intensity.

2.6. *In vivo* verification of the efficacy and safety of Syne in photo-sonodynamic treatments

Anesthetized with isoflurane in a special chamber exposed to 5% isoflurane mixed with 95% O_2 for 4 min (*12*), 42 BALB/c mice were injected with 4T1 cells (1×10^7 cells/mL, 0.1 mL) on the outer posterior side of the right lower limb root to create the breast tumor-bearing mouse model. After the injection, animals were returned to normal conditions. Once the tumor grew to experimental size (approximately 0.1 cm^3), animals were used in subsequent experiments.

Six mice were used to confirm tumor targeting by Syne. Twenty μL of Cy5.5 (10 mM, 1 mL in DMSO, Thermo Fisher Scientific, USA) was added to the Syne solution (5×10^8 CFU/mL, 2mL), and the mixture was incubated for 60 min at room temperature. Then, the solutions were adjusted to 5×10^8 CFU/mL to prepare the CY5.5-labeled Syne solutions. CY5.5-labeled Syne (0.1 mL) was injected into the animals *via* the tail vein. After injection of the CY5.5-labeled Syne for 20 min, animals were anesthetized with isoflurane and placed into a fluorescence imager for small animals (IVIS, Caliper Life Sciences, USA) to observe the distribution and accumulation of Syne over time. Data were recorded at 7 time points, namely 20 min, 3, 6, 12, 24, 48, and 72 h after injection.

The remaining animals were divided into 6 groups (n = 6 for each group): The Control groups included 3 groups, namely the PBS group (injection of 0.1 mL of PBS *via* the tail vein), the L + US group (animals underwent laser irradiation followed by ultrasound treatment), the Syne group (injection of Syne *via* the tail vein), the Syne + L group (injection of Syne and treatment with laser irradiation), the Syne + US group (injection of Syne and treatment with ultrasound), and the Syne + L + US group (injection of Syne and treatment with laser irradiation followed by ultrasound treatment). Parameters for treatments were: injection of Syne (0.1 mL, 5×10^8 CFU/mL); laser irradiation (λ = 660 nm, 0.1 W/cm^2, 30 min); and ultrasound treatment (1.0 W/cm^2, 50% duty cycle, 5 min). Tumor size and body weight were monitored for 16 days. Standard hematoxylin and eosin (HE) staining was used to check for changes in the major organs (heart, liver, spleen, lungs, and kidneys) of animals after observation for 16 days. In addition, HE staining and TUNEL staining were also used to compare the tumor in the PBS group and the Syne + L + US group. Animals were euthanized by asphyxiation with CO_2, and the major organs (heart, liver, spleen, lungs, and kidneys) were removed and fixed with 4% paraformaldehyde for 1 h and then dehydrated with a sucrose solution. Then, the organs were placed in optimal cutting temperature medium (Sakura Tissue Tek, West Chester, PA) overnight at −80 °C. A Leica cryomicrotome (CM1510, Leica Nussloch, Germany) was used to make frozen sections (6 μm), which were subjected to HE and TUNEL staining. For HE staining, the frozen sections were washed in water and stained in hematoxylin for 2 min. Then, the slides were rinsed in 95% ethanol and stained with eosin for 10 sec and washed with tap water.

The remaining slides were subjected to TUNEL staining. Slides were washed with PBS and placed in 0.1% Triton X-100 and 0.1% sodium citrate for 2 min on ice. Then, slides were incubated with TUNEL reaction mixture with deoxyribonucleotide transferase (TdT) and the fluorescent label (tetramethlylrhodamine-conjugated nucleotides) in a humidified chamber in the dark for 1 hour at 37℃. After slides were washed with PBS, they were mounted with 50% glycerin in PBS. All of the stained slides were observed with a microscope (BX53, Olympus, Tokyo, Japan)

2.7. Statistical analysis

The software GraphPad Prism (V8.0.2, GraphPad Software, MA, USA) was used for statistical analysis. The normal distribution of experimental data was checked using the Kolmogorov-Smirnov test. Data are expressed as the mean ± standard deviation. A two-tailed analysis of variance (ANOVA) with Tukey post-hoc correction was used for multi-comparisons. Each experiment was repeated at least 3 times, and the results were averaged. $P < 0.05$ was considered to be a significant difference.

3. Results

3.1. Characterization of Syne

UV-visible spectrophotometry indicated that Syne exhibited relatively strong absorption peaks at 631 nm and 683 nm (Figure 2), which confirmed that the Syne used in this study was activated by strong near-infrared light and enabled photosynthetic oxygen production (*13*).

3.2. Evaluation of Syne-related photosynthetic oxygen production and its photo-sonodynamic effects

Figure 3 shows the results of verifying Syne's photosynthetic oxygen production and photo-sonodynamic effects. Oxygen bubbles were observed when the Syne solution was irradiated with laser light (λ = 660 nm, Figure 3A). With increasing concentrations of Syne, the release of oxygen increased accordingly (Figure 3B). With an increasing irradiation time, the release of oxygen increased accordingly (Figure 3C). The FCFH-DA FL intensity ratio increased over time. Results were Syne + L + US > Syne + US > Syne (Figure 3D). These results confirmed the photosynthetic oxygen production and photo-sonodynamic effects of the Syne solution used in this study.

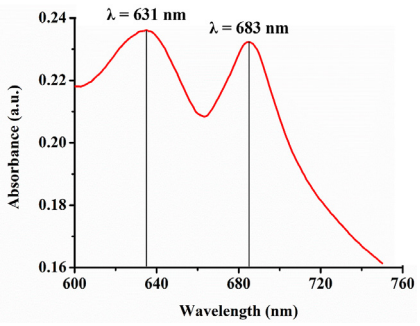

Figure 2. Data from UV-visible spectrophotometry.

3.3. Verification of the efficacy of Syne in photo-sonodynamic treatments *in vitro*

Figure 4 shows the efficacy of photo-sonodynamic treatments with Syne *in vitro*. Compared to the control, the four groups stained green, indicating the generation of ROS. The volume of ROS production was Syne + L + US > Syne + US > Syne + L > Syne (Figure 4A). Semi-quantitative analyses confirmed that production of ROS in the Syne + L + US group was significantly higher than that in the other groups ($p < 0.05$, Figure 4B). In terms of the cellular viability of breast cancer cells assessed with a CCK8 assay, 61% of cells in the Syne + L + US group died. The cellular survival rates were control > Syne > Syne + L > Syne + US > Syne + L + US, where Syne + L + US was the lowest ($p < 0.001$, *vs.* Syne + US group, Figure 4C). In terms of cellular cytotoxicity, PI intensity (red, dead cells) was Syne + L + US > Syne + US > Syne + L > Syne ($p < 0.001$, *vs.* Syne + US group, Figures 4D, E), indicating that cytotoxic effects were strongest in the Syne + L + US group. These experiments yielded similar results, namely the efficacy against

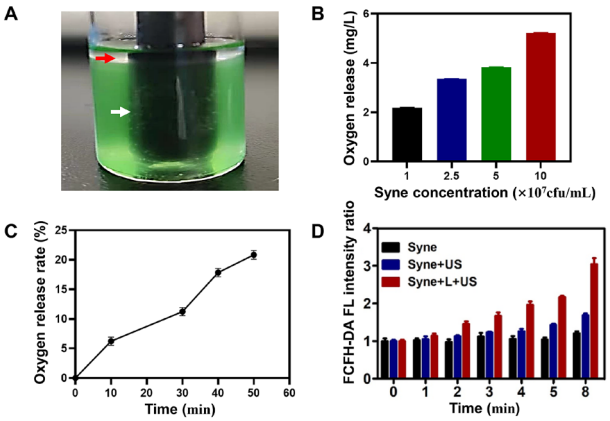

Figure 3. Verification of the photosynthetic oxygen production by and photo-sonodynamic effects of Syne solutions. (A), Oxygen bubbles appeared once the Syne solution was irradiated with a laser light (λ = 660 nm). The white arrow points to oxygen bubbles, and the red arrow points to an ethyl acetate layer at the top of solution. **(B)**, Release of oxygen increased in Syne solutions with increasing concentrations (1–10 × 10^7 CFU/mL) when they were irradiated for 30 min under a laser light (λ = 660 nm). **(C)**, Release of oxygen increased with the increasing irradiation time (0–60 min) when a Syne solution (1 × 10^8 CFU/mL) was irradiated under a laser light (λ = 660 nm). **(D)**, Verification of the photo-sonodynamic effects on the Syne solutions (1 × 10^8 CFU/mL) which were used in ultrasonic therapy (Syne + US, 1.0 Wcm^{-2}, 50% duty cycle, 8 min) or ultrasonic therapy with laser irradiation (Syne + L + US, 660 nm laser irradiation, 8 min). An intact solution (Syne) was used as the control.

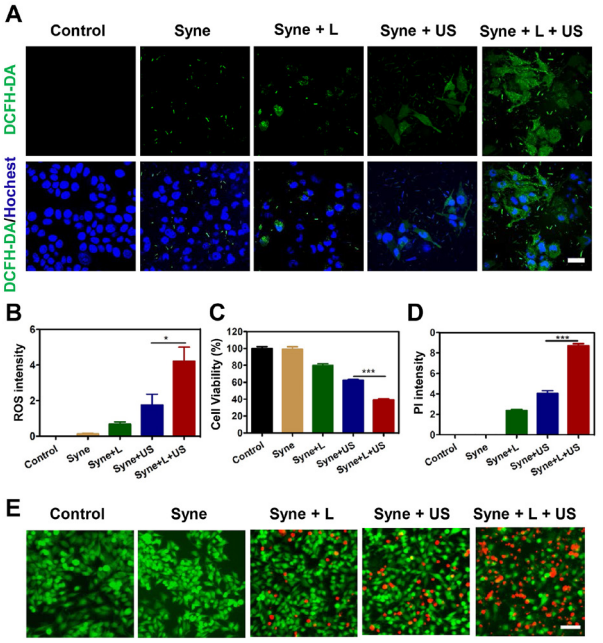

Figure 4. Evaluation of the efficacy of photo-sonodynamic treatments involving Syne *in vitro*. (A), Generation of singlet oxygen by different treatments involving Syne according to ROS staining. ROS are in green, and Hochest+ 4T1 cells are in blue. Bar = 20 μm. **(B)**, Semi-quantitative analysis of ROS average fluorescence intensity in different groups. **(C)**, Cell viability of 4T1 cells in different groups (n = 3). **(D)**, Semi-quantitative analysis of average PI fluorescence intensity in different groups. **(E)**, CLSM of 4T1 cells stained with Calcein-AM (green) and PI (red) as a result of different treatments involving Syne, Bar = 50 μm. Syne + L = laser irradiation, Syne + US = ultrasonic therapy, Syne + US + L = laser irradiation + ultrasonic therapy. Data = mean ± standard deviation, *means $p < 0.05$, ***means $p < 0.001$.

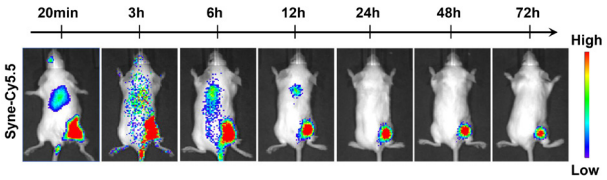

Figure 5. Confirmation of the delivery of tumor-targeting Syne with Syne-Cy5.5 fluorescence images in 4T1 tumor-bearing mice.

breast cancer cells was Syne + L + US > Syne + US > Syne + L. Accordingly, the strongest efficacy of photo-sonodynamic treatments was verified *in vitro*.

3.4. Verification of the efficacy of Syne in photo-sonodynamic treatments *in vivo*

Figure 5 shows the tumor targeting by Syne in a breast tumor-bearing mouse model. The fluorescence signal was detected throughout the body after administration of CY5.5-labeled Syne *via* the tail vein. Then, the labeled Syne gradually distributed and accumulated around the tumor over time. These results indicated that Syne satisfactorily targeted tumors and could be potentially used in subsequent photo-sonodynamic treatments (Figure 5).

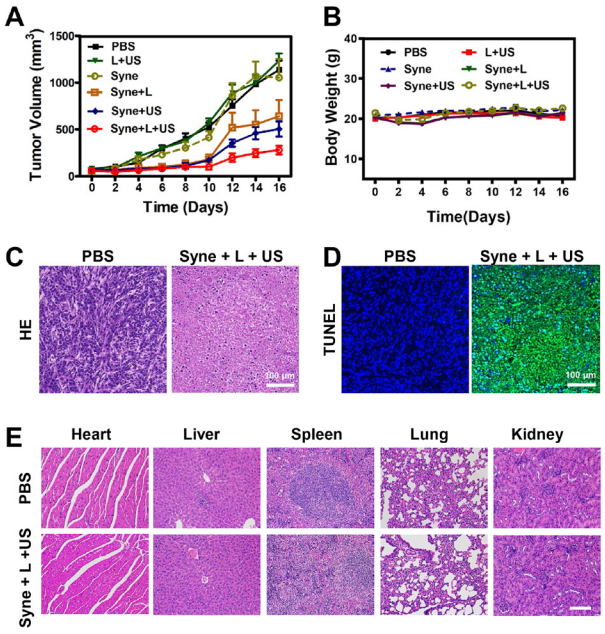

Figure 6. Verification of the efficacy of Syne in photo-sonodynamic treatment of tumors *in vivo*. (A), Data on tumor volumes (n = 6). **(B)**, Body weight of animal subjects (n = 6). **(C)**, Representative images of HE staining of tumor sections. **(D)**, Representative images of TUNEL staining of tumor sections. **(E)**, Representative images of HE staining of sections of major organs. Bar = 100 μm.

Figure 6 shows the efficacy and safety of Syne in treating the breast tumor-bearing mice. Tumor volume increased over time. Tumor growth was slowest in the Syne + L + US group. The speed of tumor growth was non-Syne groups (PBS, L + US, Syne) > Syne + L > Syne + US > Syne + L + US (Figure 6A). The results of HE staining (Figure 6C) and TUNEL staining (Figure 6D) indicated a large amount of cell death and histological disintegration in the Syne + L + US group (*vs.* PBS group). This verified the apoptosis and necrosis of tumor lesions induced by Syne + L + US treatment.

In terms of safety, the body weights of animals in each group did not change during the 16-day treatments, indicating that treatments had negligible toxicity (Figure 6B). Moreover, examination of the HE stained images of major organs in the treatment groups, including the heart, liver, spleen, lungs, and kidneys, revealed no significant histopathological lesions. The safety of photo-sonodynamic treatment was therefore verified (Figure 6E).

4. Discussion

The current study verified the value of Syne as a sensitizer for PSDT to treat breast cancer in 4T1 breast cancer cells and a breast tumor-bearing mouse model. Experiments *in vitro* indicated that Syne had the capacity to trigger the generation of oxygen and ROS during PSDT, thereby inducing cell death in 4T1 cells. *in vivo* results revealed ideal efficacy and safety when animals underwent PSDT. The current results suggest that Syne

is an ideal photosensitizer and sonosensitizer that may mediate efficacious PSDT in treating animals with breast cancer. To the extent known, this is the first study to evaluate the value of Syne as a sensitizer for PSDT. The findings of the current study are useful for further developing Syne-mediated PSDT as an alternative therapy to treat breast cancer.

4.1. Characterization of Syne

When irradiated with laser light (λ = 660 nm), Syne significantly triggered the generation of oxygen (Figures 3A-C). This effect was dose-dependent (Figure 3B) and time-dependent (Figure 3C), indicating that Syne can serve as a photosensitizer. These results agree with those of a previous study (*11*). A time-effect relationship was evident in the Syne + US group (Figure 4C), indicating that Syne also can be used as a sonosensitizer. Efficacy was significantly higher in the Syne + L + US group than in the Syne + US group, indicating a remarkable synergistic effect of PDT and SDT (Figure 3D). Thus, Syne is an ideal sensitizer for PSDT. In addition, these experiments were performed using the Syne monomer without any modification like integration with nanoparticles, which suggests that Syne itself can be used directly as a sensitizer in subsequent experiments without sophisticated modifications.

4.2. Verification of the efficacy of Syne in PSDT *in vitro*

When 4T1 breast cancer cells were used, Syne triggered the generation of ROS (Figures 4A, B) and induced the death of tumor cells (Figures 4A, C-E) as part of Syne + L, Syne + US, and Syne + L + US. In addition, the effect intensity was Syne + L + US (PSDT) > Syne + US (SDT) > Syne + L (PDT) > Syne (Control). These results confirmed that Syne was efficacious in combined PDT and SDT, and this efficacy was significantly better than that of PDT or SDT alone. Moreover, results seem to imply that the tumor cells were more sensitive to SDT (*vs.* PDT) mediated by Syne. These results differed from those of previous studies in which therapy was mediated by Ce6 (*14*) and DBDMS (*9*), which indicated that cells were more sensitive to PDT (*vs.* SDT). A plausible interpretation might be that the sensitivity of PDT and SDT varies with different sensitizers. This issue warrants further investigation in the future.

4.3. Verification of the efficacy of Syne in PSDT *in vivo*

Results suggested that Syne satisfactorily targeted tumors without any complicated processes such as integration with nanoparticles (Figure 5). Importantly, this confirmed the satisfactory availability of Syne. It is easy to prepare and produce in comparison to the previously reported sensitizers. Thus, Syne is a good candidate for future clinical use. In terms of efficacy, Syne-mediated PDST resulted in the slowest tumor growth, and the speed of tumor growth was Syne + L > Syne + US > Syne + L + US (Figure 6A). These results were in accordance with the current results *in vitro*, confirming that Syne mediated the efficacy of SDT > PDT. Moreover, HE staining (Figure 6C) and TUNEL staining (Figure 6D) indicated that PSDT was efficacious against tumor cells *in vivo*. In terms of safety, PSDT mediated by Syne did not affect the body weight (Figure 6B) and major organs (Figure 6E) of the animal subjects. Accordingly, the safety and efficacy of PDST mediated by Syne were verified.

4.4. Limitations

This study had several limitations that might have led to biased conclusions: *i*) The sample size of animals in each group was too small, and *ii*) The effects of Syne + US + L (SPDT) were not evaluated since previous studies revealed marked differences between PSDT and SPDT (*9,14*). All of these limitations will be addressed in subsequent studies.

5. Conclusions

The current study characterized Syne and it investigated the efficacy and safety of Syne-mediated PSDT to treat breast cancer *in vitro* and *in vivo*. Results indicated that Syne is effective at triggering the generation of ROS. Syne-mediated PSDT exhibited satisfactory efficacy against 4T1 breast cells and in a breast tumor-bearing mouse model. The safety of Syne-mediated PSDT was also verified. Moreover, Syne exhibited ideal availability since it did not require sophisticated modifications. Accordingly, Syne is an efficient, safe, and readily available sensitizer, which is ideal for potential clinical use in PSDT to treat breast cancer.

Funding: This work was supported by the National Key R&D Program of China (nos.: 2023YFA0915600, 2023YFC2308300), the Natural Science Foundation of China (nos.: 82372271 and 22107045), Key Area Projects for Universities in Guangdong Province (no.: 2022DZX2022), the Guangdong Provincial Key Laboratory of Advanced Biomaterials (no.: 2022B1212010003), the Shenzhen Science and Technology Program (nos.: JCYJ20220530163005012, JCYJ20210324115611032, and JCYJ20210324132012035), the Shenzhen Clinical Medical Center for Emerging infectious diseases (no.: LCYSSQ20220823091203007), the Shenzhen Clinical Research Center for Tuberculosis (no.: 20210617141509001), the Shenzhen High-level Hospital Construction Fund (nos.: 23274G1001, 23250G1005, 24250G1027, and 24250G1019), and the National Cancer Center/National Clinical Research Center for Cancer/ Cancer Hospital & Shenzhen Hospital, Chinese Academy

of Medical Sciences and Peking Union Medical College, Shenzhen (nos.: E010221005 and CFA202201006).

Conflict of Interest: The authors have no conflicts of interest to disclose.

References

1. Hu H, Zhao J, Ma K, Wang J, Wang X, Mao T, Xiang C, Luo H, Cheng Y, Yu M, Qin Y, Yang K, Li Q, Sun Y, Wang S. Sonodynamic therapy combined with phototherapy: Novel synergistic strategy with superior efficacy for antitumor and antiinfection therapy. J Control Release. 2023; 359:188-205.
2. Jin ZH, Miyoshi N, Ishiguro K, Umemura S, Kawabata K, Yumita N, Sakata I, Takaoka K, Udagawa T, Nakajima S, Tajiri H, Ueda K, Fukuda M, Kumakiri M. Combination effect of photodynamic and sonodynamic therapy on experimental skin squamous cell carcinoma in C3H/HeN mice. J Dermatol. 2000; 27:294-306.
3. Liu Z, Li J, Chen W, Liu L, Yu F. Light and sound to trigger the Pandora's box against breast cancer: A combination strategy of sonodynamic, photodynamic and photothermal therapies. Biomaterials. 2020; 232:119685.
4. Zheng Y, Li Z, Yang Y, Shi H, Chen H, Gao Y. A nanosensitizer self-assembled from oleanolic acid and chlorin e6 for synergistic chemo/sono-photodynamic cancer therapy. Phytomedicine. 2021; 93:153788.
5. Moshfegh S, Jadidi M, Hasanzadeh H, Nasr R, Mirmohammadkhani M. Efficacy of Hematoporphyrin mediated photo-sonodynamic therapy on mice breast cancer. Intl J Rad Res. 2022; 20:555-561.
6. Yang Y, Fan Z, Zheng K, Shi D, Su G, Ge D, Zhao Q, Fu X, Hou Z. A novel self-targeting theranostic nanoplatform for photoacoustic imaging-monitored and enhanced chemo-sonodynamic therapy. J Mater Chem B. 2021; 9:5547-5559.
7. Sun D, Zhang Z, Chen M, Zhang Y, Amagat J, Kang S, Zheng Y, Hu B, Chen M. Co-immobilization of Ce6 sono/photosensitizer and protonated graphitic carbon nitride on PCL/gelation fibrous scaffolds for combined sono-photodynamic cancer therapy. ACS Appl Mater Interfaces. 2020; 12:40728-40739.
8. Nene LC, Nyokong T. Photo-sonodynamic combination activity of cationic morpholino-phthalocyanines conjugated to nitrogen and nitrogen-sulfur doped graphene quantum dots against MCF-7 breast cancer cell line *in vitro*. Photodiagnosis Photodyn Ther. 2021; 36:102573.
9. Liu Y, Wang P, Liu Q, Wang X. Sinoporphyrin sodium triggered sono-photodynamic effects on breast cancer both *in vitro* and *in vivo*. Ultrason Sonochem. 2016; 31:437-448.
10. Cohen JE, Goldstone AB, Paulsen MJ, *et al*. An innovative biologic system for photon-powered myocardium in the ischemic heart. Sci Adv. 2017; 3:e1603078.
11. Liu L, He H, Luo Z, Zhou H, Liang R, Pan H, Ma Y, Cai L. In situ photocatalyzed oxygen generation with photosynthetic bacteria to enable robust immunogenic photodynamic therapy in triple-negative breast cancer. Advanced Functional Materials. 2020; 30:1910176.
12. Gielis JF, Jungraithmayr W, Boulet GA, Bogers JP, Weder W, Cos P, Van Schil PEY. A murine model of lung ischemia and reperfusion injury: Tricks of the trade. J Surg Res. 2015; 194:659-666.
13. Fushimi K, Narikawa R. Cyanobacteriochromes: Photoreceptors covering the entire UV-to-visible spectrum. Curr Opin Struct Biol. 2019; 57:39-46.
14. Wang P, Li C, Wang X, Xiong W, Feng X, Liu Q, Leung AW, Xu C. Anti-metastatic and pro-apoptotic effects elicited by combination photodynamic therapy with sonodynamic therapy on breast cancer both *in vitro* and *in vivo*. Ultrason Sonochem. 2015; 23:116-127.

Received July 24, 2024; Revised August 14, 2024; Accepted August 18, 2024.

[§]These authors contributed equally to this work.
**Address correspondence to:*
Xin Kuang, Department of Anesthesiology, People's Hospital of Longhua, 38 Jinglong construction Road, Shenzhen, Guangdong Province 518109, China.
E-mail: kx6924@126.com

Tetsuya Asakawa, Mingbin Zheng, and Pengfei Zhao, Institute of Neurology, National Clinical Research Center for Infectious Diseases, Shenzhen Third People's Hospital, 29 Bulan Road, Shenzhen, Guangdong Province 518112, China.
E-mail: asakawat1971@gmail.com (TA), mingbinzheng@126.com (MZ), pengfeizhao@aliyun.com (PZ)

Released online in J-STAGE as advance publication August 22, 2024.

Original Article

DOI: 10.5582/bst.2024.01149

SEC24C suppresses the propagation and chemoresistance of hepatocellular carcinoma by promoting unfolded protein response-related apoptosis

Xuewen Tao[1,2,§], Haowei Wei[3,§], Shuai Mao[2,4,§], Jincheng Wang[2,5,§,*], Cailin Xue[3], Weiwei Yu[3], Yuze Shi[3], Yang Liu[1,2,*], Beicheng Sun[1,2,*]

[1] School of Medicine, Southeast University, Nanjing, Jiangsu, China;
[2] Department of General Surgery, The First Affiliated Hospital of Anhui Medical University, Hefei, Anhui, China;
[3] The Affiliated Drum Tower Hospital of Nanjing University Medical School, Nanjing, Jiangsu, China;
[4] Lianyungang oriental hospital, Lianyungang, Jiangsu, China;
[5] Graduate School of Medical Science and Engineering, Hokkaido University, Sapporo, Japan.

SUMMARY Cells routinely utilize the unfolded protein response (UPR) to alleviate endoplasmic reticulum (ER)-stress or trigger about apoptotic death under extreme ER-stress conditions. Tumor cells are subjected to persistent ER-stress due to their crowded microenvironment, but can maintain hyperactive proliferation under most stressful conditions. Therefore, understanding strategies employed by cancer cells to escape from UPR-related apoptosis has important medical implications. SEC24 homolog C (SEC24C) was found decreased in later colorectal cancer (CRC) stages, but its exact role in response to ER-stress and activation of UPR in hepatocellular carcinoma (HCC) remains to be elucidated. Here, we have identified the downregulation of SEC24C in human HCC sample and its suppressive role in regulating HCC proliferation and chemoresistance. Mechanistically, SEC24C was found to interact with eukaryotic translation initiation factor 2 alpha kinase 3 (EIF2AK3 or PERK) and activate the downstream UPR-related apoptosis. During this process, SEC24C was observed to be anchored in nucleus under normal condition but responded immediately to ER-stress and could subsequently translocate to the ER. Furthermore, overexpression of SEC24C significantly augmented the efficacy of bortezomib in HCC treatment. In conclusion, our findings revealed a novel role of SEC24C in regulating HCC proliferation and chemoresistance by modulating UPR activation.

Keywords hepatocellular carcinoma (HCC), unfolded protein response, chemotherapy

1. Introduction

Hepatocellular carcinoma (HCC) remains one of the most common cancers worldwide (*1*). Although significant advancements have been made, effective systemic therapies for management of HCC are limited. Recently, targeting the unfolded protein response (UPR) and redirecting it towards apoptosis has emerged as a promising approach in cancer therapy (*2,3*). The proteostasis of the ER is exquisitely maintained, but it has been found that various factors can disrupt the processes of protein synthesis and provoke the state of ER-stress. The intrinsic factors related to hyperactive proliferation and external factors of hypoxia as well as nutrient deprivation can cause cancer cells to experience persistent ER-stress (*4*). It has been reported that to alleviate the ER stress condition, a series of signaling pathways called UPR are induced (*5*). The different branches of the UPR act synergistically or antagonistically to promote the cell survival or induce apoptosis if ER stress remains unmitigated (*6*). The selective lysosomal degradation of specific ER fragments, termed ER-phagy, could also relieve ER-stress (*7*). And SEC24C, a subunit of the coat protein complex II (COPII), was observed to exhibit a noncanonical function in participating ER-phagy (*8*). Activating transcription factor 4 (ATF4), an important component of the UPR, has also been reported to function in ER-phagy (*9*), so we hypothesized that SEC24C may participate in the regulation of UPR. Besides, the downregulated expression of SEC24C in later colorectal cancer stages was both validated with gene expression commons platform meta-analysis and IHC experiments (*10*). Overall, it is speculated that SEC24C could effectively respond to ER-stress and

affect UPR to impact HCC progression. In the present study, we have shown that SEC24C could promote UPR-related apoptosis by promoting the dissociation of Bip from PERK, thus suppressing the proliferation and chemoresistance of HCC cells.

2. Materials and Methods

2.1. Human samples

HCC samples (including tumor and adjacent nontumor samples) were collected from patients between August 2019 and September 2022 at Nanjing Drum Tower Hospital. Normal human liver samples were obtained from hepatic hemangioma patients with no evidence of chronic liver disease, diabetes, or hypertension. All patients provided written consent. All studies were approved by the Institutional Ethics Committee of Nanjing Drum Tower Hospital in compliance with the 1975 Declaration of Helsinki.

2.2. *In vivo* experiments

BABL/c male nude mice, 6 weeks of age, were purchased from the animal center of Nanjing University (Nanjing, Jiangsu, China), raised and permitted by the Nanjing University animal studies committee. In the subcutaneous transplantation model, mice were distributed at random to each group (n = 6 or 5) and implanted with Huh7 sgSEC24C, Huh7 sgNC, MHCC97H OE-SEC24C, or MHCC97H NC cells in the right groin. The mice were euthanized at 4 weeks after implantation and calculated the volume of the tumors. The equation (length × height × width) × 0.52 was used to calculate the tumor volume. For tumor drug resistance research, each group was given an intravenous injection of bortezomib (1 mg/kg body weight) or Sal003 (2.5 mg/kg body weight) once per week for 3 weeks.

For the primary liver cancer model, $Trp53^{flox/flox}$ mice were a kind gift from Southern Medical University. $Trp53^{flox/flox}$ mice were crossed with Alb-Cre mice to generate hepatocyte-specific Trp53 knockout ($Trp53^{\Delta hep}$) mice. The mixture used for hydrodynamic intravenous injection included a sterile 0.9% NaCl solution/plasmid mix containing 5 μg of pSB-U6-sgSEC24C-TBG-Cas9 or 5 μg of pSB-TBG-SEC24C-FLAG, 5 μg of pSB-EF1α-Myc and 2.5 μg of CMV-SB_{13} transposase plasmids. A total volume of mixture corresponding to 10% of body weight was injected *via* the tail vein in 7 s into 8-week-old male $Trp53^{\Delta hep}$ mice. After 6 weeks, mice were humanely sacrificed by CO_2 asphyxiation. The equation (length × $width^2$) × 0.52 was used to calculate the tumor volume. All animal experiments were approved by the Animal Core Facility of Nanjing Drum Tower Hospital and were performed in accordance with guidelines for the care and use of laboratory animals.

2.3. Statistical analysis

All data presented were based on at least 3 independent experiments both *in vivo* and *in vitro*. Student's *t* test was used for comparisons among two groups and One-way ANOVA was used for comparisons between more than two groups. Survival analysis was performed with the Kaplan–Meier method. Statistically significant differences were considered only if $P < 0.05$. SPSS 19.0 and Prism 8 were utilized for data analysis. Additional experimental procedures are described in the Supplementary Materials and Methods (*https://www.biosciencetrends.com/supplementaldata/207*).

3. Results

3.1. SEC24C, a member of COPII, is frequently downregulated in HCC

To confirm the potential function of SEC24C in HCC, the mRNA and protein levels of SEC24C in HCC and corresponding adjacent normal tissues were first measured. As depicted in Figure 1A, The Cancer Genome Atlas (TCGA) and Genotype-Tissue Expression (GTEx) database indicated that expression of SEC24C was downregulated in the tumor tissues compared to normal tissues, which was also validated with qRT-PCR experiment of HCC samples from our tissue bank. Next, we examined the protein level of SEC24C in HCC tissues using immunohistochemical (IHC) staining and found downregulated SEC24C protein levels in HCC tissues (Figure 1B). Notably, SEC24C was primarily concentrated in the nucleus in the peritumor tissues but the tumor tissues have an obvious deficiency of SEC24C expression in the nucleus. Thereafter, we employed western blotting (WB) in 10 paired samples from HCC patients and 10 normal liver samples to confirm the downregulated SEC24C expression in HCC (Figures. 1C, 1D). And the downregulation of SEC24C was also found in the liver cirrhosis tissues (Supporting Figure S1A, *https://www.biosciencetrends.com/supplementaldata/207*). To further identify its prognostic value in HCC, Kaplan–Meier Plotter was used, and the results displayed that low expression of SEC24C was significantly correlated with the poor progression-free survival (PFS) and relapse-free survival (RFS). However, analysis of overall survival (OS) only exhibited a significant correlation between low SEC24C expression and poor prognosis for the male patients infected with hepatitis virus but not for all the patients (Figure 1E). Taken together, these results suggest that SEC24C might play a critical role in the development of HCC and significantly correlate with the prognosis of HCC patients.

3.2 SEC24C attenuates malignant phenotypes of HCC cells *in vitro*

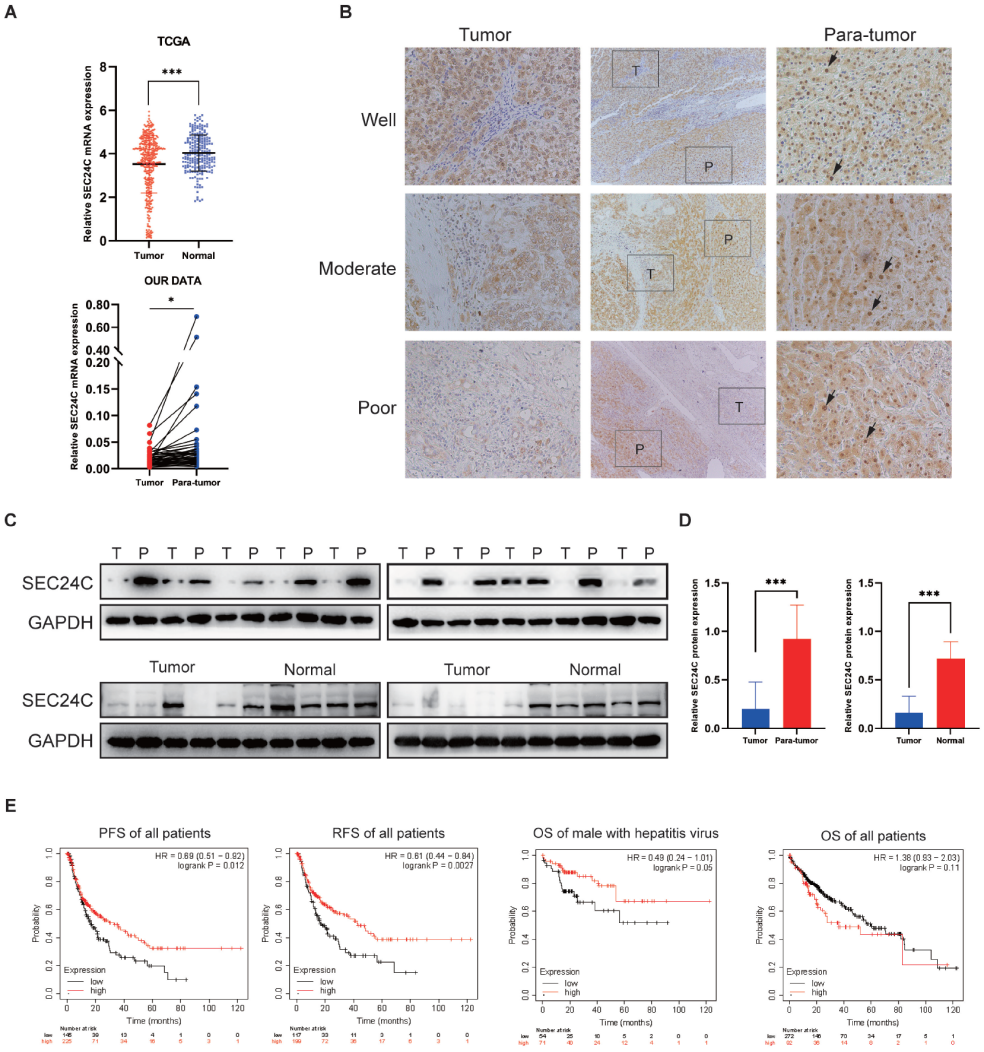

Figure 1. Downregulation of SEC24C in human HCC tissues. (A) The data regarding RNA expression of SEC24C for HCC patients obtained from the Cancer Genome Atlas, Genotype-Tissue Expression and our tissues bank were statistically analyzed (*$P < 0.05$; **$P < 0.01$; ***$P < 0.001$). **(B)** Representative IHC staining images of SEC24C in HCC tissues of different differentiation grades from HCC sections. Arrows: nuclear staining. **(C)** Representative expression levels of SEC24C protein in 10 paired HCC (T) and corresponding peritumor tissues (P), as well as 10 normal liver tissues, were analyzed by western blotting, and the quantification of SEC24C protein levels is depicted in **(D)** (**$P < 0.01$; ***$P < 0.001$). **(E)** Kaplan–Meier Plotter was used for the prognosis analysis in HCC patients stratified by high and low expression of SEC24C.

To confirm the antitumor activity of SEC24C in HCC, we first detected the protein levels of SEC24C in four different HCC cell lines as well as the immortalized hepatocytenormal liver cell line (HepaRG) by western blot analysis (Supporting Figure S1B, *https://www.biosciencetrends.com/supplementaldata/207*). Then, MHCC97H cells was selected to construct an *in vitro* overexpressing (OE) model as they showed relatively low expression of SEC24C. Similarly, Hep3B cells was chosen to establish SEC24C-silenced cell lines whereas SEC24C expression in the Huh7 cells was knocked out by CRISPR Cas9. WB verified SEC24C expression levels in the generated cell lines (Supporting Figure S1C, *https://www.biosciencetrends.com/supplementaldata/207*). Thereafter, plate colony formation and cell counting kit-8 (CCK8) assays showed that knockdown of SEC24C in Hep3B cells or knockout of SEC24C in Huh7 cells both significantly promoted the clone formation ability as well as proliferation rate. However, decreased colony formation and proliferation rates were observed in MHCC97H OE-SEC24C cells in comparison with control cells (Figure 2A-B). In addition, the effect of SEC24C on HCC migration and invasion was investigated *in vitro* (Figures 2C, 2D). Moreover, flow cytometry experiments were also performed and displayed that deletion of SEC24C in HCC cells significantly reduced the apoptotic rates (Figures 2E, 2F). These results indicated the suppressive role of SEC24C in regulating HCC cell proliferation and metastasis.

3.3. SEC24C weakens HCC progression *in vivo*

To further validate the impact of SEC24C on HCC, we performed tumorigenesis assays under *in vivo* conditions. A subcutaneous xenograft model was developed, and the results revealed that SEC24C overexpression

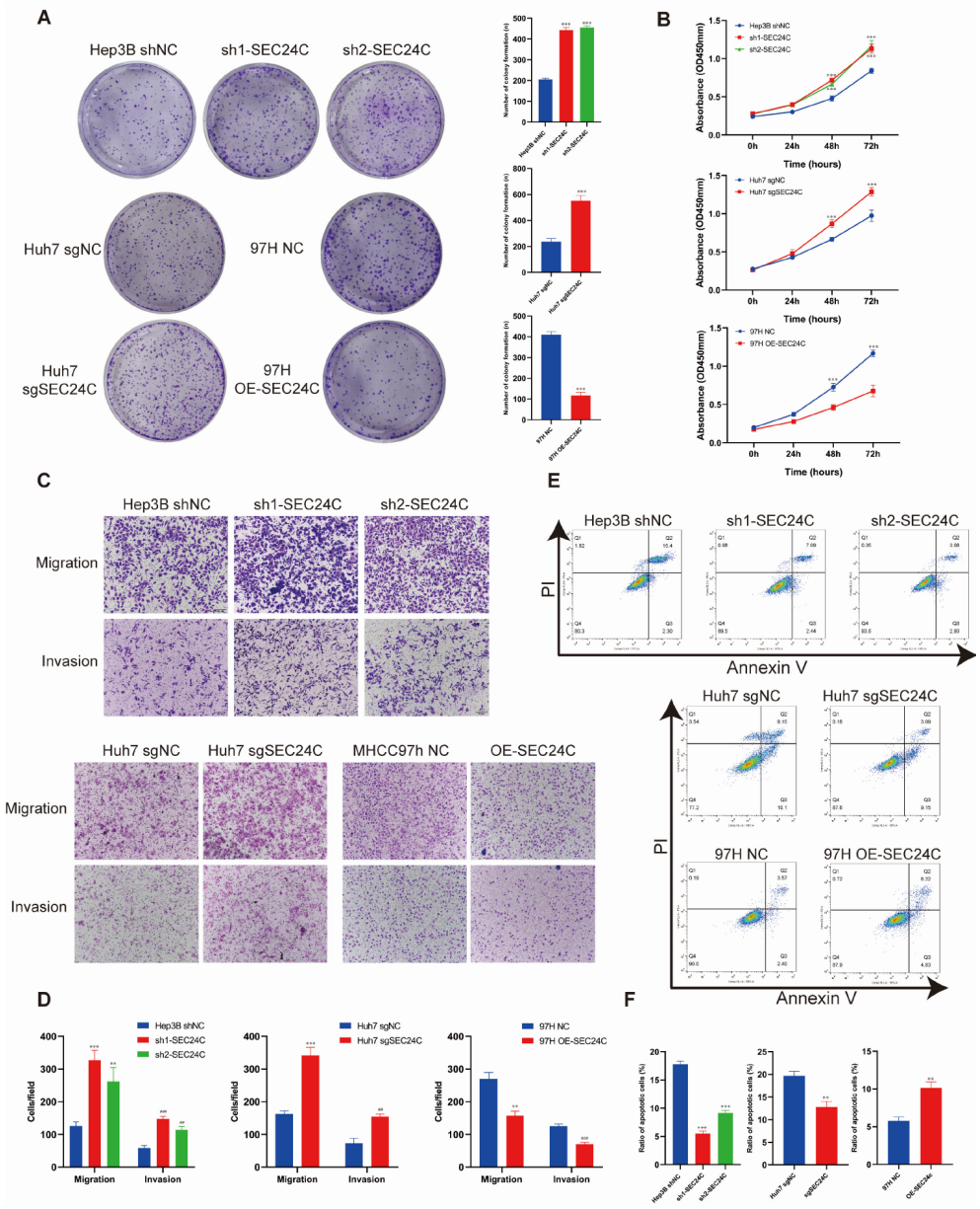

Figure 2. Tumor-suppressive functions of SEC24C in HCC cells. (A) Representative images of colony formation induced by Hep3B shNC, Hep3B sh1-SEC24C, Hep3B sh2-SEC24C, Huh7 sgNC, Huh7 sgSEC24C, MHCC97H NC and MHCC97H OE-SEC24C cells respectively. The numbers of colonies were counted and are shown in the right bar graph. **(B)** CCK8 assays of Hep3B sh1-SEC24C&sh2-SEC24C, Huh7 sgSEC24C, MHCC97H OE-SEC24C cells and the corresponding control cells. **(C)** Invasion and migration assays were performed in the presence or absence of matrix. The number of invaded and migrated cells was calculated and have been shown in bar graph **(D)**. **(E)** Apoptosis assays for Hep3B sh1-SEC24C&sh2-SEC24C, Huh7 sgSEC24C, MHCC97H OE-SEC24C cells and the corresponding control cells were performed after treatment with H_2O_2 using flow cytometry analysis. The apoptosis rate of the cells was measured and has been shown in the bar graph **(F)**. All experiments were performed in triplicate, and the data has been expressed as the mean ± SD from three independent experiments ($n = 3$, $^{**}P < 0.01$; $^{***}P < 0.001$; $^{\#\#}P < 0.01$; $^{\#\#\#}P < 0.001$)

significantly inhibited the tumor growth, whereas the SEC24C knockout promoted this process (Figure 3A). Furthermore, we created a primary liver cancer model (*11*) with liver-specific knockout or overexpression of SEC24C. We first generated the mice with hepatocyte-specific deletion of Trp53 ($Trp53^{\Delta hep}$) by crossing $Trp53^{flox/flox}$ mice with Alb-Cre mice, as 58% of HCC patients have been reported possess the Trp53 mutation (*12*). Thereafter, a CRISPR–Cas9 fraction of SEC24C (sgSEC24C-Cas9) and the SEC24C cDNA were cloned into the Sleeping Beauty (SB) vector respectively. These plasmids along with their control plasmids were then hydrodynamically injected in combination with pSB-EF1α-Myc and CMV-SB_{13} transposase plasmids through the tail vein in $Trp53^{\Delta hep}$ mice (Figures 3C, 3D). At 6 weeks after injection, the tumors from mice injected with SB-sgSEC24C-Cas9 plasmids exhibited a significantly increased number and volume in comparison with the controls. In contrast, tumors obtained from the mice injected with SB-SEC24C plasmids displayed a significant reduced number and volume in comparison with the controls (Figure 3E). Immunostaining with

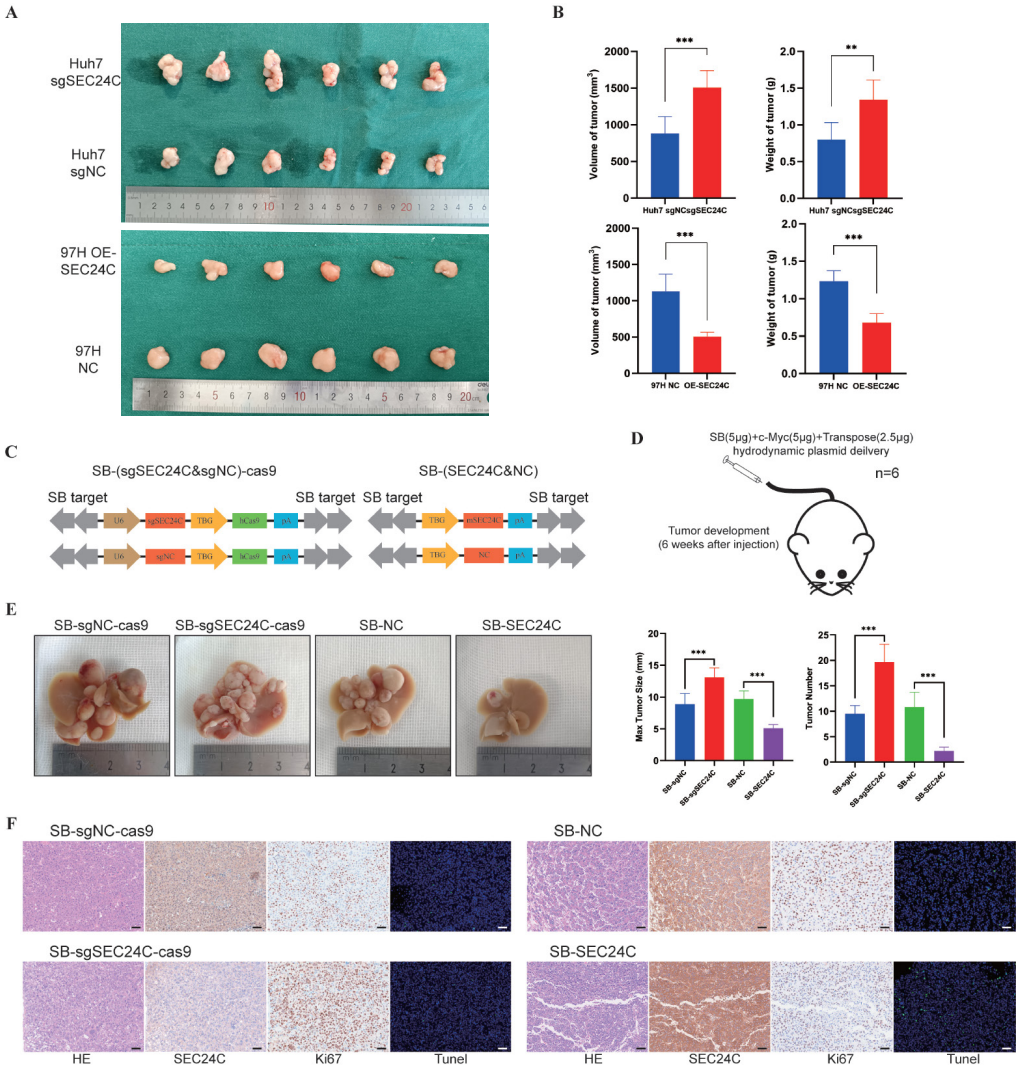

Figure 3. Tumor-suppressive effects of SEC24C *in vivo*. (A) Representative images have been shown for the tumors derived from the nude mice induced by Huh7 sgSEC24C and Huh7 sgNC cells (upper panel) and MHCC97H OE-SEC24C as well as MHCC97H NC cells (lower panel) after the subcutaneous injection. **(B)**The tumor volume and tumor weight were measured 30 days after implantation after sacrificing the mice ($n = 6$). **(C)** and **(D)** $Trp53^{\Delta hep}$ mice were utilized to establish a primary liver cancer model by hydrodynamic injection of SB-sgSEC24C-cas9 or SB-SEC24C and the corresponding control plasmids, as well as c-Myc and transpose plasmids. **(E)** Representative HCC samples of $Trp53^{\Delta hep}$ mice ($n = 6$) with the different plasmids. The number of the tumors was measured and has been shown in the right bar graph. **(F)** HE, SEC24C, ki67 and TUNEL staining were performed in HCC sections (scale bar: 50 μm). All results have been presented as the mean ± SD (**$P < 0.01$; ***$P < 0.001$).

Ki67 and TUNEL confirmed increased proliferation and alleviated apoptosis after specific knockout of SEC24C, whereas SEC24C overexpression led to an opposite outcome *in vivo* (Figure 3F). All these results suggested that depletion of SEC24C led to liver tumorigenesis as well as tumor progression.

3.4. SEC24C translocates from nucleus to ER upon ER-stress

In Figure 1B, we found that SEC24C was concentrated in the nucleus of peritumor tissues, but tumor tissues lacked the protein expression of SEC24C in nucleus. As SEC24C was mainly reported as a cytosolic protein to locate at the ER surface and could participate in ER-phagy (*8*), we deduced that SEC24C may be transferred from the nucleus to the ER surface under stressed conditions and then be degraded by autolysosome. Starvation and ER-stress both have been found to activate ER-phagy to restore ER homeostasis (*13,14*), so Earle's Balanced Salt Solution Earle's Balanced Salt Solution (EBSS) and tunicamycin (TM) are both employed to investigate whether SEC24C could be degraded during ER-phagy process. In support of our hypothesis, application of TM and EBSS resulted in a gradual upregulation of LC3 II protein levels and a reduction in receptor accessory protein 5 (REEP5), degradation of which was a marker for ER-phagy (*15*) (Figure 4A, and Supporting Figure S2A, *https://www.biosciencetrends.com/supplementaldata/207*). As the autophagy level was frequently active in multiple types of cancer, we further investigated whether ER-phagy was more hyperactive in HCC than in peritumor tissues by examining the protein levels of reticulon-3-long (RTN3L) (Figure 4B),

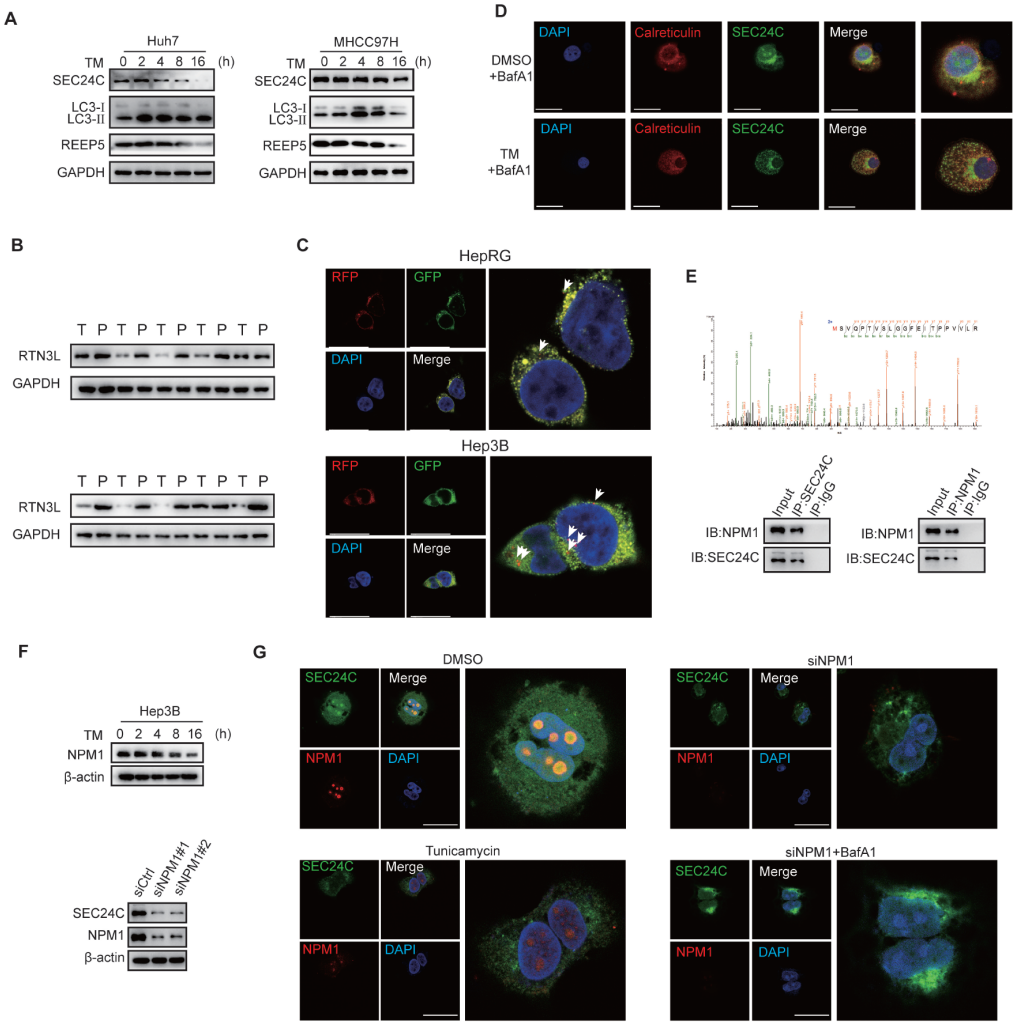

Figure 4. Degradation and shuttle of SEC24C under stress in HCC cells. (A) Representative images depicting the protein levels of SEC24C, LC3-I/II and REEP5 following TM treatment. **(B)** Representative expression levels of RTN3L protein in 10 paired HCC (T) and corresponding peritumor tissues (P) analyzed by western blotting. **(C)** Stable ssRFP-GFP-KDEL-expressing HepRG and Hep3B cells are under confocal microscopy of ssRFP$^+$/GFP$^-$KDEL$^-$ and ssRFP$^+$/GFP-KDEL$^+$ structures. Arrows highlight ssRFP$^+$/GFP-KDEL$^-$ puncta. **(D)** Representative images displaying the localization of SEC24C in Hep3B cells treated with DMSO or TM. **(E)** Collision-induced dissociation mass spectrum demonstrating the structural diagram of NPM1 protein (upper panel). SEC24C interacts with NPM1, as evidenced by a Co-IP assay in Hep3B cells (lower panel). **(F)** Representative images showing the protein levels of NPM1 upon TM treatment in Hep3B cells (upper panel) and SEC24C after NPM1 knockdown (lower panel). **(G)** Representative images depicting the localization of SEC24C and NPM1 with DMSO or TM (left panel). The concentration of SEC24C in the nucleus was attenuated by NPM1 knockdown and administration of BafA1 was able to restore the expression of SEC24C in the perinuclear area (right panel) in Hep3B cells (Scale bar: 50 μm). All experiments were performed in triplicate. Abbreviations: DAPI, 4′,6-diamidino-2-phenylindole; IgG, immunoglobulin.

which degradation are vital indicators of ER-phagy (*16*). Subsequently the ssRFP-GFP tandem fluorescently tagged KDEL plasmid was also employed to verify the specific ER-phagy process (*17*) and results revealed that Hep3B cell showed more numerous ssRFP$^+$/GFP-KDEL$^-$ puncta than HepRG cell (Figure 4C). Above data found that SEC24C are frequently degraded during ER-phagy and HCC has a hyperactive ER-phagy in most cases, suggesting that the decline of SEC24C in tumor tissue maybe partial due to persistent autolysosome degradation by ER-phagy in HCC.

Next, results of double immunofluorescent (IF) staining demonstrated that SEC24C could distribute in the nucleus and mainly localized within the nucleoli under normal condition, but upon TM treatment, SEC24C in the nucleus could effectively translocate at perinuclear ER surface (Figure 4D). In addition, cell fractionation analysis also confirmed the preferred localization of SEC24C in the nucleus under normal condition (Supporting Figure S2B, *https://www.biosciencetrends.com/supplementaldata/207*). To further unravel the shuttling mechanism of SEC24C, we performed liquid chromatography–tandem mass spectrometry (LC–MS/MS) and found that SEC24C interacted with nucleophosmin1 (NPM1) under normal condition, which could shuttle between cytoplasm and nucleus, and regulate protein nuclear translocation (*18-20*). Co-immunoprecipitation (Co-IP) experiments confirmed a direct interaction between SEC24C and NPM1 (Figure 4E). Then WB results found that NPM1

level was also decreased upon TM treatment (Figure 4F, upper panel). Thereafter, siRNAs targeted against NPM1 were used and an interesting fact was discovered that the SEC24C protein level decreased concomitantly with NPM1 reduction (Figure 4F, lower panel), but not the mRNA level of SEC24C (Supporting Figure S2C, *https://www.biosciencetrends.com/supplementaldata/207*). Use of bafilomycin A1 (BafA1) could restored the protein expression of SEC24C after NPM1 knockdown (Supporting Figure S2D, *https://www.biosciencetrends.com/supplementaldata/207*), implying that NPM1 may help SEC24C restore in the nucleus. Finally, IF analysis further verified that SEC24C was colocalized with NPM1 in the nucleus under normal condition. However, when ER-stress was induced, SEC24C dissociated from NPM1 and concentrated specifically in the perinuclear area (Figure 4G, left panel). After NPM1 knockdown, the distribution of SEC24C in nucleus was dismissed and application of BafA1 could rescue partial SEC24C expression in the perinuclear area (Figure 4G, right panel), which was also examined by cell fractionation analysis (Supporting Figure S2D, *https://www.biosciencetrends.com/supplementaldata/207*). To decrease possible interference from non-specific immunoreactivity of SEC24C antibody, SEC24C-Flag were constructed and transfected into Hep3B cells. Results of Co-IP and IF showed direct interaction of SEC24C and NPM1 in the nucleus by employing Flag antibody (Supporting Figures S2E, S2F, *https://www.biosciencetrends.com/supplementaldata/207*). Collectively, NPM1 could help SEC24C reserve in the nucleus under normal conditions, but upon ER-stress, SEC24C in the nucleus rapidly shuttled to the ER surface in HCC cells.

3.5. Loss of SEC24C facilitates HCC progression by suppressing the UPR

A number of studies have shown that the crowded molecular microenvironment can cause malignant cells particularly vulnerable to ER-stress (*4,21*) , and that activated UPR plays a critical role in HCC progression as well as survival (*22,23*). Our results have revealed the rapid response of SEC24C to ER-stress and demonstrated the shuttling of SEC24C from the nucleus to ER, thereby prompting us to speculate that SEC24C could participate in the process of ER-stress after localization in ER and thus suppress HCC proliferation by modulating the UPR. Interestingly, various past studies have revealed that SEC24C can effectively regulate specific cellular functions by interacting with the specific protein partners (*24,25*), hence we performed LC–MS/MS to qualitatively analyze the components of the SEC24C binding protein and identified a novel combination with both PERK (Figure 5A) and Bip (Supporting Figure S3A, *https://www.biosciencetrends.com/supplementaldata/207*). Co-IP experiments also showed a direct interaction between SEC24C and PERK (Figure 5B). However, considering that Bip is mainly localized in the ER lumen, but SEC24C lacks a transmembrane domain that can facilitate its access to the ER lumen, the association between SEC24C and Bip could be indirect and mediated by PERK.

Since the PERK branch remains the main studied signal for contributing to apoptotic death in UPR (*6,21,26*) and above results indicated that SEC24C had a strong impact on HCC apoptosis under both *in vitro* and *in vivo* settings (Figure 2F, 3F), we hypothesized that SEC24C could influence HCC cell apoptosis by modulating the PERK branch of UPR. WB results further verified that SEC24C knockout significantly decreased the protein levels of DNA damage inducible transcript 3 (DDIT3, also known as CHOP), a transcription factor downstream of PERK to promote apoptosis (*27*) (Figure 5C). Furthermore, immunoblotting data confirmed that SEC24C knockout significantly reduced the protein levels of phosphorylated PERK (p-PERK) in comparison to PERK and phosphorylated eukaryotic translation initiation factor 2 subunit alpha (eIF2α) (p-eIF2α) in comparison to eIF2α and ATF4, which was opposite in SEC24C-overexpressing group (Figure 5C), but was consistent in SEC24C knockdown cells (Supporting Figure S3B, *https://www.biosciencetrends.com/supplementaldata/207*). Moreover, results of qRT–PCR confirmed that the mRNA levels of CHOP and protein phosphatase 1 regulatory subunit 15A (PPP1R15A, also known as GADD34), which are transcriptional regulated downstream of UPR, were significantly positively correlated with SEC24C levels (Figure 5D). Interestingly, similar results were also obtained by WB analysis of HCC samples from $Trp53^{\Delta hep}$ mice injected with different SB plasmids (Figure 5E). And representative images of IHC staining showed that SEC24C knockout significantly reduced the protein expression and nuclear localization of p-PERK and CHOP, which was significantly enhanced upon SEC24C overexpression (Figure 5F).

To further analyze the function of SEC24C on PERK signaling, we examined the potential correlation between SEC24C and CHOP or GADD34 in TCGA database and observed significant positive correlations between SEC24C and all of them (Supporting Figure S3C, *https://www.biosciencetrends.com/supplementaldata/207*). In addition, we examined whether SEC24C affect UPR activation partly through its secretory role. As Sec24 isoforms have displayed overlapping selectivity for the different transport signals and some similarities in their secretory functions (*28*), we overexpressed the expression of three remain Sec24 isoforms in Huh7 sgSEC24C cells and knocked them down in MHCC97H OE-SEC24C cells. The results demonstrated no significant differences in the protein levels of CHOP after switching the three remaining Sec24 isoforms, thus suggesting that SEC24C can promote the activation of PERK signaling independent of its secretory function

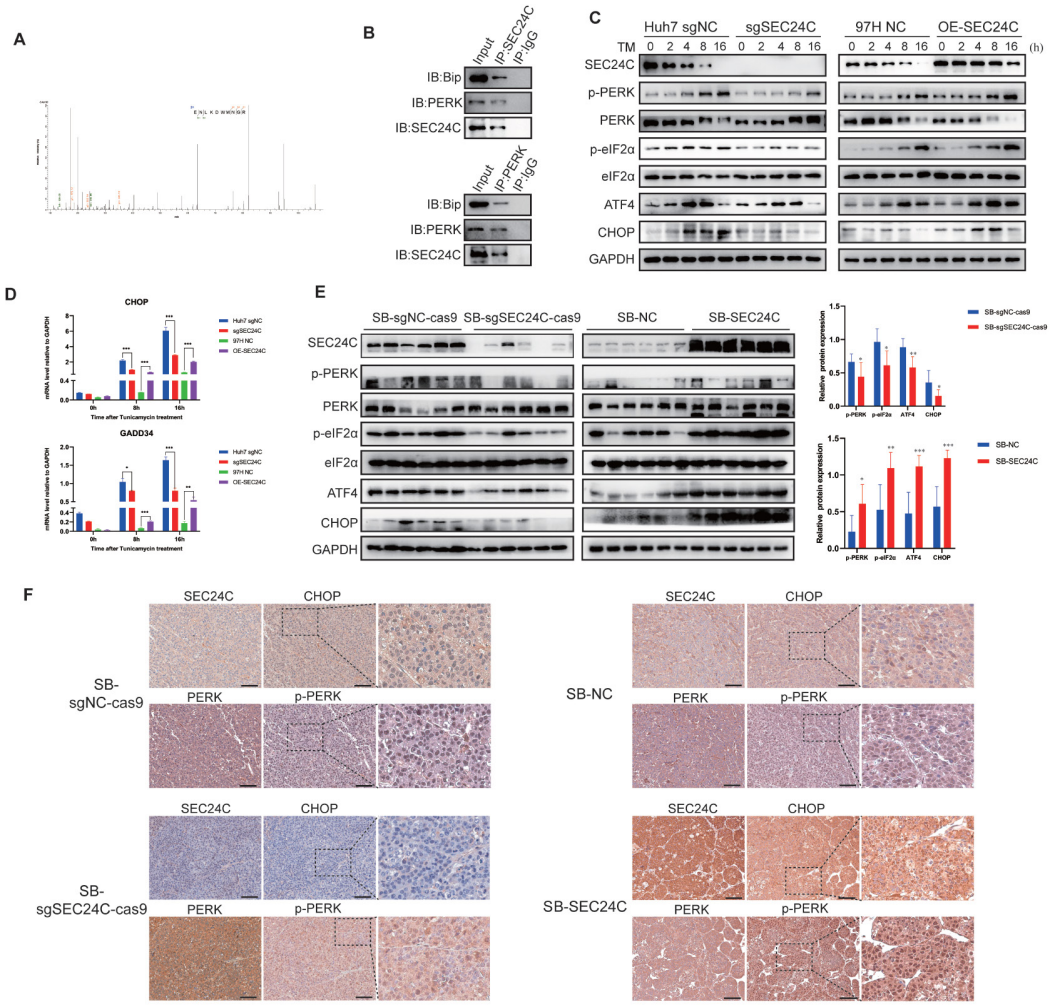

Figure 5. SEC24C modulates activation of the UPR *in vitro* and *in vivo*. (A) A representative PERK tryptic peptide identified in mass spectrometry (MS) analysis of SEC24C-interacting proteins. **(B)** Interaction of the endogenous SEC24C with PERK and Bip determined by Co-IP analysis in Hep3B cells. **(C)** Western blot analysis of the protein levels of phosphorylated PERK, PERK, phosphorylated eIF2α, eIF2α, ATF4 and CHOP after SEC24C knockout or overexpression following tunicamycin treatment. **(D)** qRT–PCR analysis of the mRNA levels of CHOP and GADD34 after SEC24C knockout or overexpression following tunicamycin treatment. (n = 3) **(E)** Western blot analysis of the protein levels of phosphorylated PERK, PERK, phosphorylated eIF2α, eIF2α, ATF4 and CHOP in HCC samples obtained from the $Trp53^{Ahep}$ mice injected with the different plasmids. The quantification of bands is represented in the right bar graph. **(F)** Representative IHC staining images of SEC24C, p-PERK, PERK and CHOP in HCC samples derived from $Trp53^{Ahep}$ mice injected with the different plasmids. Scale bar: 100 μm. All results are presented as the mean ± SD (*P < 0.05; **P < 0.01; ***P < 0.001).

(Supporting Figure S3D, *https://www.biosciencetrends.com/supplementaldata/207*). We also found the significant positive correlations between SEC24C and other UPR target genes (Supporting Figure S3E, *https://www.biosciencetrends.com/supplementaldata/207*). Overall, our data strongly suggested that SEC24C can promote the activation of the PERK-eIF2α-ATF4 branch of the UPR to increase UPR-related apoptosis in HCC.

3.6. SEC24C promotes the UPR by interfering with the interaction between Bip and PERK

To understand the underlying molecular mechanisms by which SEC24C promoted PERK activation in HCC, we sought to explore the potential interaction between Bip, PERK and SEC24C (*4*). First, Co-IP experiments demonstrated the dissociation of Bip away from PERK and SEC24C with BafA1 under ER-stress conditions (Figure 6A, left panel). However, the direct interaction between SEC24C and PERK was increased under ER-stress (Figure 6A, right panel), which suggested that SEC24C could suppress the interaction between Bip and PERK. As expected, SEC24C knockout increased the interaction between Bip and PERK after TM treatment, whereas SEC24C overexpression limited this interaction even under the normal conditions (Figure 6B). Moreover, consistent with the Co-IP results, IF staining demonstrated an interaction between SEC24C and PERK, which was found to be upregulated under ER-stress (Figure 6C). To better understand the roles of precise SEC24C domains that could be essential for this interaction, SEC24C-Flag truncations were constructed and transfected into the Hep3B cells. Co-IP results revealed that residues 748–843 of SEC24C

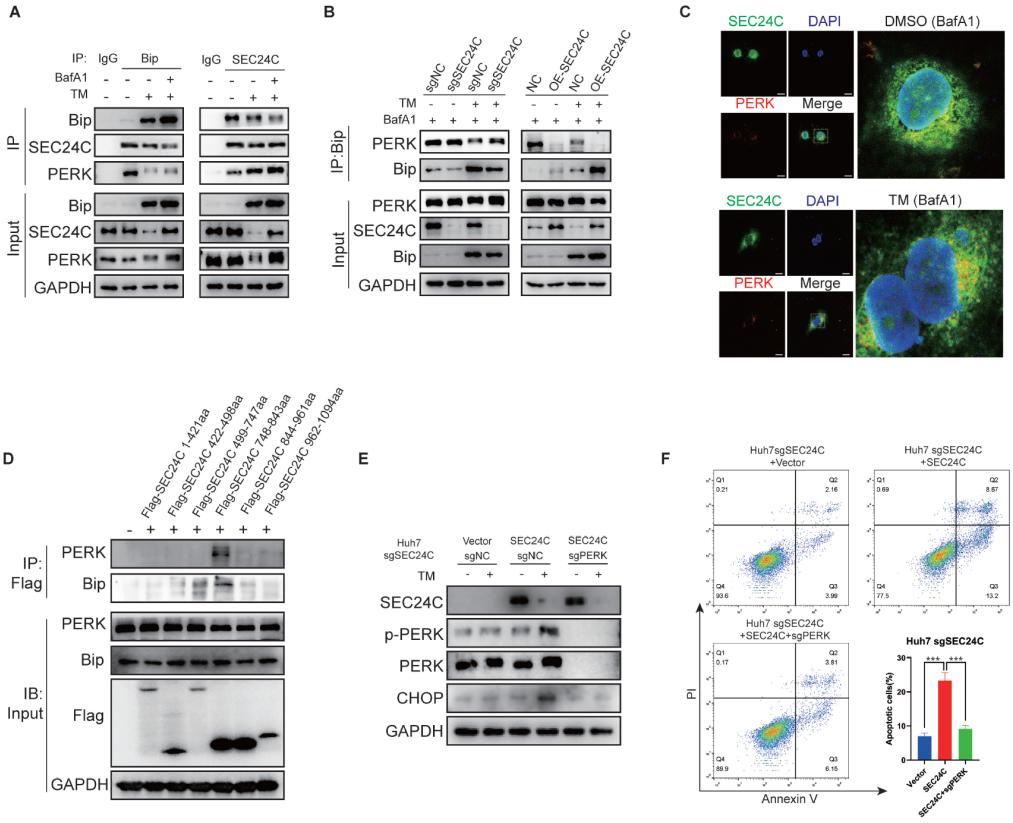

Figure 6. SEC24C interacts with PERK and facilitates the disassociation of Bip from PERK. (A) Immunoprecipitation was performed in Hep3B cells to analyze the protein levels of PERK interacting with Bip (left panel) or SEC24C (right panel) after tunicamycin treatment. **(B)** Immunoprecipitation analysis of PERK and SESC24C proteins interacting with Bip after treatment with DMSO or tunicamycin upon SEC24C variation in the corresponding Huh7 or MHCC97H cells. **(C)** Representative immunofluorescence staining images displaying the colocalization of SEC24C and PERK in HCC cells treated with DMSO or TM in Huh7 cells (scale bar: 25 μm). **(D)** Hep3B cells were transfected with the different Flag-SEC24C truncations. Immunoprecipitations were performed with anti-Flag antibodies to identify the individual binding sites of SEC24C. **(E)** Huh7 sgSEC24C cells were transfected with the various indicated plasmids, such as vector, SEC24C, sgNC or sgPERK-cas9, and treated with DMSO or TM to examine the CHOP expression upon variation of SEC24C and PERK. **(F)** Apoptosis assays for Huh7 sgSEC24 cells transfected with indicated plasmids were performed after the treatment with DMSO or TM for 36 hours using flow cytometry analysis. The apoptosis rate of the cells was measured and has been shown in right lower bar graph. All experiments were performed in triplicate, and the data has been expressed as the mean ± SD from three independent experiments ($n = 3$, $^{***}P < 0.001$). Abbreviations: DAPI, 4′,6-diamidino-2-phenylindole; IgG, immunoglobulin.

were indispensable for binding to PERK (Figure 6D). Furthermore, we noted that re-expressing SEC24C in Huh7 sgSEC24C cells restored the restrained protein levels of p-PERK and CHOP, which was subsequently inhibited upon PERK knockout (Figure 6E). The results of apoptosis assays also showed that re-expressing SEC24C in SEC24C knockout cells attenuated the anti-apoptotic effect under ER-stress, which was reversed by PERK knockout (Figure 6F).

To further investigate whether loss of SEC24C promotes HCC progression through affecting the PERK-eIF2α-ATF4 pathway, we used various pharmacological modulators targeting the UPR. The results indicated that administration of Sal003, an inhibitor targeting eIF2α phosphatases to prevent the dephosphorylation of eIF2α (*29*), was able to cause upregulated expression of CHOP independent of SEC24C level and significantly suppress upregulated proliferation ability of Huh7 sgSEC24C cells (Supporting Figure S4A-C, *https://www.biosciencetrends.com/supplementaldata/207*). Besides, ISRIB, a potent inhibitor of PERK signaling, significantly rescued the downregulated proliferation ability of MHCC97H OE-SEC24C cells, which also caused a reduction in endogenous production of CHOP (Supporting Figure S4D-S4F, *https://www.biosciencetrends.com/supplementaldata/207*). Thus, our findings indicated that SEC24C increased the dissociation of Bip from PERK and activated downstream CHOP-related apoptosis, which in turn could attenuate the malignant phenotypes of HCC cells.

3.7. SEC24C increases the chemosensitivity of HCC to Bortezomib

In recent years, induction of lethal ER-stress or suppression of the cytoprotective UPR has emerged as a new target for cancer therapy (*2,4*).As bortezomib (BTZ) was reported to fulfil its anti-tumor function partly through activating UPR and the effect could be strongly inhibited by suppression of ATF4 (*30*), we wondered whether SEC24C could influence the chemosensitivity of HCC to BTZ through regulating

UPR activation. As expected, BTZ obviously upregulated the activation of the PERK-eIF2α-ATF4 axis, and knockdown of SEC24C significantly downregulated but SEC24C overexpression increased the CHOP level in HCC cells treated with BTZ (Figure 7A). Results showed that BTZ significantly inhibited the colony formation and metastatic ability of HCC cells, especially in SEC24C-overexpressing group (Figure 7B). And in SEC24C knockout Huh7 cells, the half-maximal inhibitory concentration (IC_{50}) of BTZ was increased from 12.88 to 19.94 compared with control cells. In SEC24C overexpressing 97H cells, the IC50 of BTZ was decreased from 11.7 to 8.284 compared with control cells (Figure 7C). Next, experiment conducted in xenograft tumor model revealed that SEC24C rendered HCC tumors more sensitive to BTZ toxicity (Figure 7D, 7E). And histological analysis revealed a significantly greater extent of necrosis in the SEC24C-overexpressing group upon BTZ treatment in comparison to any other group (Figure 7F). Sal003 was also administered to immunodeficient xenograft mice with Huh7 sgNC or Huh7 sgSEC24C tumors, and results indicated that both Huh7 sgSEC24C and Huh7 sgNC tumors showed similar sensitivity to Sal003 (Supporting Figure S5, *https://www.biosciencetrends.com/supplementaldata/207*). Overall, these findings indicated that SEC24C overexpression markedly enhanced the chemosensitivity of HCC cells to BTZ induced UPR.

4. Discussion

SEC24C, a member of the Sec24 subfamily of the Sec23/Sec24 family, is an important member of the coat protein complex—COPII. However, to date, little research has been performed to understand the functions of SEC24C in cancer, especially in HCC. In the present study, we have found that SEC24C protein levels were frequently downregulated in HCC tissues in comparison to the peritumor and normal

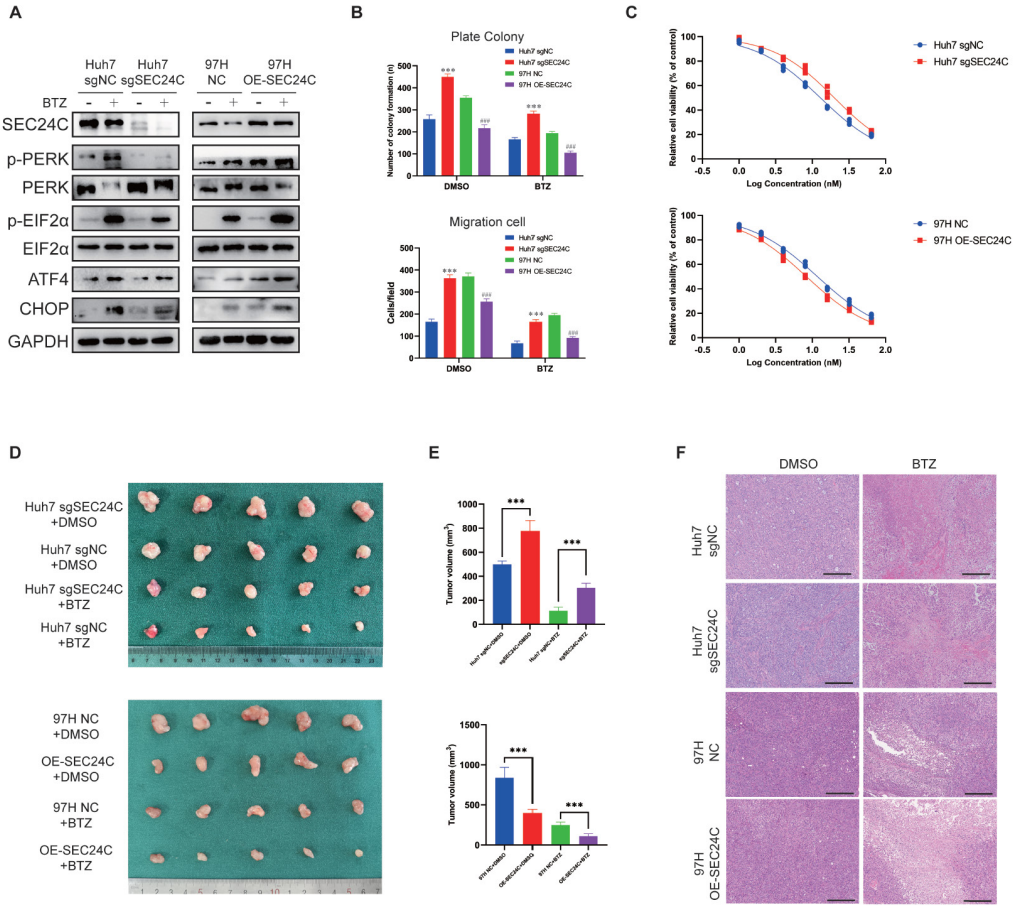

Figure 7. SEC24C promotes the chemosensitivity of HCC to bortezomib. (A) Analysis of protein levels of the PERK-eIF2α-ATF4 axis and CHOP with bortezomib in Huh7 sgSEC24C, MHCC97H OE-SEC24C and their respective control cells. **(B)** The colony formation and migration assays are induced by Huh7 sgSEC24C, MHCC97H OE-SEC24C and their control cells with DMSO or BTZ. The number of colonies and migrated cells were measured and shown in the bar graph ($n = 3$). **(C)** The cell viability was measured with CCK8 assay in Huh7 sgSEC24C, MHCC97H OE-SEC24C and their control cells with the indicated concentrations of BTZ. **(D)** Representative images are shown for the tumors derived from nude mice induced by Huh7 sgSEC24C and Huh7 sgNC cells (upper panel) and MHCC97H OE-SEC24C and MHCC97H NC cells (lower panel) with tail vein injection of vehicle or bortezomib. The tumor weight and volume of each group of mice have been summarized in right panels **(E)** ($n = 5$). **(F)** Xenografts were fixed and embedded in the paraffin and stained with hematoxylin and eosin for analysis of tumor necrosis induced by BTZ. All the data has been expressed as the mean ± SD from three independent experiments. Scale bars = 250 μm. (*$P < 0.05$; **$P < 0.01$; ***$P < 0.001$).

liver tissues. In addition, SEC24C levels were found to be negatively correlated with poor prognosis in HCC patients. Thereafter, through a series of *in vitro* as well as *in vivo* experiments, the potential role of SEC24C in regulating HCC cell proliferation, migration, invasion and apoptosis resistance was examined.

The basic UPR pathway is primarily divided into three branches initiated by three distinct ER transmembrane protein sensors: PERK, inositol-requiring enzyme 1α and activating transcription factor 6 (*31*). Under conditions of ER homeostasis, Bip bind to these sensors and prevent their activation. But upon ER-stress, BiP display higher affinity for various misfolded proteins and dissociate from these sensors (*32*). Thereafter PERK can phosphorylate itself and leads to the activation of eIF2α, which in turn can reduce global protein synthesis and suppresses proliferation, while selectively increasing ATF4 expression. Prolonged or extreme ER-stress lead to the subsequent transcriptional upregulation of CHOP and GADD34. As a transcription factor, CHOP can translocate to the nucleus and can facilitate programmed cell death by upregulating various genes involved in apoptosis (*33*). The loss of CHOP can render the cells and mice more resistant to ER-stress (*34*). In summary, moderate ER-stress responses caused by conditions of the tumor microenvironment promote cancer cell proliferation, metastasis and chemoresistance, but extreme ER-stress lead to a terminal UPR to induce cell death (*4*).

Our data clearly showed that SEC24C could localize in the nucleus with NPM1 under normal condition but respond rapidly to ER-stress and subsequently translocate at the ER surface. In previous report, NPM1 could shuttle to cytoplasm under stressed conditions, and our study also found its reduction upon ER-stress. As SEC24C has no classic nuclear localization signal, the localization of SEC24C in nucleus may rely on the interaction with NPM1, which could regulate nuclear import of protein without nuclear localization signal (*20*). When ER-stress are continuously activated, the expression of NPM1 in nucleus would be decreased, then SEC24C in the nucleus would shuttle to the ER surface for replenishing its deficiency by autolysosome degradation. The mechanism of NPM1 reduction upon ER-stress and the function of SEC24C in nucleus need our future exploration. In addition, we also found that SEC24C overexpression provoke extreme activation of the PERK-eIF2α-ATF4 axis and redirect the cells to CHOP-related apoptotic death. Thus, the shuttling ability of SEC24C between nucleus and ER are significant for the rapid response of hepatocytes to ER-stress and help prevent massive localization of SEC24C on ER for UPR activation under normal conditions. So, the hyperactive ER-phagy in HCC may partially account for the deficiency of SEC24C and subsequently enable HCC cells to tolerate to extreme ER-stress and escape from final UPR-related apoptosis.

BTZ, an FDA-approved drug, has been reported to markedly decrease the viability of HCC cells partly through UPR and the effect could be strongly inhibited by suppression of ATF4 (*30*). We found that overexpression of SEC24C significantly promote the sensitivity of HCC cells to BTZ treatment under both *in vitro* and *in vivo* settings. In addition, prior studies have also reported that the eIF2α-specific phosphatase inhibitor salubrinal inhibit the progression of HCC cells and its derivative Sal003 could also inhibit breast cancer progression (*30,35*). Our results demonstrated that the tumor volume of the nude mice with Huh7 sgNC and Huh7 sgSEC24C was reduced to a similar volume after the treatment with Sal003, thus suggesting that targeting downstream eIF2α could be a promising strategy to treat HCC tumors with low SEC24C expression.

In summary, our findings revealed that SEC24C can significantly suppress both HCC propagation and chemoresistance by promoting activation of the PERK-CHOP related apoptotic death, which could also partly explain the underlined mechanism of HCC cells escaping from apoptosis and maintaining proliferation under persistent ER-stress *via* SEC24C deficiency. Besides, by employing BTZ and several modulators targeting UPR signaling pathway, this present study can also provide opportunities for selecting appropriate chemotherapeutic drugs according to SEC24C expression levels in HCC tumors.

Acknowledgements

We would like to thank all laboratory members for their critical discussion of this manuscript.

Funding: This work was supported by grants from National Natural Science Foundation of China (82101850) & Project funded by China Postdoctoral Science Foundation (2021M701679) To Y.L.

Conflict of Interest: The authors have no conflicts of interest to disclose.

Ethics Approval and Consent to Participate: HCC samples (including tumor and adjacent nontumor samples) were collected from patients between August 2019 and September 2022 at Nanjing Drum Tower Hospital. Normal human liver samples were obtained from hepatic hemangioma patients with no evidence of chronic liver disease, diabetes, or hypertension. All patients provided written consent. All studies were approved by the Institutional Ethics Committee of Nanjing Drum Tower Hospital in compliance with the 1975 Declaration of Helsinki.

Availability of Data and Materials: The data generated in this study are available within the article and its

supplementary data files. Extra expression profile data analyzed in this study were obtained from TGCA dataset for tumor and GTEx dataset for normal. Prognosis data of patients with HCC were obtained from Kaplan-Meier Plotter database (*http://kmplot.com/analysis/index.php?p=service&cancer=liver_rnaseq*).

References

1. Vogel A, Meyer T, Sapisochin G, Salem R, Saborowski A. Hepatocellular carcinoma. Lancet. 2022; 400:1345-1362.
2. Li Z, Ge Y, Dong J, Wang H, Zhao T, Wang X, Liu J, Gao S, Shi L, Yang S, Huang C, Hao J. BZW1 Facilitates Glycolysis and Promotes Tumor Growth in Pancreatic Ductal Adenocarcinoma Through Potentiating eIF2alpha Phosphorylation. Gastroenterology. 2022; 162:1256-1271. e1214.
3. Hetz C, Chevet E, Harding HP. Targeting the unfolded protein response in disease. Nat Rev Drug Discov. 2013; 12:703-719.
4. Chen X, Cubillos-Ruiz JR. Endoplasmic reticulum stress signals in the tumour and its microenvironment. Nat Rev Cancer. 2021; 21:71-88.
5. Hetz C, Zhang K, Kaufman RJ. Mechanisms, regulation and functions of the unfolded protein response. Nat Rev Mol Cell Biol. 2020; 21:421-438.
6. Walter P, Ron D. The unfolded protein response: from stress pathway to homeostatic regulation. Science. 2011; 334:1081-1086.
7. Bernales S, McDonald KL, Walter P. Autophagy counterbalances endoplasmic reticulum expansion during the unfolded protein response. PLoS Biol. 2006; 4:e423.
8. Cui Y, Parashar S, Zahoor M, Needham PG, Mari M, Zhu M, Chen S, Ho HC, Reggiori F, Farhan H, Brodsky JL, Ferro-Novick S. A COPII subunit acts with an autophagy receptor to target endoplasmic reticulum for degradation. Science. 2019; 365:53-60.
9. Zielke S, Kardo S, Zein L, Mari M, Covarrubias-Pinto A, Kinzler MN, Meyer N, Stolz A, Fulda S, Reggiori F, Kogel D, van Wijk S. ATF4 links ER stress with reticulophagy in glioblastoma cells. Autophagy. 2021; 17:2432-2448.
10. Quesada-Calvo F, Massot C, Bertrand V, *et al*. OLFM4, KNG1 and Sec24C identified by proteomics and immunohistochemistry as potential markers of early colorectal cancer stages. Clin Proteomics. 2017; 14:9.
11. Xin C, Diego F CJAJP. Hydrodynamic transfection for generation of novel mouse models for liver cancer research. 2014; 184.
12. Gao Q, Zhu H, Dong L, *et al*. Integrated Proteogenomic Characterization of HBV-Related Hepatocellular Carcinoma. Cell. 2019; 179:1240.
13. Ferro-Novick S, Reggiori F, Brodsky JL. ER-Phagy, ER Homeostasis, and ER Quality Control: Implications for Disease. Trends Biochem Sci. 2021; 46:630-639.
14. Wilkinson S. ER-phagy: shaping up and destressing the endoplasmic reticulum. FEBS J. 2019; 286:2645-2663.
15. Chen Q, Xiao Y, Chai P, Zheng P, Teng J, Chen J. ATL3 Is a Tubular ER-Phagy Receptor for GABARAP-Mediated Selective Autophagy. Curr Biol. 2019; 29:846-855 e846.
16. Klionsky DJ, Abdel-Aziz AK, Abdelfatah S, *et al*. Guidelines for the use and interpretation of assays for monitoring autophagy (4th edition). Autophagy. 2021; 17:1-382.
17. Chino H, Hatta T, Natsume T, Mizushima NJMc. Intrinsically Disordered Protein TEX264 Mediates ER-phagy. 2019; 74:909-921.e906.
18. Grisendi S, Mecucci C, Falini B, Pandolfi PP. Nucleophosmin and cancer. Nat Rev Cancer. 2006; 6:493-505.
19. Borer RA, Lehner CF, Eppenberger HM, Nigg EA. Major nucleolar proteins shuttle between nucleus and cytoplasm. Cell. 1989; 56:379-390.
20. Gao H, Jin S, Song Y, Fu M, Wang M, Liu Z, Wu M, Zhan Q. B23 regulates GADD45a nuclear translocation and contributes to GADD45a-induced cell cycle G2-M arrest. J Biol Chem. 2005; 280:10988-10996.
21. Clarke HJ, Chambers JE, Liniker E, Marciniak SJ. Endoplasmic reticulum stress in malignancy. Cancer Cell. 2014; 25:563-573.
22. Hong F, Lin CY, Yan J, Dong Y, Ouyang Y, Kim D, Zhang X, Liu B, Sun S, Gu W, Li Z. Canopy Homolog 2 contributes to liver oncogenesis by promoting unfolded protein response-dependent destabilization of tumor protein P53. Hepatology. 2022; 76:1587-1601.
23. Tang J, Guo YS, Zhang Y, Yu XL, Li L, Huang W, Li Y, Chen B, Jiang JL, Chen ZN. CD147 induces UPR to inhibit apoptosis and chemosensitivity by increasing the transcription of Bip in hepatocellular carcinoma. Cell Death Differ. 2012; 19:1779-1790.
24. Parashar S, Chidambaram R, Chen S, Liem CR, Griffis E, Lambert GG, Shaner NC, Wortham M, Hay JC, Ferro-Novick S. Endoplasmic reticulum tubules limit the size of misfolded protein condensates. Elife. 2021; 10.
25. Adolf F, Rhiel M, Reckmann I, Wieland FT. Sec24C/D-isoform-specific sorting of the preassembled ER-Golgi Q-SNARE complex. Mol Biol Cell. 2016; 27:2697-2707.
26. Liu Z, Lv Y, Zhao N, Guan G, Wang J. Protein kinase R-like ER kinase and its role in endoplasmic reticulum stress-decided cell fate. Cell Death Dis. 2015; 6:e1822.
27. Marciniak SJ, Yun CY, Oyadomari S, Novoa I, Zhang Y, Jungreis R, Nagata K, Harding HP, Ron D. CHOP induces death by promoting protein synthesis and oxidation in the stressed endoplasmic reticulum. Genes Dev. 2004; 18:3066-3077.
28. Wendeler MW, Paccaud JP, Hauri HP. Role of Sec24 isoforms in selective export of membrane proteins from the endoplasmic reticulum. EMBO Rep. 2007; 8:258-264.
29. Yahiro K, Tsutsuki H, Ogura K, Nagasawa S, Moss J, Noda M. Regulation of subtilase cytotoxin-induced cell death by an RNA-dependent protein kinase-like endoplasmic reticulum kinase-dependent proteasome pathway in HeLa cells. Infect Immun. 2012; 80:1803-1814.
30. Ord T, Ord D, Kaikkonen MU, Ord T. Pharmacological or TRIB3-Mediated Suppression of ATF4 Transcriptional Activity Promotes Hepatoma Cell Resistance to Proteasome Inhibitor Bortezomib. Cancers (Basel). 2021; 13.
31. Ron D, Walter P. Signal integration in the endoplasmic reticulum unfolded protein response. Nat Rev Mol Cell Biol. 2007; 8:519-529.
32. Wang M, Wey S, Zhang Y, Ye R, Lee AS. Role of the unfolded protein response regulator GRP78/BiP in development, cancer, and neurological disorders. Antioxid Redox Signal. 2009; 11:2307-2316.
33. Samanta S, Yang S, Debnath B, Xue D, Kuang Y, Ramkumar K, Lee AS, Ljungman M, Neamati N. The Hydroxyquinoline Analogue YUM70 Inhibits GRP78

to Induce ER Stress-Mediated Apoptosis in Pancreatic Cancer. Cancer Res. 2021; 81:1883-1895.
34. Han J, Back SH, Hur J, Lin YH, Gildersleeve R, Shan J, Yuan CL, Krokowski D, Wang S, Hatzoglou M, Kilberg MS, Sartor MA, Kaufman RJ. ER-stress-induced transcriptional regulation increases protein synthesis leading to cell death. Nat Cell Biol. 2013; 15:481-490.
35. Darini C, Ghaddar N, Chabot C, *et al*. An integrated stress response *via* PKR suppresses HER2+ cancers and improves trastuzumab therapy. Nat Commun. 2019; 10:2139.

Received June 4, 2024; Revised July 10, 2024; Accepted July 23, 2024.

[§]These authors contributed equally to this work.

*Address correspondence to:
Beicheng Sun, School of Medicine, Southeast University, Nanjing 210009, Jiangsu, China.
E-mail: sunbc@nju.edu.cn

Yang Liu, Department of General Surgery, The First Affiliated Hospital of Anhui Medical University, Hefei 230022, Anhui, China.
E-mail: liuyang_1005@163.com

Jincheng Wang, Graduate School of Medical Science and Engineering, Hokkaido University, Sapporo, Japan.
E-mail: jcwang_med@hotmail.com

Released online in J-STAGE as advance publication August 1, 2024.

Original Article

DOI: 10.5582/bst.2024.01120

Effect and mechanism of Hashimoto thyroiditis on female infertility: A clinical trial, bioinformatics analysis, and experiments-based study

Meijun Pan[1,2,3,4,§], Qing Qi[5,§], Chuyu Li[1,2,3,§], Jing Wang[1,2,3], Xinyao Pan[1,2,3], Jing Zhou[6], Hongmei Sun[1,2,3], Lisha Li[1,2,3], Ling Wang[1,2,3,*]

[1] Laboratory for Reproductive Immunology, Obstetrics and Gynecology Hospital of Fudan University, Shanghai, China;
[2] The Academy of Integrative Medicine of Fudan University, Shanghai, China;
[3] Shanghai Key Laboratory of Female Reproductive Endocrine-related Diseases, Shanghai, China;
[4] The Second Clinical Medical College of Guangzhou University of Traditional Chinese Medicine, Guangzhou, China;
[5] Wuhan Business University, Wuhan, Hubei, China;
[6] Department of Obstetrics and Gynecology, Nanfang Hospital of Southern Medical University, Guangzhou, China.

SUMMARY Diagnosing Hashimoto thyroiditis (HT) relies on thyroglobulin antibody (TgAb) and thyroid peroxidase antibody (TPOAb) titers. The influence of these antibodies on female infertility remains a subject of debate. This study aims to explore the effect and mechanism of HT on female infertility. First, a single-center cross-sectional study was conducted to investigate whether TgAb and TPOAb are the key factors leading to female infertility. Second, bioinformatic analysis was performed to investigate the potential target molecules and pathways. Third, *in vivo* experiments were performed to explore the effects of elevated TgAb levels on embryo implantation in a mouse model of autoimmune thyroiditis (AIT). Four hundred and five infertile women and 155 healthy controls were enrolled in the cross-sectional study. Results indicated that the TPOAb titer was associated with female infertility, while the TgAb titer showed no significant association. The increased levels of TgAb and TPOAb are not significantly correlated with anti-Mullerian hormone. Bioinformatic analysis indicated that the common target molecules for HT and female infertility include interleukin (IL)-6, IL-10, matrix metalloproteinase 9, and tumor necrosis factor, suggesting potential regulation through multiple signaling pathways such as HIF-1, VEGF, MAPK, and Th17 cell differentiation. A certain dose of porcine thyroglobulin can successfully establish a mouse model of AIT. In this mouse model, embryo implantation and ovarian reserve remain unaffected by elevated TgAb levels. In conclusion, the serum TPOAb titer was associated with infertility due to female factors but the TgAb titer showed no significant association. A simple increase in serum TgAb titer does not affect embryo implantation and ovarian reserve in the AIT model.

Keywords female infertility, Hashimoto thyroiditis, thyroglobulin antibody, thyroid peroxidase antibody, embryo implantation

1. Introduction

Infertility is defined as the inability of a couple to achieve a clinical pregnancy after 12 months of regular, unprotected sexual contact (*1*). Over 186 million people are suffering from infertility (*2*), impacting 8 to 12% of couples of reproductive age globally (*3*). About 85% of infertile couples have a clear etiology. The most common reason is ovulation dysfunction, male infertility factors, and fallopian tubes, and the remaining 15% of infertile couples have unexplained infertility (*4*). Immune factors associated with infertility primarily encompass non-organ-specific antibodies, organ-specific antibodies, and natural killer cells. Although studies have shown that immune factors are involved in various links of reproduction, the mechanism has not been clarified (*5-11*). Insufficient evidence exists to identify the causal relationship between immune factors and infertility.

Hashimoto thyroiditis (HT), a chronic inflammation of the thyroid gland, is currently recognized as the most prevalent autoimmune disease, with a population prevalence of approximately 4.6% (*12,13*). The prevalence of HT in women is at least 8 times higher

than in men, and it is more prevalent among Whites and Asians compared to African-Americans. The diagnosis of HT relies on identification of thyroglobulin antibody (TgAb) and thyroid peroxidase antibody (TPOAb) (*12*). TgAb and TPOAb are collectively referred to as antithyroid antibodies (ATAb). Several clinical studies have suggested a relationship between TgAb, TPOAb, and fertility decline (*5-9*). However, the specific causal relationship between TgAb and TPOAb and fertility decline has not been clarified, and its mechanism still needs to be studied (*11*).

The prevalence of thyroid autoimmunity features is more frequent in infertile women than in healthy fertile women (*14,15*). However, asserting causation in the relationship between fertility and thyroid autoimmunity is a challenge, even when adequately controlling for other variables (*11*). Some researchers have pointed out that numerous studies have mainly explored the association between TPOAb and infertility. They advocate that research should also explore the effect of TgAb in fertility assessment (*10*). Most recently, some researches have simultaneously or independently studied the effects of TPOAb and TgAb on infertility, the pregnancy rate, outcomes of reproductive-assisted technology, and ovarian function, but the results have been inconsistent. A meta-analysis revealed an association between the presence of thyroid antibodies in euthyroid patients and unexplained subfertility (*16*). Research has also demonstrated that TPO-Ab is associated with reduced ovarian reserve and decreased embryo quality. High titers of TPO-Ab can reduce live birth rates. However, a recent prospective study has shown that while higher TPOAb titers should be considered one of the risk factors for miscarriage in infertile women, fertility is not affected by any thyroid-related factors (*17*). A population-based study and a case-control study have found no significant correlation between thyroid autoimmune antibodies and female infertility or cumulative pregnancy rate (*17,18*). TPOAb and/or TgAb's association with and causation of infertility are related to intervention with levothyroxine (L-T4) and other treatment regimens (*19,20*). This relationship also affects the rationality of screening infertile women for thyroid antibodies. At present, the causal relationship is still a subject of debate, and further research is of great value.

The current study sought to explore whether there is a correlation between infertility and HT and to elucidate the mechanisms underlying HT's impact on female infertility. This study consists of the following three parts. The first part explored whether TgAb and TPOAb are associated with female infertility based on clinical data. In the second part, the common target molecules for HT and female infertility were analyzed bioinformatically. The third part explored whether TgAb affects embryo implantation and ovarian reserve through animal experiments. This study combined clinical data, bioinformatics, and animal experiments to provide evidence for the treatment of HT and the improvement of female fertility.

2. Materials and Methods

2.1. A single-center cross-sectional study

2.1.1. Trial oversight

This study adopted a single-center cross-sectional design and was divided into two parts. The first part investigated the association between female infertility and peripheral blood TgAb and TPOAb positivity. The second part explored the correlation between peripheral blood TgAb or TPOAb titers and AMH levels.

The study included a group of infertile females and a control group. A total of 927 participants were screened. In the group of infertile females, 729 individuals were screened and 324 individuals were excluded, resulting in a remaining sample size of 405 individuals. Based on etiological factors, the group of infertile females was further divided into a group with ovulation disorders (47 individuals) and a group with pelvic factors (358 individuals, including 78 patients with endometriosis). Age-matched healthy adults made up the control group. In the control group, 198 people were screened, and 155 people were finally enrolled. The 405 individuals in the group of infertile females and the 155 individuals in the control group were used to study thyroid function and the association of peripheral blood TgAb and TPOAb with the disease (Figure 1).

Further screening of these patients was conducted to exclude confounding factors affecting the odds ratio (*21,22*). Of the 405 individuals in the group with infertility due to female factors, 300 were excluded, leaving 105 individuals. In the control group, 155 individuals were excluded, leaving 83 individuals. The association between peripheral blood TgAb titers, TPOAb titers, and AMH levels was examined based on the remaining 105 participants in the group of infertile females and the 83 participants in the control group. The study flow is shown in Figure 1. The Ethics Committee of the Obstetrics and Gynecology Hospital of Fudan University approved this clinical investigation (Kyy2018-85), which was conducted from January 1, 2018 to December 31, 2020.

2.1.2. Inclusion and exclusion criteria

The inclusion criteria were: 1) patients who were unable to achieve a clinical pregnancy after 12 months of regular sexual contact (*23,24*); 2) patients who have undergone hysterosalpingography, ultrasound, and a reproductive endocrine hormone examination suggesting female factors for infertility; 3) age between 20 and 40; 4) patients who have undergone a full set of thyroid laboratory examinations. Exclusion criteria were: 1)

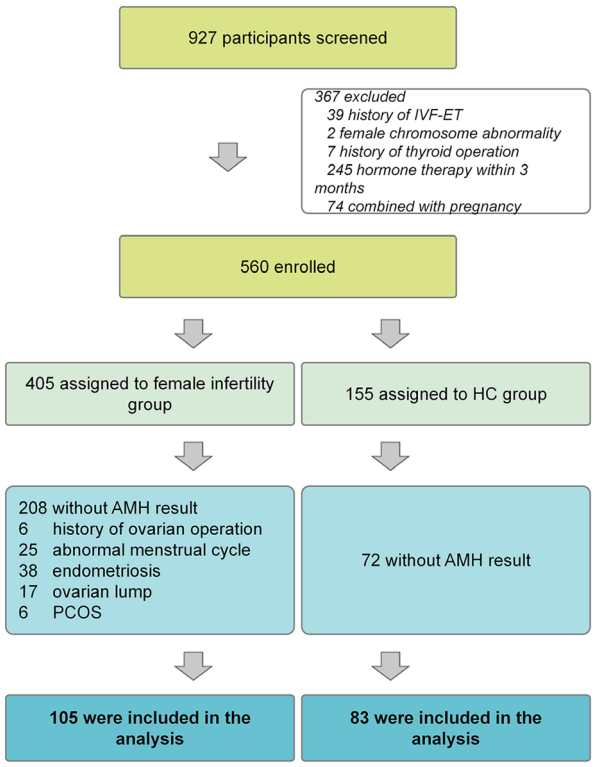

Figure 1. Flow chart showing the categorization of 560 participants based on diagnosis.

a history of significant respiratory, neurological, or cardiovascular diseases, or gastrointestinal, genitourinary system disorders; 2) severe infections, tumors, or immune deficiencies; 3) having previously undergone *in vitro* fertilization and embryo transfer; 4) female chromosomal abnormalities; 5) having previously undergone thyroid surgery; 6) the use of hormonal medications (such as L-T4, phenobarbital, and carbimazole) within three months of the determination of thyroxine hormones and antibodies; 7) patients whose thyroid hormone (TH), TgAb, and TPOAb results were only available during pregnancy; 8) having previously undergone an abortion within 6 months of measuring TH, TgAb, and TPOAb; 9) patients with factors affecting AMH, such as no measurement of AMH, having previously undergone ovarian surgery, an abnormal menstrual cycle, not having undergone a gynecological ultrasound examination, a gynecological ultrasound suggesting ovarian mass, endometriosis diagnosed *via* laparoscopy, and polycystic ovary syndrome (PCOS) diagnosed according to the 2003 Rotterdam diagnostic criteria. Participants in the control group had regular menstrual cycles, no history of adverse pregnancy, no abnormal gynecologic ultrasound examination, age 20-40 years, and had undergone a full set of laboratory thyroid examinations.

2.1.3. Medical evaluation

The basic information on each participant was collected in detail, including age, menstrual cycle, history of the present illness, pregnancy history, surgical history, past medical history, and family history. Venous blood samples were taken from the patients when seen, and the samples were centrifuged for five minutes at 3,000 r/min and 4°C. Before determination, serum samples were collected and kept at -20°C.

The serum AMH level was measured using sandwich immunoassay with a direct chemiluminescence technique. The serum thyrotropin (TSH) level was measured using the double antibody sandwich method; serum free thyroxine (FT4), TgAb, and TPOAb (Roche from Shanghai, China) were measured using the competition method. Transvaginal or transrectal ultrasonography was performed to determine ovarian and uterine morphology. Hysterosalpingography was performed 3-7 days after the patient experienced a clean menstrual period to observe the morphology of the uterus.

2.2. Bioinformatic analysis to explore the mechanism of female infertility caused by HT

2.2.1. Screening of disease-related target molecules

"Female infertility" and "Hashimoto thyroiditis" were used as keywords, which were input respectively into the DrugBank database (*https://go.drugbank.com/*), OMIM database (*https://omim.org/*), GeneCards database (*https://www.genecards.org/*), and Therapeutic Target Database (*http://db.idrblab.net/ttd/*). Information on target molecules related to diseases was downloaded from every database. After duplicates were removed, validated human target genes were screened by specifying "Homo sapiens" and "Reviewed" in the UniProt database (*https://www.uniprot.org/*). All relevant target molecules for female infertility and HT were identified. Cytoscape 3.8.2 was subsequently used to establish separate disease-target networks for female infertility and HT.

2.2.2. Construction of a protein-protein interaction network

A Venn diagram (*http://www.bioinformatics.com.cn/plot_basic_proportional_2_or_3_venn_diagram_028*) was drawn to obtain overlapping target molecules for female infertility-HT. The String 11.5 database *(https://cn.string-db.org/*) was used to construct a protein-protein interaction (PPI) network of overlapping target molecules. "Homo sapiens" was designated as the species, and a confidence level of 0.4 was the parameter.

2.2.3. Analysis of core target molecules

The network underwent topological analysis using CytoHubba (*25*), a plug-in of Cytoscape, to identify the top 20 core target molecules. The parameters for

CytoHubba were set as follows: Core target molecule = the top 20 nodes in order of highest clique centrality.

2.2.4. Gene Ontology (GO) and Kyoto Encyclopedia of Genes and Genomes (KEGG) enrichment analysis

The target molecules interacting in female infertility and HT were subjected to KEGG and GO enrichment analysis using the Metascape database (*https://metascape.org/gp/index.html*), with "Homo sapiens" and "$P < 0.01$" serving as the screening conditions. The acquired data included cellular components (CC), biological processes (BP), molecular function (MF), and signal pathways that are closely related to HT and female infertility. The results were plotted for visualization (*https://cloud.oebiotech.cn/spa#/bio/detail?number=5f6b0540-9c97-4d95-9528-bd0f3ed9d412*, *http://www.ehbio.com/ImageGP/index.php/Home/Index/GOenrichmentplot.html*).

2.3. Animal experiments

2.3.1. Reagents

Collagenase, Chicago Sky Blue, complete and incomplete Freund's adjuvants (CFA and IFA), and porcine thyroglobulin (pTg) were acquired from Sigma. A hematoxylin and eosin (HE) staining kit was obtained from Wuhan Servicebio Technology Co., Ltd. Tribromoethyl alcohol was purchased from Jiangsu Yihe Scientific Instrument Co., Ltd.

2.3.2. Animals

Four-week-old female NOD/LtJ mice were procured from Jiangsu JiCui Yaokang Biotechnology Co., Ltd. (Nanjing, Jiangsu). The mice were housed in a climate-controlled setting with a 12-hour light/dark cycle, where they had unlimited access to food and drink. A constant temperature of 25°C was kept. After one week of acclimation, the mice were used in experiments. All operations were carried out in strict compliance with the National Institutes of Health's Guide for the Care and Use of Laboratory Animals (publication number 85-23, amended in 1985) and Fudan University's (Shanghai, China) relevant guidelines.

2.3.3. Establishment of a mouse model of AIT

Forty-two specific pathogen-free NOD/LtJ female mice were randomly divided into three groups - a normal group, a control group, and a Tg group - with each group consisting of 14 mice. Mice in the Tg group were immunized with pTg. The 0.375 g/L pTg solution was fully emulsified with an equivalent volume of CFA on ice, and 0.1 ml of emulsified agent was injected subcutaneously 1 cm proximal to the root of the tail of each mouse. Two weeks after the primary immunization, a booster immunization with pTg and IFA emulsifier was administered again to establish a mouse model of AIT (*26,27*). The control group served as the solvent control group, while the normal group did not undergo any treatment. Six weeks after the establishment of AIT, some mice were sacrificed. The thyroid, lymph nodes, spleen, and serum samples were collected. Serum TH levels, the TgAb titer, and the TPOAb titer were determined using electrochemiluminescence immunoassay (ECLIA). HE staining was used to count the follicles at different developmental stages. The remaining mice were mated. The pregnant mice were injected with Chicago blue dye during the window of implantation (WOI) period (4.5 days of gestation) to count the number of embryo implantation sites, and HE staining was used to observe and count the uterine glands during WOI.

2.3.4. Measurement of serum TgAb, TPOAb, FT3, and FT4

Following anesthesia, blood samples were extracted from the mice. After the blood was left stand for 4-6 hours, it was centrifuged for 10 minutes at 4000 g. The upper serum was then collected and stored at -20°C. ECLIA was used to determine the serum TgAb titer, TPOAb titer, FT3 level, and FT4 level.

2.3.5. HE staining of the thyroid, ovaries, and uterus

Ovarian, uterine, and thyroid tissues were dissected and promptly fixed in 4% paraformaldehyde solution for 24 hours. After dehydration and embedding in paraffin, the sections underwent HE staining. The main process was as follows: after baking in an oven at 60°C, the slices were deparaffinized with xylene and ethanol and then hydrated. Tissues were stained with hematoxylin for 3-5 minutes, rinsed with running water, and differentiated with a differentiation solution. They were then washed with running water, treated with blue liquid, and rinsed again with running water. Afterwards, the slices were stained with eosin for 5 min, dehydrated with absolute ethanol and xylene, and sealed with neutral gum. Ultimately, microscopy and image acquisition were performed. HE-stained sections of ovaries were observed under a microscope. The count of primordial, primary, secondary, antral, and preovulatory follicles was determined, followed by statistical analysis. The number of uterine glands was also quantified under a microscope based on HE-stained uterine sections.

2.3.6. Measurement of implantation sites

After the mice were anesthetized, 0.25 ml Chicago blue dye was injected into the inner canthus vein, and the palms and soles of the mice could be observed to turn blue. After waiting for 10 minutes, blood and the uterus were collected. The implantation sites were stained light

blue by the Chicago blue dye. The uterine glands were photographed, and the number of embryo implantation sites during the WOI period was counted.

2.4. Statistical analysis

Data were processed and analyzed utilizing SPSS 25.0. In clinical trials, for the two groups of quantitative data, an independent samples *t*-test was used if the data followed a normal distribution and displayed homogeneity of variances. A Mann-Whitney *U* test was utilized if not. If there were three or more groups of quantitative data, analysis of variance was used for intergroup comparisons. The Kruskal-Wallis test and the Conover test were used to perform intergroup comparisons in the event that the data did not satisfy the requirements of normality and homogeneity of variances. A chi-square test or Fisher's exact test was used for unordered categorical data. The associations between serum TgAb titers, TPOAb titers, gravidity, parity, TSH levels, FT4 levels, age, antral follicle count (MOV), and AMH were analyzed using the Spearman correlation coefficient.

For animal experiments, in the three groups of quantitative data that were normally distributed and had homogeneity of variance, analysis of variance and the Least Significant Difference test were used. The Kruskal-Wallis rank sum test was used for between-group comparisons if the conditions were not met. Image pro plus 6.0.0 was used to compute the ovarian area. Scale addition was performed using ImageJ 1.5.3. Graphs were created using GraphPad Prism 8.0.2. A two-tailed $P < 0.05$ indicated a significant difference.

3. Results

3.1. Comparison of general information, thyroid function, peripheral blood TgAb, and TPOAb between infertile female patients and the control group

In comparison to the control group, the female infertility cohort exhibited a marked increase in pregnancies ($P < 0.001$) and a markedly increased FT4 level ($P = 0.027$). The TPOAb titer in peripheral blood was elevated ($P = 0.031$), and positivity for TPOAb was markedly higher ($P = 0.019$) compared to that in the control group. Positivity for TgAb or/and TPOAb was also significantly higher compared to that in controls ($P = 0.013$). Conversely, there were no significant differences in age, TSH level, TgAb titer, positivity for TgAb, double positivity for TgAb and TPOAb, the rate of congenital hypothyroidism (CH), the rate of subclinical hypothyroidism (SCH), and the rate of normal thyroid function between the infertile female group and the control group ($P > 0.05$) (Table 1).

In accordance with the etiology of the disease, infertile female patients were stratified into those with ovulatory dysfunction and pelvic factors. Results indicated that the ovulation disorder group tended to be younger than the control group ($P < 0.001$) and exhibited a notably higher pregnancy rate ($P = 0.004$). The TSH level in the ovulation disorder group was significantly elevated compared to that in the control group ($P =$

Table 1. Distributions of age and serological thyroid function indicators between infertile female patients and the control group

Items	Female infertility			Control (n = 155)
	Ovulatory dysfunction (n = 47)	Pelvic factor (n = 358)	Total (n = 405)	
Age (year)	27.66 ± 0.51***	29.43 ± 0.21	29.23 ± 0.2	29.83 ± 0.32
Serum hormone levels				
TSH (μIU/mL)	3.92 ± 0.51**	2.72 ± 0.1	2.86 ± 0.1	2.51 ± 0.12
FT4 (pmol/L)	16.69 ± 0.32	17.35 ± 0.14*	17.27 ± 0.13*	16.82 ± 0.19
Serum antibody levels				
TgAb (IU/mL)	10.89 (10-4000)	11.92 (10-4000)	11.86 (10-4000)	11.68 (10-4000)
TPOAb (IU/mL)	12.34 (5-600)	14.13 (5-600)*	13.87 (5-600)*	12.78 (5-600)
TgAb-positive [n (%)]	12 (25.53)**	51 (14.25)	63 (15.56)	15 (9.68)
TPOAb-positive [n (%)]	9 (19.15)*	56 (15.64)*	65 (16.05)*	13 (8.39)
TgAb or/and TPOAb-positive [n (%)]	14 (29.79)**	73 (20.39)*	87 (21.48)*	19 (12.26)
TgAb and TPOAb-positive [n (%)]	7 (14.89)	34 (9.5)	41 (10.12)	9 (5.81)
Clinical diagnosis				
EU [n (%)]	37 (78.72)	298 (83.24)	335 (82.72)	133 (85.81)
CH [n (%)]	1 (2.13)	1 (0.28)	2 (0.49)	0 (0)
SCH [n (%)]	9 (19.15)	45 (12.57)	54 (13.33)	19 (12.26)

Data are means ± SD or Median (Min-Max) for continuous variables, or n (%) for categorical variables. AMH: anti-Müllerian hormone; MOV: mean ovarian volume; TSH: thyroid stimulating hormone; FT3: free triiodothyronine; FT4: free thyroxine; TgAb: thyroglobulin antibody; TPOAb: thyroid peroxidase antibody; CH: clinical hypothyroidism; SCH: subclinical hypothyroidism; EU: euthyroid. *$P < 0.05$ *vs.* controls, **$P < 0.01$ *vs.* controls, ***$P < 0.001$ *vs.* controls.

0.004). Moreover, there was a significant increase in the positivity for TgAb in peripheral blood ($P = 0.005$) and an elevation in the positivity for TPOAb ($P = 0.038$) in the ovulation disorder group compared to controls. Positivity for TgAb or/and TPOAb was also higher ($P = 0.004$). However, the FT4 level, TPOAb titer, TgAb titer, double positivity for TgAb and TPOAb, the rate of CH rate, the rate of SCH, and the rate of normal thyroid function did not differ significantly compared to those indices in the control group ($P > 0.05$).

In the pelvic factor group, the number of pregnancies was notably higher than that in the control group ($P < 0.001$). Significantly elevated FT4 levels ($P = 0.016$) and TPOAb titers ($P = 0.027$) were noted compared to levels and titers in controls. Positivity for TPOAb and positivity for TgAb or/and TPOAb were both considerably higher than those in the control group ($P = 0.027$). There were significant differences in age, the TSH level, TgAb titer, positivity for TgAb, double positivity for TgAb and TPOAb, the rate of CH, the rate of SCH, and the rate of normal thyroid function compared to those indices in the control group ($P > 0.05$).

3.2. Peripheral blood TgAb and TPOAb levels lead to differences in the proportion of patients in different stages of clinical hypothyroidism

In accordance with the development of CH caused by TgAb and TPOAb, CH can be divided into four stages: Normal thyroid function and double negativity for TgAb and TPOAb, normal thyroid function and positivity for TgAb or/and TPOAb, SCH and positivity for TgAb or/and TPOAb, and CH and positivity for TgAb or/and TPOAb. An analysis of the distribution of these stages among all patients showed that individuals with SCH and positivity for TgAb or/and TPOAb were substantially more prevalent in the group of infertile females compared to controls ($P = 0.038$). There were no substantial differences in the proportion of patients with normal thyroid function and double negativity for TgAb and TPOAb, normal thyroid function and positivity for TgAb and/or TPOAb, and CH and positivity for TgAb and/or TPOAb ($P > 0.05$) (Table 2).

3.3. No correlation between serum TgAb, TPOAb, and AMH

3.3.1. No correlation between the serum TgAb titer, TPOAb titer, and serum AMH level

Spearman correlation analysis was performed between AMH levels in the two groups and other quantitative data. Results revealed a substantial positive association with MOV ($r = 0.459$, $P < 0.001$) and a significant negative correlation with age in the group of infertile females ($r = -0.346$, $P < 0.001$). In the control group, the AMH level also exhibited a significant association with MOV ($r = 0.41$, $P < 0.001$). However, the AMH level and antibody titer were not significantly correlated in either group ($P > 0.05$) (Table 3).

3.3.2. No correlation between ATAb positivity and peripheral blood AMH

TgAb titers and TPOAb titers are used to determine whether TgAb and TPOAb are positive in clinical practice, so TgAb and TPOAb were converted into categorical variables to explore the association between TgAb, TPOAb, and ovarian reserve. The two groups were subdivided according to TgAb and/or TPOAb

Table 2. Proportion of participants in each group at different development stages of CH

Items	Female infertility ($n = 405$)	Control ($n = 155$)	P value
EU and double negative for TgAb and TPOAb [n (%)]	280 (69.14)	118 (76.13)	0.102
EU and positive for TgAb or/and TPOAb [n (%)]	55 (13.58)	15 (9.68)	0.211
SCH and positive for TgAb or/and TPOAb [n (%)]	21 (5.19)*	2 (1.29)	0.038
CH and positive for TgAb or/and TPOAb [n (%)]	2 (0.49)	0 (0)	1

Data are n (%). EU: euthyroid; TgAb: thyroglobulin antibody; TPOAb: thyroid peroxidase antibody; SCH: subclinical hypothyroidism; CH: clinical hypothyroidism. *$P < 0.05$ *vs.* controls.

Table 3. Correlation analysis between serum AMH and quantitative data

Correlation coefficient	Female infertility ($n = 105$)	P value	Control ($n = 83$)	P value
Age	-0.346***	< 0.001	-0.19	0.085
MOV	0.459**	< 0.001	0.41***	< 0.001
TSH	0.056	0.571	-0.11	0.321
FT4	0.105	0.286	0.018	0.870
TgAb	0.103	0.297	-0.114	0.305
TPOAb	-0.056	0.572	-0.096	0.389

Data are r. MOV: mean ovarian volume; TSH: thyroid stimulating hormone; FT4: free thyroxine; TgAb: thyroglobulin antibody; TPOAb: thyroid peroxidase antibody. **$P < 0.01$ *vs.* controls, ***$P < 0.001$. *vs.* controls.

positivity. Among them, 21 were positive for TgAb and/or TPOAb , and 84 were negative in the group of infertile females. In the control group, 14 patients were positive for TgAb or/and TPOAb, and 69 were negative. The age, MOV, TSH, FT4, and AMH levels of the positive and negative groups were compared. Results indicated that, in both the group of infertile females and control group, there were no notable differences in age, MOV, TSH, FT4, and AMH levels between the TgAb- or/and TPOAb-positive subgroup and the double-negative TgAb and TPOAb subgroup ($P > 0.05$) (Table 4).

3.4. Analysis of intersecting target molecules for infertility due to female factors and HT

3.4.1. Overlapping target molecules for female infertility-HT

Nine hundred ninety-five target molecules related to female infertility and 1,282 target molecules related to HT were screened, respectively, using GeneCards and other databases. There were 427 overlapping target molecules for female infertility-HT (Figure 2A).

3.4.2. PPI network analysis of core target molecules

A PPI network was established from 427 overlapping target molecules utilizing the String database and the software Cytoscape. The female infertility-HT network consists of 426 nodes and 14,839 edges. Each node represents a target of the interaction between female infertility and HT, the magnitude of which is proportional to the value for the target molecule. An edge indicates an interaction between the two target molecules, and its thickness is proportional to the strength of the interaction (Figure 2B). The PPI network was entered into the software Cytoscape and analyzed using a CytoHubba plug-in to obtain the highest 20 core target molecules according to the MCC (Figure 2C). Core target molecules for female infertility-HT include glyceraldehyde-3-phosphate dehydrogenase, vascular endothelial growth factor A, interleukin-6 (IL-

Table 4. Comparison of peripheral blood AMH after subgrouping according to ATAb positivity

Items	Female infertility			Control		
	ATAb positive ($n = 21$)	ATAb negative ($n = 84$)	P value	ATAb positive ($n = 14$)	ATAb negative ($n = 69$)	P value
Age (year)	31 ± 0.94	29.7 ± 0.48	0.293	31.57 ± 0.8	30.35 ± 0.5	0.131
MOV (cm^3)	6.98 ± 0.47	7.07 ± 0.27	0.882	6.96 ± 0.59	7.61 ± 0.27	0.323
TSH (μIU/mL)	3.54 ± 0.75	2.45 ± 0.16	0.767	2.57 ± 0.35	2.59 ± 0.22	0.481
FT4 (pmol/L)	16.56 ± 0.4	17.17 ± 0.23	0.231	17.9 ± 1.57	16.63 ± 0.19	0.913
AMH (ng/mL)	3.86 ± 0.55	3.05 ± 0.19	0.087	3.38 ± 0.52	3.45 ± 0.21	0.675

Data are the mean ± SD. MOV: mean ovarian volume; TSH: thyroid stimulating hormone; FT4: free thyroxine; ATAb: antithyroid antibody; TgAb: thyroglobulin antibody; TPOAb: thyroid peroxidase antibody; AMH: anti-Müllerian hormone.

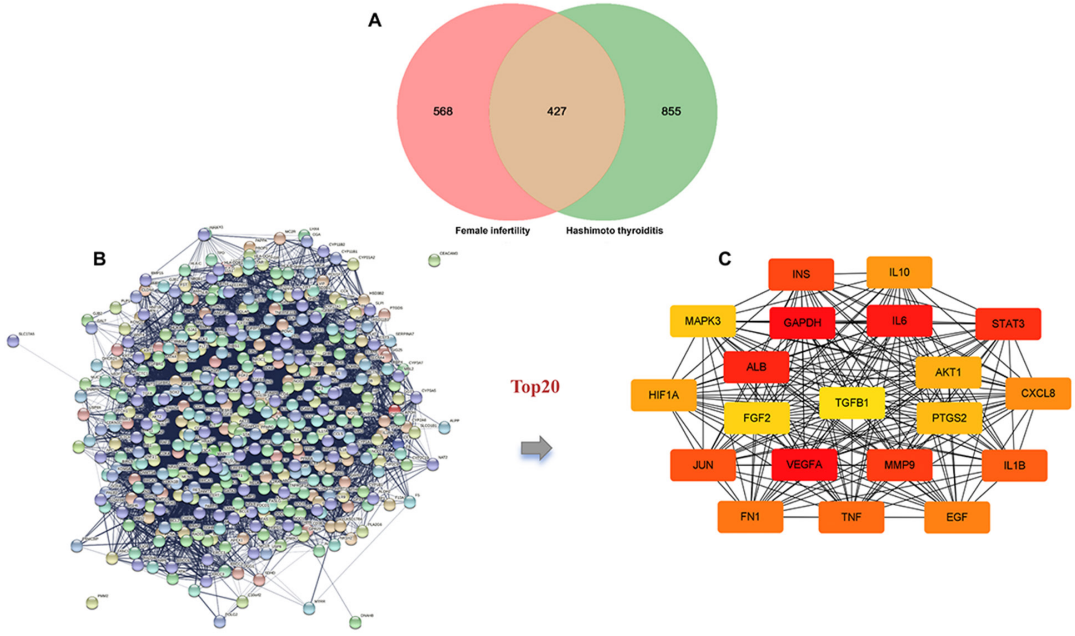

Figure 2. Analysis of target molecules for infertility due to female factors and HT. (A) Overlapping target molecules for female infertility-HT. **(B)** PPI network of overlapping target molecules for female infertility-HT. **(C)** PPI network of the top 20 target molecules. Rounded rectangles represent target molecules and those that are darker in color represent a greater degree of centrality. HT: Hashimoto thyroiditis, PPI: protein-protein interaction.

6), serum albumin, signal transducer and activator of transcription 3, matrix metalloproteinase 9 (MMP9), insulin, transcription factor AP-1, IL-1β, tumor necrosis factor (TNF), fibronectin 1, pro-epidermal growth factor (EGF), IL-8, IL-10, hypoxia-inducible factor 1-α (HIF 1-α), RAC-alpha serine/threonine-protein kinase (AKT1), prostaglandin G/H synthase, mitogen activated protein kinase 3 (MAPK3), fibroblast growth factor 2, and transforming growth factor-β1 (TGF-β1).

3.4.3. GO enrichment analysis and KEGG pathway enrichment analysis

GO enrichment and KEGG pathway enrichment analysis were performed for the top 20 target molecules to systematically explore their biological function. GO enrichment analysis revealed the function of genes by BP (green bars), CC (blue bars), and MF (red bars). A $P < 0.01$ was used, resulting in 671 entries. These included 634 BP entries, 15 CC entries, and 22 MF entries. The BP of female infertility-HT interaction, the positive regulation of cell migration, cell movement, and cell component movement were at the forefront. The endoplasmic reticulum lumen, cell membrane, outer cytoplasmic membrane, extracellular matrix, and membrane microdomain were at the forefront of CC. At the forefront of MF were cytokine activity, cytokine receptor binding, growth factor activity, chemokine receptor binding, and chemokine activity (Figure 3A).

KEGG signaling pathway enrichment analysis

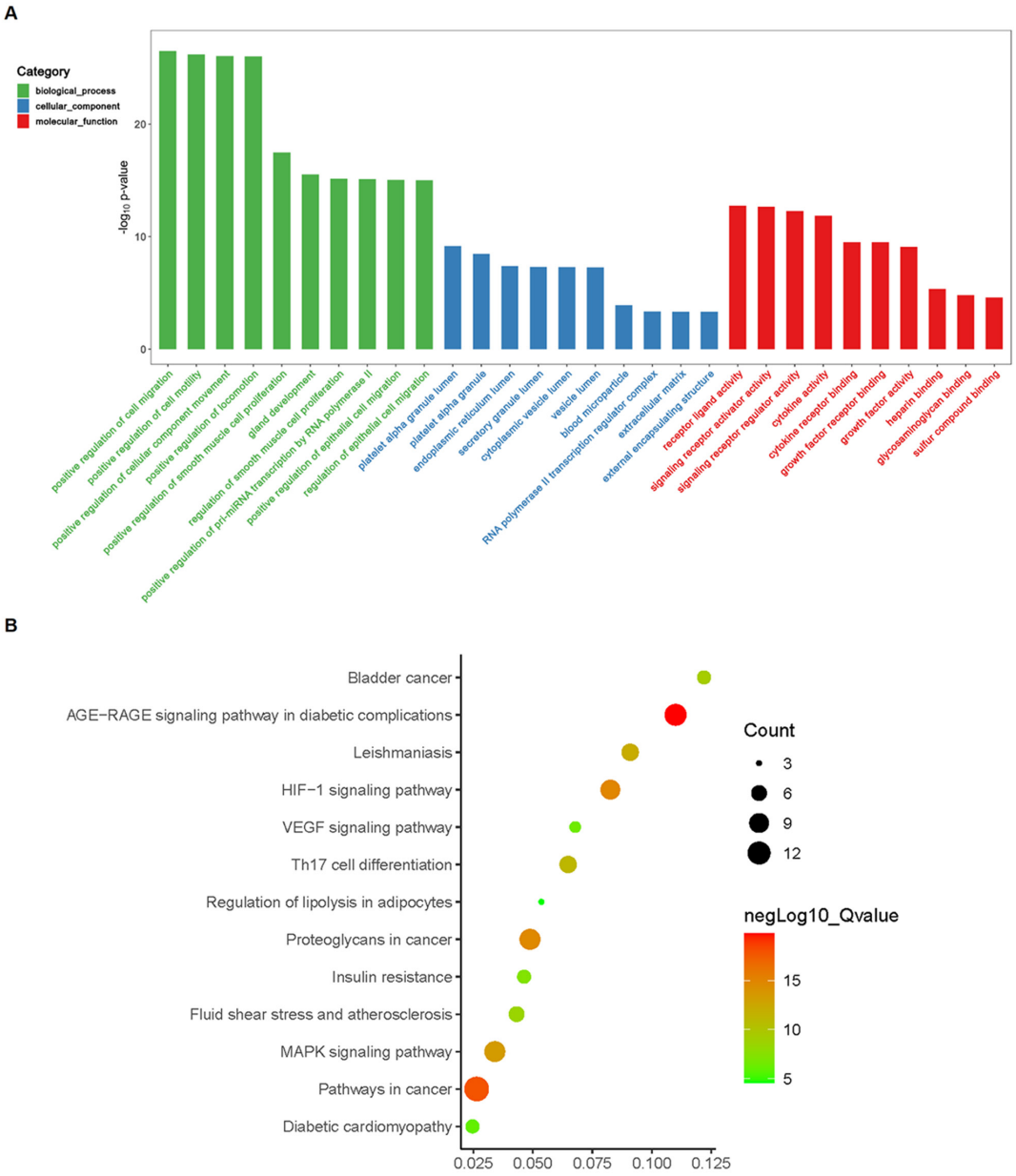

Figure 3. GO enrichment analysis and KEGG pathway enrichment analysis. **(A)** GO enrichment analysis. **(B)** KEGG pathway enrichment analysis. HT: Hashimoto's thyroiditis; GO: gene ontology; KEGG: Kyoto Encyclopedia of Genes and Genomes; AGE-RAGE: advanced glycosylated end product-glycosylated end product receptor; HIF-1: hypoxia-inducing factor 1; VEGF: vascular endothelial growth factor; TH17: type 17 helper T cells; MAPK: mitogen-activated protein kinase.

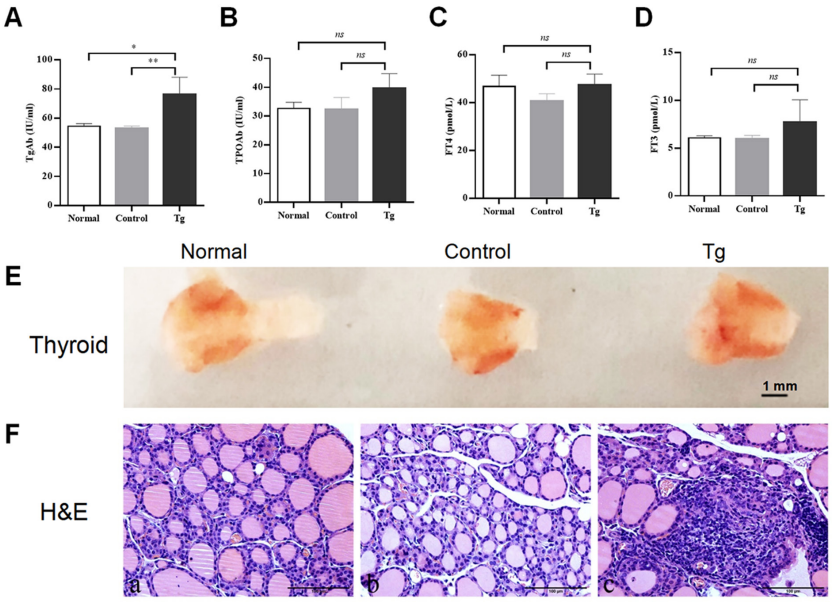

Figure 4. Serum thyroid hormone levels, antibody titers, and thyroid changes in each group. Comparison of serum **(A)** TgAb, **(B)** TPOAb, **(C)** FT4, and **(D)** FT3 in mice among the normal, control, and Tg groups. **(E)** Appearance of thyroid specimens in each group. Scale bars, 1mm. **(F)** Hematoxylin and eosin staining of thyroid tissue from rats. Magnification, ×400. Scale bars, 100 μm.

showed that the core target molecule for female infertility-HT was mainly enriched in 119 signaling pathways ($P < 0.01$) (Figure 3B). The pathways mainly included the advanced glycosylation end product (AGE) - receptor of AGE (RAGE) signaling pathway in diabetic complications, the cancer pathway, Chagas disease, HIF-1 pathway, and Kaposi sarcoma-associated herpes virus infection (Figure 3B).

3.5. Serum thyroid hormone levels and antibody titers in mice in each group

In this study, pTg was used to establish a mouse AIT model. On day 43, serum antibody titers and hormone levels in peripheral blood were determined. The serum TgAb titer in the Tg group was considerably higher than that in the normal group and control group ($P = 0.010$ in the normal group and $P = 0.008$ in the control group). The TPOAb titer tended to increase, while the serum FT4 and FT3 levels did not change substantially ($P > 0.05$), indicating that the model was successfully established (Figures 4A-4D).

3.6. Changes in the thyroid of mice in each group

The Tg group had larger thyroid volume, darker color, and tougher texture compared to both the normal and control groups. The HE-stained thyroid specimens from the normal, control, and Tg groups were observed under a light microscope. In the normal group and the control group, the thyroid follicle structure was intact, robust, and had a clear boundary. There was also no obvious destruction of the follicular epithelium. The cytoplasm was red, and the nucleus was blue. The follicular cavity had an abundance of glia-like substances and was pink. No lymphocytes were seen in the interfollicular space. The Tg group exhibited lymphocyte aggregation and partial destruction of follicular structures (Figures 4E and 4F).

3.7. Embryo implantation in mice in each group

Visual inspection of the uterus after Chicago staining revealed a V-shaped mouse uterus. Embryo implantation sites are stained dark blue and can be clearly counted in each uterus. No discernible difference in implantation sites was noted among the three groups ($P > 0.05$) (Figure 5G).

3.8. Changes in pathological sections of the mice uterus in each group

Pathological sections of the uterus showed that the mouse uterine cavity was located in the middle of the transverse section of the uterus and was surrounded by the luminal epithelium (Le), which was a single layer of columnar epithelium with the cytoplasm in red and nucleus in blue. Deep in the luminal epithelium is the lamina propria, which occupies most of the cross-sectional area of the mouse uterus and which contains stromal cells (S) and glands. The glands consist of glandular epithelium (Ge), which varies in size, with the cytoplasm in red and nucleus in blue. The Tg group's uterine pathological alterations did not differ markedly from those in the other two groups. The number of uterine glands did not differ significantly among the

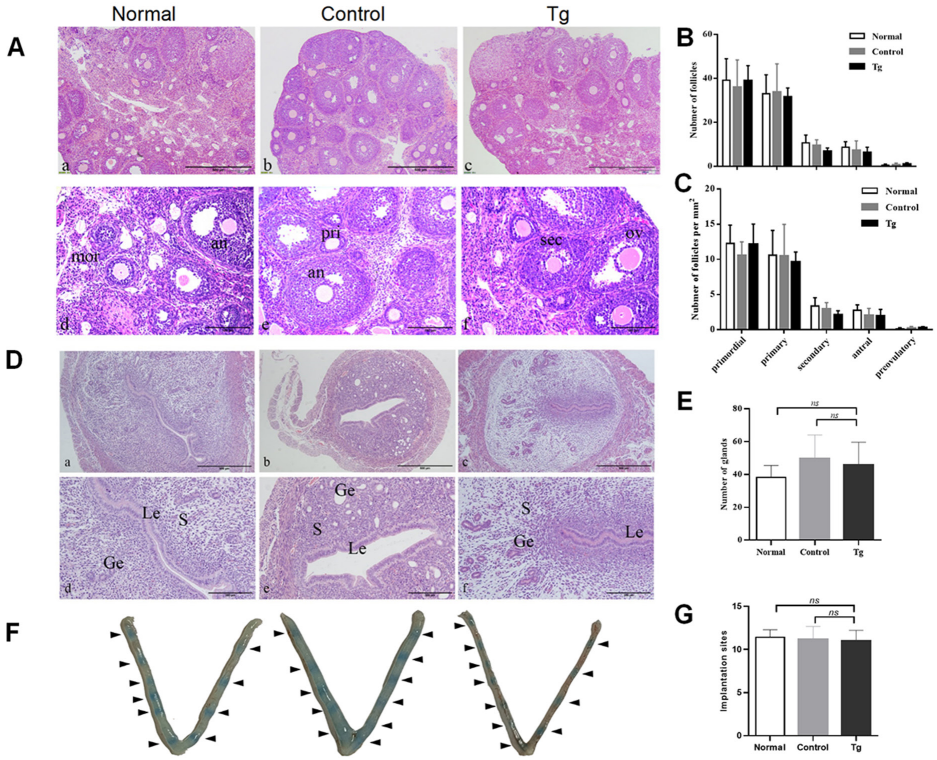

Figure 5. The ovaries, uterus, embryo implantation sites, and follicles of mice in each group. (A) Hematoxylin and eosin staining of mouse ovaries. a, b, c: Magnification, ×100. Scale bars, 500 μm. d, e, f: Magnification, ×200. Scale bars, 100 μm. mor: primordial follicle; pri: primary follicle; sec: secondary follicle; an: antral follicle; ov: preovulatory follicle. **(B)** Number of different types of follicles. **(C)** Number of different types of follicles per mm^2. **(D)** Hematoxylin and eosin staining of the uterus. a, b, c: Magnification, ×200. Scale bars, 500 μm. d, e, f: Magnification, ×200. Scale bars, 500 μm. Le: uterine luminal epithelium; S: uterine stromal cells; Ge: uterine glandular epithelium. **(E)** Comparison of counts in mouse uterine glands. ns: There was no significant difference. **(F)** Chicago Sky blue staining at the implantation site of mouse embryos in each group. **(G)** Comparison of the number of embryo implantation sites.

three groups ($P > 0.05$) (Figures 5D and 5E).

3.9. Ovarian pathological changes in mice in each group

The pathological sections of the mouse ovary suggested that the follicles were mainly distributed in the cortex and were of different sizes and shapes. Primordial follicles are formed by a single layer of spindle-shaped pregranulosa cells surrounding the primary oocyte (mor in Figure 5A). The primary follicle is larger in volume than the primordial follicle and consists of 1-2 layers of cuboid cells surrounding the oocyte (pri in Figure 5A). Secondary follicles further increased in size and had more cuboidal cell layers (sec in Figure 5A). The accumulation of follicular fluid between the granulosa cells increased, and fluid-filled spaces coalesced to form a follicular antrum, at which point the follicle is called antral (an in Figure 5A). Mature follicles are the final stage of follicular development, with a sharp increase in follicular fluid, enlargement of the follicular cavity, a significant increase in follicular volume, and the beginning of follicular projection toward the ovarian surface (ov in Figure 5A). The number of follicles at different developmental stages did not differ significantly among the normal, control, and Tg groups ($P > 0.05$). Similarly, the number of follicles per square millimeter at various developmental stages did not differ significantly among these groups ($P > 0.05$).

4. Discussion

The marked decrease in infertility is currently a substantial challenge for numerous countries (*28*). The etiology of female infertility is multifaceted, with ongoing exploration into immunological factors (*23,29*). However, the relationship between infertility due to female factors and HT remains inconclusive (*11,30*). In the current work, a cross-sectional study was designed to explore whether TgAb and TPOAb are associated with infertility due to female factors. Additionally, we conducted in-depth research based on bioinformatics and a murine AIT model to investigate the mechanism of TgAb and TPOAb on female fertility. Our findings verified the association between peripheral blood TPOAb and infertility due to female factors and suggested that peripheric TgAb may be not associated with infertility due to female factors or that TPOAb and TgAb may influence female reproductive capability synergistically. Elevated TgAb titers in the peripheral blood of mice were not significantly correlated with embryo implantation and ovarian reserve, which is consistent with our clinical results.

The thyroid gland, the body's largest endocrine organ, serves as a primary target of autoimmune assault, with HT regarded as the most prevalent autoimmune disorder (*10*). Our cross-sectional study found a positive correlation between serum TPOAb levels and infertility due to female factors, which accords with previous results (*11,14*). In a study by Poppe *et al*., among 197 patients with infertility due to female factors, positivity for TPOAb was considerably higher compared to that in the control group (18% *vs.* 8%, $P < 0.05$). Among these 197 patients with infertility due to female factors, 116 had ovulatory disorders, with no discernible difference in positivity for TPOAb compared to controls (16% *vs.* 8%, $P > 0.05$). In 21 patients with endometriosis, however, positivity for TPOAb was substantially higher than that in the control group (29% *vs.* 8%, $P < 0.05$) (*14*). The results of our investigation align closely with these findings, revealing a significantly higher positivity for TPOAb in patients with infertility due to female factors. Positivity for TPOAb was markedly higher in patients with ovulatory disorders, suggesting a potential correlation between TPOAb and infertility due to female factors.

The study by Poppe *et al*. did not include TgAb, whereas our study did, and we found a higher positivity for TgAb in the group with ovulatory disorders but no significant difference in any of the infertile female patients. Additionally, all of the patients with infertility due to female factors in our study demonstrated significantly higher parity compared to controls, which is probably because of the inclusion of mostly secondary infertility patients with a history of prior pregnancies. In summary, our results suggested a potential association between TPOAb and female infertility. However, it remains unclear whether TPOAb acts independently or in synergy with TgAb, whether TgAb and TPOAb are associated with clinical conditions manifesting as female infertility (*e.g.*, endometriosis, PCOS, primary ovarian insufficiency), or whether TgAb and TPOAb are directly related to female infertility. The diagnosis of infertility spans a year, adding to the complexity of cohort studies investigating the relationship between TgAb and TPOAb positivity and infertility. Consequently, further comprehensive clinical or foundational research needs to be conducted to provide conclusive evidence.

Several researchers have explored the relationship between TgAb, TPOAb, TSH, and AMH, but their conclusions have been inconsistent (*31-39*). The study by Poppe *et al*. and our research observed an increase in TSH levels in the group with ovulatory disorders (Poppe: 1.5 *vs.* 1.1, $P < 0.05$; ours: 3.92 *vs.* 2.51, $P < 0.01$). However, there is currently no evidence to suggest that TSH levels above the reference range (*i.e.*, SCH) impact ovarian response, oocyte/embryo quality, or pregnancy rates (*10*). AMH is mainly affected by biological characteristics, reproductive factors, environment, and lifestyle. In terms of reproductive factors, ovarian suppression, pregnancy status, and having previously undergone ovarian surgery have been linked to reduced AMH levels. Conditions like PCOS, granulosa cell tumors, and multiparity have been associated with elevated AMH levels. Smoking, chemotherapy, and low vitamin D levels have been linked to decreased AMH levels (*40,41*). Ovarian reserve is influenced by age and is negatively correlated with age (*40*). Few studies have focused on the impact of TgAb or TPOAb on AMH, and they did not exclude relevant factors. In our study, we excluded the factors that could interfere with AMH as much as possible to investigate the impact of TgAb and TPOAb on AMH. However, we found no correlation between AMH and TSH, FT4, TPOAb, or TgAb either in subjects with infertility due to female factors or in controls. Moreover, grouping based on TgAb and/or TPOAb positivity versus double negativity did not reveal any significant differences in AMH levels, indicating that TgAb and TPOAb do not affect ovarian reserve. A review by Zhu *et al*. posited that TPOAb may negatively affect oocyte fertilization, embryo, and placenta development (*42*). In contrast, other studies noted no impact of TgAb and TPOAb on assisted reproductive technology outcomes (*43-45*). Moreover, abnormal TH levels may lead to ovarian dysfunction throughout life, and especially during puberty and childbearing (*46*). Therefore, TgAb and TPOAb may affect ovarian reserve by influencing thyroid function. However, whether TgAb and TPOAb can directly influence ovarian reserve, oocyte development, fertilization, and other physiological processes remains unclear. Given our relatively small sample size and the fact that we did not exclude all potential factors influencing AMH (such as smoking and vitamin D levels), further well-designed clinical studies need to be conducted to establish whether there is an association among AMH, TgAb, and TPOAb.

Elevated peripheral blood TPOAb titers affecting infertility due to female factors may be related to inflammation. Our bioinformatic results indicated that the intersecting target molecules for HT and infertility due to female factors included IL-6, IL-10, TNF, and MMP-9, involving various signaling pathways such as HIF-1, VEGF, MAPK, and Th17 cell differentiation. The etiology of HT is a combination of genetic susceptibility and environmental factors, leading to the loss of immune tolerance (*47*). Lymphocyte infiltration, and especially T-cell infiltration, and follicular disruption are histological characteristics of HT (*47*). Cytokines and chemokines play crucial roles in the pathogenesis of HT, participating in the initiation and perpetuation of the autoimmune process (*47*). Infertility due to female factors can result from various factors, including age, anatomy, endocrine, and immunological factors. Pathological conditions affecting the uterine lining can also lead to implantation failure within the maternal uterus, thereby compromising fertility. Leukemia inhibitory factor, a cytokine belonging to the IL-6 family, can activate the Janus kinase-signal

transducer and activator of transcription pathway, which is essential for embryo implantation. The robust invasive capacity of trophoblast cells is attributed to the production of abundant MMPs, and particularly MMP2 and MMP9. The secretion of MMPs by trophoblast cells is regulated by factors such as IL-1β, TNF-α, IL-1α, macrophage colony-stimulating factor, TGF-β, EGF, and human chorionic gonadotropin, all of which are released by several types of cells at the fetal-maternal interface to promote trophoblast invasion. In addition, VEGF promotes embryo development, enhances endometrial receptivity, and facilitates interaction between developing embryos and the endometrium during implantation. Researchers have discovered that trophoblast cell migration and invasion are regulated by epidermal growth factor-like domain 7, which activates the NOTCH1, MAPK, and AKT signaling pathways in both trophoblast cell lines and primary cells. IL-10, an anti-inflammatory cytokine with important immune regulatory functions, plays a critical role in successful pregnancy. Starting from embryo implantation, fetal cells must survive under extremely adverse conditions within the maternal uterus, including severe hypoxia, lack of vascularization, and potential attacks from the maternal immune system.

The embryo implantation site serves as an indicator reflecting the uterine endometrial receptivity in mice. We constructed a murine model of AIT to investigate changes in implantation sites and ovarian reserve when peripheral blood TgAb titer increased. In this study, we used pTg instead of TPO for the AIT animal model due to various force majeure factors. During our exploratory phase of dosage modeling, we noticed that administering a dose of 25 μg led to a significant elevation in the peripheral blood FT4 levels in mice. When given a dose of 12.5 μg, murine serum antibody titers did not change markedly. Therefore, we opted for a dose of 18.75 μg in our study, resulting in a significant rise in serum TgAb titers and a noticeable rise in TPOAb titers. The results suggest that this model does not affect embryo implantation or ovarian reserve in mice, aligning with the results of our clinical cross-sectional study, in which patients with infertility due to female factors did not exhibit a notable increase in positivity for serum TgAb. This might be attributable to interspecies differences or the possibility that TPOAb plays a more dominant role during embryo implantation. TgAb is a diagnostic criterion for HT, but research has shown that women with isolated TgAb positivity exhibit significantly elevated blood TSH levels (*48*). However, TgAb cannot fix complement and is believed to have a less prominent role in thyroid damage, so it is considered less significant than TPOAb (*49*). Peripheral blood TPOAb and TgAb might play different roles or have a synergistic effect, influencing female fertility. TPOAb may act alone or synergistically with TgAb to affect female fertility.

Limitations of this study include its retrospective nature as a cross-sectional analysis, which makes it susceptible to selection bias (*21,22*). The study data rely on patient medical records, leading to the exclusion of some individuals due to the absence of relevant diagnostic indicators. Future research would benefit from prospective studies with larger sample sizes. Additionally, due to constraints in the modeling approach, mice in this study only exhibited an elevation in peripheral blood TgAb levels, hampering investigation of the influence of peripheral blood TPOAb on embryo implantation and ovarian reserve.

5. Conclusion

An elevated TPOAb titer in peripheral blood is associated with female infertility but has no significant correlation with AMH. The relative mechanisms may be related to the regulation of multiple signaling pathways such as HIF-1, VEGF, MAPK, and Th17 cell differentiation. The serum TgAb titer may be not associated with both female infertility and AMH. A certain dose of pTg can successfully establish a murine model of AIT, in which elevated peripheral blood TgAb levels did not affect embryo implantation and ovarian reserve.

Funding: This work was supported by grants from a project under the National Natural Science Foundation of China (grant no. 82374243 to L Wang), a project of the Chinese Association of Integration of Traditional and Western Medicine special foundation for Obstetrics and Gynecology (grant no. FCK-ZSYTW-04 to Q Qi), and a project of the Wuhan Business University project (grant no. 2024KB021 to Q Qi).

Conflict of Interest: The authors have no conflicts of interest to disclose.

References

1. Vander Borght M, Wyns C. Fertility and infertility: Definition and epidemiology. Clin Biochem. 2018; 62:2-10.
2. Inhorn MC, Patrizio P. Infertility around the globe: New thinking on gender, reproductive technologies and global movements in the 21st century. Hum Reprod Update. 2015; 21:411-426.
3. Ombelet W, Cooke I, Dyer S, Serour G, Devroey P. Infertility and the provision of infertility medical services in developing countries. Hum Reprod Update. 2008; 14:605-621.
4. Carson SA, Kallen AN. Diagnosis and management of infertility: A review. JAMA. 2021; 326:65-76.
5. Arduc A, Aycicek Dogan B, Bilmez S, Imga Nasiroglu N, Tuna MM, Isik S, Berker D, Guler S. High prevalence of Hashimoto's thyroiditis in patients with polycystic ovary syndrome: Does the imbalance between estradiol and progesterone play a role? Endocr Res. 2015; 40:204-210.
6. Ho CW, Chen HH, Hsieh MC, Chen CC, Hsu SP, Yip HT, Kao CH. Increased risk of polycystic ovary syndrome

and it's comorbidities in women with autoimmune thyroid disease. Int J Environ Res Public Health. 2020; 17.
7. Negro R, Formoso G, Mangieri T, Pezzarossa A, Dazzi D, Hassan H. Levothyroxine treatment in euthyroid pregnant women with autoimmune thyroid disease: Effects on obstetrical complications. J Clin Endocrinol Metab. 2006; 91:2587-2591.
8. Poppe K, Glinoer D, Tournaye H, Devroey P, van Steirteghem A, Kaufman L, Velkeniers B. Assisted reproduction and thyroid autoimmunity: An unfortunate combination? J Clin Endocrinol Metab. 2003; 88:4149-4152.
9. Sieiro Netto L, Medina Coeli C, Micmacher E, Mamede Da Costa S, Nazar L, Galvao D, Buescu A, Vaisman M. Influence of thyroid autoimmunity and maternal age on the risk of miscarriage. Am J Reprod Immunol. 2004; 52:312-316.
10. Unuane D, Velkeniers B. Impact of thyroid disease on fertility and assisted conception. Best Pract Res Clin Endocrinol Metab. 2020; 34:101378.
11. Tanska K, Gietka-Czernel M, Glinicki P, Kozakowski J. Thyroid autoimmunity and its negative impact on female fertility and maternal pregnancy outcomes. Front Endocrinol (Lausanne). 2022; 13:1049665.
12. Caturegli P, De Remigis A, Rose NR. Hashimoto thyroiditis: Clinical and diagnostic criteria. Autoimmun Rev. 2014; 13:391-397.
13. Hollowell JG, Staehling NW, Flanders WD, Hannon WH, Gunter EW, Spencer CA, Braverman LE. Serum TSH, T(4), and thyroid antibodies in the United States population (1988 to 1994): National Health and Nutrition Examination Survey (NHANES III). J Clin Endocrinol Metab. 2002; 87:489-499.
14. Poppe K, Glinoer D, Van Steirteghem A, Tournaye H, Devroey P, Schiettecatte J, Velkeniers B. Thyroid dysfunction and autoimmunity in infertile women. Thyroid. 2002; 12:997-1001.
15. Iravani AT, Saeedi MM, Pakravesh J, Hamidi S, Abbasi M. Thyroid autoimmunity and recurrent spontaneous abortion in Iran: A case-control study. Endocr Pract. 2008; 14:458-464.
16. van den Boogaard E, Vissenberg R, Land JA, van Wely M, van der Post JA, Goddijn M, Bisschop PH. Significance of (sub)clinical thyroid dysfunction and thyroid autoimmunity before conception and in early pregnancy: A systematic review. Hum Reprod Update. 2011; 17:605-619.
17. Inagaki Y, Takeshima K, Nishi M, Ariyasu H, Doi A, Kurimoto C, Uraki S, Morita S, Furukawa Y, Inaba H, Iwakura H, Shimokawa T, Utsunomiya T, Akamizu T. The influence of thyroid autoimmunity on pregnancy outcome in infertile women: A prospective study. Endocr J. 2020; 67:859-868.
18. Birjandi B, Ramezani Tehrani F, Amouzegar A, Tohidi M, Bidhendi Yarandi R, Azizi F. The association between subclinical hypothyroidism and TPOAb positivity with infertility in a population-based study: Tehran thyroid study (TTS). BMC Endocr Disord. 2021; 21:108.
19. Dosiou C. Thyroid and Fertility: Recent Advances. Thyroid. 2020; 30:479-486.
20. Poppe K. Management of endocrine disease: Thyroid and female infertility: More questions than answers?! Eur J Endocrinol. 2021; 184:R123-R135.
21. Richiardi L, Bellocco R, Zugna D. Mediation analysis in epidemiology: Methods, interpretation and bias. Int J Epidemiol. 2013; 42:1511-1519.
22. Chen CW, Huang YL, Tzeng CR, Huang RL, Chen CH. Idiopathic low ovarian reserve is associated with more frequent positive thyroid peroxidase antibodies. Thyroid. 2017; 27:1194-1200.
23. Practice Committee of the American Society for Reproductive Medicine. Definitions of infertility and recurrent pregnancy loss: A committee opinion. Fertil Steril. 2020; 113:533-535.
24. Practice Committee of the American Society for Reproductive Medicine. Fertility evaluation of infertile women: A committee opinion. Fertil Steril. 2021; 116:1255-1265.
25. Chin CH, Chen SH, Wu HH, Ho CW, Ko MT, Lin CY. CytoHubba: Identifying hub objects and sub-networks from complex interactome. BMC Syst Biol. 2014; 8 Suppl 4:S11.
26. Liu H, Li Y, Zhu Y, Ma L, Xue H. Notch signaling pathway promotes Th17 cell differentiation and participates in thyroid autoimmune injury in experimental autoimmune thyroiditis mice. Mediators Inflamm. 2023; 2023:1195149.
27. McLachlan SM, Atherton MC, Nakajima Y, Napier J, Jordan RK, Clark F, Rees Smith B. Thyroid peroxidase and the induction of autoimmune thyroid disease. Clin Exp Immunol. 1990; 79:182-188.
28. Sang Q, Ray PF, Wang L. Understanding the genetics of human infertility. Science. 2023; 380:158-163.
29. Deroux A, Dumestre-Perard C, Dunand-Faure C, Bouillet L, Hoffmann P. Female infertility and serum auto-antibodies: A systematic review. Clin Rev Allergy Immunol. 2017; 53:78-86.
30. De Leo S, Pearce EN. Autoimmune thyroid disease during pregnancy. Lancet Diabetes Endocrinol. 2018; 6:575-586.
31. Shi CJ, Shao TR, Zhao X, Wang B. Evaluation of the ovarian reserve in women and adolescent girls with Hashimoto's thyroiditis by serum anti-Mullerian hormone level: A systematic review and meta-analysis. Heliyon. 2023; 9:e19204.
32. Ozalp Akin E, Aycan Z. Evaluation of the ovarian reserve in adolescents with Hashimoto's thyroiditis using serum anti-Mullerian hormone levels. J Clin Res Pediatr Endocrinol. 2018; 10:331-335.
33. Tuten A, Hatipoglu E, Oncul M, Imamoglu M, Acikgoz AS, Yilmaz N, Ozcil MD, Kaya B, Misirlioglu AM, Sahmay S. Evaluation of ovarian reserve in Hashimoto's thyroiditis. Gynecol Endocrinol. 2014; 30:708-711.
34. Vega M, Barad DH, Yu Y, Darmon SK, Weghofer A, Kushnir VA, Gleicher N. Anti-Mullerian hormone levels decline with the presence of antiphospholipid antibodies. Am J Reprod Immunol. 2016; 76:333-337.
35. Osuka S, Iwase A, Goto M, Takikawa S, Nakamura T, Murase T, Kato N, Bayasula, Kotani T, Kikkawa F. Thyroid autoantibodies do not impair the ovarian reserve in euthyroid infertile women: A cross-sectional study. Horm Metab Res. 2018; 50:537-542.
36. Weghofer A, Barad DH, Darmon S, Kushnir VA, Gleicher N. What affects functional ovarian reserve, thyroid function or thyroid autoimmunity? Reprod Biol Endocrinol. 2016; 14:26.
37. Erol O, Parlak M, Ellidag HY, Parlak AE, Derbent AU, Eren E, Yilmaz N. Serum anti-Mullerian hormone levels in euthyroid adolescent girls with Hashimoto's thyroiditis: Relationship to antioxidant status. Eur J Obstet Gynecol Reprod Biol. 2016; 203:204-209.

38. Saglam F, Onal ED, Ersoy R, Koca C, Ergin M, Erel O, Cakir B. Anti-Mullerian hormone as a marker of premature ovarian aging in autoimmune thyroid disease. Gynecol Endocrinol. 2015; 31:165-168.
39. Magri F, Schena L, Capelli V, Gaiti M, Zerbini F, Brambilla E, Rotondi M, De Amici M, Spinillo A, Nappi RE, Chiovato L. Anti-Mullerian hormone as a predictor of ovarian reserve in ART protocols: The hidden role of thyroid autoimmunity. Reprod Biol Endocrinol. 2015; 13:106.
40. Tal R, Seifer DB. Ovarian reserve testing: A user's guide. Am J Obstet Gynecol. 2017; 217:129-140.
41. Fleming R, Seifer DB, Frattarelli JL, Ruman J. Assessing ovarian response: Antral follicle count versus anti-Mullerian hormone. Reprod Biomed Online. 2015; 31:486-496.
42. Zhu Q, Xu QH, Xie T, Wang LL, Liu H, Muyayalo KP, Huang XB, Zhao SJ, Liao AH. Recent insights into the impact of immune dysfunction on reproduction in autoimmune thyroiditis. Clin Immunol. 2021; 224:108663.
43. Zhang S, Yang M, Li T, Yang M, Wang W, Chen Y, Ding Y, Liu J, Xu X, Zhang J, Wang Z, Liu J. High level of thyroid peroxidase antibodies as a detrimental risk of pregnancy outcomes in euthyroid women undergoing ART: A meta-analysis. Mol Reprod Dev. 2023; 90:218-226.
44. Poppe K, Autin C, Veltri F, Sitoris G, Kleynen P, Praet JP, Rozenberg S. Thyroid disorders and *in vitro* outcomes of assisted reproductive technology: An unfortunate combination? Thyroid. 2020; 30:1177-1185.
45. So S, Yamaguchi W, Murabayashi N, Miyano N, Tawara F. Effect of moderately increased thyroid-stimulating hormone levels and presence of thyroid antibodies on pregnancy among infertile women. Reprod Med Biol. 2020; 19:82-88.
46. Colella M, Cuomo D, Giacco A, Mallardo M, De Felice M, Ambrosino C. Thyroid hormones and functional ovarian reserve: Systemic *vs.* peripheral dysfunctions. J Clin Med. 2020; 9.
47. Ragusa F, Fallahi P, Elia G, Gonnella D, Paparo SR, Giusti C, Churilov LP, Ferrari SM, Antonelli A. Hashimotos' thyroiditis: Epidemiology, pathogenesis, clinic and therapy. Best Pract Res Clin Endocrinol Metab. 2019; 33:101367.
48. Unuane D, Velkeniers B, Anckaert E, Schiettecatte J, Tournaye H, Haentjens P, Poppe K. Thyroglobulin autoantibodies: Is there any added value in the detection of thyroid autoimmunity in women consulting for fertility treatment? Thyroid. 2013; 23:1022-1028.
49. Frohlich E, Wahl R. Thyroid autoimmunity: Role of anti-thyroid antibodies in thyroid and extra-thyroidal diseases. Front Immunol. 2017; 8:521.

Received May 9, 2024; Revised June 20, 2024; Accepted June 23, 2024.

[§]These authors contributed equally to this work.
**Address correspondence to:*
Ling Wang, Laboratory for Reproductive Immunology, Obstetrics and Gynecology Hospital of Fudan University, 419 Fangxie Road, Shanghai 200011, China.
E-mail: Dr.wangling@fudan.edu.cn

Released online in J-STAGE as advance publication June 26, 2024.

Original Article

DOI: 10.5582/bst.2024.01227

Unveiling the unexplored secret: Aggressive behavior and poor survival in intrahepatic mucinous adenocarcinoma compared to conventional adenocarcinoma

Wenhui Wang[1,§], Hongjun Lin[2,§], Qiang Lu[1,*], Yulong Cai[3,*]

[1] Department of Ultrasound, West China Hospital, Sichuan University, Chengdu, Sichuan, China;
[2] Department of Operation Room, West China Hospital, Sichuan University, Chengdu, Sichuan, China;
[3] Department of Biliary Tract Surgery, General Surgery, West China Hospital, Sichuan University, Chengdu, Sichuan, China.

SUMMARY Intrahepatic bile duct mucinous adenocarcinoma (IHBDMAC) is a rare pathological subtype of intrahepatic cholangiocarcinoma (IHCC), and its tumor biological features and survival outcomes have rarely been explored, especially when compared to the most common subtype, intrahepatic bile duct adenocarcinoma (IHBDAC). Therefore, the aim of this study was to explore the clinical features and survival outcomes of IHBDAC and IHBDMAC using the Surveillance, Epidemiology, and End Results (SEER) database from 2000 to 2021. A total of 1,126 patients were included, with 1,083 diagnosed with IHBDAC and 43 diagnosed with IHBDMAC. Patients with IHBDMAC presented with a more advanced T stage (55.8% *vs.* 36.9%, $P = 0.012$) and higher rate of lymph node metastasis (37.2% *vs.* 24.9%, $P = 0.070$). Cox regression identified advanced T stage, lymph node metastasis, and distant metastasis as poor survival predictors, while chemotherapy and surgery were protective factors. Survival analyses revealed significantly worse overall survival (OS) and cancer-specific survival (CSS) for IHBDMAC compared to IHBDAC ($P < 0.05$). Even after matching, patients with IHBDMAC still had a worse prognosis than those with IHBDAC. These findings highlight the aggressive nature of IHBDMAC and the need for tailored therapeutic strategies. Future research should focus on prospective studies and molecular insights to develop targeted treatments for IHBDMAC.

Keywords mucinous adenocarcinoma, surgery, intrahepatic cholangiocarcinoma, prognosis

1. Introduction

Intrahepatic cholangiocarcinoma (IHCC) is the second most common primary liver malignancy, originating from the bile ducts within the liver. It represents a heterogeneous group of tumors with varying biological behaviors and clinical outcomes (*1*). For IHCC, surgical treatment achieving R0 resection has always been the cornerstone of therapy (*1*). In addition, recent studies have shown that adjuvant immunotherapy and targeted therapy can also significantly improve the prognosis of patients with this type of tumor (*2*). IHCC can be broadly classified into different histological subtypes, the most prominent of which are intrahepatic bile duct adenocarcinoma (IHBDAC) and intrahepatic bile duct mucinous adenocarcinoma (IHBDMAC) (*3*). IHBDAC is the most prevalent subtype and is characterized by tubular and glandular structures formed by malignant biliary epithelial cells. It has been extensively studied, with well-documented clinical features and prognostic factors. In contrast, IHBDMAC is less common and its clinic-pathological features have not been fully evaluated, especially when compared to IHBDAC. Distinct differences in these two different pathological subtypes are evident in HE-stained images. As shown in Figure 1, mucinous production is less prominent in IHBDAC (Figure 1A) while extensive mucinous production and the presence of mucin lakes are evident in IHBDMAC (Figure 1B). In addition, the cells in IHCC are tightly arranged with well-defined ductal or acinar structures, whereas the cells in IHBDMAC are loosely arranged with irregular glandular structures within the mucin lakes. Only Azchar *et al*. evaluated the prognostic value of mucinous component in patients with IHCC (*4*). However, further more in-depth analysis was not performed, especially in the post-matched cohort (*4*). According to the latest (8th) American Joint Committee on Cancer (AJCC) staging system, apart from three most conventional staging factors, including the T, N, and M stage, concurrent liver cirrhosis,

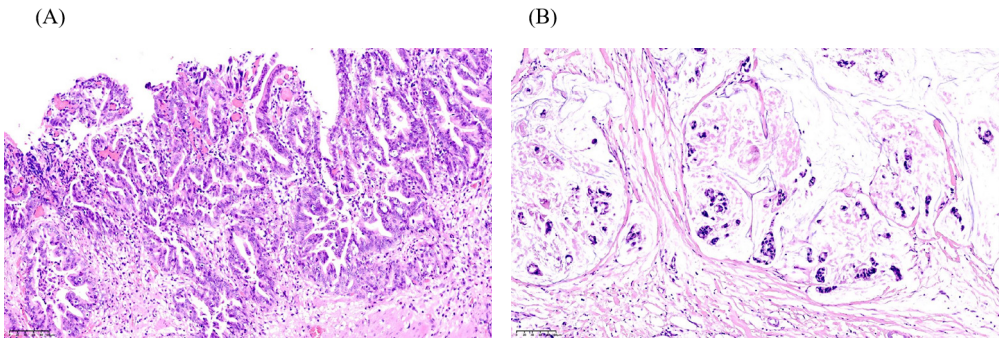

Figure 1. Representative images of pure IHBDAC and IHBDMAC (hematoxylin and eosin staining, 20×). A, pure adenocarcinoma; B, mucinous adenocarcinoma.

the serum CA199 level, and primary sclerosing cholangitis are cited as prognostic factors requiring additional clinical care. The prognostic significance of a mucinous component in IHCC is still being evaluated. Undoubtedly, understanding these differences is crucial to tailoring therapeutic strategies and improving patient management.

The Surveillance, Epidemiology, and End Results (SEER) database provides a valuable resource for examining large-scale cancer trends and outcomes. Utilizing this extensive database, the current study sought to perform a retrospective analysis to compare the clinical features and survival outcomes of patients with IHBDAC and IHBDMAC. Specifically, this study sought to identify distinct prognostic factors and treatment modalities that may influence survival in these two subtypes, thereby contributing to a more nuanced understanding of IHBDMAC and informing future clinical practice.

2. Materials and Methods

2.1. Patients

The SEER database is the largest publicly-available cancer database, covering almost 28% of the American population (*5*). Patients diagnosed with IHCC from the SEER database [released in April 2024: version 8.4.3; SEER 17 Regs Custom Data (with SEER Plus data, from 2000 to 2021)] were retrospectively reviewed and analyzed. The "Primary Site—labeled-liver/intrahepatic bile duct" variable was used to identify patients with tumors primarily located in the liver. The variable "behavior-malignant" was used to focus on malignancies. Only patients with pathologically confirmed IHBDAC or IHBDMAC were considered eligible. The pathologically diagnosed variables were restricted to "Positive histology." Given the similarities between the 7th edition and 8th edition of AJCC staging criteria for IHCC, cancers staged according to the 7th AJCC criteria [Derived AJCC TNM, 7th ed (2010-2015)] and the 8th AJCC criteria [Derived EOD 2018 TNM (2018+)] were combined. Consequently, T stages were broadly classified into T1-T2 and T3-T4, and N stages were similarly classified into node-negative (N-) and node-positive (N+). Moreover, only patients with survival information (greater than 0 months) were included.

2.2. Variable identification

A total of fourteen variables were identified for further analysis, including age, sex, race, marital status, T stage, N stage, pathological subtypes, tumor differentiation grade, radiotherapy, chemotherapy, cancer-related death (CRD), AFP level, and cirrhosis status. The continuous variable "Age" was categorized into ≤60 and >60. Minor adjustments were also applied to other categorical variables. For instance, marital status was simplified into two groups: married and single/unknown. Race was simplified into two major groups: white and other. Tumor differentiation status was simplified into three groups: well to moderately differentiated, poorly differentiated to undifferentiated, and unknown.

2.3. Study design

First, a basic comparison of clinicopathological features and long-term survival was made between patients with IHBDAC and IHBDMAC. Overall survival (OS) and cancer-specific survival (CSS) between the two pathological subtypes were compared. Univariate and multivariate Cox regression analyses were performed to identify potential and independent prognostic factors for OS in the entire cohort and in patients with IHBDMAC. Finally, propensity score matching (PSM) analysis was utilized to control for various factors significantly influencing OS, allowing for further investigation.

2.4. Statistical analysis

The software R version 4.2.2 was used for statistical analysis. The R package tableone was used for baseline comparison and subsequent table output. Categorical data were expressed as numbers (percentages). Categorical variables were evaluated *via* Chi-Squared and Fisher's

exact tests. Survival analyses were performed using the R packages survminer and survival. Kaplan–Meier curves and the corresponding risk tables were produced using the R command ggsurvplot. OS was defined as the time from the date of radical surgery to the date of death or last follow-up. The R packages survminer, dplyr, survival, and rms were used to construct a Cox proportional hazards model, which showed hazard ratios (HR) and their 95% confidence intervals (CI). P values lower than 0.05 indicated statistical significance. PSM analysis was performed using the R package MatchIt with the method="nearest," caliper=0.05, and ratio=1, matching factors that mainly consisted of age, sex, and other independent prognostic factors for OS.

3. Results

3.1. Comparative analysis of baseline characteristics

The baseline characteristics of the study population are summarized in Table 1. The cohort consisted of 1,126 patients, 1,083 of whom had IHBDAC and 43 of whom had IHBDMAC. The distribution of demographic and clinical variables, including age, sex, race, tumor grade, T stage, N stage, M stage, surgery status, radiotherapy, chemotherapy, CRD, marital status, AFP levels, and cirrhosis status, were compared between the two groups. Significant differences were noted in the T stage distribution (P = 0.012); patients with IHBDMAC more

Table 1. Baseline features before PSM

Variables	Overall (n = 1126)	IHBDAC (n = 1083)	IHBDMAC (n = 43)	P value
Age (%)				0.234
≤60	328 (29.1)	312 (28.8)	16 (37.2)	
>60	798 (70.9)	771 (71.2)	27 (62.8)	
Sex (%)				0.903
Male	592 (52.6)	569 (52.5)	23 (53.5)	
Female	534 (47.4)	514 (47.5)	20 (46.5)	
Race (%)				0.536
White	901 (80.0)	865 (79.9)	36 (83.7)	
Other	225 (20.0)	218 (20.1)	7 (16.3)	
Grade (%)				0.332
Well to moderately differentiated	311 (27.6)	297 (27.4)	14 (32.6)	
Poorly differentiated to undifferentiated	261 (23.2)	255 (23.5)	6 (14.0)	
Unknown	554 (49.2)	531 (49.0)	23 (53.5)	
T stage (%)				0.012
T1-T2	702 (62.3)	683 (63.1)	19 (44.2)	
T3-T4	424 (37.7)	400 (36.9)	24 (55.8)	
N stage (%)				0.070
N0	840 (74.6)	813 (75.1)	27 (62.8)	
N1	286 (25.4)	270 (24.9)	16 (37.2)	
M stage (%)				0.192
M0	782 (69.4)	756 (69.8)	26 (60.5)	
M1	344 (30.6)	327 (30.2)	17 (39.5)	
Surgery (%)				0.211
Not undergone	942 (83.7)	909 (83.9)	33 (76.7)	
Undergone	184 (16.3)	174 (16.1)	10 (23.3)	
Radiotherapy (%)				0.216
Not undergone	1086 (96.4)	1046 (96.6)	40 (93.0)	
Undergone	40 (3.6)	37 (3.4)	3 (7.0)	
Chemotherapy (%)				0.887
Not undergone	588 (52.2)	566 (52.3)	22 (51.2)	
Undergone	538 (47.8)	517 (47.7)	21 (48.8)	
CRD (%)				0.302
No	196 (17.4)	186 (17.2)	10 (23.3)	
Yes	930 (82.6)	897 (82.8)	33 (76.7)	
Marital status (%)				0.908
Single/unknown	514 (45.6)	494 (45.6)	20 (46.5)	
Married	612 (54.4)	589 (54.4)	23 (53.5)	
AFP (%)				0.958
Positive	345 (33.7)	331 (33.6)	14 (35.0)	
Negative	143 (14.0)	138 (14.0)	5 (12.5)	
No/unknown	537 (52.4)	516 (52.4)	21 (52.5)	
Cirrhosis (%)				0.055
No	45 (4.0)	42 (3.9)	3 (7.0)	
Yes	114 (10.1)	114 (10.5)	0 (0.0)	
No/unknown	967 (85.9)	927 (85.6)	40 (93.0)	

IHBDAC: intrahepatic bile duct adenocarcinoma; IHBDMAC: intrahepatic bile duct mucinous adenocarcinoma; CRD: cancer-related death; PSM: propensity score matching.

likely to present with an advanced T stage (T3-T4) (55.8% *vs.* 36.9%, $P = 0.012$). Moreover, lymph node metastasis was more frequently detected among patients with IHBDMAC (37.2% *vs.* 24.9%, $P = 0.070$).

3.2. Comparative analysis of survival outcomes

Kaplan-Meier survival curves revealed significant differences in OS and CSS between patients with IHBDAC and patients with IHBDMAC. Patients with IHBDMAC had a much worse OS (Figure 2A) and CSS (Figure 2B) than those with IHBDMAC ($P < 0.05$ for both).

3.3. Univariate and multivariate cox regression analysis

Univariate and multivariate cox regression analyses were performed to identify prognostic factors for the entire cohort (Table 2) and specifically for patients with IHBDMAC (Table 3). For the entire cohort, as is summarized in Table 2, age, tumor differentiation grade, T stage, N stage, M stage, chemotherapy, radiotherapy, and surgery status were found to be prognostic factors in univariate analyses. In multivariate analyses, patients over the age of 60 had a significantly higher risk of mortality (HR = 1.270, 95% CI: 1.109-1.454, $P = 0.001$). Poorly differentiated to undifferentiated tumors were associated with worse outcomes (HR = 1.420, 95% CI: 1.198-1.683, $P < 0.001$). An advanced T stage (T3-T4) was a significant predictor of poor survival (HR = 1.417, 95% CI: 1.244-1.615, $P < 0.001$). Positive nodal status (N1) was also associated with worse survival (HR = 1.283, 95% CI: 1.109-1.485, $P = 0.001$). Distant metastasis (M1) significantly increased the mortality risk (HR = 1.477, 95% CI: 1.285-1.698, $P < 0.001$). Undergoing chemotherapy (HR = 0.576, 95% CI: 0.506-0.656, $P < 0.001$) and surgery (HR = 0.335, 95% CI: 0.277-0.405, $P < 0.001$) were protective factors for survival.

For patients with IHBDMAC, the M stage and surgery status were found to be prognostic factors in univariate analyses. In multivariate analyses, distant metastasis (M1) significantly increased the mortality risk in patients with IHBDMAC (HR = 2.427, 95% CI: 1.207-4.878, $P = 0.013$). Undergoing surgery was a protective factor for survival in patients with IHBDMAC (HR = 0.394, 95% CI: 0.178-0.874, $P = 0.022$).

3.4. Propensity score matching analysis

PSM analysis was performed account for confounding factors, resulting in 40 patients with IHBDAC matched to 40 patients with IHBDMAC. Post-matching baseline characteristics (Table 4) revealed no significant differences in key variables, ensuring balanced groups for comparison. Post-PSM survival analysis confirmed that IHBDMAC was still associated with a worse OS (Figure 3A) and CSS (Figure 3B) compared to IHBDAC.

4. Discussion

The prognostic value of mucinous components has been explored in patients with various solid tumors, including colon cancer (*6*), rectal cancer (*7*), ovary cancer (*8*), and pulmonary cancer (*9*). These studies consistently indicated that the mucinous component was associated with a more aggressive tumor biological features, reduced response to chemotherapy, and worse prognosis. However, in patients with IHCC, the differences in clinicopathological factors and long-term prognosis brought about by the mucinous component compared

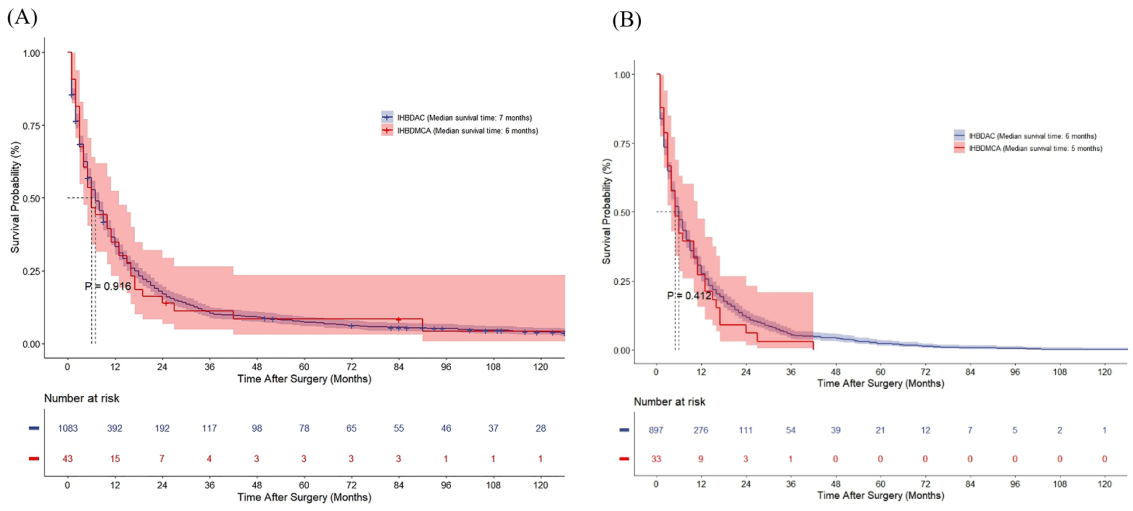

Figure 2. KM curves showing survival differences between patients with IHBDAC and patients with IHBDMAC. A, OS; B, CSS. IHBDAC: intrahepatic bile duct adenocarcinoma carcinoma; IHBDMAC: intrahepatic bile duct mucinous adenocarcinoma. OS: overall survival; CSS: cancer-specific survival.

Table 2. Univariate and multivariate Cox regression of the entire cohort

Variables	Univariate		Multivariate	
	HR (95% CI)	*P* value	HR (95% CI)	*P* value
Age				
≤60				
>60	1.209 (1.058,1.382)	0.005	1.270 (1.109,1.454)	0.001
Sex				
Male				
Female	0.910 (0.807,1.026)	0.122		
Race				
White				
Other	0.956 (0.821,1.114)	0.566		
Grade				
Well to moderately differentiated				
Poorly differentiated to undifferentiated	1.477 (1.247,1.749)	< 0.001	1.420 (1.198,1.683)	< 0.001
Unknown	1.321 (1.144,1.524)	< 0.001	1.075 (0.929,1.244)	0.334
AFP				
Positive				
Negative	0.893 (0.730,1.091)	0.267		
No/unknown	1.021 (0.889,1.172)	0.770		
Marital status				
Single/unknown				
Married	0.957 (0.849,1.079)	0.474		
Pathology				
IHBDAC				
IHBDMAC	1.015 (0.740,1.393)	0.925		
Cirrhosis				
No				
Yes	1.242 (0.871,1.771)	0.232		
No/unknown	1.248 (0.916,1.700)	0.161		
T stage				
T1-T2				
T3-T4	1.532 (1.352,1.737)	< 0.001	1.417 (1.244,1.615)	< 0.001
N stage				
N0				
N1	1.375 (1.199,1.576)	< 0.001	1.283 (1.109,1.485)	0.001
M stage				
M0				
M1	1.621 (1.422,1.847)	< 0.001	1.477 (1.285,1.698)	< 0.001
Chemotherapy				
Not undergone				
Undergone	0.799 (0.708,0.901)	< 0.001	0.576 (0.506,0.656)	< 0.001
Radiotherapy				
Not undergone				
Undergone	0.520 (0.373,0.725)	< 0.001	1.086 (0.764,1.545)	0.644
Surgery				
Not undergone				
Undergone	0.334 (0.280,0.398)	< 0.001	0.335 (0.277,0.405)	< 0.001

HR: hazard ratio; CI: confidence interval; IHBDAC: intrahepatic bile duct adenocarcinoma; IHBDMAC: intrahepatic bile duct mucinous adenocarcinoma.

to conventional IHCC have not yet been systematically explored. Consequently, the current study represents the first systematic evaluation of the clinical and pathological features and survival outcomes of patients with IHBDAC and IHBDMAC. Through meticulous data collection and analysis, several key insights have been gained, shedding light on the distinct characteristics and prognostic factors associated with these two subtypes of IHCC.

The baseline characteristics of the cohort revealed that patients with IHBDMAC tend to have a more advanced T stage compared to those with IHBDAC. This finding suggests a potentially more aggressive disease course in IHBDMAC, which is further supported by the survival analyses showing a significantly worse OS and CSS in patients with IHBDMAC. These findings were consistent with observations as mentioned earlier (*6-9*). This aggressive behavior of IHBDMAC could be attributed to the unique biological and molecular properties of mucinous tumors, which are known to exhibit higher invasiveness and metastatic potential. Using single-cell profiling, researchers have indicated that mucinous adenocarcinoma cancer cells exhibit goblet cell-like properties and express high levels of goblet cell markers (REG4, SPINK4, FCGBP, and

Table 3. Univariate and multivariate Cox regression of patients with IHBDMAC

Variables	Univariate		Multivariate	
	HR (95% CI)	*P* value	HR (95% CI)	*P* value
Age				
≤60				
>60	2.025 (1.038,3.953)	0.039	1.718 (0.855,3.452)	0.129
Sex				
Male				
Female	0.843 (0.447,1.592)	0.599		
Race				
White				
Other	0.466 (0.181,1.198)	0.113		
Grade				
Well to moderately differentiated				
Poorly differentiated to undifferentiated	0.943 (0.357,2.491)	0.905		
Unknown	0.650 (0.323,1.309)	0.228		
AFP				
Positive				
Negative	0.967 (0.310,3.017)	0.954		
No/unknown	1.182 (0.580,2.411)	0.645		
Marital status				
Single/unknown				
Married	1.045 (0.559,1.953)	0.891		
Cirrhosis				
No				
No/unknown	2.095 (0.502,8.742)	0.310		
T stage				
T1-T2				
T3-T4	1.120 (0.598,2.099)	0.723		
N stage				
N0				
N1	1.285 (0.675,2.448)	0.446		
M stage				
M0				
M1	2.766 (1.396,5.480)	0.004	2.427 (1.207,4.878)	0.013
Chemotherapy				
Not undergone				
Undergone	1.219 (0.648,2.295)	0.539		
Radiotherapy				
Not undergone				
Undergone	0.504 (0.153,1.660)	0.260		
Surgery				
Not undergone				
Undergone	0.338 (0.157,0.728)	0.006	0.394 (0.178,0.874)	0.022

HR: hazard ratio; CI: confidence interval; IHBDMAC: intrahepatic bile duct mucinous adenocarcinoma.

MUC2) compared to classical adenocarcinoma cancer cells. TFF3 is essential for the transcriptional regulation of these molecules and may cooperate with RPS4X to ultimately lead to the mucinous adenocarcinoma mucus phenotype (*10*). Moreover, Kaplan-Meier survival curves showed that patients with IHBDMAC have markedly poorer survival outcomes compared to those with IHBDAC, both before and after PSM. The persistence of significant survival differences post-PSM indicates that the worse prognosis associated with IHBDMAC is intrinsic to the tumor biology rather than due to differences in patient demographics or treatment modalities. This underscores the need for tailored therapeutic strategies for patients with IHBDMAC to improve their survival outcomes. In addition, the Cox regression analyses identified several prognostic factors for the entire cohort and for IHBDMAC specifically. For the entire cohort, age, tumor grade, T stage, N stage, M stage, chemotherapy, and surgery were significant predictors of survival. Notably, age and advanced T stage were associated with increased mortality while chemotherapy and surgical interventions were protective factors. This aligns with existing literature emphasizing the importance of early detection and aggressive treatment in improving outcomes for patients with IHCC. In the IHBDMAC subgroup, metastatic status (M1) emerged as a significant adverse prognostic factor, whereas surgical resection was associated with improved survival. The pronounced impact of metastasis on survival in patients with IHBDMAC highlights the critical need for effective systemic therapies to manage distant disease spread. Moreover, the benefit of surgery

Table 4. Baseline features after PSM

Variables	Overall (*n* = 80)	IHBDAC (*n* = 40)	IHBDMAC (*n* = 40)	*P* value
Age (%)				1.000
≤60	28 (35.0)	14 (35.0)	14 (35.0)	
>60	52 (65.0)	26 (65.0)	26 (65.0)	
Sex (%)				0.654
Male	42 (52.5)	20 (50.0)	22 (55.0)	
Female	38 (47.5)	20 (50.0)	18 (45.0)	
Race (%)				0.108
White	62 (77.5)	28 (70.0)	34 (85.0)	
Other	18 (22.5)	12 (30.0)	6 (15.0)	
Grade (%)				1.000
Well to moderately differentiated	24 (30.0)	12 (30.0)	12 (30.0)	
Poorly differentiated to undifferentiated	10 (12.5)	5 (12.5)	5 (12.5)	
Unknown	46 (57.5)	23 (57.5)	23 (57.5)	
T stage (%)				1.000
T1-T2	38 (47.5)	19 (47.5)	19 (47.5)	
T3-T4	42 (52.5)	21 (52.5)	21 (52.5)	
N stage (%)				1.000
N0	54 (67.5)	27 (67.5)	27 (67.5)	
N1	26 (32.5)	13 (32.5)	13 (32.5)	
M stage (%)				1.000
M0	48 (60.0)	24 (60.0)	24 (60.0)	
M1	32 (40.0)	16 (40.0)	16 (40.0)	
Surgery (%)				1.000
Not undergone	64 (80.0)	32 (80.0)	32 (80.0)	
Undergone	16 (20.0)	8 (20.0)	8 (20.0)	
Radiotherapy (%)				0.556
Not undergone	77 (96.2)	39 (97.5)	38 (95.0)	
Undergone	3 (3.8)	1 (2.5)	2 (5.0)	
Chemotherapy (%)				1.000
Not undergone	42 (52.5)	21 (52.5)	21 (52.5)	
Undergone	38 (47.5)	19 (47.5)	19 (47.5)	
CRD (%)				0.793
No	19 (23.8)	9 (22.5)	10 (25.0)	
Yes	61 (76.2)	31 (77.5)	30 (75.0)	
Marital status (%)				0.501
Single/unknown	43 (53.8)	23 (57.5)	20 (50.0)	
Married	37 (46.2)	17 (42.5)	20 (50.0)	
AFP (%)				0.873
Positive	26 (35.1)	12 (32.4)	14 (37.8)	
Negative	11 (14.9)	6 (16.2)	5 (13.5)	
No/unknown	37 (50.0)	19 (51.4)	18 (48.6)	
Cirrhosis (%)				0.038
No	4 (5.0)	2 (5.0)	2 (5.0)	
Yes	6 (7.5)	6 (15.0)	0 (0.0)	
No/unknown	70 (87.5)	32 (80.0)	38 (95.0)	

IHBDAC: intrahepatic bile duct adenocarcinoma; IHBDMAC: intrahepatic bile duct mucinous adenocarcinoma; CRD: cancer-related death; PSM: propensity score matching.

underscores the importance of considering surgical options even in advanced stages, provided the patient's condition permits.

The current findings have several important implications for clinical practice. First, the distinct survival outcomes between IHBDAC and IHBDMAC necessitate a differential approach to diagnosis, treatment, and management. Given the poorer prognosis of IHBDMAC, clinicians should remain highly suspicious of aggressive disease and consider comprehensive staging and early systemic therapy to manage potential metastases. Second, the identification of key prognostic factors such as tumor grade, T stage, and metastatic status can aid in stratifying patients based on their risk profiles. This stratification can inform treatment decisions, enabling a more personalized approach to patient care. For instance, patients with high-risk features may benefit from more intensive monitoring and adjuvant therapies to address micro-metastatic disease and improve survival outcomes. Third, in the latest version of the AJCC staging system, pathological subtype is not considered a prognostic factor for IHCC. However, based on our research and previous studies, we believe that pathological subtype should also be regarded as a key prognostic factor for IHCC. In addition, more comprehensive and precise prognostic models for IHCC

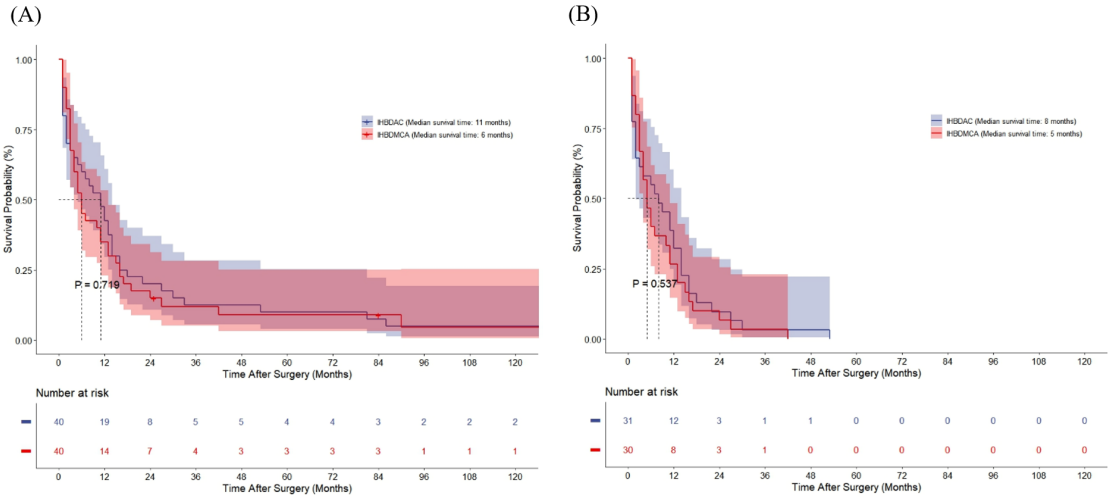

Figure 3. KM curves showing survival differences between patients with IHBDAC and patients with IHBDMAC after matching. A, OS; B, CSS. IHBDAC: intrahepatic bile duct adenocarcinoma carcinoma; IHBDMAC: intrahepatic bile duct mucinous adenocarcinoma. OS: overall survival; CSS: cancer-specific survival.

should be developed in larger clinical cohorts in the future, incorporating pathological subtype and other reported factors.

Despite the strengths of this study, including a robust sample size and thorough statistical analysis, several limitations warrant consideration. The retrospective nature of this study may introduce selection bias, and the reliance on registry data means that certain clinical details, such as comorbidities and detailed treatment regimens, were not available. In addition, the relatively small number of patients with IHBDMAC might limit the generalizability of findings to all mucinous adenocarcinomas of the intrahepatic bile ducts. In addition, mucinous colorectal adenocarcinoma is a distinct subtype of colorectal cancer that is characterized by the presence of abundant extracellular mucin, which accounts for at least 50% of the tumor volume (*6*). However, the specific definition of IHBDMAC has not yet been clarified, particularly regarding the optimal cut-off value for the mucinous component when defining IHBDMAC. Future research should focus on prospective studies with larger cohorts to validate our findings and explore the underlying molecular mechanisms driving the aggressive behavior of IHBDMAC. Understanding the genetic and epigenetic alterations specific to mucinous tumors could reveal novel therapeutic targets and lead to the development of more effective treatment strategies.

In conclusion, the current study has highlighted significant differences in the clinical and pathological characteristics and survival outcomes of IHBDAC and IHBDMAC. Patients with IHBDMAC have a worse prognosis, driven by more advanced disease at presentation and a higher metastatic potential. Key prognostic factors identified in our analysis, such as tumor grade, T stage, and metastatic status, can guide risk stratification and personalized treatment approaches. Surgical resection remains a critical component of the management strategy, even in advanced cases, and systemic therapies are crucial to controlling metastatic disease. Future research should aim to elucidate the molecular underpinnings of IHBDMAC to develop targeted therapies that can improve survival outcomes for this challenging subtype of intrahepatic cholangiocarcinoma.

Funding: This study was supported by a grant from the Sichuan Science and Technology Program (2024NSFSC1936).

Conflict of Interest: The authors have no conflicts of interest to disclose.

References

1. Sugawara Y, Hibi T. Recent trends and new developments in liver transplantation. Biosci Trends. 2024; 18:206-211.
2. Chen L, Yin G, Wang Z, Liu Z, Sui C, Chen K, Song T, Xu W, Qi L, Li X. A predictive radiotranscriptomics model based on DCE-MRI for tumor immune landscape and immunotherapy in cholangiocarcinoma. Biosci Trends. 2024; 18:263-276.
3. Sumiyoshi T, Shima Y, Okabayashi T, Ishikawa A, Matsumoto M, Iwata J, Morita S, Sueda T. Mucinous cholangiocarcinoma: Clinicopathological features of the rarest type of cholangiocarcinoma. Annals Gastroentero Surg. 2017; 1:114-121.
4. Azhar MS, Zhang ZJ, Liu ZT, Huang YP, Wang YX, Zhou H, Xiong L, Wen Y, Zou H. Prognostic models for mucinous and non-specific adeno cholangiocarcinoma: A population-based retrospective study. Frontiers Endocrin. 2024; 15:1284283.
5. Mao W, Zhang Z, Huang X, Fan J, Geng J. Marital status and survival in patients with penile cancer. J Cancer. 2019; 10:2661-2669.
6. Luo C, Cen S, Ding G, Wu W. Mucinous colorectal adenocarcinoma: Clinical pathology and treatment options. Cancer Comm (London, England). 2019; 39:13.

7. McCawley N, Clancy C, O'Neill BD, Deasy J, McNamara DA, Burke JP. Mucinous rectal adenocarcinoma is associated with a poor response to neoadjuvant chemoradiotherapy: A systematic review and meta-analysis. Diseases Colon Rectum. 2016; 59:1200-1208.
8. Shimada M, Kigawa J, Ohishi Y, Yasuda M, Suzuki M, Hiura M, Nishimura R, Tabata T, Sugiyama T, Kaku T. Clinicopathological characteristics of mucinous adenocarcinoma of the ovary. Gynecol Oncol. 2009; 113:331-334.
9. Boland JM, Maleszewski JJ, Wampfler JA, Voss JS, Kipp BR, Yang P, Yi ES. Pulmonary invasive mucinous adenocarcinoma and mixed invasive mucinous/nonmucinous adenocarcinoma-A clinicopathological and molecular genetic study with survival analysis. Human Path. 2018; 71:8-19.
10. Hu FJ, Li YJ, Zhang L, Ji DB, Liu XZ, Chen YJ, Wang L, Wu AW. Single-cell profiling reveals differences between human classical adenocarcinoma and mucinous adenocarcinoma. Comm Bio. 2023; 6:85.

Received August 7, 2024; Revised August 26, 2024; Accepted August 28, 2024.

[§]These authors contributed equally to this work.
*Address correspondence to:
Qiang Lu, Department of Ultrasound, West China Hospital, Sichuan University, Chengdu 610041, Sichuan Province, China.
E-mail: luqiang@scu.edu.cn

Yulong Cai, Department of Biliary Tract Surgery, General Surgery, West China Hospital, Sichuan University, Chengdu 610041, Sichuan province, China.
E-mail: caiyulong@wchscu.cn

Released online in J-STAGE as advance publication August 29, 2024.

Original Article

DOI: 10.5582/bst.2024.01230

Unmasking the silent killer: The hidden aggressiveness of signet-ring cell carcinoma in gallbladder cancer

Zhimeng Cheng[1,§], Zilin Jia[2,§], Xiaoling Li[2], Liping Chen[1,*], Yulong Cai[1,*]

[1] Department of Biliary Tract Surgery, General Surgery, West China Hospital, Sichuan University, Chengdu, Sichuan, China;
[2] West China School of Nursing, West China Hospital, Sichuan University, Chengdu, Sichuan, China.

SUMMARY The prognostic significance of the signet-ring cell component in gallbladder carcinoma (GBC) has not been systematically evaluated. The aim of this study was to assess the similarities and differences between gallbladder signet-ring cell carcinoma (GBSRCA) and gallbladder adenocarcinoma (GBAC) in terms of clinicopathological features and long-term survival. Using the Surveillance, Epidemiology, and End Results (SEER) database, we analyzed 6,612 patients diagnosed with gallbladder cancer between 2000 and 2021. The cohort included 147 patients with GBSRCA and 6,465 with GBAC. Patients with GBSRCA were significantly younger, with 33.3% being age 60 or younger compared to 23.9% of patients with GBAC ($P = 0.009$). There was a higher proportion of females in the GBSRCA group (77.6%) compared to the GBAC group (70.1%, $P = 0.049$). GBSRCA was associated with a more advanced tumor stage (T3-T4: 56.5% *vs*. 44.4%, $P = 0.004$), higher rates of lymph node metastasis (43.5% *vs*. 28.0%, $P < 0.001$), and poorer differentiation status (poorly to undifferentiated: 80.3% *vs*. 29.7%, $P < 0.001$). Survival analysis revealed that patients with GBSRCA had significantly worse overall survival (OS) and cancer-specific survival (CSS) compared to patients with GBAC ($P < 0.001$). GBSRCA was an independent prognostic factor for OS ($P = 0.001$) in the entire cohort, while the T stage and N stage were independent prognostic factors for OS and CSS in patients with GBSRCA. Even after propensity score matching, patients with GBSRCA still had a poorer prognosis.

Keywords gallbladder carcinoma, adenocarcinoma, signet-ring cell carcinoma, prognosis

1. Introduction

According to the latest (8th) edition of the American Joint Committee on Cancer (AJCC) staging system for gallbladder carcinoma (GBC), in addition to the three most common staging factors – T stage, N stage, and M stage – various other factors can affect the overall prognosis for patients with GBC (*1*). Histological subtypes are considered a crucial prognostic factor that requires additional clinical attention. Cases with papillary differentiation have been associated with a favorable prognosis (*2*). Studies have also shown that gallbladder adeno-squamous/squamous carcinoma has a significantly worse prognosis compared to pure adenocarcinoma (*3*). Moreover, gallbladder mucinous adenocarcinoma (*4*) or sarcomatoid carcinoma (*5*) has been found to have a less favorable prognosis than gallbladder adenocarcinoma (GBAC).

Signet-ring cell carcinoma (SRCC) is a type of adenocarcinoma that produces mucin and is characterized by the presence of significant amounts of mucin within the cytoplasm, which displaces the nucleus towards one side of the cell. When SRCC spreads beyond the submucosa, the signet-ring cells spread widely and establish distant metastases (*6*). This aggressive behavior of SRCC signifies a poor prognosis for adenocarcinoma. Primary SRCC is typically found in the stomach, making up about 15.1-28.2% of cases of primary gastric cancer (*7-9*). It can also develop, although less frequently, in other organs such as the breasts, lungs, esophagus, gallbladder, bladder, and pancreas (*10-16*). To the extent known, few studies have systematically evaluated the clinical significance of the signet-ring component in patients with GBC. Zou *et al*. comparatively analyzed the inconsistencies of clinic-pathological features and long-term survival in patients with GBAC and patients with gallbladder signet-ring cell carcinoma (GBSRCA) (*4*). However, their sample size was too limited to draw a convincing conclusion.

Therefore, the current study evaluated the similarities and differences between patients with GBAC and patients with GBSRCA in terms of short- and long-term outcomes.

2. Materials and Methods

2.1. Data source

The study utilized data from the Surveillance, Epidemiology, and End Results (SEER) database, which collects and publishes cancer incidence and survival data from population-based cancer registries covering approximately 34.6% of the US population (*3*). The dataset included patients diagnosed with gallbladder cancer between 2000 and 2021. Patients who were staged according to the 6th AJCC staging system were first evaluated. Moreover, only patients with pathologically confirmed GBAC and GBMCA were considered eligible. In order to guarantee the quality of this study, patients with recorded survival periods less than 1 month were excluded. The specific process of patient selection and identification is shown in Figure 1.

2.2. Identification of variables

Clinical and pathological variables analyzed included age, sex, race, marital status, tumor differentiation grade, pathological subtypes, stage at diagnosis, treatment modalities (radiotherapy, chemotherapy, and surgery), and cancer-related death (CRD). The variables were compared between the GBSRCA and GBAC groups using appropriate statistical tests to identify significant differences. The continuous variable "Age" was categorized into ≤60 and >60. Minor adjustments were also applied to other categorical variables. For instance, Marital status was simplified into two groups: Married and Single/unknown. Race was simplified into two major groups: White and Others. Tumor differentiation status was simplified into three groups: well to moderate differentiated, poorly to undifferentiated, and unknown.

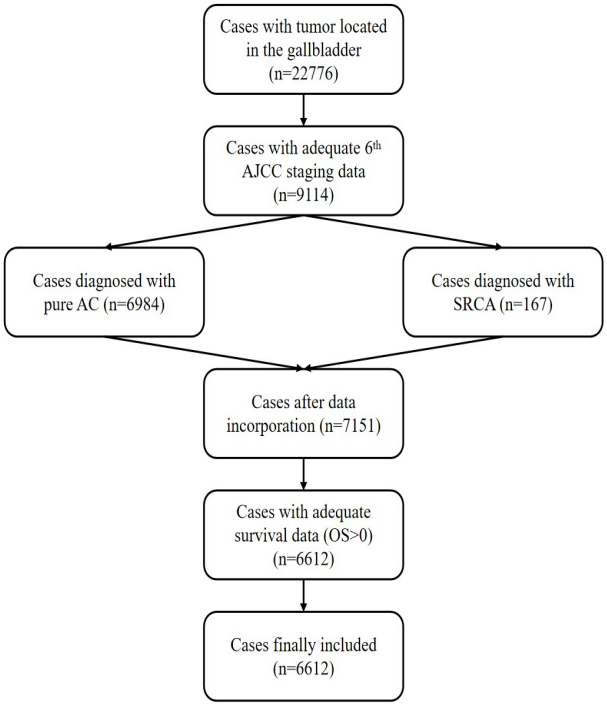

Figure 1. Flowchart illustrating the process of patient selection and identification.

2.3. Statistical analysis

The software R version 4.2.2 was used for statistical analysis. The R package tableone was used for baseline comparison and subsequent table output. Categorical data were expressed as numbers (percentages). Categorical variables were evaluated *via* the chi-squared and Fisher's exact tests. Survival analyses were performed using the R packages survminer and survival. Kaplan–Meier (KM) curves and the corresponding risk tables were generated using the R command ggsurvplot. OS was defined as the time from the date of radical surgery to the date of death or last follow-up. The R packages survminer, dplyr, survival, and rms were used to construct a Cox proportional hazards model, which produced hazard ratios (HR) and their 95% confidence intervals (CI). *P* values lower than 0.05 indicated statistical significance. The PSM analysis was performed using the R package MatchIt with the method="nearest," caliper = 0.05, and ratio = 1, matching factors that mainly consisted of independent prognostic factors for OS.

3. Results

3.1. Clinical and pathological characteristics before and after PSM

Table 1 summarizes the basic clinical and pathological features of the entire cohort. The cohort consisted of 6,612 patients, 147 (2.2%) of whom were diagnosed with GBSRCA and 6,465 (97.8%) of whom were diagnosed with GBAC. The age distribution revealed a significant difference between the two groups. Patients ≤ the age of 60 comprised 24.2% of the total cohort. Of them, 33.3% were in the GBSRCA group, while 23.9% were in the GBAC group, indicating that patients with GBSRCA tended to be younger (P = 0.009). There was also a significant difference in the sex distribution. Males represented 29.8% of the entire cohort. Within the GBSRCA group, males accounted for 22.4%, compared to 29.9% in the GBAC group, indicating a higher prevalence of GBSRCA among females (P = 0.049). Regarding tumor-related pathological features, GBSRCA was associated with a more advanced tumor stage. The proportions of patients with T3-T4 disease (56.5% *vs*. 44.0%, P = 0.004), lymph node metastasis (43.5% *vs*. 28.0%, P < 0.001), and poorly to undifferentiated disease (80.3% *vs*. 29.7%, P < 0.001) were significantly higher in patients with GBSRCA. Moreover, CRD was more frequent in patients with

Table 1. Basic clinical and pathological features in patients with GBSRCA or GBAC

Variables	Overall number (n = 6,612)	GBSRCA (n = 157)	GBAC (n = 6465)	P value
Age (%)				0.009
≤ 60	1,597 (24.2)	49 (33.3)	1,548 (23.9)	
> 60	5,015 (75.8)	98 (66.7)	4,917 (76.1)	
Sex (%)				0.049
Male	1,969 (29.8)	33 (22.4)	1,936 (29.9)	
Female	4,643 (70.2)	114 (77.6)	4,529 (70.1)	
Race (%)				0.708
Asian	694 (10.5)	14 (9.5)	680 (10.5)	
White	5,069 (76.7)	111 (75.5)	4,958 (76.7)	
Other	849 (12.8)	22 (15.0)	827 (12.8)	
Marital status (%)				0.191
No/Unknown	3,231 (48.9)	64 (43.5)	3,167 (49.0)	
Married	3,381 (51.1)	83 (56.5)	3,298 (51.0)	
Grade (%)				< 0.001
Well to moderately differentiated	3,318 (50.2)	13 (8.8)	3,305 (51.1)	
Poorly to undifferentiated	2,038 (30.8)	118 (80.3)	1,920 (29.7)	
Unknown	1,256 (19.0)	16 (10.9)	1,240 (19.2)	
T stage (%)				0.004
T1-T2	3,659 (55.3)	64 (43.5)	3,595 (55.6)	
T3-T4	2,953 (44.7)	83 (56.5)	2,870 (44.4)	
N stage (%)				< 0.001
N-	4,738 (71.7)	83 (56.5)	4,655 (72.0)	
N+	1,874 (28.3)	64 (43.5)	1,810 (28.0)	
M stage (%)				0.133
M-	4,940 (74.7)	102 (69.4)	4,838 (74.8)	
M+	1,672 (25.3)	45 (30.6)	1,627 (25.2)	
Radiotherapy (%)				0.441
Not performed	5,635 (85.2)	122 (83.0)	5,513 (85.3)	
Performed	977 (14.8)	25 (17.0)	952 (14.7)	
Chemotherapy (%)				0.221
Not performed	4,230 (64.0)	87 (59.2)	4,143 (64.1)	
Performed	2,382 (36.0)	60 (40.8)	2,322 (35.9)	
CRD (%)				< 0.001
No	2,558 (38.7)	32 (21.8)	2,526 (39.1)	
Yes	4,054 (61.3)	115 (78.2)	3,939 (60.9)	
Surgery (%)				0.168
Not performed	1,085 (16.4)	18 (12.2)	1,067 (16.5)	
Performed	5,527 (83.6)	129 (87.8)	5,398 (83.5)	

GBSRCA: gallbladder signet-ring cell carcinoma; GBAC: gallbladder adenocarcinoma; CRD: cancer-related death.

GBSRCA (78.2% *vs*. 60.9%, $P < 0.001$).

Table 2 shows the clinical and pathological features of the cohort after PSM, ensuring a balanced comparison between groups. Post-PSM, the age and sex distribution between the GBSRCA and GBAC groups were well balanced, and no significant differences were noted (Age: $p = 1.000$; Sex: $P = 0.657$). Other clinical and pathological features also showed a balanced distribution, ensuring that the survival differences observed are attributable to the histological subtype rather than confounding factors. Provided here is a comprehensive analysis of the differences in clinical characteristics and survival outcomes between patients with GBSRCA and those with GBAC, highlighting the poorer prognosis associated with GBSRCA. The use of PSM helps ensure that these findings are robust and not confounded by baseline differences in patient characteristics.

3.2. Survival analysis before and after PSM

Figure 2 shows the KM survival curves for overall survival (OS) and cancer-specific survival (CSS) before PSM. The median OS for patients with GBSRCA was significantly shorter compared to that for patients with GBAC ($P < 0.001$). The KM curves (Figure 2A) depict a sharp decline in survival for patients with GBSRCA, emphasizing their poorer prognosis. Similarly, CSS analysis (Figure 2B) indicated that patients with GBSRCA had a significantly worse CSS compared to patients with GBAC ($P < 0.001$). Figure 3 shows the KM survival curves for OS and CSS after adjusting for potential confounders through PSM. Even after PSM, the median OS for patients with GBSRCA remained significantly shorter than that for patients with GBAC ($P < 0.001$), as shown in Figure 3A. The CSS results post-PSM (Figure 3B) also indicated that patients with GBSRCA continued to have a significantly poorer prognosis compared to patients with GBAC ($P < 0.001$).

3.3. Univariate and multivariate Cox regression analysis

Table 2. Basic clinical and pathological features in patients with GBSRCA and GBAC after PSM

Variables	Overall number (n = 284)	GBSRCA (n = 142)	GBAC (n = 142)	P value
Age (%)				1.000
≤ 60	90 (31.7)	45 (31.7)	45 (31.7)	
> 60	194 (68.3)	97 (68.3)	97 (68.3)	
Sex (%)				0.657
Male	57 (20.1)	30 (21.1)	27 (19.0)	
Female	227 (79.9)	112 (78.9)	115 (81.0)	
Race (%)				0.881
Asian	26 (9.2)	12 (8.5)	14 (9.9)	
White	218 (76.8)	109 (76.8)	109 (76.8)	
Other	40 (14.1)	21 (14.8)	19 (13.4)	
Marital status (%)				0.720
No/Unknown	127 (44.7)	62 (43.7)	65 (45.8)	
Married	157 (55.3)	80 (56.3)	77 (54.2)	
Grade (%)				1.000
Well to moderately differentiated	26 (9.2)	13 (9.2)	13 (9.2)	
Poorly to undifferentiated	232 (81.7)	116 (81.7)	116 (81.7)	
Unknown	26 (9.2)	13 (9.2)	13 (9.2)	
T stage (%)				1.000
T1-T2	126 (44.4)	63 (44.4)	63 (44.4)	
T3-T4	158 (55.6)	79 (55.6)	79 (55.6)	
N stage (%)				1.000
N-	158 (55.6)	79 (55.6)	79 (55.6)	
N+	126 (44.4)	63 (44.4)	63 (44.4)	
M stage (%)				1.000
M-	198 (69.7)	99 (69.7)	99 (69.7)	
M+	86 (30.3)	43 (30.3)	43 (30.3)	
Radiotherapy (%)				1.000
Not performed	234 (82.4)	117 (82.4)	117 (82.4)	
Performed	50 (17.6)	25 (17.6)	25 (17.6)	
Chemotherapy (%)				0.719
Not performed	161 (56.7)	82 (57.7)	79 (55.6)	
Performed	123 (43.3)	60 (42.3)	63 (44.4)	
CRD (%)				0.399
No	66 (23.2)	30 (21.1)	36 (25.4)	
Yes	218 (76.8)	112 (78.9)	106 (74.6)	
Surgery (%)				1.000
Not performed	32 (11.3)	16 (11.3)	16 (11.3)	
Performed	252 (88.7)	126 (88.7)	126 (88.7)	

GBSRCA: gallbladder signet-ring cell carcinoma; GBAC: gallbladder adenocarcinoma; CRD: cancer-related death; PSM: propensity score matching.

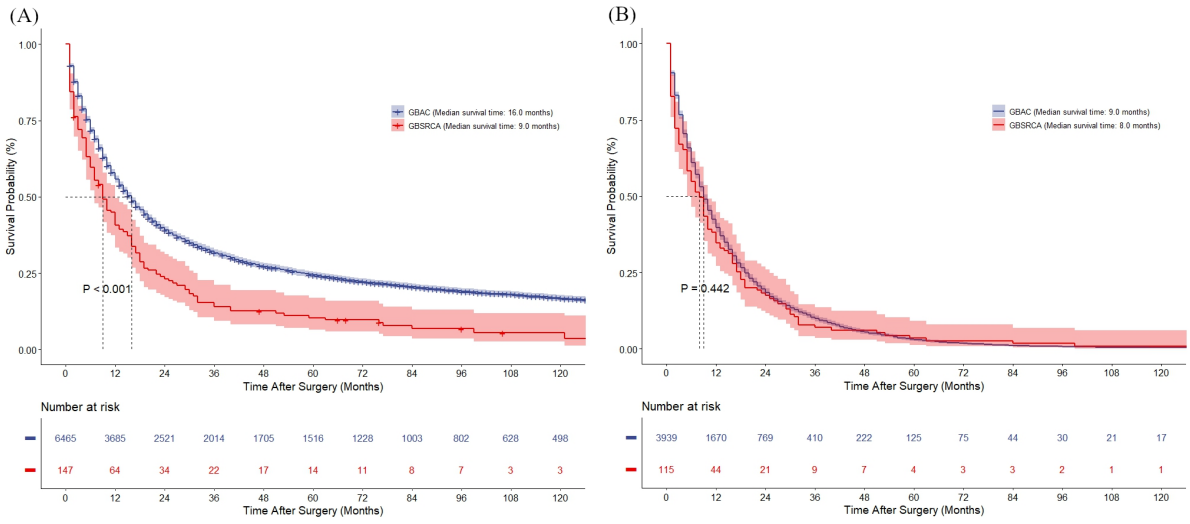

Figure 2. KM curves showing survival differences between patients with GBAC and those with GBSRCA. (A), OS. **(B)**, CSS. GBAC: gallbladder adenocarcinoma; GBSRCA: gallbladder signet-ring cell carcinoma. OS: overall survival. CSS: cancer-specific survival.

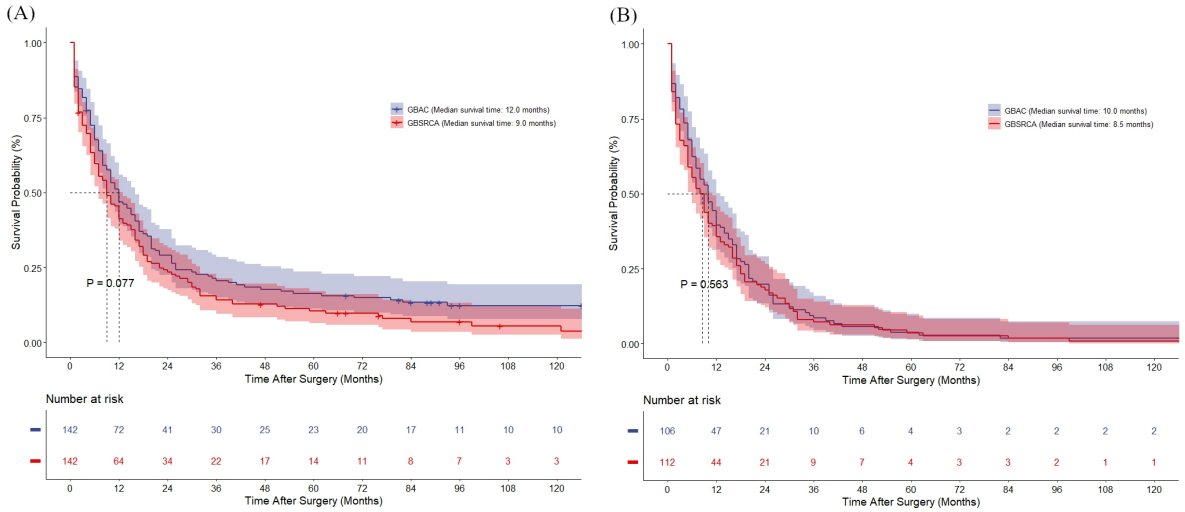

Figure 3. KM curves showing survival differences between patients with GBAC and those with GBSRCA after PSM. (A), OS. **(B)**, CSS. GBAC: gallbladder adenocarcinoma; GBSRCA: gallbladder signet-ring cell carcinoma. OS: overall survival. CSS: cancer-specific survival. PSM: propensity score matching.

Table 3 shows the results of the univariate and multivariate Cox regression analyses for prognostic factors affecting OS and CSS in the entire cohort. In univariate analysis, patients > the age of 60 had an HR for OS of 0.791 (95% CI: 0.552-1.135; $P = 0.204$) and an HR for CSS of 0.765 (95% CI: 0.517-1.134; $P = 0.182$), indicating a trend, albeit not a significant one. Being female was associated with a better OS (HR: 0.786, 95% CI: 0.659-0.937; $P = 0.008$) and CSS (HR: 0.798, 95% CI: 0.667-0.954; $P = 0.013$). In multivariate analysis of the histological subtypes (GBSRCA *vs*. GBAC), GBSRCA was found to be an independent adverse prognostic factor for both OS (HR: 1.839, 95% CI: 1.474-2.297; $P < 0.001$) and CSS (HR: 1.871, 95% CI: 1.494-2.343; $P < 0.001$). Advanced tumor stage was independently associated with a poorer OS and CSS, emphasizing the importance of early detection and treatment.

In the prognostic analyses of cases with GBSRCA, as summarized in Table 4, tumor differentiation grade, T stage, M stage, and surgical status were identified as significant prognostic factors in the univariate analyses. In the multivariate analyses, T stage (HR: 1.721, 95% CI: 1.137-2.605; $P = 0.010$) and M stage (HR: 1.816, 95% CI: 1.192-2.767; $P = 0.005$) emerged as independent prognostic factors. Additionally, while surgery was shown to be a protective factor, it was not found to be an independent prognostic factor (HR: 0.667, 95% CI: 0.373-1.191; $P = 0.171$).

4. Discussion

Previous studies have indicated that the presence of SRCC components is a significantly poor prognostic factor for patients with solid tumors, and particularly in those with gastric cancer (*17-21*). In these patients, early peritoneal dissemination and lymph node metastasis are common, leading to a worse prognosis than that for conventional adenocarcinoma. In GBC, however, the differences in clinicopathological factors and long-term prognosis associated with SRCC compared to conventional adenocarcinoma have not been systematically explored. Using data from the SEER database, the current study has provided an in-depth comparative analysis of these two subtypes, emphasizing differences in demographic characteristics, clinical features, and survival outcomes.

Results revealed significant differences in the age and sex distribution between patients with GBSRCA and those with GBAC. In specific terms, patients with GBSRCA were significantly younger ($p = 0.009$), with a notable 33.3% being age 60 or younger compared to 23.9% of patients with GBAC. This younger age at diagnosis of GBSRCA suggests a potentially distinct etiopathogenesis that might involve genetic predispositions or environmental factors not typically associated with GBAC. This finding is consistent with previous studies indicating that SRCC is more prevalent among younger individuals. The sex distribution also differed significantly, with a higher proportion of females in the GBSRCA group (77.6%) compared to the GBAC group (70.1%, $p = 0.049$). This female predominance aligns with the overall higher incidence of gallbladder disease in women, which is often attributed to hormonal influences and a higher prevalence of gallstones that are known risk factors for gallbladder cancer. In addition, results confirmed that SRCC is associated with a higher likelihood of lymph node metastasis, later-stage diagnosis, and poorer prognosis. Even after PSM, which adjusts for potential confounders such as age, sex, and other clinical variables, patients with GBSRCA continued to share a significantly worse OS and CSS compared to

Table 3. Univariate and multivariate Cox regression of prognostic factors for OS and CSS of the entire cohort

Variables	OS				CSS			
	Univariate		Multivariate		Univariate		Multivariate	
	Crude HR (95%CI)	uni-*P* value	Adj HR (95%CI)	Multi *P* value	Crude HR (95%CI)	Uni *P* value	Adj HR (95%CI)	Multi *P* value
Age								
≤ 60								
> 60	1.409 (1.320,1.505)	< 0.001	1.434 (1.342,1.533)	< 0.001	1.092 (1.016,1.173)	0.017	1.112 (1.033,1.196)	0.005
Sex								
Male								
Female	0.939 (0.886,0.995)	0.032	0.850 (0.801,0.902)	< 0.001	1.006 (0.940,1.076)	0.864		
Race								
Asian								
White	1.120 (1.024,1.226)	0.013	1.083 (0.989,1.184)	0.084	1.054 (0.951,1.168)	0.314		
Other	1.148 (1.026,1.284)	0.016	1.088 (0.972,1.218)	0.143	1.092 (0.960,1.242)	0.179		
Marital status								
No/Unknown								
Married	0.860 (0.815,0.907)	< 0.001	0.801 (0.758,0.847)	< 0.001	0.899 (0.845,0.956)	0.001	0.870 (0.818,0.926)	< 0.001
Grade								
Well to moderately differentiated								
Poorly to undifferentiated	1.788 (1.683,1.900)	< 0.001	1.400 (1.314,1.491)	< 0.001	1.484 (1.384,1.591)	< 0.001	1.368 (1.275,1.469)	< 0.001
Unknown	1.563 (1.455,1.679)	< 0.001	0.943 (0.867,1.026)	0.171	1.968 (1.810,2.141)	< 0.001	1.087 (0.977,1.209)	0.124
T stage								
T1-T2								
T3-T4	2.996 (2.834,3.168)	< 0.001	2.183 (2.046,2.329)	< 0.001	1.835 (1.720,1.957)	< 0.001	1.594 (1.485,1.711)	< 0.001
N stage								
N-								
N+	1.666 (1.572,1.765)	< 0.001	1.266 (1.188,1.348)	< 0.001	1.133 (1.062,1.209)	< 0.001	1.123 (1.049,1.202)	0.001
M stage								
M-								
M+	3.559 (3.345,3.787)	< 0.001	2.320 (2.156,2.497)	< 0.001	2.174 (2.034,2.324)	< 0.001	1.904 (1.763,2.056)	< 0.001
Pathology subtypes								
GBAC								
GBSRCA	1.614 (1.361,1.914)	< 0.001	1.341 (1.127,1.594)	0.001	1.077 (0.894,1.297)	0.434		
Chemotherapy								
Not performed								
Performed	1.283 (1.214,1.356)	< 0.001	0.704 (0.656,0.754)	< 0.001	0.864 (0.811,0.919)	< 0.001	0.578 (0.536,0.624)	< 0.001
Radiotherapy								
Not performed								
Performed	0.816 (0.757,0.880)	< 0.001	0.978 (0.896,1.067)	0.613	0.663 (0.609,0.721)	< 0.001	1.018 (0.924,1.121)	0.717
Surgery								
Not performed								
Performed	0.264 (0.246,0.283)	< 0.001	0.485 (0.442,0.533)	< 0.001	0.405 (0.375,0.437)	< 0.001	0.531 (0.477,0.590)	< 0.001

GBSRCA: gallbladder signet-ring cell carcinoma; GBAC: gallbladder adenocarcinoma; OS: overall survival; CSS: cancer-specific survival.

Table 4. Univariate and multivariate Cox regression of prognostic factors for the OS and CSS of patients with GBSRCA

Variables	OS				CSS			
	Univariate		Multivariate		Univariate		Multivariate	
	HR (95%CI)	*P* value	HR (95%CI)	*P* value	HR (95%CI)	*P* value	HR (95%CI)	*P* value
Age								
≤ 60								
> 60	0.791 (0.552,1.135)	0.204			0.765 (0.517,1.134)	0.182		
Sex								
Male								
Female	0.735 (0.490,1.105)	0.139			0.749 (0.483,1.162)	0.197		
Race								
Asian								
White	0.758 (0.422,1.364)	0.356			1.044 (0.553,1.971)	0.894		
Other	0.827 (0.406,1.681)	0.599			0.985 (0.456,2.131)	0.970		
Marital status								
No/Unknown								
Married	1.050 (0.747,1.477)	0.777			0.868 (0.594,1.268)	0.464		
Grade								
Well to moderately differentiated								
Poorly to undifferentiated	1.514 (0.810,2.829)	0.194	1.538 (0.818,2.892)	0.182	1.110 (0.576,2.138)	0.755		
Unknown	2.353 (1.063,5.208)	0.035	1.705 (0.720,4.036)	0.225	1.446 (0.629,3.325)	0.385		
T stage								
T1-T2								
T3-T4	1.936 (1.354,2.768)	< 0.001	1.720 (1.186,2.494)	0.004	1.798 (1.205,2.683)	0.004	1.721 (1.137,2.605)	0.010
N stage								
N-								
N+	1.197 (0.849,1.688)	0.306			0.835 (0.578,1.208)	0.339		
M stage								
M-								
M+	2.562 (1.754,3.741)	< 0.001	2.421 (1.618,3.623)	< 0.001	1.949 (1.308,2.903)	0.001	1.816 (1.192,2.767)	0.005
Chemotherapy								
Not performed								
Performed	0.964 (0.684,1.360)	0.836			0.753 (0.520,1.091)	0.133		
Radiotherapy								
Not performed								
Performed	0.876 (0.563,1.364)	0.558			0.923 (0.555,1.535)	0.758		
Surgery								
Not performed								
Performed	0.420 (0.245,0.720)	0.002	0.738 (0.387,1.410)	0.358	0.448 (0.259,0.774)	0.004	0.667 (0.373,1.191)	0.171

GBSRCA: gallbladder signet-ring cell carcinoma; OS: overall survival; CSS: cancer-specific survival.

patients with GBAC ($p < 0.001$). This persistent survival disadvantage highlights the inherent aggressiveness of GBSRCA, which may be due to its distinct biological characteristics such as a higher metastatic potential and resistance to conventional therapies.

The clinical implications of this study can be summarized as follows. First, given the younger age at diagnosis of GBSRCA, considering earlier screening of at-risk populations may be worth considering. This could involve more vigilant monitoring of patients with known risk factors such as gallstones or chronic gallbladder inflammation. Second, the distinct survival disadvantage associated with GBSRCA underscores the need for personalized treatment strategies. There is a pressing need for research into targeted therapies that address the unique molecular characteristics of GBSRCA. Third, the higher prevalence of GBSRCA in females suggests that gender-specific factors may influence the development and progression of this subtype. Hormonal influences and their potential role in GBSRCA pathogenesis warrant further investigation. Fourth, comprehensive molecular and genetic profiling of GBSRCA is essential to identifying unique biomarkers and therapeutic targets. Such studies could lead to the development of novel targeted therapies and improve outcomes for patients with this aggressive subtype. Fifth, developing and validating prognostic models that incorporate clinical, pathological, and molecular variables can help predict outcomes more accurately and guide treatment decisions. These models should be tailored to account for the specific characteristics of GBSRCA.

This study had several limitations. First, the retrospective nature of the analysis may have introduced selection bias and limited the ability to establish causality. Second, the reliance on the SEER database means that certain clinical details, such as comorbidities and specific treatment regimens, were not available, potentially affecting the comprehensiveness of the findings. With the advent of adjuvant immunotherapy over the past few years, significant efficacy and improved survival have been achieved in an increasing number of patients with biliary tract malignancies after immunotherapy (*22*). However, the SEER data are not able to provide corresponding detailed raw data, which is undoubtedly a drawback to this study. Third, the relatively small sample of patients with GBSRCA may limit the generalizability of the results and the statistical power to detect differences. Fourth, the study did not include molecular and genetic analyses, which could provide deeper insights into the distinct etiopathogenesis of and therapeutic targets for GBSRCA.

In conclusion, this study has highlighted the significant clinical and pathological differences between GBSRCA and GBAC, emphasizing the poorer prognosis associated with GBSRCA. The findings underscore the need for early detection, personalized treatment strategies, and targeted research efforts to address the unique challenges posed by this rare and aggressive subtype of gallbladder cancer. Enhanced understanding and management of GBSRCA could lead to improved survival outcomes and better quality of life for affected patients.

Funding: This study was supported by a grant from the Sichuan Science and Technology Program (2024NSFSC1936).

Conflict of Interest: The authors have no conflicts of interest to disclose.

References

1. Midorikawa Y. Treatment of biliary tract carcinoma over the last 30 years. Biosci Trends. 2022; 16:189-197.
2. Wang Z, Wang L, Hua Y, Zhuang X, Bai Y, Wang H. Development and validation of a prognostic nomogram for gallbladder papillary adenocarcinoma. Front Oncol. 2023; 13:1157057.
3. Song HW, Chen C, Shen HX, Ma L, Zhao YL, Zhang GJ, Geng ZM, Wang L. Squamous/adenosquamous carcinoma of the gallbladder: Analysis of 34 cases and comparison of clinicopathologic features and surgical outcomes with adenocarcinoma. J Surg Oncol. 2015; 112:677-680.
4. Zou RQ, Hu HJ, Lv TR, Liu F, Ma WJ, Wang JK, Dai YS, Yang SQ, Hu YF, Li FY. Clinicopathological characteristics and outcome of primary sarcomatoid carcinoma of the gallbladder. Front Oncol. 2022; 12:1009673.
5. Zou RQ, Hu HJ, Liu F, Lv TR, Wang JK, Regmi P, Li FY. Comparison of clinicopathological characteristics of mucinous adenocarcinoma and conventional adenocarcinoma of gallbladder. Asian J Surg. 2023; 46:283-290.
6. Wu SG, Chen XT, Zhang WW, Sun JY, Li FY, He ZY, Pei XQ, Lin Q. Survival in signet ring cell carcinoma varies based on primary tumor location: a Surveillance, Epidemiology, and End Results database analysis. Expert Rev Gastroenterol Hepatol. 2018; 12:209-214.
7. Zhang M, Zhu G, Zhang H, Gao H, Xue Y. Clinicopathologic features of gastric carcinoma with signet ring cell histology. J Gastrointest Surg. 2010; 14:601-606.
8. Chiu CT, Kuo CJ, Yeh TS, Hsu JT, Liu KH, Yeh CN, Hwang TL, Jan YY, Lin CJ. Early signet ring cell gastric cancer. Digest Diseases Sci. 2011; 56:1749-1756.
9. Kunisaki C, Shimada H, Nomura M, Matsuda G, Otsuka Y, Akiyama H. Therapeutic strategy for signet ring cell carcinoma of the stomach. Br J Surg. 2004; 91:1319-1324.
10. Thomas AA, Stephenson AJ, Campbell SC, Jones JS, Hansel DE. Clinicopathologic features and utility of immunohistochemical markers in signet-ring cell adenocarcinoma of the bladder. Hum Pathol. 2009; 40:108-116.
11. Ou SH, Ziogas A, Zell JA. Primary signet-ring carcinoma (SRC) of the lung: A population-based epidemiologic study of 262 cases with comparison to adenocarcinoma of the lung. J Thorac Oncol. 2010; 5:420-427.

12. Pavić I, Marusić Z, Mijić A, Balicević D, Kruslin B, Tomas D. A case of signet-ring cell carcinoma of the gallbladder: Immunohistochemistry and differential diagnosis. Acta Clin Croat. 2010; 49:159-162.
13. Wu X, Zhang Z, Li X, Lin Q, Chen G, Lu J, Zeng Y, Hu D, Huang K, Lin Z, Yan J. Poorer prognosis of primary signet-ring cell carcinoma of the breast compared with mucinous carcinoma. PloS One. 2016; 11:e0162088.
14. Yendamuri S, Huang M, Malhotra U, Warren GW, Bogner PN, Nwogu CE, Groman A, Demmy TL. Prognostic implications of signet ring cell histology in esophageal adenocarcinoma. Cancer. 2013; 119:3156-3161.
15. Hiraki M, Ueda J, Kai K, Ide T, Asai M, Ohtsuka T, Kohya N, Mukai S, Kitahara K, Noshiro H. A case of signet ring cell carcinoma of the gallbladder which was treated by aggressive surgery and intensive adjuvant chemotherapy. J Gastrointest Cancer. 2017; 48:83-86.
16. Kaji K, Seishima J, Yamato M, Miyazawa M, Komura T, Marukawa Y, Ohta H, Kasashima S, Kawashima A, Yano M, Unoura M. Clinical utility of endoscopic ultrasound-guided fine-needle aspiration in mixed adenoneuroendocrine carcinoma with signet-ring cells of the pancreas: A case report and review of the literature. Clin J Gastroenterol. 2016; 9:43-48.
17. Bleaney CW, Barrow M, Hayes S, Ang Y. The relevance and implications of signet-ring cell adenocarcinoma of the oesophagus. J Clin Pathol. 2018; 71:201-206.
18. Börger ME, Gosens MJ, Jeuken JW, van Kempen LC, van de Velde CJ, van Krieken JH, Nagtegaal ID. Signet ring cell differentiation in mucinous colorectal carcinoma. J Pathol. 2007; 212:278-286.
19. Belkaïd S, Crumbach L, de Bernardi A, Darnis S, Bouquerel M, Neuhart A, Assaad S, Amini-Adle M. Gastric signet-ring cell adenocarcinoma masquerading as sarcoidosis. Lancet Oncol. 2024; 25:e173.
20. Roth LM, Ramzy I. Signet ring stromal cell tumor revisited and related signet ring cell lesions of the ovary. Hum Pathol. 2014; 45:636-642.
21. Murakami H, Nakanishi H, Tanaka H, Ito S, Misawa K, Ito Y, Ikehara Y, Kondo E, Kodera Y. Establishment and characterization of novel gastric signet-ring cell and non signet-ring cell poorly differentiated adenocarcinoma cell lines with low and high malignant potential. Gastric Cancer. 2013; 16:74-83.
22. Chen L, Yin G, Wang Z, Liu Z, Sui C, Chen K, Song T, Xu W, Qi L, Li X. A predictive radiotranscriptomics model based on DCE-MRI for tumor immune landscape and immunotherapy in cholangiocarcinoma. Biosci Trends. 2024; 18:263-276.

Received July 27, 2024; Revised August 20, 2024; Accepted August 23, 2024.

[§]These authors contributed equally to this work.

*Address correspondence to:
Liping Chen and Yulong Cai, Department of Biliary Tract Surgery, General Surgery, West China Hospital of Sichuan University, Chengdu, Sichuan Province, China.
E-mail: 47137417@qq.com (LC), caiyulong@wchscu.cn (YC)

Released online in J-STAGE as advance publication August 25, 2024.

Original Article

DOI: 10.5582/bst.2024.01108

The role of cholesterol-modified prognostic nutritional index in nutritional status assessment and predicting survival after liver resection for hepatocellular carcinoma

Kunlin Chen, Guangjun Li, Yiwen Qiu, Ming Yang, Tao Wang, Yi Yang, Haizhou Qiu, Ting Sun, Wentao Wang*

Department of Liver Surgery, West China Hospital, Sichuan University, Chengdu, Sichuan, China.

SUMMARY Malnutrition, which is often underestimated in patients with hepatocellular carcinoma (HCC), has a proven adverse effect on survival rates. The purpose of this study was to verify the effectiveness of the cholesterol-modified prognostic nutritional index (CPNI) in determining the nutritional status and predicting overall survival (OS) and recurrence-free survival (RFS) in patients with HCC by comparing it with several other nutritional indicators. This retrospective single-center study enrolled 1450 consecutive HCC patients who underwent curative liver resection from January 2015 to November 2019. We evaluated the prognostic significance of several nutritional indicators, including CPNI, the controlling nutritional status (CONUT), the nutritional risk index (NRI), and the prognostic nutritional index (PNI), by applying time-dependent receiver operating characteristic (ROC) curves, Kaplan–Meier survival analysis, and Cox proportional hazards regression analysis. Among several objective nutrition evaluations (including CPNI, CONUT, NRI, and PNI), CPNI demonstrated the greatest prognostic predictive power for predicting OS. Meanwhile, CPNI demonstrated marginally higher accuracy in predicting RFS compared to PNI, and significantly outperformed CONUT and NRI. Univariate and multivariate analyses suggested that CPNI was an independent risk factor for the OS and RFS of patients with HCC undergoing curative liver resection. In most subgroups, malnutrition as identified by CPNI demonstrates strong stratification ability in predicting both OS and RFS. CPNI serves as an accurate and stable instrument for evaluating nutritional status and forecasting survival outcomes in HCC patients following liver resection, which has the potential to markedly influence clinical decision-making processes and the management of patient care.

Keywords malnutrition, cholesterol-modified prognostic nutritional index, hepatocellular carcinoma

1. Introduction

Malnutrition is a common problem among patients with cancer, although it is frequently undiagnosed (*1*). It is estimated that 32% of the individuals diagnosed with cancer experience malnutrition (*2*). Malnutrition can weaken immunity and treatment tolerance, potentially affecting cancer therapy outcomes and patient prognosis (*3,4*). Hepatocellular carcinoma (HCC) is the primary type of liver cancer, representing 90% of such cases, and is the fourth leading cause of cancer-related deaths worldwide (*5*). Hepatectomy is widely recognized as a curative therapeutic approach for HCC (*6*). Most HCC cases are associated with liver cirrhosis (*7*). Malnutrition often affects 20-50% of patients with liver cirrhosis, representing a significant health burden (*4*). Therefore, assessing the nutritional status before liver resection is essential to ensure positive patient outcomes.

Despite the development of several screening instruments to detect malnutrition in cancer patients, a universally accepted gold standard has yet to be established. The Controlling Nutritional Status (CONUT) score, proposed by Ulibarri *et al*. in 2005, is designed to screen the nutritional condition of patients in a hospital setting, utilizing parameters such as serum albumin concentration, total cholesterol, and lymphocyte count (*8*). The CONUT score has been demonstrated to serve as a prognostic indicator and predictor of complications across a variety of cancer types, including HCC (*9-12*). The Nutritional Risk Index (NRI) has become a simple tool for predicting

nutritional risk and has shown strong prognostic value in medical and surgical patients (*13,14*). The Prognostic Nutritional Index (PNI) is an indicator formulated using serum albumin levels and lymphocyte counts. It offers a convenient metric to describe the association between a patient's nutritional health and immunological status and correlates with the prognosis following liver resection (*15-18*). Recently, the Cholesterol-modified Prognostic Nutritional Index (CPNI), which was proposed as a new nutritional assessment based on PNI, has shown greater predictive accuracy for overall survival (OS) in breast cancer patients than other indices, including PNI, CONUT, NRI, global leadership initiative on malnutrition (GLIM), and patient-generated subjective nutrition assessment (PGSGA) (*19*).

However, the performance of CPNI in determining the nutritional status and forecasting survival outcome among patients with HCC following liver resection remains unclear. This study explored the relationship between CPNI and OS and recurrence-free survival (RFS) in HCC patients and assessed its predictive accuracy relative to other objective nutritional indicators such as CONUT, NRI, and PNI.

2. Materials and Methods

2.1. Patient election

This retrospective cohort study was approved by the Ethics Committee of West China Hospital, Sichuan University and was conducted in accordance with the Declaration of Helsinki (NO.2024(189)). Between January 2015 and November 2019, 1,450 consecutive HCC patients who underwent curative liver resection were retrospectively enrolled in this study at the West China Hospital of Sichuan University. Due to the nature of this retrospective analysis, consent forms were not required.

The inclusion criteria were patients with HCC who underwent R0 liver resection and had HCC confirmed by histopathological examination.

The exclusion criteria were: (1) the presence of other types of primary liver cancer (such as cholangiocarcinoma or combined hepatocellular-cholangiocarcinoma) and a history of cancer in another organ at the same time or in the past; (2) bile duct invasion; (3) vascular invasion; (4) lymph node metastases; and (5) invasion of the adjacent organs. (6) Patients with incomplete clinicopathological information or follow-up data. The process for selecting patients is shown in Supplemental Figure S1 (*https://www.biosciencetrends.com/supplementaldata/206*).

2.2. Patient characteristics, surgical procedures and endpoints

Clinicodemographic factors such as sex, age, body mass index (BMI), the albumin-bilirubin (ALBI) grade, hepatitis B infection, hepatitis C infection, tumor stage, comorbidities, preoperative blood test results, serum α-fetoprotein (AFP) level, type of resection and pathological findings were collected from electronic medical records.

Major hepatectomy is defined as the surgical removal of three or more segments from the liver, according to Couinaud's classification. In contrast, a minor hepatectomy involves the excision of less than three segments. Liver resection is classified either as anatomical, conforming to the Brisbane 2000 liver anatomy nomenclature, or as non-anatomical, which includes limited forms of resection such as wedge resections. The Edmondson-Steiner classification system was used to grade tumor differentiation.

Patients underwent necessary imaging modalities such as enhanced abdominal computed tomography (CT), chest CT, contrast-enhanced ultrasound, or magnetic resonance imaging (MRI) for a thorough assessment. Comprehensive laboratory tests including liver function, hepatitis B and C screenings, and tumor markers were also performed. The volume of the remaining liver was gauged using CT or MRI to ensure post-surgery viability. Liver function was assessed using the Child-Pugh scores and ALBI grades. Candidates for liver resection had adequate liver volumes and potential for complete tumor removal. The surgical approach was tailored to the tumor characteristics, with intraoperative ultrasound utilized as required to guide the procedure.

In the study, the primary endpoint was overall survival (OS), defined as the time from the date of surgery until the patient's death or the last follow-up date. The secondary endpoint was recurrence-free survival (RFS), which was measured from the date of surgery to the date of confirmation of recurrence and/or metastasis. Recurrent HCC is diagnosed through CT and/or MRI imaging, along with elevated AFP tumor marker levels. Patients experiencing HCC recurrence would undergo suitable treatments, preferably radiofrequency ablation or another liver resection for curative intent. The vital status of patients discharged alive was monitored through outpatient visits, telephone calls every two months, or during hospital admissions. Starting from the third year after discharge, the follow-up frequency was adjusted to every three months. We continued to follow-up with the patients until they died of any cause or were lost to follow-up.

2.3. Malnutrition assessment

For every patient, BMI = weight (kg)/height^2 (m). Then, all patients were sorted in four categories based on their BMI: underweight (< 18.5 kg/m^2), normal weight (18.5 to 24.0 kg/m^2), overweight (24.0 to 28.0 kg/m^2), and obese (≥ 28.0 kg/m^2) (*19,20*).

The CONUT score is an assessment tool that

evaluates an individual's nutritional status by three biomarkers: serum albumin, total cholesterol, and lymphocyte count. Scores for albumin, lymphocytes, and cholesterol are as follows: albumin: >35 g/L = 0 points, 30-34 g/L = 2 points, 25-29 g/L = 4 points, <25 g/L = 6 points; lymphocytes: ≥ 1.6×10^9/L = 0 points, 1.2-1.59 × 10^9/L = 1 points, 0.8-1.19 × 10^9/L = 2 points, < 0.8×10^9/L = 3 points; cholesterol: ≥180 mg/dL = 0 points, 140-179 mg/dL = 1 points, 100-139 mg/dL = 2 points, <100 mg/dL = 3 points (*20*). This scoring system ranges from 0 to 12, with a score > 2 indicating malnutrition (19). To calculate the NRI: ideal body weight (IBW) = Height^2 (m) × 22; NRI = 1.519 × albumin (g/L) + 41.7 × (current weight/IBW) (*19*). An NRI of < 100 indicates malnutrition. The PNI = albumin (g/L) + 5 × lymphocyte count ($\times 10^9$) (*20*). The Cholesterol-modified Prognostic Nutritional Index (CPNI) = 4.8 × cholesterol (mmol/L) - 1.5 × albumin (g/L) - 7.7 × lymphocyte ($\times 10^9$) + 126 (*19*).

2.4. Statistics analysis

Continuous variables are expressed as a median with interquartile range (25th to 75th percentiles). The Student's *t*-test was used to evaluate distributed continuous variables, while the Mann–Whitney *U* test was used to assess non-normally distributed variables. Categorical data were reported as percentages and analyzed using $\chi 2$ or Fisher's exact tests. The prognostic effectiveness of several nutritional indices for OS and RFS was examined using the time-dependent ROC curves. The relationships between the malnutrition markers and OS were examined using restricted cubic spline (RCS) plots. Continuous nutritional indicators were split into two groups using optimal cut-offs, which were determined by maximally selected rank statistics. Kaplan-Meier curves and the log-rank tests were used for survival comparisons between the groups. To determine the independent predictive significance of nutritional markers for OS in HCC, univariate and multivariate Cox regression analyses were performed. Four nutritional indicators were evaluated using separate multivariate models designed to assess the impact of malnutrition on OS and RFS. Variables with *p*-values < 0.05 in the univariate Cox regression were included in the multivariate Cox regression analysis. Statistical analysis was considered significant when the two-tailed *P*-value was less than 0.05. All statistical procedures were conducted using R software, version 4.3.2.

3. Results

3.1. Patents' characteristic

Finally, 1,450 patients with hepatocellular carcinoma were included in this retrospective study. The cohort comprised 219 (15.1%) females and 1231 (84.9%) males, with a median age of 53 years. 1194 (82.3%) patients had HBV infection, whereas 24 patients had HCV infection. The median BMI of the patients was 23 kg/m^2, 804 (55.6%) were classified as normal weight, 446 (30.8%) were classified as overweight, 114 (16.4%) as obese, and 84 (5.79%) as underweight. Patients were classified according to the BCLC staging system: 146 (10.1%) were in BCLC stage 0, 1132 (78.1%) were in BCLC stage A, and 172 (11.9%) were in BCLC stage B. Additionally, we compared the baseline data of male and female patients; the detailed baseline characteristics of the patients are shown in Table 1.

3.2. Assessment of malnutrition

There was a nonlinear relationship between nutritional indices (PNI and CPNI) and OS of HCC patients, according to RCS analysis using the Cox proportional hazards model, as depicted in Figure 1. According to maximally selected log rank statistics, the optimal cutoffs for PNI and CPNI were 50.25 and 70.48 points, respectively (Supplemental Figure S2, *https://www.biosciencetrends.com/supplementaldata/206*). PNI ≤ 50.25 points indicates malnutrition, while CPNI > 70.48 points indicates malnutrition. The incidence of malnutrition in patients with HCC was notably inconsistent, ranging from 21.2% under the NRI criteria to 62.8% when assessed with CONUT. Evaluations using different indicators, CONUT score, NRI, PNI, and CPNI, diagnosed malnutrition in 911 (62.8%), 308 (21.2%), 721 (49.7%), and 695 (47.9%) patients, respectively (Table 1). A total of 198 cases were identified as malnutrition using four nutritional indicators (CONUT, NRI, PNI, and CPNI), as shown in Figure 2. The frequency of malnutrition within both sex and BMI groups was established using each of the nutritional indices and is shown in Supplemental Figure S3 (*https://www.biosciencetrends.com/supplementaldata/206*). Under the CONUT diagnostic criteria, females showed a higher incidence of malnutrition than males. However, according to the NRI, PNI, and CPNI criteria, no notable difference was found in the malnutrition rates between the two groups. When evaluated using the CONUT, NRI, PNI, and CPNI criteria, the incidence of malnutrition decreased as the BMI increased.

3.3. Evaluating the prognostic effectiveness of nutritional indices

The time-dependent ROC analysis assessing the prognostic predictive power of CONUT, NRI, PNI, and CPNI in HCC patients showed that CPNI was the most accurate in predicting OS compared to the other nutritional indices (Figure 3A). Additionally, CPNI demonstrated marginally higher accuracy in predicting RFS compared to PNI, and was clearly superior to both CONUT and NRI (Figure 3B). Detailed information,

Table 1. Baseline table of patients' characteristics

Characteristic	Overall (*n* = 1,450)	Female (*n* = 219)	Male (*n* = 1,231)	*P* value
Age, years, median (IQR)	53.0 [46.0;62.0]	54.0 [45.0;63.0]	53.0 [46.0;62.0]	0.713
Height, cm, median (IQR)	165 [160;170]	156 [152;160]	167 [163;170]	< 0.001
Weight, kg, median (IQR)	63.0 [56.0;70.0]	56.0 [50.0;61.2]	65.0 [58.0;71.0]	< 0.001
BMI, kg/m^2, median (IQR)	23.0 [20.9;25.3]	22.6 [20.7;25.2]	23.1 [21.0;25.3]	0.159
BMI group, *n* (%)				0.216
Normal weight	806 (55.6)	121 (55.3)	685 (55.6)	
Obesity	114 (7.86)	18 (8.22)	96 (7.80)	
Overweight	446 (30.8)	61 (27.9)	385 (31.3)	
Underweight	84 (5.79)	19 (8.68)	65 (5.28)	
HBV, yes, *n* (%)	1194 (82.3)	183 (83.6)	1011 (82.1)	0.677
HCV, yes, *n* (%)	24 (1.66)	6 (2.74)	18 (1.46)	0.243
AFP, ng/mL, *n* (%)				0.496
< 400	1,224 (84.4)	181 (82.6)	1,043 (84.7)	
≥ 400	226 (15.6)	38 (17.4)	188 (15.3)	
Hemoglobin, g/L, median (IQR)	144 [132;155]	128 [118;136]	147 [136;157]	< 0.001
Platelets, 10^9/L, median (IQR)	130 [93.0;179]	121 [86.0;181]	131 [94.0;179]	0.224
WBC, 10^9/L, median (IQR)	5.24 [4.23;6.55]	4.31 [3.54;5.68]	5.38 [4.41;6.65]	< 0.001
NE, 10^9/L, median (IQR)	3.08 [2.33;4.05]	2.53 [1.99;3.62]	3.14 [2.42;4.13]	< 0.001
LY, 10^9/L, median (IQR)	1.45 [1.15;1.85]	1.31 [1.06;1.61]	1.49 [1.17;1.88]	< 0.001
ALT, U/L, median (IQR)	35.0 [24.0;52.0]	26.0 [19.0;37.0]	37.0 [25.0;53.0]	< 0.001
AST, U/L, median (IQR)	35.0 [27.0;50.0]	35.0 [26.0;49.0]	36.0 [27.0;50.0]	0.313
Cholesterol, mmol/L, median (IQR)	4.02 [3.50;4.61]	4.04 [3.54;4.56]	4.00 [3.49;4.61]	0.581
Prothrombin time, s, median (IQR)	12.0 [11.4;12.7]	12.0 [11.4;12.8]	12.0 [11.4;12.7]	0.733
Tbil, μmol/L, median (IQR)	13.7 [10.5;17.9]	13.5 [10.1;17.1]	13.7 [10.6;18.2]	0.187
Total protein, g/L, median (IQR)	70.4 [66.6;74.1]	71.6 [68.5;75.8]	70.2 [66.4;73.8]	< 0.001
Albumin, g/L, median (IQR)	42.5 [39.9;45.1]	42.6 [39.8;45.5]	42.5 [39.9;45.0]	0.663
Triglyceride, mmol/L, median (IQR)	0.94 [0.72;1.28]	0.92 [0.69;1.29]	0.94 [0.72;1.27]	0.433
HDL, mmol/L, median (IQR)	1.20 [0.98;1.47]	1.40 [1.15;1.69]	1.17 [0.96;1.42]	< 0.001
LDL, mmol/L, median (IQR)	2.30 [1.88;2.80]	2.21 [1.83;2.60]	2.33 [1.89;2.83]	0.006
ALBI grade, *n* (%)				0.855
1	1,142 (78.8)	174 (79.5)	968 (78.6)	
2	308 (21.2)	45 (20.5)	263 (21.4)	
Tumor diameter, cm, *n* (%)				1.000
< 5	731 (50.4)	110 (50.2)	621 (50.4)	
≥ 5	719 (49.6)	109 (49.8)	610 (49.6)	
Number of tumors, *n* (%)				0.411
multiple	229 (15.8)	30 (13.7)	199 (16.2)	
single	1,221 (84.2)	189 (86.3)	1,032 (83.8)	
BCLC stage, *n* (%)				0.067
0	146 (10.1)	17 (7.76)	129 (10.5)	
A	1,132 (78.1)	184 (84.0)	948 (77.0)	
B	172 (11.9)	18 (8.22)	154 (12.5)	
Hypertension, yes, *n* (%)	231 (15.9)	36 (16.4)	195 (15.8)	0.903
Diabetes, yes, *n* (%)	122 (8.41)	17 (7.76)	105 (8.53)	0.807
Cardiovascular disease, yes, *n* (%)	26 (1.79)	5 (2.28)	21 (1.71)	0.578
Anatomical resection, yes, *n* (%)	494 (34.1)	68 (31.1)	426 (34.6)	0.344
Major hepatectomy, yes, *n* (%)	190 (13.1)	23 (10.5)	167 (13.6)	0.259
Transfusion, yes, *n* (%)	71 (4.90)	12 (5.48)	59 (4.79)	0.792
Differentiation, *n* (%)				0.455
I-II	818 (56.4)	118 (53.9)	700 (56.9)	
III-IV	632 (43.6)	101 (46.1)	531 (43.1)	
Microsatellites, yes, *n* (%)	106 (7.31)	8 (3.65)	98 (7.96)	0.034
Microvascular invasion, yes, *n* (%)	389 (26.8)	51 (23.3)	338 (27.5)	0.230
Cirrhosis, yes, *n* (%)	750 (51.7)	120 (54.8)	630 (51.2)	0.361
CONUT, *n* (%)				0.004
Malnutrition	911 (62.8)	157 (71.7)	754 (61.3)	
No malnutrition	539 (37.2)	62 (28.3)	477 (38.7)	
NRI, *n* (%)				0.281
Malnutrition	308 (21.2)	40 (18.3)	268 (21.8)	
No malnutrition	1,142 (78.8)	179 (81.7)	963 (78.2)	
PNI, *n* (%)				0.333
Malnutrition	721 (49.7)	116 (53.0)	605 (49.1)	
No malnutrition	729 (50.3)	103 (47.0)	626 (50.9)	
CPNI, *n* (%)				0.066
Malnutrition	695 (47.9)	118 (53.9)	577 (46.9)	
No malnutrition	755 (52.1)	101 (46.1)	654 (53.1)	

BMI, body mass index; HBV, hepatitis B virus; HCV, hepatitis C virus; AFP, a-fetoprotein; WBC, white blood cells; NE, neutrophil; LY, lymphocyte; ALT, glutamate aminotransferase; AST, aspartate aminotransferase; Tbil, total bilirubin; HDL, high-density lipoprotein; LDL, low-density lipoprotein; BCLC, Barcelona Clinic Liver Cancer; CONUT, Controlling Nutritional Status score; NRI, Nutritional Risk Index; PNI, Prognostic Nutritional Index; CPNI, Cholesterol-modified Prognostic Nutritional Index.

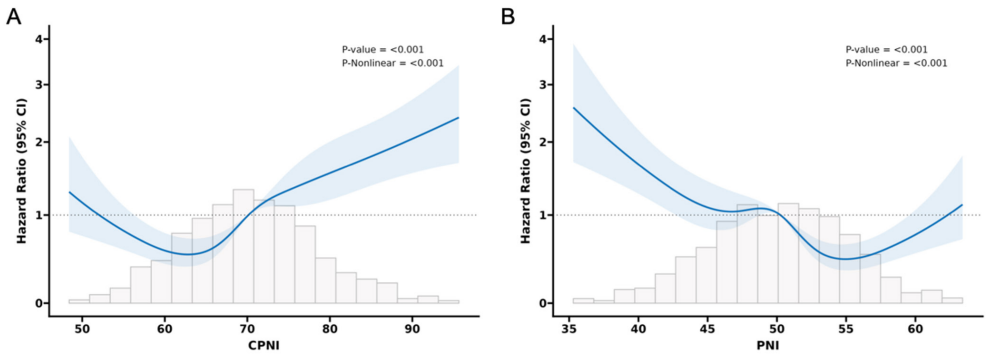

Figure 1. RCS analysis using the Cox proportional hazards model to explore the nonlinear relationship between nutritional indices (CPNI and PNI) and OS. RCS, restricted cubic spline; CPNI, Cholesterol-modified Prognostic Nutritional Index, PNI, Prognostic Nutritional Index; OS, overall survival.

including the 1-year, 3-year, and 5-year area under the curve (AUC) values for each nutritional indicator for both OS and RFS, was presented in Table 2.

The Kaplan-Meier method was employed to explore the relationship between malnutrition, as determined by various nutritional indices, and OS and RFS. Meanwhile, all subgroup analyses predicting OS and RFS based on different nutritional indicators were respectively presented in Supplementary Figures S10 and S11 (*https://www.biosciencetrends.com/supplementaldata/206*). According to the CPNI diagnostic criteria, survival curves for OS demonstrated that malnourished patients had lower survival rates across the overall cohort and within specific subgroups such as males and females, and patients classified as underweight, normal weight, and overweight, as well as those categorized as BCLC stage A and B (Figure 4). Similarly, survival curves for RFS revealed that malnourished patients had higher recurrence rates among the overall patient cohort, males, and patients of normal weight, overweight, underweight, and those classified as BCLC stage A and B (Figure 5).

Under the CONUT diagnostic criteria, survival curve comparisons predicting OS revealed no significant differences across several groups, including overall HCC patients, as well as subgroups such as males and females, patients categorized as underweight, of normal weight, overweight, or obese, and those classified in the BCLC stages 0, A, and B (Supplemental Figure S4, *https://www.biosciencetrends.com/supplementaldata/206*). However, survival curves predicting RFS indicated that malnourished patients had higher recurrence rates among female patients (Supplemental Figure S7C, *https://www.biosciencetrends.com/supplementaldata/206*).

Under the NRI diagnostic criteria, survival curves predicting OS showed that malnourished patients had lower survival rates across several groups, including the overall patient cohort and specific subgroups such as males, females, those of normal weight, and patients classified in BCLC stages A and B (Supplemental

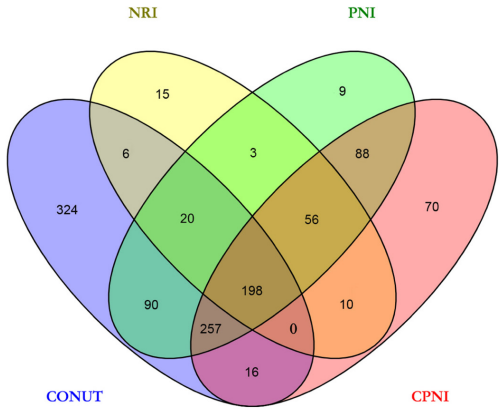

Figure 2. Venn diagram for malnutrition diagnosis criteria: overlapping patient counts. CONUT, Controlling Nutritional Status score; CPNI, Cholesterol-modified Prognostic Nutritional Index. NRI, Nutritional Risk Index; PNI, Prognostic Nutritional Index.

Figure S5, *https://www.biosciencetrends.com/supplementaldata/206*). Additionally, survival curves predicting recurrence-free survival (RFS) revealed that malnourished patients had higher recurrence rates in the overall patient cohort, among males, patients of normal weight, and those classified as BCLC stage A (Supplemental Figure S8, *https://www.biosciencetrends.com/supplementaldata/206*).

Under the PNI diagnostic criteria, survival curves predicting OS showed that malnourished patients exhibited lower survival rates in the overall cohort, as well as within specific subgroups including male and female patients, those classified as underweight, normal weight, overweight, and categorized as BCLC stage A (Supplemental Figure S6, *https://www.biosciencetrends.com/supplementaldata/206*). Furthermore, survival curves predicting RFS revealed that malnourished patients had higher recurrence rates in the overall patient cohort, among males, females, patients of normal weight, overweight, and those classified as BCLC stages 0 and A (Supplemental Figure S9, *https://www.biosciencetrends.com/supplementaldata/206*).

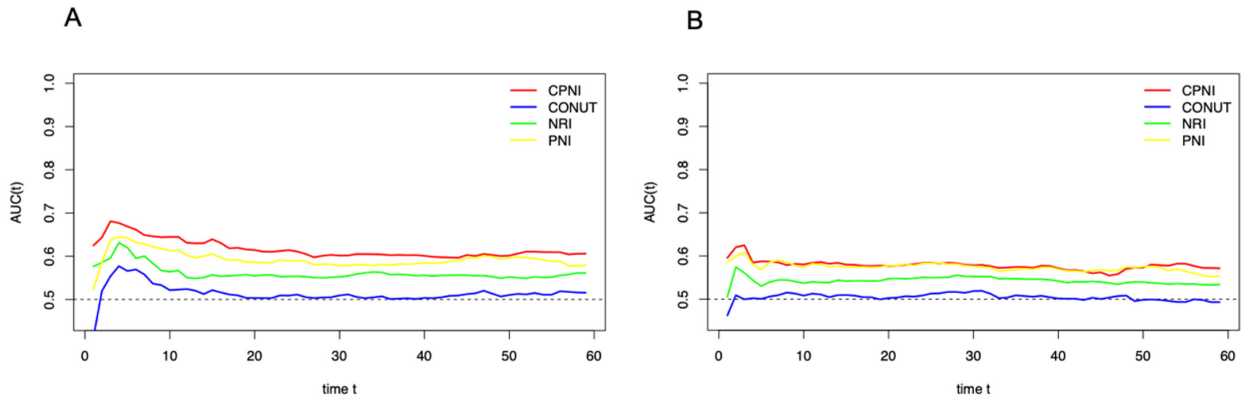

Figure 3. The time-dependent ROC of different nutritional indices predicting (A) OS and (B) RFS in patients with HCC. OS, overall survival; RFS, Recurrence-free survival; CONUT, Controlling Nutritional Status score; CPNI, Cholesterol-modified Prognostic Nutritional Index. NRI, Nutritional Risk Index; PNI, Prognostic Nutritional Index.

Table 2. The AUCs of nutrition indicators for OS and RFS in patients with HCC

Indicators	OS			RFS		
	1-year AUC	3-year AUC	5-year AUC	1-year AUC	3-year AUC	5-year AUC
CONUT	0.524	0.501	0.512	0.511	0.507	0.494
NRI	0.551	0.557	0.563	0.539	0.547	0.537
PNI	0.602	0.579	0.583	0.580	0.571	0.556
CPNI	0.631	0.602	0.612	0.586	0.575	0.573

AUC, area under the curve; OS, overall survival; HCC, hepatocellular carcinoma; RFS, Recurrence-free survival; CONUT, Controlling Nutritional Status score; NRI, Nutritional Risk Index; PNI, Prognostic Nutritional Index; CPNI, Cholesterol-modified Prognostic Nutritional Index.

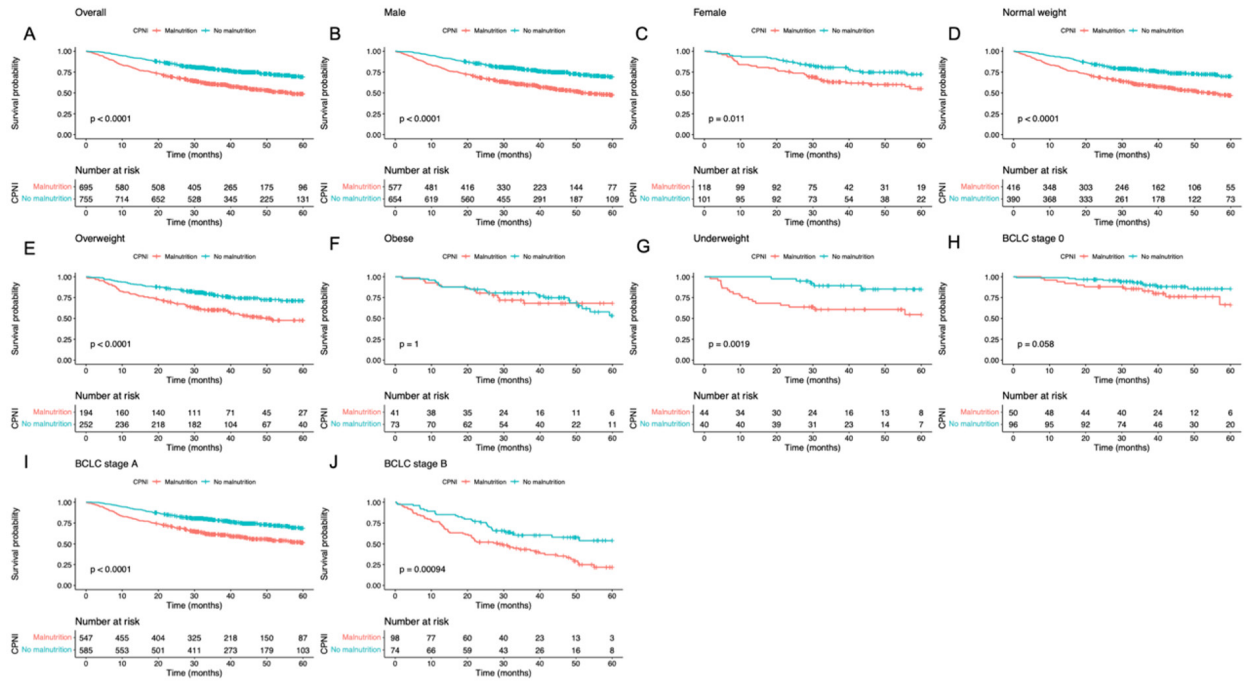

Figure 4. Kaplan-Meier analysis of OS in HCC patients classified by CPNI criteria into malnourished and non-malnourished groups across all populations and subgroups.

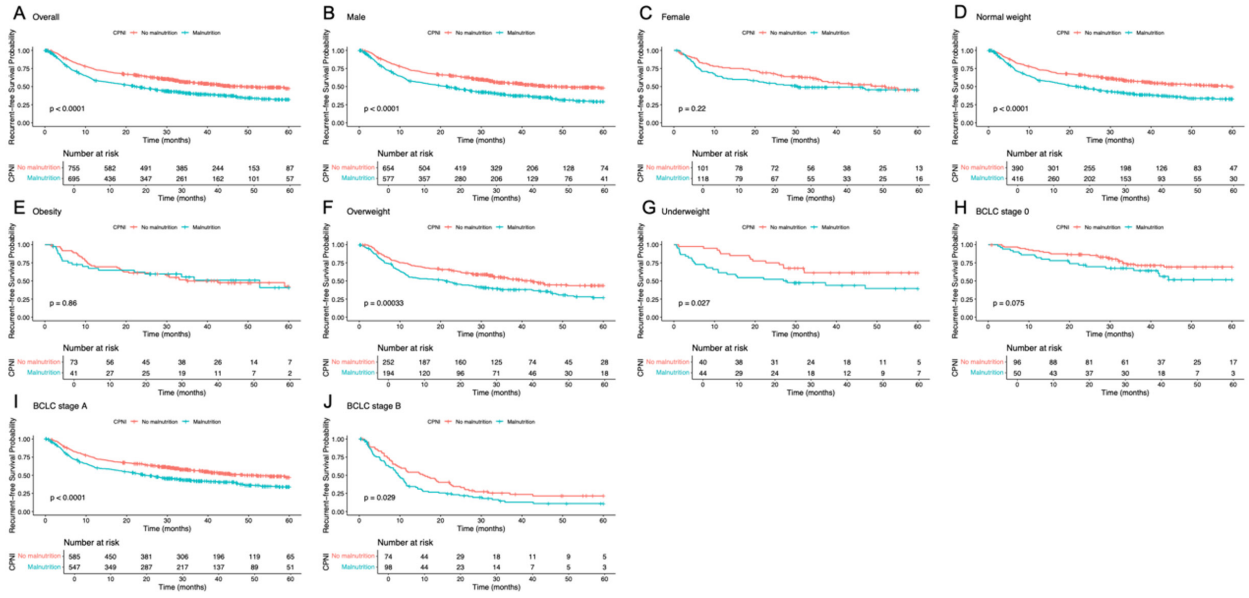

Figure 5. Kaplan-Meier analysis of RFS in HCC patients classified by CPNI criteria into malnourished and non-malnourished groups across all populations and subgroups.

3.4. Association of CPNI with clinicopathological factors in HCC patients

Among 1,450 HCC patients, 695 (47.9%) were classified as malnourished and 755 (52.1%) were not malnourished. The baseline clinicopathological characteristics of both groups are presented in Table 3. Malnutrition, as identified by the CPNI criteria, was significantly related to several clinical and pathological features: increased age, lower BMI, a higher prevalence of underweight, and reduced hemoglobin levels. Additional associations include decreased white blood cell count, neutrophil count, total bilirubin and triglyceride, as well as increased aspartate aminotransferase, prolonged prothrombin time, high-density lipoprotein and low-density lipoprotein. Malnourished patients also frequently exhibited worse liver function, larger tumor diameters, higher BCLC stages, and higher rates of major hepatectomy, and transfusion requirements. Poor tumor differentiation, microsatellites, microvascular invasion, and cirrhosis were also more common in this group.

3.5. Univariate and multivariate cox regression analyses of nutritional Indices for OS and RFS

Univariate and multivariate analyses with Cox proportional hazards model showed that CONUT scores were not significantly correlated with OS or RFS in HCC patients, as depicted in Table 4. Under the NRI criteria, univariate analysis showed a significant association between malnutrition and both OS and RFS; however, this association was not maintained in the multivariate analysis. In contrast, both PNI and CPNI were identified as independent prognostic factors in both univariate and multivariate analyses. Detailed results from these analyses for each nutritional indicator are presented separately in Supplemental Tables S1-S4 (*https://www.biosciencetrends.com/supplementaldata/206*).

Multivariable analysis for OS was adjusted by age, HBsAg, AFP, PLT, WBC, NE, ALT, AST, PT, HDL, LDL, ALBI Grade, BCLC stage, hypertension, major hepatectomy, transfusion, Differentiation, Microsatellites, MVI; Multivariable analysis for RFS was adjusted by age, HBsAg, AFP, HB, PLT, WBC, NE, ALT, AST, PT, TP, ALBI Grade, BCLC stage, hypertension, major hepatectomy, transfusion, Differentiation, Microsatellites, MVI.

4. Discussion

To our knowledge, this is the first study to explore the association between CPNI and prognosis of HCC patients undergoing liver resection. In this study, we assessed the capability of the CPNI to evaluate nutritional status and predict survival in HCC patients undergoing liver resection. Univariate and multivariate Cox regression analyses revealed that the CPNI was an independent predictor of both OS and RFS in HCC patients after liver resection. Under CPNI criteria, malnutrition was significantly associated with a range of adverse conditions including underweight, deteriorated liver function, larger tumor diameters, advanced BCLC stages, increased occurrences of major hepatectomy, and higher transfusion requirements. Additionally, malnourished patients exhibited poor tumor differentiation, the presence of microsatellites, microvascular invasion, and cirrhosis. Time-dependent ROC curves used to assess predictive accuracy over time showed that CPNI had superior prognostic performance

Table 3. Comparison of clinicopathological factors between malnourished and non-malnourished patients stratified by CPNI

Characteristics	No malnutrition *n* =755	Malnutrition *n* = 695	*P* value
Sex, male, *n* (%)	654 (86.6)	577 (83.0)	0.066
Age, years, median (IQR)	52.0 [45.0;61.0]	55.0 [47.0;64.0]	< 0.001
BMI, kg/m^2, median (IQR)	23.4 [21.3;25.7]	22.6 [20.7;24.8]	< 0.001
BMI group, n (%)			0.002
Normal weight	390 (51.7)	416 (59.9)	
Obesity	73 (9.67)	41 (5.90)	
Overweight	252 (33.4)	194 (27.9)	
Underweight	40 (5.30)	44 (6.33)	
HBsAg, positive, *n* (%)	617 (81.7)	577 (83.0)	0.562
HCV, positive, *n* (%)	15 (1.99)	9 (1.29)	0.409
AFP, ≥ 400ng/mL, *n* (%)	109 (14.4)	117 (16.8)	0.236
Hemoglobin, g/L, median (IQR)	148 [137;158]	139 [128;151]	< 0.001
Platelets, 10^9/L, median (IQR)	132 [99.0;174]	129 [89.0;184]	0.442
WBC, 10^9/L, median (IQR)	5.57 [4.60;6.82]	4.89 [3.97;6.10]	< 0.001
NE, 10^9/L, median (IQR)	3.19 [2.43;4.10]	2.91 [2.22;3.95]	0.001
LY, 10^9/L, median (IQR)	1.67 [1.31;2.10]	1.29 [1.00;1.59]	< 0.001
Cholesterol, mmol/L, median (IQR)	3.85 [3.40;4.36]	4.22 [3.64;4.83]	< 0.001
Albumin, g/L, median (IQR)	44.7 [42.7;46.8]	40.0 [37.7;42.1]	< 0.001
ALT, U/L, median (IQR)	34.0 [24.0;50.0]	35.0 [24.0;53.0]	0.410
AST, U/L, median (IQR)	33.0 [26.0;43.0]	40.0 [28.0;56.0]	< 0.001
Prothrombin time, s, median (IQR)	11.9 [11.3;12.6]	12.2 [11.5;12.9]	< 0.001
Tbil, μmol/L, median (IQR)	14.0 [10.8;18.0]	13.3 [10.1;17.9]	0.035
Total protein, g/L, median (IQR)	72.1 [68.8;75.8]	68.2 [64.8;71.7]	< 0.001
Triglyceride, mmol/L, median (IQR)	0.97 [0.74;1.33]	0.91 [0.70;1.21]	0.007
HDL, mmol/L, median (IQR)	1.18 [0.96;1.42]	1.22 [1.00;1.52]	0.011
LDL, mmol/L, median (IQR)	2.21 [1.82;2.66]	2.40 [2.00;2.99]	< 0.001
ALBI grade, 2, *n* (%)	26 (3.44)	282 (40.6)	< 0.001
Tumor diameter, ≥ 5cm, *n* (%)	307 (40.7)	412 (59.3)	< 0.001
Number of tumors, multiple, *n* (%)	110 (14.6)	119 (17.1)	0.208
BCLC stage, *n* (%)			< 0.001
0	96 (12.7)	50 (7.19)	
A	585 (77.5)	547 (78.7)	
B	74 (9.80)	98 (14.1)	
Hypertension, yes, *n* (%)	140 (18.5)	91 (13.1)	0.006
Diabetes, yes, *n* (%)	66 (8.74)	56 (8.06)	0.708
Cardiovascular disease, yes, *n* (%)	16 (2.12)	10 (1.44)	0.437
Anatomical resection, yes, *n* (%)	247 (32.7)	247 (35.5)	0.281
Major hepatectomy, yes, *n* (%)	79 (10.5)	111 (16.0)	0.002
Transfusion, yes, *n* (%)	22 (2.91)	49 (7.05)	< 0.001
Differentiation, III-IV, *n* (%)	310 (41.1)	322 (46.3)	0.049
Microsatellites, yes, *n* (%)	45 (5.96)	61 (8.78)	0.050
Microvascular invasion, yes, *n* (%)	182 (24.1)	207 (29.8)	0.017
Cirrhosis, yes, *n* (%)	370 (49.0)	380 (54.7)	0.035

CPNI, Cholesterol-modified Prognostic Nutritional Index.

Table 4. Univariate and multivariate analyses with Cox proportional hazards in the entire population

	OS				RFS			
	Univariable analysis		Multivariable analysis		Univariable analysis		Multivariable analysis	
	HR (95% CI)	*p*	HR (95% CI)	*p*	HR (95% CI)	*p*	HR (95% CI)	*p*
CONUT	1.06 (0.88-1.27)	0.522	1.15 (0.93-1.43)	0.202	1.02 (0.88-1.17)	0.756	1.00 (0.86-1.19)	0.913
NRI	1.74 (1.44-2.11)	< 0.001	1.12 (0.88-1.43)	0.345	1.50 (1.27-1.76)	< 0.001	1.08 (0.88-1.32)	0.481
PNI	1.81 (1.51-2.16)	< 0.001	1.48 (1.19-1.83)	< 0.001	1.54 (1.34-1.78)	< 0.001	1.43 (1.19-1.71)	< 0.001
CPNI	2.08 (1.73-2.49)	< 0.001	1.77 (1.43-2.18)	< 0.001	1.60 (1.38-1.84)	< 0.001	1.50 (1.26-1.77)	< 0.001

OS, overall survival; RFS, Recurrence-free survival; CONUT, Controlling Nutritional Status score; NRI, Nutritional Risk Index; PNI, Prognostic Nutritional Index; CPNI, Cholesterol-modified Prognostic Nutritional Index.

for OS compared to other nutritional indices such as CONUT, NRI, and PNI. Additionally, CPNI showed marginally higher accuracy in predicting RFS than PNI and significantly outperformed both CONUT and NRI. Subgroup analyses indicated that malnutrition, as identified by CPNI criteria, was associated with a lower

OS rate across various groups. This included males and females, and those categorized as underweight, normal weight, and overweight, as well as patients classified in BCLC stages A and B. Similarly, the analyses showed a higher recurrence rate associated with malnutrition in similar groups, including males, those classified as underweight, normal weight, or overweight, and patients categorized in BCLC stages A and B.

Malnutrition was prevalent in HCC patients who underwent liver resection, with rates ranging from 21.2% to 62.8% according to four different nutritional assessment tools. Consistent with previous studies, malnutrition represents a significant burden that is frequently underdiagnosed in patients with HCC undergoing liver resection (*4*). BMI is a widely used, clinically available objective variable for assessing malnutrition (*21,22*). However, BMI has become less universally applicable as newer nutritional assessment indices, which identify malnutrition more effectively, provide a more comprehensive evaluation of health (*23-25*). As BMI increases, the incidence of malnutrition decreases. Consistent with previous studies, this study also found a high proportion of malnutrition among overweight and obese patients(*26-28*). Malnourished patients who are overweight, normal weight and underweight faced poorer OS and RFS. Nevertheless, no significant differences in survival rates and recurrence rates were observed among the obese subgroups.

CPNI, as a newly proposed tool for malnutrition assessment, has shown more accurate and stable capabilities in assessing the nutritional status of patients than several objective malnutrition assessment indices. Owing to its objectivity calculated from regular blood test indicators and non-invasiveness, CPNI has shown greater potential to assess the nutritional status of preoperative HCC patients and predict their prognosis. The predictive value of CPNI for patient prognosis may be explained by the incorporation of key factors such as serum cholesterol, lymphocyte counts, and serum albumin. High cholesterol levels may increase cancer risk, intensify tumor aggressiveness, and worsen patient outcomes (*29-32*). Albumin is the most thoroughly investigated protein in the context of malnutrition diagnosis (*33*). Furthermore, albumin serves as an important predictor for HCC outcomes and is shown to inhibit HCC cell proliferation (*34,35*). Lower lymphocyte levels are associated with poor prognosis in solid tumors, highlighting the vital role of the immune response in HCC outcomes (*36*).

However, this study has some limitations. First, it was a retrospective single-center study, and the findings need to be confirmed through randomized controlled trials or large-cohort studies. Second, the predominance of hepatitis B in the patient sample may not represent regions such as Europe or the United States. Third, additional studies are essential to clarify the influence of CPNI in particularly smaller patient subgroups, such as those with BCLC stage 0 and those who are obese.

In conclusion, this study suggests that CPNI is a precise and stable instrument for evaluating nutritional status and forecasting survival in HCC patients who underwent liver resection, potentially offering advantages over other indicators such as CONUT, NRI, and PNI, and thus could improve clinical decision-making.

Funding: This work was supported by grants from the National Natural Science Foundation of China (Nos. 81770566, 82000599), NHC Key Laboratory of Echinococcosis Prevention and Control (No. 2021WZK1004) and Health Commission of the Tibet Autonomous Region (No.311220432).

Conflict of Interest: The authors have no conflicts of interest to disclose.

References

1. Elia M, Zellipour L, Stratton RJ. To screen or not to screen for adult malnutrition? Clin Nutr. 2005; 24:867-884.
2. Schütte K, Tippelt B, Schulz C, Röhl FW, Feneberg A, Seidensticker R, Arend J, Malfertheiner P.. Malnutrition is a prognostic factor in patients with hepatocellular carcinoma (HCC). Clin Nutr. 2015; 34:1122-1127.
3. Arends J. Struggling with nutrition in patients with advanced cancer: nutrition and nourishment-focusing on metabolism and supportive care. Ann Oncol. 2018; 29(suppl_2):ii27-ii34.
4. EASL Clinical Practice Guidelines on nutrition in chronic liver disease. J Hepatol. 2019; 70:172-193.
5. Hepatocellular carcinoma. Nat Rev Dis Primers. 2021; 7:7.
6. Lee KF, Chong CCN, Fong AKW, Fung AKY, Lok HT, Cheung YS, Wong J, Lai PBS. Pattern of disease recurrence and its implications for postoperative surveillance after curative hepatectomy for hepatocellular carcinoma: experience from a single center. Hepatobiliary Surg Nutr. 2018; 7:320-330.
7. Schütte K, Kipper M, Kahl S, Bornschein J, Götze T, Adolf D, Arend J, Seidensticker R, Lippert H, Ricke J, Malfertheiner P. Clinical characteristics and time trends in etiology of hepatocellular cancer in Germany. Digestion. 2013; 87:147-159.
8. Ignacio de Ulíbarri J, González-Madroño A, de Villar NG, González P, González B, Mancha A, Rodríguez F, Fernández G. CONUT: A tool for controlling nutritional status. First validation in a hospital population. Nutr Hosp. 2005; 20:38-45.
9. Harimoto N, Yoshizumi T, Inokuchi S, *et al.* Prognostic Significance of Preoperative Controlling Nutritional Status (CONUT) Score in Patients Undergoing Hepatic Resection for Hepatocellular Carcinoma: A Multi-institutional Study. Ann Surg Oncol. 2018; 25:3316-3323.
10. Tokunaga R, Sakamoto Y, Nakagawa S, Ohuchi M, Izumi D, Kosumi K, Taki K, Higashi T, Miyamoto Y, Yoshida N, Oki E, Watanabe M, Baba H. CONUT: A novel independent predictive score for colorectal cancer patients undergoing potentially curative resection. Int J Colorectal Dis. 2017; 32:99-106.
11. Zhang Y, Zhang X. Controlling nutritional status score, a promising prognostic marker in patients with

gastrointestinal cancers after surgery: A systematic review and meta-analysis. Int J Surg. 2018; 55:39-45.
12. Toyokawa G, Kozuma Y, Matsubara T, Haratake N, Takamori S, Akamine T, Takada K, Katsura M, Shimokawa M, Shoji F, Okamoto T, Maehara Y. Prognostic impact of controlling nutritional status score in resected lung squamous cell carcinoma. J Thorac Dis. 2017; 9:2942-2951.
13. Qian W, Xiao-Jian J, Jun H, Liang L, Xiao-Yong C. Comparison of the Value of Multiple Preoperative Objective Nutritional Indices for the Evaluation of Prognosis after Hepatectomy for Hepatocellular Carcinoma. Nutr Cancer. 2022; 74:3217-3227.
14. Bo Y, Yao M, Zhang L, Bekalo W, Lu W, Lu Q. Preoperative Nutritional Risk Index to predict postoperative survival time in primary liver cancer patients. Asia Pac J Clin Nutr. 2015; 24:591-597.
15. Imai D, Maeda T, Shimokawa M, Wang H, Yoshiya S, Takeishi K, Itoh S, Harada N, Ikegami T, Yoshizumi T, Mori M. Prognostic nutritional index is superior as a predictor of prognosis among various inflammation-based prognostic scores in patients with hepatocellular carcinoma after curative resection. Hepatol Res. 2020; 50:101-109.
16. Saito Y, Imura S, Morine Y, Ikemoto T, Yamada S, Shimada M. Preoperative prognostic nutritional index predicts short- and long-term outcomes after liver resection in patients with hepatocellular carcinoma. Oncol Lett. 2021; 21:153.
17. Sim JH, Kim SH, Jun IG, Kang SJ, Kim B, Kim S, Song JG. The Association between Prognostic Nutritional Index (PNI) and Intraoperative Transfusion in Patients Undergoing Hepatectomy for Hepatocellular Carcinoma: A Retrospective Cohort Study. Cancers (Basel). 2021; 13:2508.
18. Wang D, Hu X, Xiao L, Long G, Yao L, Wang Z, Zhou L. Prognostic Nutritional Index and Systemic Immune-Inflammation Index Predict the Prognosis of Patients with HCC. J Gastrointest Surg. 2021; 25:421-427.
19. Shi J, Liu T, Ge Y, *et al*. Cholesterol-modified prognostic nutritional index (CPNI) as an effective tool for assessing the nutrition status and predicting survival in patients with breast cancer. BMC Med. 2023; 21:512.
20. Raposeiras Roubín S, Abu Assi E, Cespón Fernandez M, *et al*. Prevalence and Prognostic Significance of Malnutrition in Patients With Acute Coronary Syndrome. J Am Coll Cardiol. 2020; 76:828-840.
21. Cederholm T, Bosaeus I, Barazzoni R, Bauer J, Van Gossum A, Klek S, Muscaritoli M, Nyulasi I, Ockenga J, Schneider SM, de van der Schueren MA, Singer P. Diagnostic criteria for malnutrition - An ESPEN Consensus Statement. Clin Nutr. 2015; 34:335-340.
22. Burman M, Säätelä S, Carlsson M, Olofsson B, Gustafson Y, Hörnsten C. Body mass index, Mini Nutritional Assessment, and their association with five-year mortality in very old people. J Nutr Health Aging. 2015; 19:461-467.
23. Mokaddem F. BMI and FFMI do not seem universally applicable in nutritional assessment and the usefulness of SGA and functional evaluation should not be overlooked. Clin Nutr. 2016; 35:236.
24. Tan S, Jiang J, Qiu L, Liang Y, Meng J, Tan N, Xiang B. Prevalence of Malnutrition in Patients with Hepatocellular Carcinoma: A Comparative Study of GLIM Criteria, NRS2002, and PG-SGA, and Identification of Independent Risk Factors. Nutr Cancer. 2024; 76:335-344.
25. Bell JJ, Pulle RC, Lee HB, Ferrier R, Crouch A, Whitehouse SL. Diagnosis of overweight or obese malnutrition spells DOOM for hip fracture patients: A prospective audit. Clin Nutr. 2021; 40:1905-1910.
26. Leibovitz E, Giryes S, Makhline R, Zikri Ditch M, Berlovitz Y, Boaz M. Malnutrition risk in newly hospitalized overweight and obese individuals: Mr NOI. Eur J Clin Nutr. 2013; 67:620-624.
27. Sharma K, Mogensen KM, Robinson MK. Under-Recognizing Malnutrition in Hospitalized Obese Populations: The Real Paradox. Curr Nutr Rep. 2019; 8:317-322.
28. Freeman AM, Aggarwal M. Malnutrition in the Obese: Commonly Overlooked But With Serious Consequences. J Am Coll Cardiol. 2020; 76:841-843.
29. Brindisi M, Fiorillo M, Frattaruolo L, Sotgia F, Lisanti MP, Cappello AR. Cholesterol and Mevalonate: Two Metabolites Involved in Breast Cancer Progression and Drug Resistance through the ERRα Pathway. Cells. 2020; 9:1819.
30. Ruan GT, Xie HL, Hu CL, *et al*. Comprehensive prognostic effects of systemic inflammation and Insulin resistance in women with breast cancer with different BMI: a prospective multicenter cohort. Sci Rep. 2023; 13:4303.
31. Che L, Chi W, Qiao Y, *et al*. Cholesterol biosynthesis supports the growth of hepatocarcinoma lesions depleted of fatty acid synthase in mice and humans. Gut. 2020; 69:177-186.
32. He M, Zhang W, Dong Y, Wang L, Fang T, Tang W, Lv B, Chen G, Yang B, Huang P, Xia J. Pro-inflammation NF-κB signaling triggers a positive feedback *via* enhancing cholesterol accumulation in liver cancer cells. J Exp Clin Cancer Res. 2017; 36:15.
33. Zhang Z, Pereira SL, Luo M, Matheson EM. Evaluation of Blood Biomarkers Associated with Risk of Malnutrition in Older Adults: A Systematic Review and Meta-Analysis. Nutrients. 2017; 9:829.
34. Fu X, Yang Y, Zhang D. Molecular mechanism of albumin in suppressing invasion and metastasis of hepatocellular carcinoma. Liver Int. 2022; 42:696-709.
35. Nojiri S, Joh T. Albumin suppresses human hepatocellular carcinoma proliferation and the cell cycle. Int J Mol Sci. 2014; 15:5163-5174.
36. Tan CS, Read JA, Phan VH, Beale PJ, Peat JK, Clarke SJ. The relationship between nutritional status, inflammatory markers and survival in patients with advanced cancer: a prospective cohort study. Support Care Cancer. 2015; 23:385-391.

Received April 30, 2024; Revised June 27, 2024; Accepted July 23, 2024.

**Address correspondence to:*
Wentao Wang, Department of Liver Surgery, West China Hospital, Sichuan University, Chengdu, Sichuan, China.
E-mail: wwtdoctor02@163.com

Released online in J-STAGE as advance publication Julr 27, 2024.

Correspondence

DOI: 10.5582/bst.2024.01235

Potential value and advances in research on bone mineral density (BMD) measurement in the auxiliary clinical assessment of hepatocellular carcinoma

Xudong Zhang[1,2], Lu Chen[2,3], Peipei Song[2], Chunfu Zhu[1], Liming Tang[1,*]

[1] Changzhou Medical Center, The Affiliated Changzhou No. 2 People's Hospital of Nanjing Medical University, Changzhou, Jiangsu, China;
[2] National Center for Global Health and Medicine, Tokyo, Japan;
[3] Department of Hepatobiliary Cancer, Liver cancer research center, Tianjin Medical University Cancer Institute and Hospital, National Clinical Research Center for Cancer, National Key Laboratory of Druggability Evaluation and Systematic Translational Medicine, Tianjin Key Laboratory of Digestive Cancer, Tianjin's Clinical Research Center for Cancer, Tianjin, China.

SUMMARY Hepatocellular carcinoma (HCC) is the fourth leading cause of cancer death worldwide and its prognosis is highly heterogeneous, being related not only to underlying chronic liver disease but also to the severity of cancer cachexia. Nutritional factors play a crucial role in influencing the prognosis of HCC. Despite musculoskeletal imbalance being consistently reported as a predictor of perioperative mortality in patients with HCC, this condition is often overlooked in clinical management. Bone mineral density (BMD), which serves as a marker of nutritional status, can be assessed through CT by measuring the pixel density of the vertebral bone. Recent clinical studies have indicated that BMD serves not only as a significant risk factor for development of HCC in cirrhotic patients but also potentially functions as an independent prognostic indicator for post-treatment outcomes in patients with HCC. Preoperative abdominal CT scans provide a convenient and cost-effective method to measure BMD, offering significant assistance in prognostic evaluation of patients with HCC. A thorough grasp of the liver-bone connection, along with the conduct of higher-quality studies and the establishment of standardized methods and cutoff values for BMD measurement, could enhance approaches to manage HCC.

Keywords hepatocellular carcinoma (HCC), bone mineral density, osteopenia, prognosis, liver-bone axis

1. Introduction

Liver cancer is recognized as the second most common cancer worldwide and constitutes the fourth leading cause of cancer-related deaths. According to estimates, there are between 500,000 and 1,000,000 new cases annually, resulting in approximately 600,000 fatalities, with hepatocellular carcinoma (HCC) being the primary type (*1*). The majority of HCC cases arise in the context of chronic liver diseases, notably viral hepatitis, non-alcoholic fatty liver disease (NAFLD), and cirrhosis. Despite advances in screening and therapeutic interventions, the prognosis for liver cancer remains unfavorable due to its aggressive nature and the high incidence of cancer cachexia (*2*). The overall health status of patients with HCC, encompassing their nutritional status, performance status, and the presence of systemic complications, are significantly correlated with their prognosis (*3,4*).

Over the past few years, the investigation of bone mineral density (BMD) has gained considerable prominence within the context of liver diseases, and particularly HCC. The relationship between liver cirrhosis, which often precedes HCC, and the subsequent development of cancer cachexia is closely associated with musculoskeletal nutritional status, encompassing conditions such as sarcopenia and osteoporosis (*5*). A significant volume of research has identified sarcopenia as a vital prognostic factor for HCC (*6*). However, evidence suggests that a low BMD frequently occurs prior to the manifestation of sarcopenia, leading to an increasing emphasis on the prognostic implications of bone changes in the context of liver cancer (*7,8*).

Recent studies have indicated that BMD is not only correlated with the incidence of HCC but also functions as a prognostic marker for HCC outcomes when assessed prior to treatment (*9,10*). A study has indicated that chronic liver disease (CLD) -HCC-cachexia can influence bone degradation and remodeling through various mechanisms, including inflammatory

processes, nutritional status, and hormonal fluctuations (*5*). Moreover, changes in bone may also influence liver function *via* the liver-bone axis (*11*).

The aim of this review was to synthesize the existing literature regarding the prognostic role of BMD in the progression of HCC, while also providing a brief description of the mechanisms involved in the liver-bone axis. Through the assessment of the overall health status of patients diagnosed with HCC and the adoption of integrated treatment approaches, this work seeks to promote additional research in this area and improve patient prognosis.

2. Predicting the development of HCC based on BMD

BMD is typically assessed with dual-energy X-ray absorptiometry (DXA), using T-scores to classify individuals as having osteopenia (1-2.5 standard deviation (SD) below the mean for a young woman at either the femur neck or the lumbar spine) or osteoporosis (more than 2.5 SD below the normal). Both conditions are influenced by various factors, including age, genetic predisposition, hormonal fluctuations, and lifestyle (*12*). In addition, computed tomography (CT)-derived Hounsfield Units (HUs) and quantitative computed tomography (QCT) are widely used diagnostic techniques (*13*). The prevalence of osteoporosis is notably elevated in patients with CLD, with an incidence of 34.5%, and is largely attributable to musculoskeletal malnutrition (*14*). As CLD progresses to HCC, the cumulative impact of cancer cachexia and therapeutic interventions for the tumor significantly aggravate bone health concerns. This situation may suggest the potential use of BMD as a predictive indicator.

A point worth noting is that individuals diagnosed with osteoporosis exhibit an elevated risk of developing liver cancer compared to those without this condition. Moreover, male patients with osteoporosis have a significantly higher risk of liver cancer than their female counterparts. Notably, more pronounced findings were identified in individuals age 64 or younger (*15*). In a retrospective-prospective analysis, BMD at the level of the 12th thoracic vertebra was found to be a risk factor for cirrhosis to progress to HCC in both training Asian (n = 126, P = 0.044) and validation American (n = 274, P = 0.030) populations (*9*). A Kaplan-Meier analysis of 347 cirrhotic patients was performed for BMD at L5 and T12 in association with the time to development of HCC, and the BMD of L5 was found to be an independent predictor, with a cutoff value of 161 HU (HR = 1.676, 95% CI: 1.022-2.748, P = 0.041) (*16*). Both studies suggest that BMD and its decline may be indicative of a higher risk for development of HCC. Researchers hypothesize that reduced BMD, akin to increased visceral fat and obesity, may act as a comprehensive marker of lifestyle factors and impaired liver function. BMD can be combined with other high-risk factors, such as active hepatitis, to create a risk model for HCC. This enables the modification of follow-up strategies for high-risk individuals, promoting the early identification of HCC. While these studies are limited in scale and retrospective in nature, they stimulate discourse regarding the correlation between nutritional status, as reflected by BMD, and the incidence of HCC. Moreover, findings suggest that vertebral BMD is a more significant predictor of HCC risk compared to femoral BMD, which is conventionally utilized to diagnose osteoporosis. The fact that various clinical studies choose different vertebral BMD and cutoff values suggests that there is still a need for more clinical evidence to standardize BMD assessment.

3. Predicting the prognosis of HCC based on BMD

The value of BMD assessment lies not only in the development of HCC but also in predicting its prognosis. Sharma *et al*. first discovered that a low BMD may indicate post-transplant survival in 118 adult recipients of living donor liver transplantation (LDLT) for HCC (HR = 0.90, 95%IC: 0.83-0.99, P = 0.03). After adjusting for sex, dorsal muscle area, number of lesions and age, a BMD below 160 HU was associated with a 2.8-fold higher hazard of post-LT mortality compared to recipients with a BMD higher than 160 HU (HR = 2.87; P = 0.018) (*10*). As shown in Table 1, recent studies increasingly corroborate these findings. Japanese studies on HCC have indicated that BMD is linked to reduced overall survival (OS) and disease-free survival (DFS) not only in LDLT patients (*17*) but also in those undergoing hepatic resection (*18,19*). Osteopenia was confirmed to be an independent risk factor for a lower OS in HCC. Studies involving 102 patients with Barcelona Cancer Liver Classification Stage A (BCLC A) HCC and 227 patients who underwent elective hepatic resection concluded that preoperative osteosarcopenia was a significant independent predictor of DFS (*20*), and osteopenia served as a risk factor for DFS and OS in univariate analysis (*21*). Moreover, studies focusing on patients with intrahepatic cholangiocarcinoma have also indicated the prognostic value of preoperative BMD in outcome assessment (*22,23*). In addition, German studies involving 151 patients who underwent partial hepatectomy for HCC and 908 patients underwent transarterial chemoembolization (TACE) confirmed that osteopenia was an independent risk factor for OS (*24,25*). These studies utilized routine pre-operative CT scans of patients with HCC to evaluate mean pixel density in the mid-vertebral core of the 11th thoracic vertebra. This approach has been proven to be equivalent to DXA and can be used without incurring additional costs, making it a recommended approach (*13*). A CT-attenuation threshold of 160 HU or less was 90% sensitive at the first lumbar vertebra and a threshold of 110 HU was more than 90% specific at distinguishing osteoporosis from osteopenia and normal BMD, which is the reason

Table 1. Summary of clinical studies on BMD reflecting liver cancer prognosis

Country (*Ref.*)	Patient characteristics	Study type	Methodology	Main findings
USA, 2016 Sharma P (*10*)	Adult patients who underwent LDLT for HCC (n = 118)	Retrospective	Preoperative BMD was evaluated with CT of pixel density in the mid-vertebral core of T11. The cutoff value of BMD was less than 160 HU.	BMD was an independent risk factor for post-LT mortality (HR = 0.90, 95%CI: 0.83-0.99, P = 0.03).
Japan, 2020 Toshima T (*17*)	Adult patients who underwent LDLT for HCC (n = 193)	Retrospective	BMD was evaluated with CT in the mid-vertebral core of the T11. Osteopenia was defined as BMD below the standard (308.82–2.49×Age in men and 311.84–2.41×Age in women).	Osteopenia was an independent risk factor for mortality after LDLT (HR = 2.106, 95%CI: 1.102–4.241, P = 0.024).
Japan, 2019 Miyachi Y (*18*)	Adult patients who underwent primary hepatectomy for HCC (n = 465)	Retrospective	BMD was evaluated with CT in the mid-vertebral core of T11. The cutoff value of BMD was less than 160 HU.	For male patients (n = 367), low BMD was an independent risk factor for cancer-specific mortality (HR = 1.720, 95%CI: 1.038–2.922, P = 0.035).
Germany, 2022 Meister FA (*24*)	Adult patients who underwent partial hepatectomy for HCC (n = 151)	Retrospective	BMD was evaluated with CT-based segmentation. Osteopenia was defined as a BMD cut-off of < 175 HU for females, <160 HU for male patients with HCC.	Osteopenia was confirmed to be an independent risk-factor for inferior overall survival (HR = 7.743, 95%CI: 2.186–27.431, P = 0.002)
Japan, 2023 Yanagaki M (*21*)	Adult patients who underwent elective hepatic resection for HCC (n = 227)	Retrospective	BMD was evaluated with CT in the mid-vertebral core of T11. Osteopenia was defined as BMD below the standard BMD (308.82–2.49×Age in men and 311.84–2.41×Age in women).	Patients with osteopenia had a worse DFS (HR = 1.67, P = 0.008) and OS (HR = 2.24, P = 0.004) according to univariate analysis. Osteosarcopenia was an independent predictor of DFS and OS.
Japan, 2024 Ishida T (*19*)	Consecutive adult patients who underwent hepatectomy (n = 188)	Retrospective	BMD was evaluated with CT in the mid-vertebral core of the T11. The cutoff value of osteopenia was 160 HU	Osteopenia was an independent risk factor in OS (HR2.52, P = 0.004) and DFS (HR1.68, P = 0.023), possibly due to mechanisms mediated *via* microvascular portal vein invasion.
Japan, 2024 Abe K (*20*)	Adult patients who underwent surgical resection (n = 45) or RFA (n = 57) for BCLC A HCC	Retrospective	BMD was evaluated with CT in the mid-vertebral core of the T11. The cutoff value of osteopenia was 160 HU. Osteosarcopenia was defined as the concomitant development of osteopenia and sarcopenia.	No significant differences in DFS (P = 0.22) and OS (P = 0.09) were noted for osteopenia. Osteosarcopenia was a significant independent predictor of DFS and OS.
Germany, 2023 Müller L (*25*)	Adult patients with HCC who underwent TACE (n = 908)	Retrospective	BMD was evaluated with CT in the mid-vertebral core of T11. The cutoff value for BMD was less than 114 HU.	Low BMD remained an independent risk factor in median OS (HR1.7, 95%CI: 1.4–2.1, P < 0.001).
*China, 2021 Zheng X (*27*)	Adult patients who underwent TACE for HCC (n = 75)	Retrospective	QCT workstation (Mindways Software) indicated the mean BMD for the first and second lumbar vertebra before and after TACE.	Changes in BMD were not associated with OS. Muscle changes and the area of subcutaneous and visceral fat were independent risk factors for HCC after TACE.
*Germany, 2023 Sven H. L (*26*)	Adult patients who underwent TACE for HCC (n = 89)	Retrospective	BMD was measured at the level of the third lumbar vertebra in a single slice CT in the venous phase. The cutoff value for BMD was the median (159.5 HU).	A low BMD was not associated with OS.
# Japan, 2023 Miki A (*22*)	Adult patients with ICC who underwent hepatectomy (n = 71)	Retrospective	BMD was evaluated with CT in the mid-vertebral core of T11. The cutoff value for osteopenia was 160 HU.	Osteopenia (HR 3.66, P = 0.0258) was an independent factor associated with OS but not an independent prognostic factor for DFS.
# Japan, 2023 Taniai T (*23*)	Adult patients who underwent hepatic resection for ICC (n = 41)	Retrospective	BMD was evaluated with CT in the mid-vertebral core of T11. Osteopenia was defined as BMD below the standard (308.82–2.49 × Age in men and 311.84–2.41 × Age in women). Osteosarcopenia was defined as the concomitant development of osteopenia and sarcopenia.	Osteosarcopenia was an independent predictor of OS (HR 6.46, P < 0.01) and DSF (HR 3.38, P < 0.01).

*Studies with negative results on the prognostic implications of BMD; # Studies on ICC. HCC, hepatocellular carcinoma; LDLT, living donor liver transplantation; BMD, bone mineral density; T11, the 11th thoracic vertebra; HU, Hounsfield unit; BCLC, Barcelona Cancer Liver Classification stage; RFA, radiofrequency ablation; TACE, transarterial chemoembolization; ICC, intrahepatic cholangiocarcinoma; QCT, quantitative computed tomography; OS, overall survival; DFS, recurrence-free survival, HR, hazard ratio; CI, confidence interval.

some studies have established that cutoff value (*10,19*). There is a discrepancy among studies regarding which vertebrae to measure. In two other studies on TACE conducted in China and Germany, different methods and thresholds were used, yet both concluded that changes in BMD were not related to OS in patients with HCC (*26,27*). This conclusion, different research strategies yield varying results, and the mixing of effects may have shifted the final result of the study in one direction or the other.

Considering the differences in populations and detection equipment, some studies have used different cutoff values to avoid age and sex biases, which hampered the determination of overall osteopenia incidence in patients with HCC and multi-center horizontal comparisons. Research in various countries reflects the similar predictive value of preoperative BMD for a poor prognosis for HCC, but subgroup analyses yield varying results, particularly in terms of sex grouping, tumor staging, and recurrence. Age and sex are crucial factors affecting BMD (*12*). Patients with HCC are predominantly middle-aged and elderly, with long-term cirrhosis and tumor conditions possibly impacting bone quality more than age differences (*25*). Due to the influence of female estrogen, changes in BMD are more useful in predicting the prognosis of HCC in males (*18*). Some studies, and especially those on LDLT, have found no correlation between BMD and DFS (*10,17,18*) or progression (*25*), suggesting that BMD is an independent factor reflecting the overall condition of the body while not being correlated with the cancer grade. However, Yanagaki *et al*. and Ishida *et al*. found that after sex differentiation, BMD has a predictive role in the DFS of patients with HCC (*19,21*). This contradiction may necessitate more precise population-specific cutoff values to yield more accurate results.

Surgical procedures and pharmacological treatments for HCC often temporarily exacerbate the burden on the liver, leading to increased bone loss and a heightened risk of pathological fractures. There is a lack of recent studies addressing the prognostic implications of BMD in patients with HCC undergoing targeted therapies. Evidence regarding immune checkpoint inhibitors (ICIs) suggests that a lower baseline BMD is correlated with poorer clinical outcomes in patients receiving ICIs for other malignancies (*28*). Further study is warranted to validate the role of changes in BMD in evaluating the efficacy of immunotherapy in HCC.

4. Regulation of the liver-bone axis in HCC

Whether BMD loss clearly promotes the progression of HCC or whether a consistent BMD prevents cancer invasion is unclear. Conclusive biological evidence to substantiate the predictive role of BMD has not yet been obtained (*17*). The pathophysiological mechanisms underlying osteopenia associated with liver cancer are intricate, and particularly in individuals with NAFLD, end-stage CLD, or cachexia.

Proposed molecular mechanisms that may elucidate the relationship between BMD and CLD-HCC include the receptor activator of nuclear factor kappa (RANK) - RANK ligand (RANKL) - osteoprotegerin (OPG) signaling pathway, the upregulation of pro-inflammatory cytokines such as interleukin-1 (IL-1), IL-6, and tumor necrosis factor alpha (TNF-α), as well as variations in levels of erythropoietin (EPO), testosterone, and insulin-like growth factor (IGF) (*29*) . In addition, deficiencies in nutritional elements such as vitamin D, calcium, and vitamin K have been linked to osteoblast apoptosis, osteoclast differentiation, and osteoporosis in cachectic patients (*5*) (Figure.1).

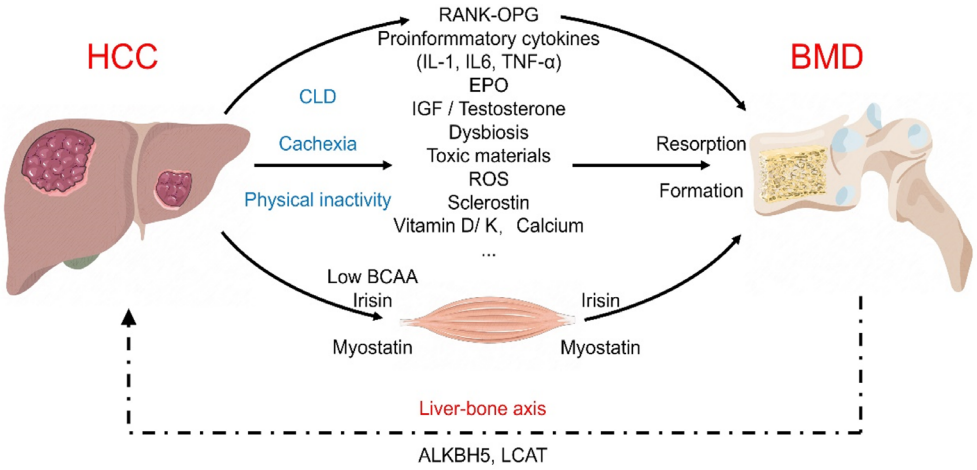

Figure 1. Diagram of the potential signaling mechanisms of bone density changes in patients with HCC. Shown are the possible signaling pathways between HCC and bone destruction and remodeling, as well as the intermediary regulatory role of muscles in the liver-bone axis. HCC, hepatocellular carcinoma; BMD, bone mineral density; CLD, chronic liver disease; RANK, the receptor activator of nuclear factor kappa; RANKL, RANK ligand; OPG, osteoprotegerin; IL-1, interleukin-1; TNF-α, tumor necrosis factor alpha; EPO, erythropoietin; ROS, reactive oxygen species; BCAA, branch-chain amino acid; GDF11, insulin-like growth factor 11, ALKBH5, AlkB homolog 5; LCAT, hepatokine lecithin-cholesterol acyltransferase.

The bidirectional regulation of the liver-bone axis has garnered considerable scholarly attention, which may be crucial to understanding the role of BMD in the progression of HCC. Lu *et al*. indicated that during osteoporosis, the downregulation of hepatokine lecithin-cholesterol acyltransferase can disrupt bone homeostasis and intensify liver fibrosis by hindering cholesterol transport from the bone to the liver, thereby highlighting the reciprocal regulatory relationship inherent in the liver-bone axis (*11*). Moreover, extracellular vesicles derived from bone-metastasized HCC cells have the capacity to target orthotopic HCC cells *via* AlkB homolog 5, thereby promoting and initiating prometastatic cascades (*30*). These findings underscore the bidirectional interplay between liver health and bone status, wherein various factors can concurrently impact both bone health and the progression of HCC.

5. BMD and therapeutic strategies for HCC

There is a lack of clinical evidence demonstrating a significant effect of improved BMD on the prognosis of HCC. Nevertheless, enhancing bone quality through exercise and nutritional interventions is not incompatible with the supportive therapies necessary for HCC management (*31*). The relationship between atezolizumab and osteoporosis appears to be particularly pronounced compared to other ICIs, necessitating special consideration for female patients due to their increased vulnerability (*32*). A study has suggested that osteoporosis therapies, such as denosumab, combined with ICIs may enhance clinical outcomes for patients with bone metastases (*33*). In addition, a reduction in fracture incidence is associated with improvement of quality of life (*5,34*). Identifying factors linked to a low BMD prior to treatment and those associated with BMD loss during treatment would be useful. Future research should aim to further elucidate the impact of treatment-related changes in BMD.

6. Conclusion

In summary, evaluating BMD may improve the assessment of prognosis in HCC. BMD has been found to be a prognostic risk factor in digestive cancers (*7*), but the current evidence from small-scale retrospective studies and limited etiopathogenesis research is insufficient to conclusively demonstrate a direct impact of BMD on the prognosis of HCC. Nevertheless, as a manifestation of overall nutritional status, BMD warrants attention during the screening and treatment of HCC. This focus may potentially contribute to improved patient outcomes, which highlights the urgent need for further interdisciplinary research. Conducting higher-quality research and establishing standardized methods of measuring BMD and cutoff values could significantly enhance its clinical use in patients with HCC.

Funding: This work was supported by grants from the Changzhou Project to Train High-level Medical Personnel (GW2023019 and LC20242022CZBJ064) and the Changzhou Medical Center of Nanjing Medical University Program (PCMCB202212, PCMCM202204, and BSH202209).

Conflict of Interest: The authors have no conflicts of interest to disclose.

References

1. Vogel A, Meyer T, Sapisochin G, Salem R, Saborowski A. Hepatocellular carcinoma. Lancet. 2022; 400:1345-1362.
2. Wang J, Wu R, Sun J-Y, Lei F, Tan H, Lu X. An overview: Management of patients with advanced hepatocellular carcinoma. Biosci Trends. 2022; 16:405-425.
3. Ma YN, Jiang X, Song P, Tang W. Neoadjuvant therapies in resectable hepatocellular carcinoma: Exploring strategies to improve prognosis. Biosci Trends. 2024; 18:21-41.
4. Cabibbo G, Celsa C, Rimassa L, Torres F, Rimola J, Kloeckner R, Bruix J, Cammà C, Reig M. Navigating the landscape of liver cancer management: Study designs in clinical trials and clinical practice. J Hepatol. 2024; 80:957-966.
5. Jadzic J, Djonic D. Hepatocellular carcinoma and musculoskeletal system: A narrative literature review. World J Gastroenterol. 2024; 30:2109-2117.
6. Chen B-B, Liang P-C, Shih TT-F, Liu T-H, Shen Y-C, Lu L-C, Lin Z-Z, Hsu C, Hsu C-H, Cheng A-L, Shao Y-Y. Sarcopenia and myosteatosis are associated with survival in patients receiving immunotherapy for advanced hepatocellular carcinoma. Eur Radiol. 2023; 33:512-522.
7. Watanabe J, Saitsu A, Miki A, Kotani K, Sata N. Prognostic value of preoperative low bone mineral density in patients with digestive cancers: A systematic review and meta-analysis. Arch Osteoporos. 2022; 17:33.
8. Pereira FB, Leite AF, de Paula AP. Relationship between pre-sarcopenia, sarcopenia and bone mineral density in elderly men. Arch Endocrinol Metab. 2015; 59:59-65.
9. Liang KH, Zhang P, Lin CL, Wang SC, Hu TH, Yeh CT, Su GL. Morphomic signatures derived from computed tomography predict hepatocellular carcinoma occurrence in cirrhotic patients. Dig Dis Sci. 2020; 65:2130-2139.
10. Sharma P, Parikh ND, Yu J, Barman P, Derstine BA, Sonnenday CJ, Wang SC, Su GL. Bone mineral density predicts posttransplant survival among hepatocellular carcinoma liver transplant recipients. Liver Transpl. 2016; 22:1092-1098.
11. Lu K, Shi T-S, Shen S-Y, *et al*. Defects in a liver-bone axis contribute to hepatic osteodystrophy disease progression. Cell Metab. 2022; 34.
12. Pinheiro MB, Naganathan V. Appraisal of Clinical Practice Guideline: Clinical practice guideline for management of osteoporosis and fracture prevention in Canada: 2023 update. J Physiother. 2024; 70:241.
13. Pickhardt PJ, Pooler BD, Lauder T, del Rio AM, Bruce RJ, Binkley N. Opportunistic screening for osteoporosis using abdominal computed tomography scans obtained for other indications. Ann Intern Med. 2013; 158:588-595.
14. Lu Z, Li X, Qi Y, Li B, Chen L. Genetic evidence of the causal relationship between chronic liver diseases and

musculoskeletal disorders. J Transl Med. 2024; 22:138.
15. Sun L-M, Liang J-A, Lin C-L, Lin M-C, Chang N-J, Kao C-H. Cancer risk in patients with osteoporosis: A population-based cohort study. Curr Med Res Opin. 2017; 33:733-739.
16. Yeh C, Lai MW, Yeh CT, Lin YH, Tseng JH. Bone densities assessed by Hounsfield Units at L5 in computed tomography image independently predict hepatocellular carcinoma development in cirrhotic patients. J Clin Med. 2022; 11.
17. Toshima T, Yoshizumi T, Kosai-Fujimoto Y, Inokuchi S, Yoshiya S, Takeishi K, Itoh S, Harada N, Ikegami T, Soejima Y, Mori M. Prognostic impact of osteopenia in patients who underwent living donor liver transplantation for hepatocellular carcinoma. World J Surg. 2020; 44:258-267.
18. Miyachi Y, Kaido T, Yao S, Shirai H, Kobayashi A, Hamaguchi Y, Kamo N, Yagi S, Uemoto S. Bone mineral density as a risk factor for patients undergoing surgery for hepatocellular carcinoma. World J Surg. 2019; 43:920-928.
19. Ishida T, Miki A, Sakuma Y, Watanabe J, Endo K, Sasanuma H, Teratani T, Kitayama J, Sata N. Preoperative bone loss predicts decreased survival associated with microvascular invasion after resection of hepatocellular carcinoma. Cancers (Basel). 2024; 16:2087.
20. Abe K, Furukawa K, Matsumoto M, Futagawa Y, Shiozaki H, Onda S, Haruki K, Shirai Y, Okamoto T, Ikegami T. Osteosarcopenia impacts treatment outcomes for Barcelona Cancer Liver Classification stage A hepatocellular carcinoma. Surg Oncol. 2024; 53:102043.
21. Yanagaki M, Haruki K, Taniai T, Igarashi Y, Yasuda J, Furukawa K, Onda S, Shirai Y, Tsunematsu M, Ikegami T. The significance of osteosarcopenia as a predictor of the long-term outcomes in hepatocellular carcinoma after hepatic resection. J Hepatobiliary Pancreat Sci. 2023; 30:453-461.
22. Miki A, Sakuma Y, Watanabe J, Endo K, Sasanuma H, Teratani T, Lefor AK, Kitayama J, Sata N. Osteopenia is associated with shorter survival in patients with intrahepatic cholangiocarcinoma. Curr Oncol. 2023; 30:1860-1868.
23. Taniai T, Haruki K, Yanagaki M, Igarashi Y, Furukawa K, Onda S, Yasuda J, Matsumoto M, Tsunematsu M, Ikegami T. Osteosarcopenia predicts poor prognosis for patients with intrahepatic cholangiocarcinoma after hepatic resection. Surg Today. 2023; 53:82-89.
24. Meister FA, Verhoeven S, Mantas A, Liu W-J, Jiang D, Heij L, Heise D, Bruners P, Lang SA, Ulmer TF, Neumann UP, Bednarsch J, Czigany Z. Osteopenia is associated with inferior survival in patients undergoing partial hepatectomy for hepatocellular carcinoma. Sci Rep. 2022; 12:18316.
25. Müller L, Mähringer-Kunz A, Auer TA, *et al*. Low bone mineral density is a prognostic factor for elderly patients with HCC undergoing TACE: Results from a multicenter study. Eur Radiol. 2023; 33:1031-1039.
26. Loosen SH, Jördens MS, Schoon B, Antoch G, Luedde T, Minko P, Loberg C, Roderburg C. Sarcopenia indicate poor survival in patients undergoing transarterial chemoembolization (TACE) for hepatic malignancies. J Cancer Res Clin Oncol. 2023; 149:6181-6190.
27. Zheng X, Cao F, Qian L, Dong J. Body composition changes in hepatocellular carcinoma: prediction of survival to transcatheter arterial chemoembolization in combination with clinical prognostic factors. Cancer Control. 2021; 28:10732748211038445.
28. Lou J, Gong B, Li Y, Guo Y, Li L, Wang J, Liu W, You Z, Zhang H, Pan F, Liang B, Yang L, Zhou G. Bone mineral density as an individual prognostic biomarker in NSCLC patients treated with immune checkpoint inhibitors. Front Immunol. 2024; 15:1332303.
29. Yang YJ, Kim DJ. An overview of the molecular mechanisms contributing to musculoskeletal disorders in chronic liver disease: Osteoporosis, sarcopenia, and osteoporotic sarcopenia. Int J Mol Sci. 2021; 22.
30. Han S, Xue L, Wei Y, *et al*. Bone lesion-derived extracellular vesicles fuel prometastatic cascades in hepatocellular carcinoma by transferring ALKBH5-targeting miR-3190-5p. Adv Sci (Weinh). 2023; 10:e2207080.
31. Hu Y, Cai Y, Ma W, Hu H, Gu H, Jin Y, Li F. The prognostic nutritional index and tumor pathological characteristics predict the prognosis of elderly patients with early-stage hepatocellular carcinoma after surgery. Biosci Trends. 2023; 17:369-380.
32. Liu H, Li Y, Li J, Zhang Q, Wu J, Li X, Meng L, Cao S, Li H. Musculoskeletal adverse events induced by immune checkpoint inhibitors: A large-scale pharmacovigilance study. Front Pharmacol. 2023; 14:1199031.
33. Asano Y, Yamamoto N, Demura S, Hayashi K, Takeuchi A, Kato S, Miwa S, Igarashi K, Higuchi T, Taniguchi Y, Okuda M, Matsumoto I, Yano S, Tsuchiya H. Combination therapy with immune checkpoint inhibitors and denosumab improves clinical outcomes in non-small cell lung cancer with bone metastases. Lung Cancer. 2024; 193:107858.
34. Park Y, Kang D, Sinn DH, Kim H, Hong YS, Cho J, Gwak GY. Effect of lifestyle modification on hepatocellular carcinoma incidence and mortality among patients with chronic hepatitis B. World J Gastroenterol. 2023; 29:3843-3854.

Received July 11, 2024; Revised August 16, 2024; Accepted August 19, 2024.

**Address correspondence to:*
Liming Tang, Changzhou Medical Center, The Affiliated Changzhou No. 2 People's Hospital of Nanjing Medical University, Changzhou, Jiangsu 213000, China
E-mail: tangliming@njmu.edu.cn

Released online in J-STAGE as advance publication August 22, 2024.

BST
BioScience Trends

Guide for Authors

1. Scope of Articles

BioScience Trends (Print ISSN 1881-7815, Online ISSN 1881-7823) is an international peer-reviewed journal. *BioScience Trends* devotes to publishing the latest and most exciting advances in scientific research. Articles cover fields of life science such as biochemistry, molecular biology, clinical research, public health, medical care system, and social science in order to encourage cooperation and exchange among scientists and clinical researchers.

2. Submission Types

Original Articles should be well-documented, novel, and significant to the field as a whole. An Original Article should be arranged into the following sections: Title page, Abstract, Introduction, Materials and Methods, Results, Discussion, Acknowledgments, and References. Original articles should not exceed 5,000 words in length (excluding references) and should be limited to a maximum of 50 references. Articles may contain a maximum of 10 figures and/or tables. Supplementary Data are permitted but should be limited to information that is not essential to the general understanding of the research presented in the main text, such as unaltered blots and source data as well as other file types.

Brief Reports definitively documenting either experimental results or informative clinical observations will be considered for publication in this category. Brief Reports are not intended for publication of incomplete or preliminary findings. Brief Reports should not exceed 3,000 words in length (excluding references) and should be limited to a maximum of 4 figures and/or tables and 30 references. A Brief Report contains the same sections as an Original Article, but the Results and Discussion sections should be combined.

Reviews should present a full and up-to-date account of recent developments within an area of research. Normally, reviews should not exceed 8,000 words in length (excluding references) and should be limited to a maximum of 10 figures and/or tables and 100 references. Mini reviews are also accepted, which should not exceed 4,000 words in length (excluding references) and should be limited to a maximum of 5 figures and/or tables and 50 references.

Policy Forum articles discuss research and policy issues in areas related to life science such as public health, the medical care system, and social science and may address governmental issues at district, national, and international levels of discourse. Policy Forum articles should not exceed 3,000 words in length (excluding references) and should be limited to a maximum of 5 figures and/or tables and 30 references.

Communications are short, timely pieces that spotlight new research findings or policy issues of interest to the field of global health and medical practice that are of immediate importance. Depending on their content, Communications will be published as "Comments" or "Correspondence". Communications should not exceed 1,500 words in length (excluding references) and should be limited to a maximum of 2 figures and/or tables and 20 references.

Editorials are short, invited opinion pieces that discuss an issue of immediate importance to the fields of global health, medical practice, and basic science oriented for clinical application. Editorials should not exceed 1,000 words in length (excluding references) and should be limited to a maximum of 10 references. Editorials may contain one figure or table.

News articles should report the latest events in health sciences and medical research from around the world. News should not exceed 500 words in length.

Letters should present considered opinions in response to articles published in *BioScience Trends* in the last 6 months or issues of general interest. Letters should not exceed 800 words in length and may contain a maximum of 10 references. Letters may contain one figure or table.

3. Editorial Policies

For publishing and ethical standards, *BioScience Trends* follows the Recommendations for the Conduct, Reporting, Editing, and Publication of Scholarly Work in Medical Journals issued by the International Committee of Medical Journal Editors (ICMJE, *https://icmje.org/recommendations*), and the Principles of Transparency and Best Practice in Scholarly Publishing jointly issued by the Committee on Publication Ethics (COPE, *https://publicationethics.org/resources/guidelines-new/principles-transparency-and-best-practice-scholarly-publishing*), the Directory of Open Access Journals (DOAJ, *https://doaj.org/apply/transparency*), the Open Access Scholarly Publishers Association (OASPA, *https://oaspa.org/principles-of-transparency-and-best-practice-in-scholarly-publishing-4*), and the World Association of Medical Editors (WAME, *https://wame.org/principles-of-transparency-and-best-practice-in-scholarly-publishing*).

BioScience Trends will perform an especially prompt review to encourage innovative work. All original research will be subjected to a rigorous standard of peer review and will be edited by experienced copy editors to the highest standards.

Ethical Approval of Studies and Informed Consent: For all manuscripts reporting data from studies involving human participants or animals, formal review and approval, or formal review and waiver, by an appropriate institutional review board or ethics committee is required and should be described in the Methods section. When your manuscript contains any case details, personal information and/or images of patients or other individuals, authors must obtain appropriate written consent, permission and release in order to comply with all applicable laws and regulations concerning privacy and/or security of personal information. The consent form needs to comply with the relevant legal requirements of your particular jurisdiction, and please do not send signed consent form to *BioScience Trends* to respect your patient's and any other individual's privacy. Please instead describe the information clearly in the Methods (patient consent) section of your manuscript while retaining copies of the signed forms in the event they should be needed. Authors should also state that the study conformed to the provisions of the Declaration of Helsinki (as revised in 2013, *https://wma.net/what-we-do/medical-ethics/declaration-of-helsinki*). When reporting experiments on animals, authors should indicate whether the institutional and national guide for the care and use of laboratory animals was followed.

Reporting Clinical Trials: The ICMJE (*https:// icmje.org/recommendations/browse/publishing-and-editorial-issues/clinical-trial-registration.html*) defines a clinical trial as any research project that prospectively assigns people or a group of people to an intervention, with or without concurrent comparison or control groups, to study the relationship between a health-related intervention and a health outcome. Registration of clinical trials in a public trial registry at or before the time of first patient enrollment is a condition of consideration for publication in *BioScience Trends*, and the trial registration number will be published at the end of the Abstract. The registry must be independent of for-profit interest and publicly accessible. Reports of trials must conform to CONSORT 2010 guidelines (*https://consort-statement.org/consort-2010*). Articles reporting the results of randomized trials must include the CONSORT flow diagram showing the progress of patients throughout the trial.

Conflict of Interest: All authors are required to disclose any actual or potential conflict of interest including financial interests or relationships with other people or organizations that might raise questions of bias

in the work reported. If no conflict of interest exists for each author, please state "There is no conflict of interest to disclose".

Submission Declaration: When a manuscript is considered for submission to *BioScience Trends*, the authors should confirm that 1) no part of this manuscript is currently under consideration for publication elsewhere; 2) this manuscript does not contain the same information in whole or in part as manuscripts that have been published, accepted, or are under review elsewhere, except in the form of an abstract, a letter to the editor, or part of a published lecture or academic thesis; 3) authorization for publication has been obtained from the authors' employer or institution; and 4) all contributing authors have agreed to submit this manuscript.

Initial Editorial Check: Immediately after submission, the journal's managing editor will perform an initial check of the manuscript. A suitable academic editor will be notified of the submission and invited to check the manuscript and recommend reviewers. Academic editors will check for plagiarism and duplicate publication at this stage. The journal has a formal recusal process in place to help manage potential conflicts of interest of editors. In the event that an editor has a conflict of interest with a submitted manuscript or with the authors, the manuscript, review, and editorial decisions are managed by another designated editor without a conflict of interest related to the manuscript.

Peer Review: *BioScience Trends* operates a single-anonymized review process, which means that reviewers know the names of the authors, but the authors do not know who reviewed their manuscript. All articles are evaluated objectively based on academic content. External peer review of research articles is performed by at least two reviewers, and sometimes the opinions of more reviewers are sought. Peer reviewers are selected based on their expertise and ability to provide quality, constructive, and fair reviews. For research manuscripts, the editors may, in addition, seek the opinion of a statistical reviewer. Every reviewer is expected to evaluate the manuscript in a timely, transparent, and ethical manner, following the COPE guidelines (*https://publicationethics.org/files/cope-ethical-guidelines-peer-reviewers-v2_0.pdf*). We ask authors for sufficient revisions (with a second round of peer review, when necessary) before a final decision is made. Consideration for publication is based on the article's originality, novelty, and scientific soundness, and the appropriateness of its analysis.

Suggested Reviewers: A list of up to 3 reviewers who are qualified to assess the scientific merit of the study is welcomed. Reviewer information including names, affiliations, addresses, and e-mail should be provided at the same time the manuscript is submitted online. Please do not suggest reviewers with known conflicts of interest, including participants or anyone with a stake in the proposed research; anyone from the same institution; former students, advisors, or research collaborators (within the last three years); or close personal contacts. Please note that the Editor-in-Chief may accept one or more of the proposed reviewers or may request a review by other qualified persons.

Language Editing: Manuscripts prepared by authors whose native language is not English should have their work proofread by a native English speaker before submission. If not, this might delay the publication of your manuscript in *BioScience Trends*.

The Editing Support Organization can provide English proofreading, Japanese-English translation, and Chinese-English translation services to authors who want to publish in *BioScience Trends* and need assistance before submitting a manuscript. Authors can visit this organization directly at *https://www.iacmhr.com/iac-eso/support.php?lang=en*. IAC-ESO was established to facilitate manuscript preparation by researchers whose native language is not English and to help edit works intended for international academic journals.

Copyright and Reuse: Before a manuscript is accepted for publication in *BioScience Trends*, authors will be asked to sign a transfer of copyright agreement, which recognizes the common interest that both the journal and author(s) have in the protection of copyright. We accept that some authors (*e.g.*, government employees in some countries) are unable to transfer copyright. A JOURNAL PUBLISHING AGREEMENT (JPA) form will be e-mailed to the authors by the Editorial Office and must be returned by the authors by mail, fax, or as a scan. Only forms with a hand-written signature from the corresponding author are accepted. This copyright will ensure the widest possible dissemination of information. Please note that the manuscript will not proceed to the next step in publication until the JPA Form is received. In addition, if excerpts from other copyrighted works are included, the author(s) must obtain written permission from the copyright owners and credit the source(s) in the article.

4. Cover Letter

The manuscript must be accompanied by a cover letter prepared by the corresponding author on behalf of all authors. The letter should indicate the basic findings of the work and their significance. The letter should also include a statement affirming that all authors concur with the submission and that the material submitted for publication has not been published previously or is not under consideration for publication elsewhere. The cover letter should be submitted in PDF format. For an example of Cover Letter, please visit: *https://www.biosciencetrends.com/downcentre* (Download Centre).

5. Submission Checklist

The Submission Checklist should be submitted when submitting a manuscript through the Online Submission System. Please visit Download Centre (*https://www.biosciencetrends.com/downcentre*) and download the Submission Checklist file. We recommend that authors use this checklist when preparing your manuscript to check that all the necessary information is included in your article (if applicable), especially with regard to Ethics Statements.

6. Manuscript Preparation

Manuscripts are suggested to be prepared in accordance with the "Recommendations for the Conduct, Reporting, Editing, and Publication of Scholarly Work in Medical Journals", as presented at *https://www.ICMJE.org*.

Manuscripts should be written in clear, grammatically correct English and submitted as a Microsoft Word file in a single-column format. Manuscripts must be paginated and typed in 12-point Times New Roman font with 24-point line spacing. Please do not embed figures in the text. Abbreviations should be used as little as possible and should be explained at first mention unless the term is a well-known abbreviation (*e.g.* DNA). Single words should not be abbreviated.

Title page: The title page must include 1) the title of the paper (Please note the title should be short, informative, and contain the major key words); 2) full name(s) and affiliation(s) of the author(s), 3) abbreviated names of the author(s), 4) full name, mailing address, telephone/fax numbers, and e-mail address of the corresponding author; 5) author contribution statements to specify the individual contributions of all authors to this manuscript, and 6) conflicts of interest (if you have an actual or potential conflict of interest to disclose, it must be included as a footnote on the title page of the manuscript; if no conflict of interest exists for each author, please state "There is no conflict of interest to disclose").

Abstract: The abstract should briefly state the purpose of the study, methods, main findings, and conclusions. For articles that are Original Articles, Brief Reports, Reviews, or Policy Forum articles, a one-paragraph abstract consisting of no more than 250 words must be included in the manuscript. For Communications, Editorials, News, or Letters, a brief summary of main content in 150 words or fewer should be included in the manuscript. For articles reporting clinical trials, the trial registration number should be stated at the end of the Abstract. Abbreviations must be kept to a minimum and non-standard

abbreviations explained in brackets at first mention. References should be avoided in the abstract. Three to six key words or phrases that do not occur in the title should be included in the Abstract page.

Introduction: The introduction should provide sufficient background information to make the article intelligible to readers in other disciplines and sufficient context clarifying the significance of the experimental findings

Materials/Patients and Methods: The description should be brief but with sufficient detail to enable others to reproduce the experiments. Procedures that have been published previously should not be described in detail but appropriate references should simply be cited. Only new and significant modifications of previously published procedures require complete description. Names of products and manufacturers with their locations (city and state/country) should be given and sources of animals and cell lines should always be indicated. All clinical investigations must have been conducted in accordance Materials/ Patients and Methods.

Results: The description of the experimental results should be succinct but in sufficient detail to allow the experiments to be analyzed and interpreted by an independent reader. If necessary, subheadings may be used for an orderly presentation. All Figures and Tables should be referred to in the text in order, including those in the Supplementary Data.

Discussion: The data should be interpreted concisely without repeating material already presented in the Results section. Speculation is permissible, but it must be well-founded, and discussion of the wider implications of the findings is encouraged. Conclusions derived from the study should be included in this section.

Acknowledgments: All funding sources (including grant identification) should be credited in the Acknowledgments section. Authors should also describe the role of the study sponsor(s), if any, in study design; in the collection, analysis, and interpretation of data; in the writing of the report; and in the decision to submit the paper for publication. If the funding source had no such involvement, the authors should so state.

In addition, people who contributed to the work but who do not meet the criteria for authors should be listed along with their contributions.

References: References should be numbered in the order in which they appear in the text. Citing of unpublished results, personal communications, conference abstracts, and theses in the reference list is not recommended but these sources may be mentioned in the text. In the reference list, cite the names of all authors when there are fifteen or fewer authors; if there are sixteen or more authors, list the first three followed by *et al*. Names of journals should be abbreviated in the style used in PubMed. Authors are responsible for the accuracy of the references. The EndNote Style of *BioScience Trends* could be downloaded at **EndNote** (*https://ircabssagroup.com/examples/ BioScience_Trends.ens*).

Examples are given below:

Example 1 (Sample journal reference):

Inagaki Y, Tang W, Zhang L, Du GH, Xu WF, Kokudo N. Novel aminopeptidase N (APN/CD13) inhibitor 24F can suppress invasion of hepatocellular carcinoma cells as well as angiogenesis. Biosci Trends. 2010; 4:56-60.

Example 2 (Sample journal reference with more than 15 authors):

Darby S, Hill D, Auvinen A, *et al*. Radon in homes and risk of lung cancer: Collaborative analysis of individual data from 13 European case-control studies. BMJ. 2005; 330:223.

Example 3 (Sample book reference):

Shalev AY. Post-traumatic stress disorder: Diagnosis, history and life course. In: Post-traumatic Stress Disorder, Diagnosis, Management and Treatment (Nutt DJ, Davidson JR, Zohar J, eds.). Martin Dunitz, London, UK, 2000; pp. 1-15.

Example 4 (Sample web page reference):

World Health Organization. The World Health Report 2008 – primary health care: Now more than ever. *http://www.who.int/whr/2008/whr08_ en.pdf* (accessed September 23, 2022).

Tables: All tables should be prepared in Microsoft Word or Excel and should be arranged at the end of the manuscript after the References section. Please note that tables should not in image format. All tables should have a concise title and should be numbered consecutively with Arabic numerals. If necessary, additional information should be given below the table.

Figure Legend: The figure legend should be typed on a separate page of the main manuscript and should include a short title and explanation. The legend should be concise but comprehensive and should be understood without referring to the text. Symbols used in figures must be explained. Any individually labeled figure parts or panels (A, B, *etc*.) should be specifically described by part name within the legend.

Figure Preparation: All figures should be clear and cited in numerical order in the text. Figures must fit a one- or two-column format on the journal page: 8.3 cm (3.3 in.) wide for a single column, 17.3 cm (6.8 in.) wide for a double column; maximum height: 24.0 cm (9.5 in.). Please make sure that the symbols and numbers appeared in the figures should be clear. Please make sure that artwork files are in an acceptable format (TIFF or JPEG) at minimum resolution (600 dpi for illustrations, graphs, and annotated artwork, and 300 dpi for micrographs and photographs). Please provide all figures as separate files. Please note that low-resolution images are one of the leading causes of article resubmission and schedule delays.

Units and Symbols: Units and symbols conforming to the International System of Units (SI) should be used for physicochemical quantities. Solidus notation (*e.g.* mg/kg, mg/mL, mol/mm^2/min) should be used. Please refer to the SI Guide *www.bipm.org/en/si/* for standard units.

Supplemental data: Supplemental data might be useful for supporting and enhancing your scientific research and *BioScience Trends* accepts the submission of these materials which will be only published online alongside the electronic version of your article. Supplemental files (figures, tables, and other text materials) should be prepared according to the above guidelines, numbered in Arabic numerals (*e.g.*, Figure S1, Figure S2, and Table S1, Table S2) and referred to in the text. All figures and tables should have titles and legends. All figure legends, tables and supplemental text materials should be placed at the end of the paper. Please note all of these supplemental data should be provided at the time of initial submission and note that the editors reserve the right to limit the size and length of Supplemental Data.

5. Submission Checklist

The Submission Checklist will be useful during the final checking of a manuscript prior to sending it to *BioScience Trends* for review. Please visit Download Centre and download the Submission Checklist file.

6. Online Submission

Manuscripts should be submitted to *BioScience Trends* online at *https://www.biosciencetrends.com/login*. Receipt of your manuscripts submitted online will be acknowledged by an e-mail from Editorial Office containing a reference number, which should be used in all future communications. If for any reason you are unable to submit a file online, please contact the Editorial Office by e-mail at *office@ biosciencetrends.com*

8. Accepted Manuscripts

Page Charge: Page charges will be levied on all manuscripts accepted for publication in *BioScience Trends* (Original Articles / Brief Reports / Reviews / Policy Forum / Communications: $140 per page for black white pages, $340 per page for color pages; News / Letters: a total cost of $600). Under exceptional circumstances, the author(s) may apply to the editorial office for a waiver of the publication charges by stating the reason in the Cover Letter when the manuscript online.

Misconduct: *BioScience Trends* takes seriously all allegations of potential misconduct and adhere to the ICMJE Guideline (*https://icmje.org/recommendations*) and COPE Guideline (*https://publicationethics.org/files/Code_of_conduct_for_journal_editors.pdf*). In cases of suspected research or publication misconduct, it may be necessary for the Editor or Publisher to contact and share submission details with third parties including authors' institutions and ethics committees. The corrections, retractions, or editorial expressions of concern will be performed in line with above guidelines.

(As of December 2022)

BioScience Trends
Editorial and Head Office
Pearl City Koishikawa 603,
2-4-5 Kasuga, Bunkyo-ku,
Tokyo 112-0003, Japan.
E-mail: office@biosciencetrends.com